Electronic Supporting Information

Manganese germylene complexes: reactivity with dihydrogen, isonitriles, and dinitrogen

Jeffrey S. Price and David J. H. Emslie*

Department of Chemistry, McMaster University, 1280 Main Street West, Hamilton, Ontario, L8S 4M1, Canada. Fax: (905)-522-2509; Tel: (905)-525-9140 x 23307

E-mail: emslied@mcmaster.ca

Website: https://emsliegroup.mcmaster.ca/

The supplemental file Cartesian_Coordinates_for_Calculated_Structures.xyz contains the computed Cartesian coordinates of all of the molecules reported in this study. The file may be opened as a text file to read the coordinates, or opened directly by a molecular modeling program such as Mercury (version 3.3 or later, http://www.ccdc.cam.ac.uk/pages/Home.aspx) for visualization and analysis.

Selected Abbreviations: dmpe = 1,2-bis(dimethylphosphino)ethane, sat. = satellite

Overview of Literature Mn(I) Dinitrogen Chemistry

Scheme S1 provides an overview of manganese(I) dinitrogen complexes synthesized from N_2 (not including dinitrogen complexes prepared by conversion of another N-containing ligand previously installed on the metal). Many manganese(I) complexes bearing dinitrogen ligands have been prepared by substitution reactions displacing THF,[1] H_2,[2-5] ethyl vinyl ether,[4] PMe_3,[6] or (more commonly) CO[6-12] ligands on Mn(I) with dinitrogen (Scheme S1). These reactions required supercritical fluid solvents, high N_2 pressures, photochemical conditions, or (in the case of $[(dmpe)_2MnH(N_2)]$) elevated temperature. Examples of N_2 coordination to manganese(I) under mild conditions (bottom right of Scheme S1) are limited to the syntheses of a μ-N_2 complex reported by Milstein *et al.* featuring an asymmetric PNP co-ligand, which was only observed in the solid state,[13] and a series of cationic 5-coordinate tetraphosphine carbonyl manganese(I) complexes with poor stability (complete conversion to the N_2 complex was only observed for the bis(depe) derivative).[14-16] The syntheses of dinitrogen manganese complexes $[(dmpe)_2Mn(GeHR_2)(N_2)]$ (**5a**; R = Ph, **5b**; R = Et) discussed in this work also proceeded under mild conditions.

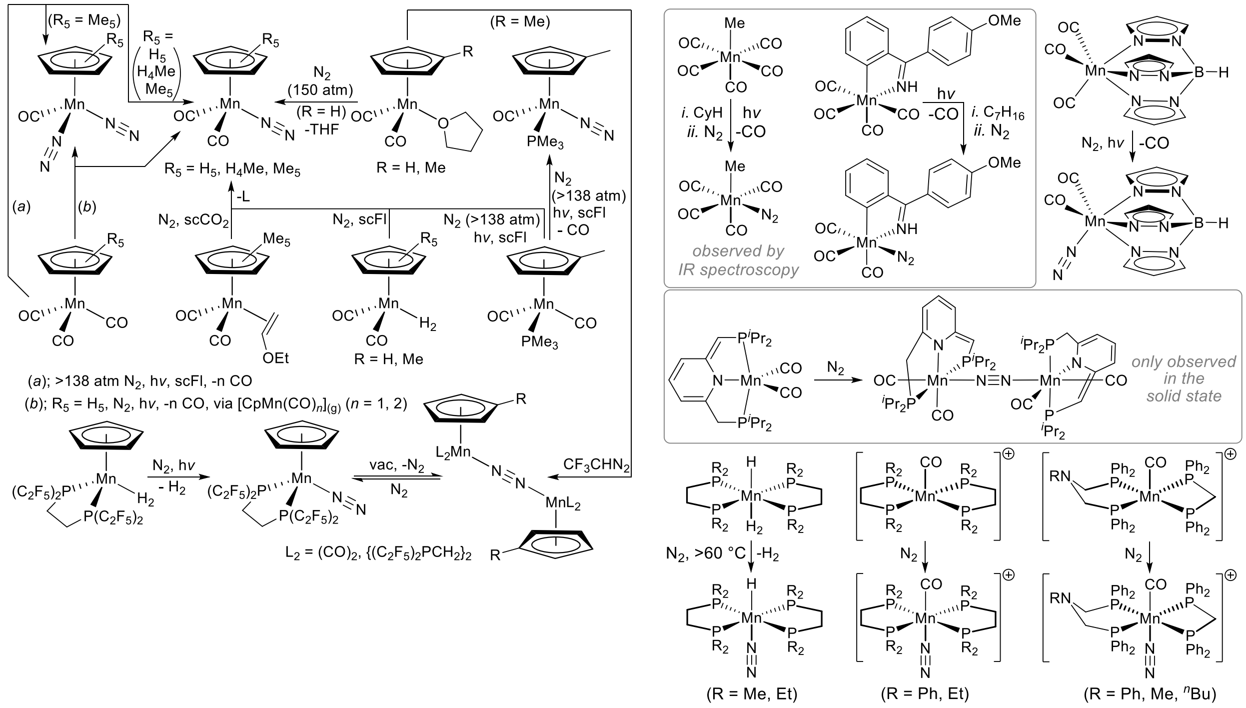

Scheme S1. Syntheses of previously reported manganese(I) dinitrogen complexes using N_2. For clarity, equilibria involving N_2 coordination/de-coordination are not indicated. scFl = supercritical fluid (CO_2 or Xe).[1-16]

Selected NMR Spectra for Solutions Containing Complexes 2a-b, *d*$_n$-2a-b, 3a-c, 5a-b, and 6

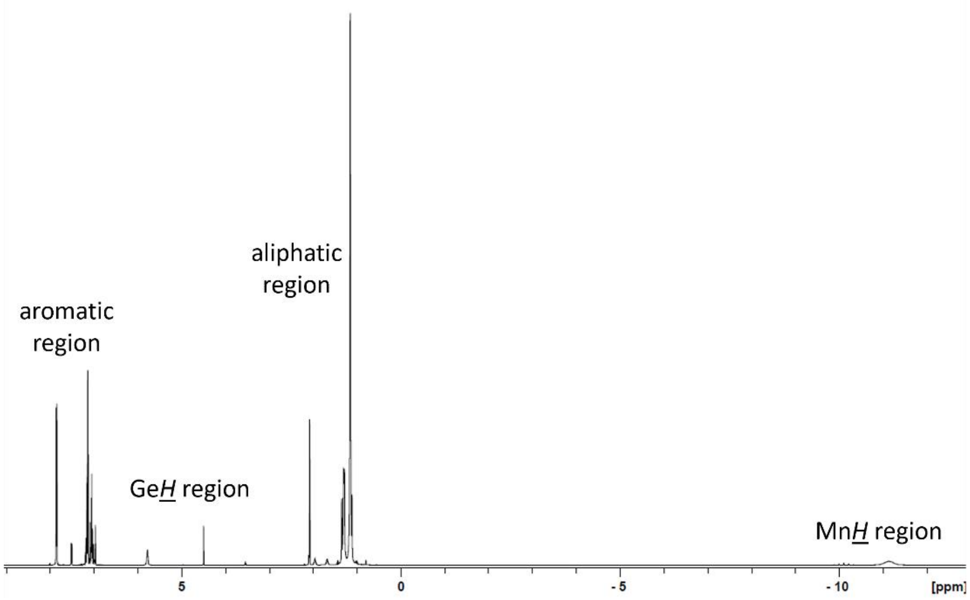

Figure S1. ^{1}H NMR spectrum of a solution containing [(dmpe)$_2$MnH$_2$(GeHPh$_2$)] (**2a**) formed from the reaction of [(dmpe)$_2$MnH(=GePh$_2$)] (**1a**) and H_2 after sitting at ambient temperature for 4 days in *d*$_8$-toluene (500 MHz, 298 K).

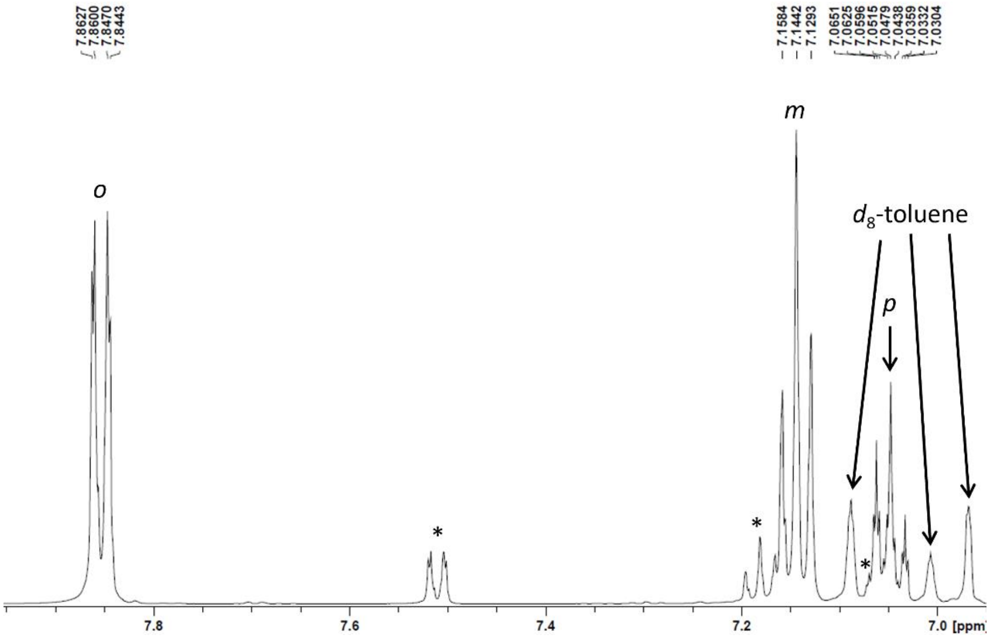

Figure S2. Expanded aromatic region of the ^{1}H NMR spectrum of a solution containing [(dmpe)$_2$MnH$_2$(GeHPh$_2$)] (**2a**) formed from the reaction of [(dmpe)$_2$MnH(=GePh$_2$)] (**1a**) and H_2 after sitting at ambient temperature for 4 days in *d*$_8$-toluene (500 MHz, 298 K). * indicates peaks from **1a**, and peak labels are for signals from **2a**.

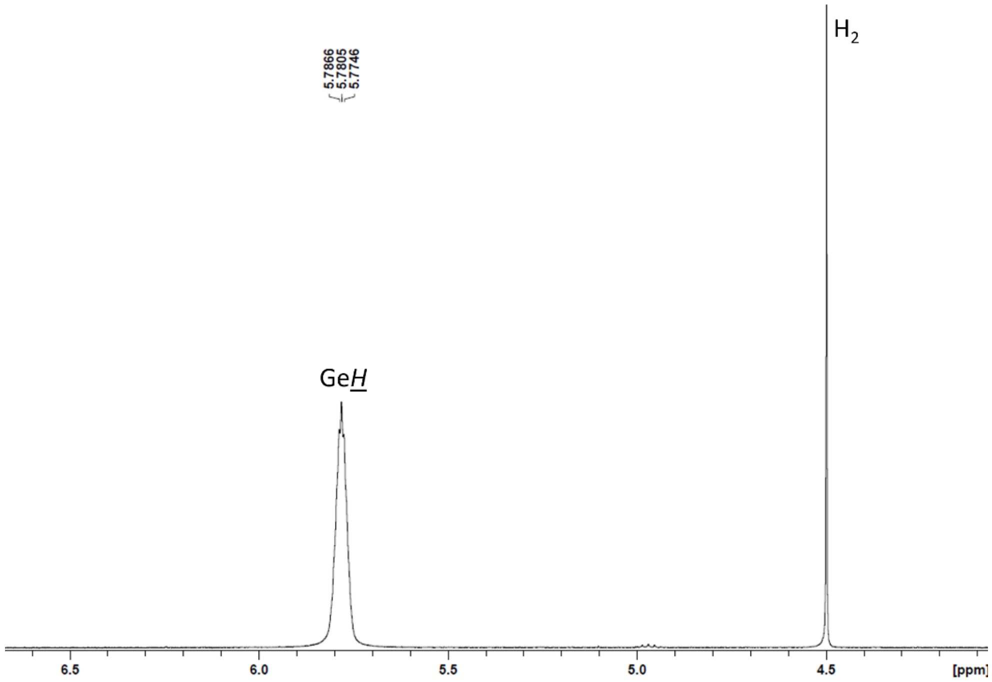

Figure S3. Expanded Ge*H* region of the ^{1}H NMR spectrum of a solution containing [(dmpe)$_2$MnH$_2$(GeHPh$_2$)] (**2a**) formed from the reaction of [(dmpe)$_2$MnH(=GePh$_2$)] (**1a**) and H_2 after sitting at ambient temperature for 4 days in *d*$_8$-toluene (500 MHz, 298 K). The peak label is for a signal from **2a**.

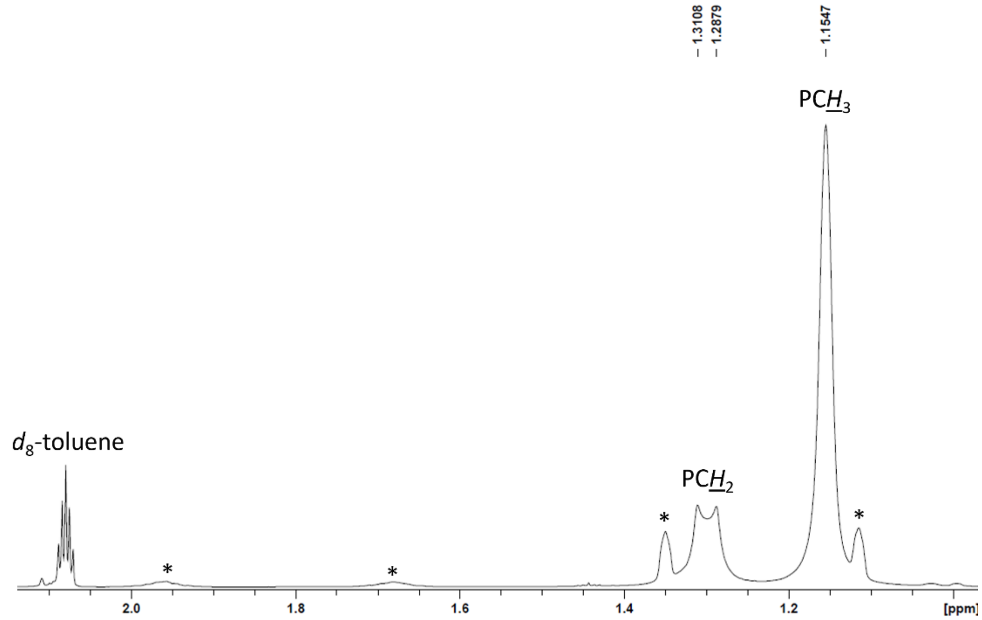

Figure S4. Expanded aliphatic region of the ^{1}H NMR spectrum of a solution containing [(dmpe)$_2$MnH$_2$(GeHPh$_2$)] (**2a**) formed from the reaction of [(dmpe)$_2$MnH(=GePh$_2$)] (**1a**) and H_2 after sitting at ambient temperature for 4 days in *d*$_8$-toluene (500 MHz, 298 K). * indicates peaks from **1a**, and peak labels are for signals from **2a**.

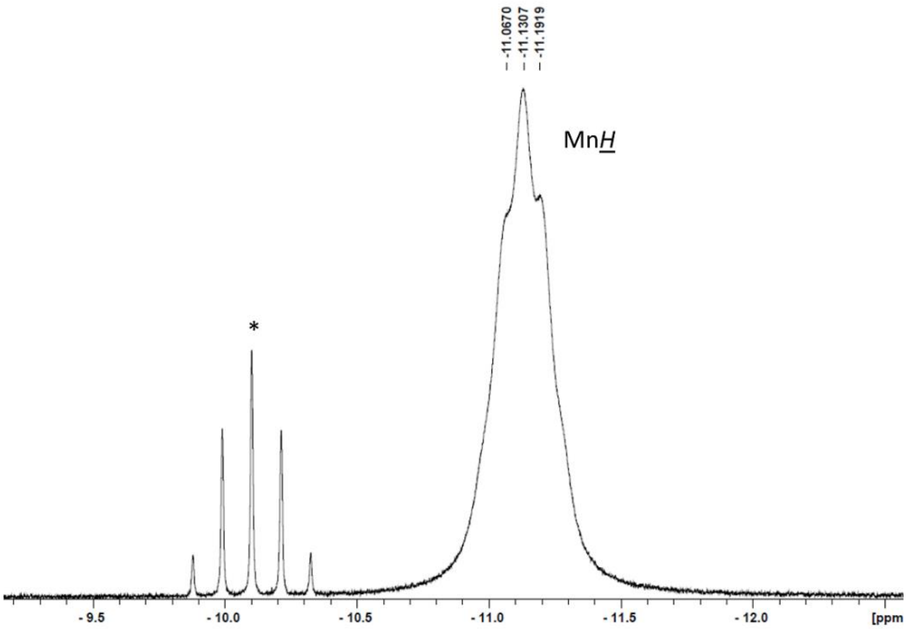

Figure S5. Expanded metal hydride region of the ^{1}H NMR spectrum of a solution containing [(dmpe)$_2$MnH$_2$(GeHPh$_2$)] (**2a**) formed from the reaction of [(dmpe)$_2$MnH(=GePh$_2$)] (**1a**) and H$_2$ after sitting at ambient temperature for 4 days in d_8-toluene (500 MHz, 298 K). * indicates a peak from **1a**, and the peak label is for a signal from **2a**.

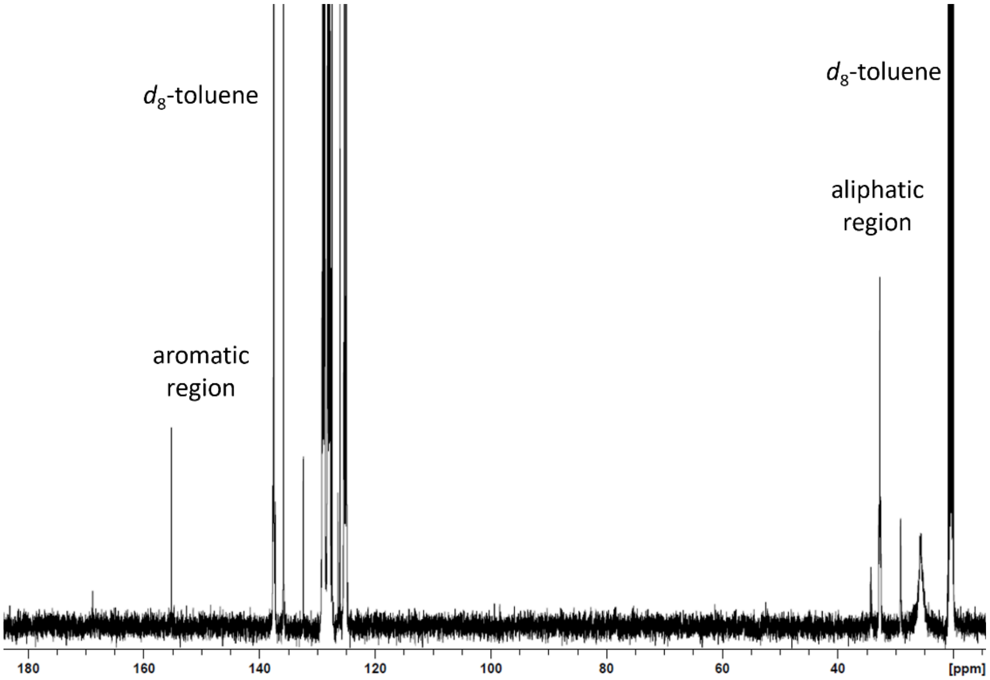

Figure S6. ^{13}C{^{1}H} NMR spectrum of a solution containing [(dmpe)$_2$MnH$_2$(GeHPh$_2$)] (**2a**) formed from the reaction of [(dmpe)$_2$MnH(=GePh$_2$)] (**1a**) and H$_2$ after sitting at ambient temperature for 4 days in d_8-toluene (126 MHz, 298 K).

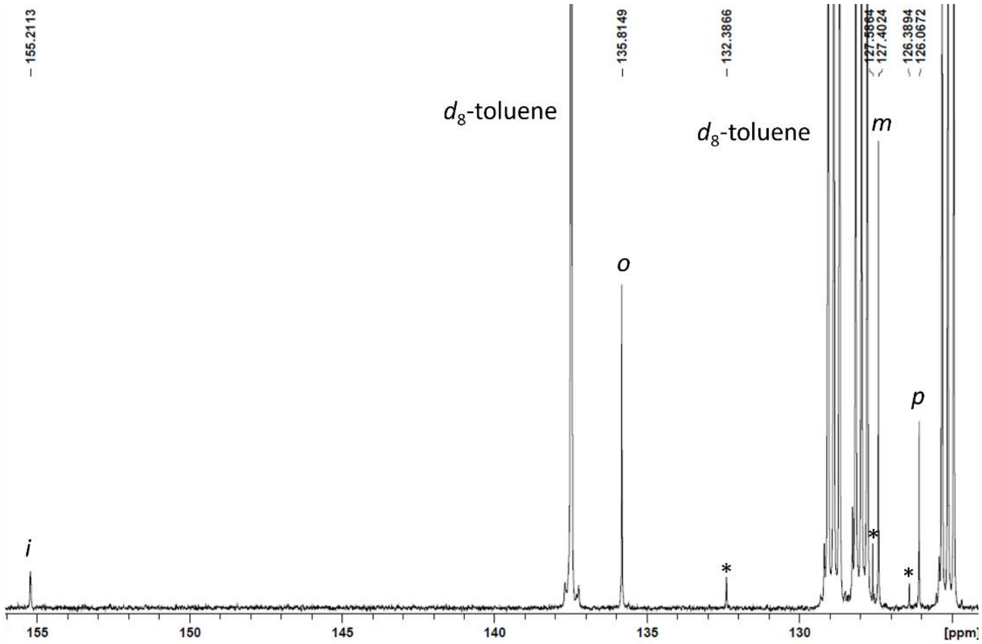

Figure S7. Expanded aromatic region of the $^{13}C\{^{1}H\}$ NMR spectrum of a solution containing [(dmpe)$_2$MnH$_2$(GeHPh$_2$)] (**2a**) formed from the reaction of [(dmpe)$_2$MnH(=GePh$_2$)] (**1a**) and H_2 after sitting at ambient temperature for 4 days in *d*$_8$-toluene (126 MHz, 298 K). * indicates peaks from **1a**, and peak labels are for signals from **2a**.

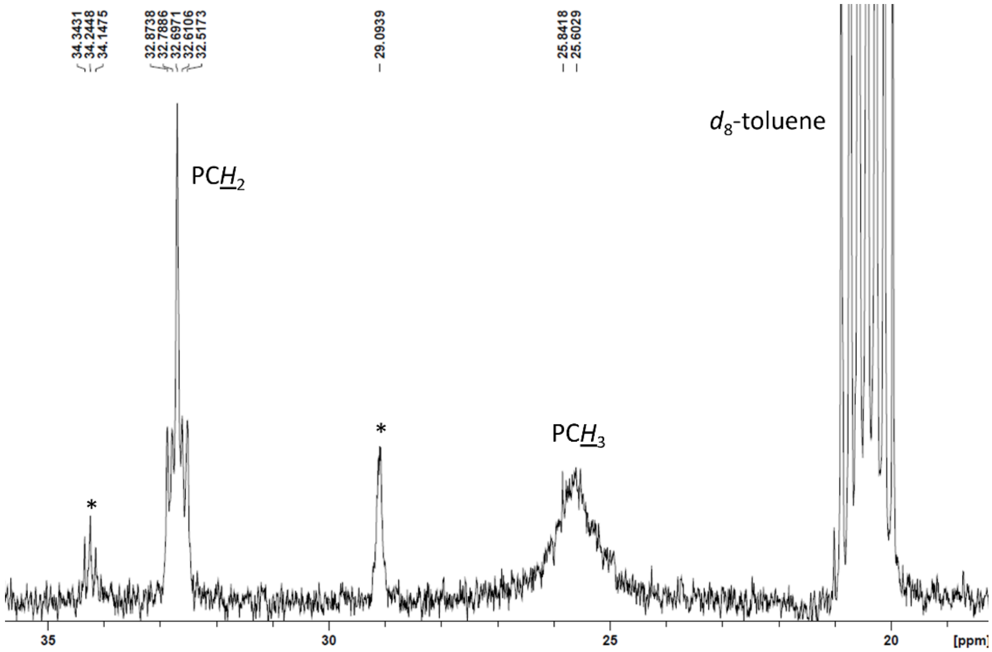

Figure S8. Expanded aliphatic region of the $^{13}C\{^{1}H\}$ NMR spectrum of a solution containing [(dmpe)$_2$MnH$_2$(GeHPh$_2$)] (**2a**) formed from the reaction of [(dmpe)$_2$MnH(=GePh$_2$)] (**1a**) and H_2 after sitting at ambient temperature for 4 days in *d*$_8$-toluene (126 MHz, 298 K). * indicates peaks from **1a**, and peak labels are for signals from **2a**.

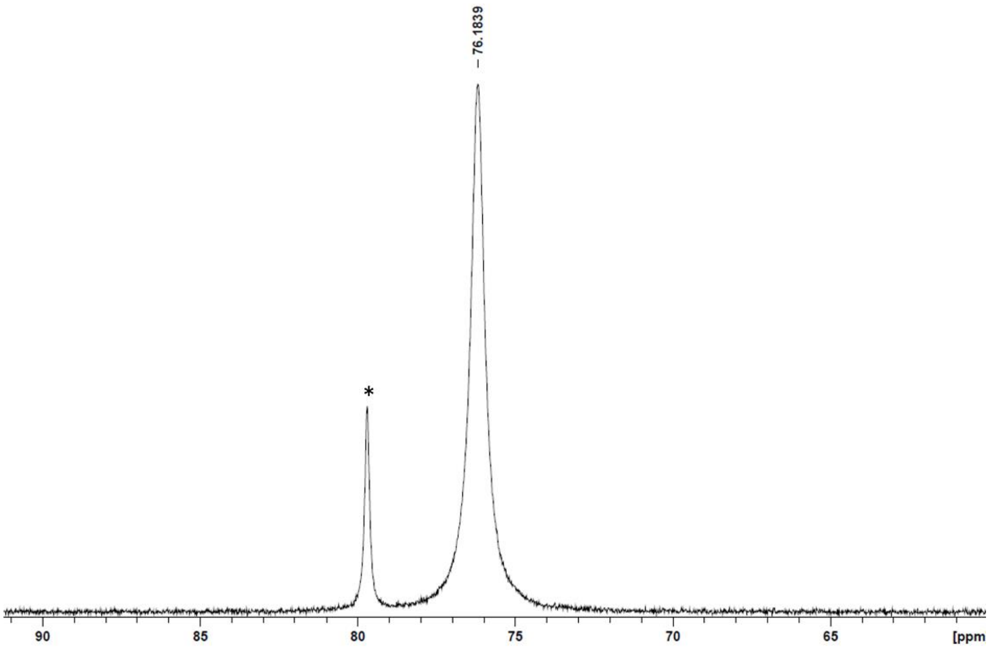

Figure S9. $^{31}P\{^{1}H\}$ NMR spectrum of a solution containing [$(dmpe)_2MnH_2(GeHPh_2)$] (**2a**) formed from the reaction of [$(dmpe)_2MnH(=GePh_2)$] (**1a**) and H_2 after sitting at ambient temperature for 4 days in d_8-toluene (202 MHz, 298 K). * indicates a peak from **1a**, and the unlabelled peak is a signal from **2a**.

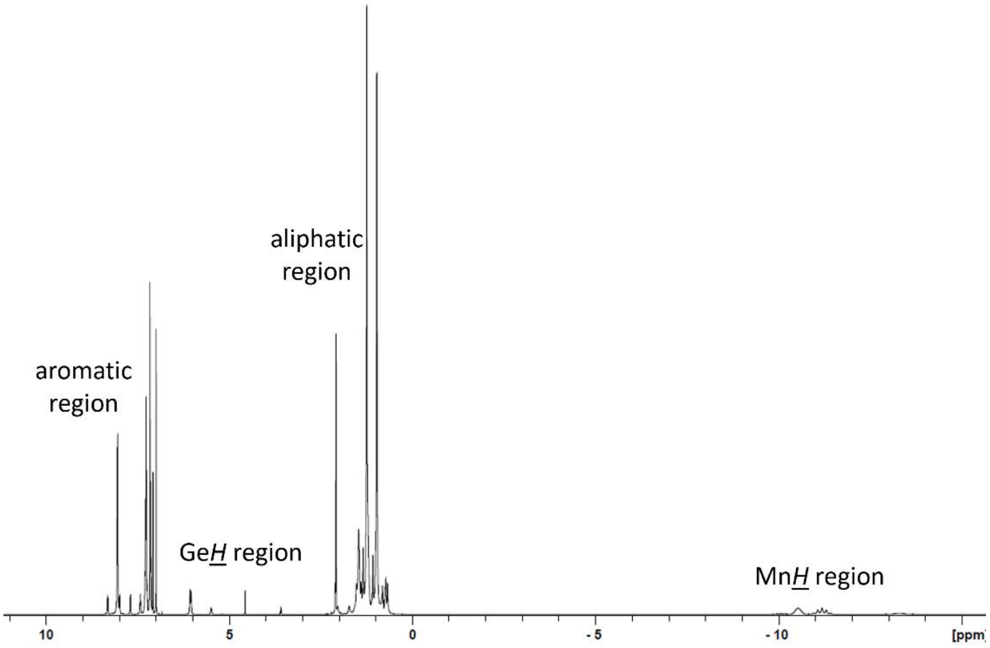

Figure S10. ^{1}H NMR spectrum of a solution containing [$(dmpe)_2MnH_2(GeHPh_2)$] (**2a**) formed from the reaction of [$(dmpe)_2MnH(=GePh_2)$] (**1a**) and H_2 after sitting at ambient temperature for 4 days in d_8-toluene (500 MHz, 176 K).

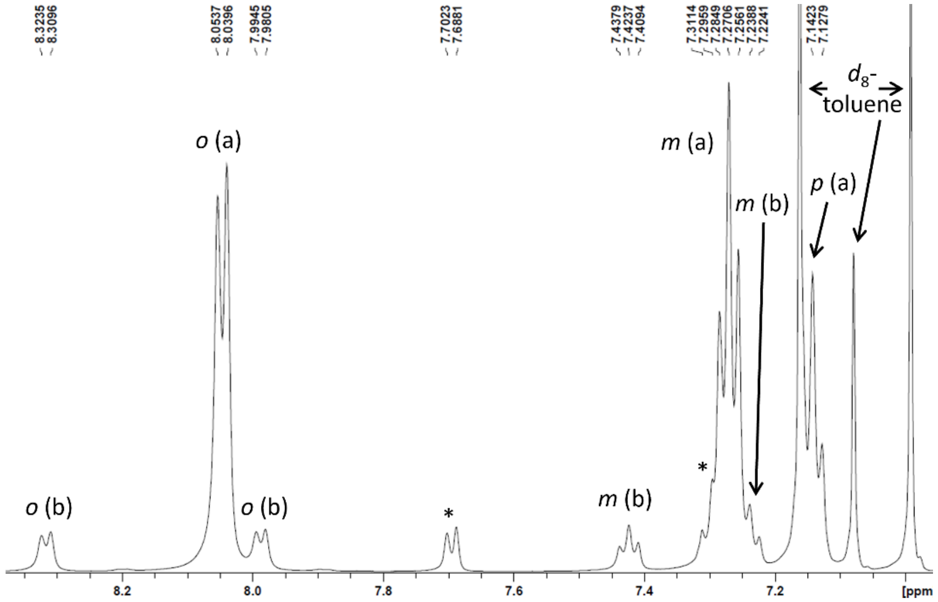

Figure S11. Expanded aromatic region of the ^{1}H NMR spectrum of a solution containing [(dmpe)$_2$MnH$_2$(GeHPh$_2$)] (**2a**) formed from the reaction of [(dmpe)$_2$MnH(=GePh$_2$)] (**1a**) and H$_2$ after sitting at ambient temperature for 4 days in d_8-toluene (500 MHz, 176 K). * indicates peaks from **1a**, peaks labelled (a) are those from *transHGe*-[(dmpe)$_2$MnH(HGeHPh$_2$)] (***transHGe*-2a**), and peaks labelled (b) are from the low symmetry isomer(s) *central*-[(dmpe)$_2$Mn(H$_2$GeHPh$_2$)] (***central*-2a**) and/or *cis*-[(dmpe)$_2$Mn(GeHPh$_2$)(H$_2$)] (***cis*-2a**).

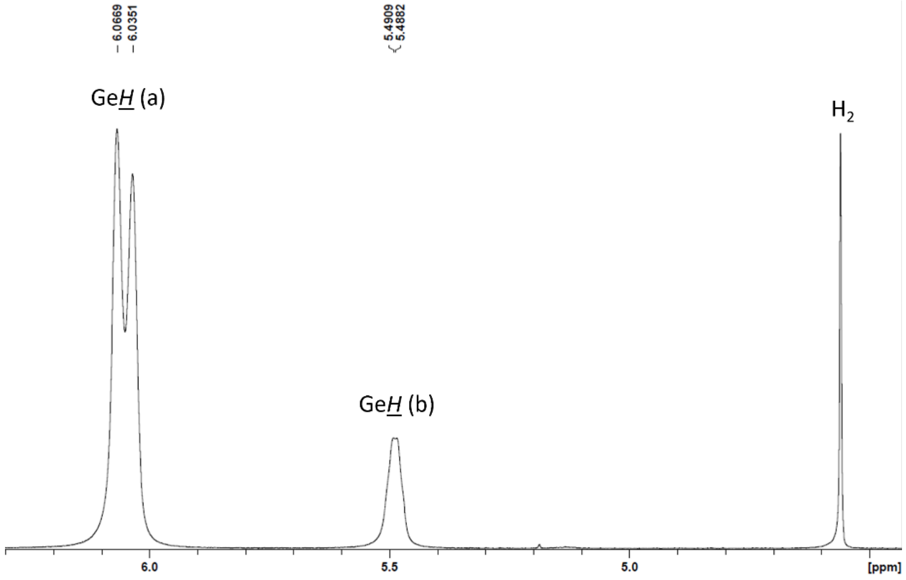

Figure S12. Expanded Ge*H* region of the ^{1}H NMR spectrum of a solution containing [(dmpe)$_2$MnH$_2$(GeHPh$_2$)] (**2a**) formed from the reaction of [(dmpe)$_2$MnH(=GePh$_2$)] (**1a**) and H$_2$ after sitting at ambient temperature for 4 days in d_8-toluene (500 MHz, 176 K). The peak labelled (a) is from *transGeH*-[(dmpe)$_2$MnH(HGeHPh$_2$)] (***transHGe*-2a**), and the peak labelled (b) is from the low symmetry isomer(s) *central*-[(dmpe)$_2$Mn(H$_2$GeHPh$_2$)] (***central*-2a**) and/or *cis*-[(dmpe)$_2$Mn(GeHPh$_2$)(H$_2$)] (***cis*-2a**).

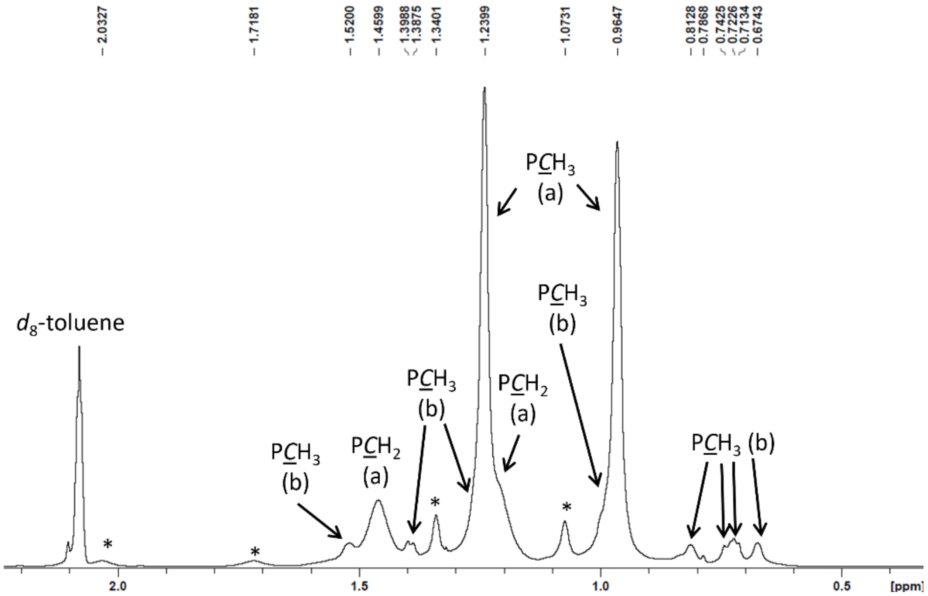

Figure S13. Expanded aliphatic region of the ^{1}H NMR spectrum of a solution containing [(dmpe)$_2$MnH$_2$(GeHPh$_2$)] (**2a**) formed from the reaction of [(dmpe)$_2$MnH(=GePh$_2$)] (**1a**) and H$_2$ after sitting at ambient temperature for 4 days in *d*$_8$-toluene (500 MHz, 176 K). * indicates peaks from **1a**, peaks labelled (a) are those from *transHGe*-[(dmpe)$_2$MnH(HGeHPh$_2$)] (***transHGe*-2a**), and peaks labelled (b) are from the low symmetry isomer(s) *central*-[(dmpe)$_2$Mn(H$_2$GeHPh$_2$)] (***central*-2a**) and/or *cis*-[(dmpe)$_2$Mn(GeHPh$_2$)(H$_2$)] (***cis*-2a**).

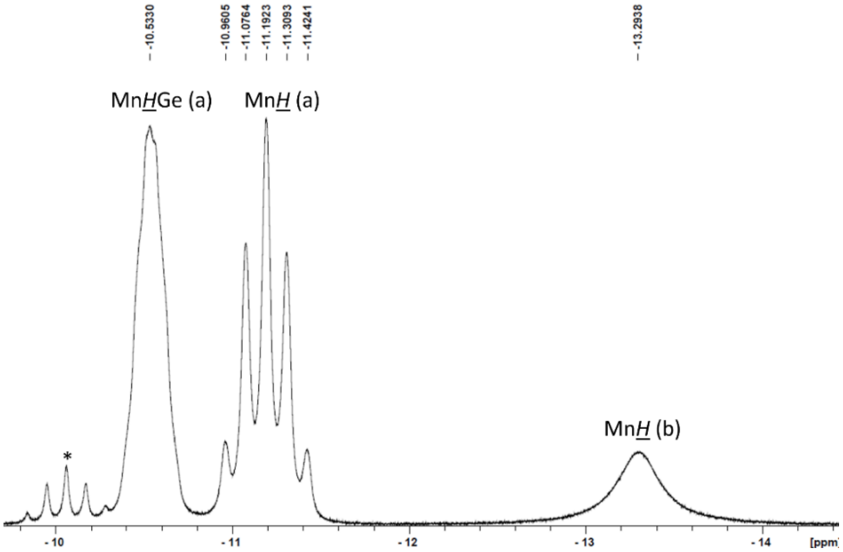

Figure S14. Expanded metal hydride region of the ^{1}H NMR spectrum of a solution containing [(dmpe)$_2$MnH$_2$(GeHPh$_2$)] (**2a**) formed from the reaction of [(dmpe)$_2$MnH(=GePh$_2$)] (**1a**) and H$_2$ after sitting at ambient temperature for 4 days in *d*$_8$-toluene (500 MHz, 176 K). * indicates a peak from **1a**, peaks labelled (a) are those from *transHGe*-[(dmpe)$_2$MnH(HGeHPh$_2$)] (***transHGe*-2a**), and the peak labelled (b) is from the low symmetry isomer(s) *central*-[(dmpe)$_2$Mn(H$_2$GeHPh$_2$)] (***central*-2a**) and/or *cis*-[(dmpe)$_2$Mn(GeHPh$_2$)(H$_2$)] (***cis*-2a**).

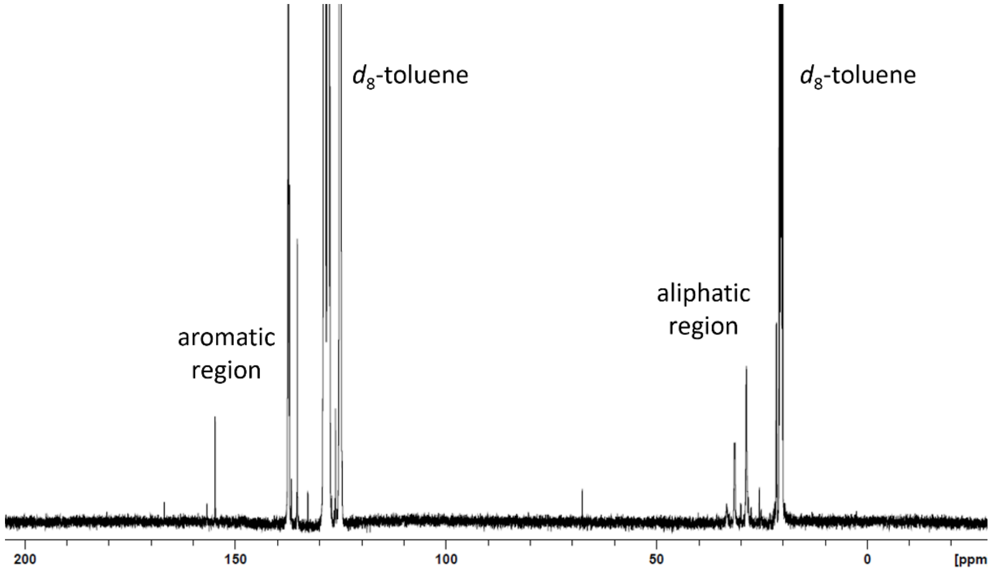

Figure S15. $^{13}C\{^1H\}$ NMR spectrum of a solution containing [(dmpe)$_2$MnH$_2$(GeHPh$_2$)] (**2a**) formed from the reaction of [(dmpe)$_2$MnH(=GePh$_2$)] (**1a**) and H_2 after sitting at ambient temperature for 4 days in d_8-toluene (126 MHz, 176 K).

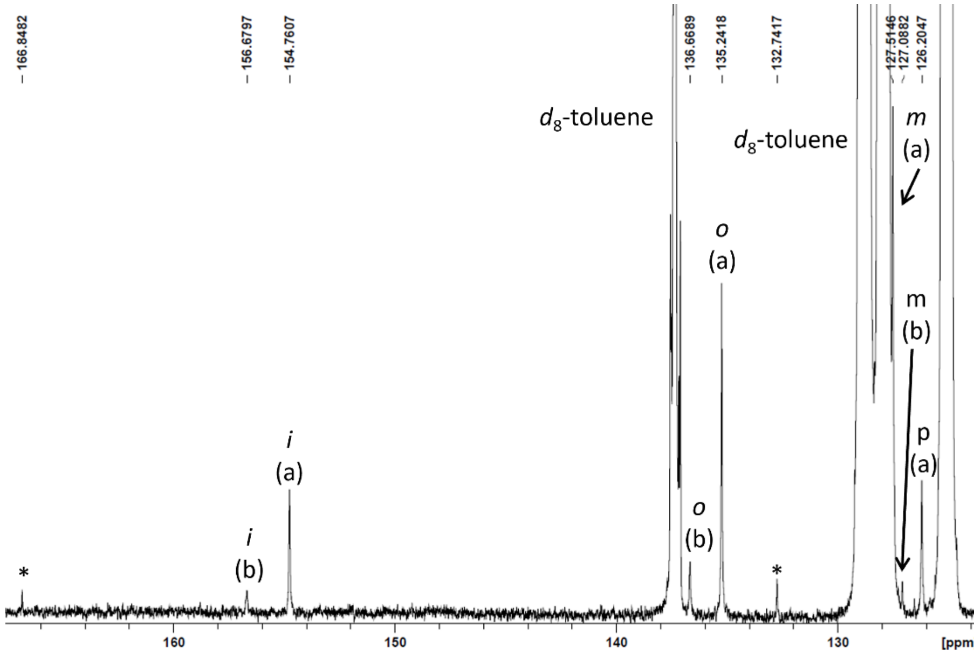

Figure S16. Expanded aromatic region of the $^{13}C\{^1H\}$ NMR spectrum of a solution containing [(dmpe)$_2$MnH$_2$(GeHPh$_2$)] (**2a**) formed from the reaction of [(dmpe)$_2$MnH(=GePh$_2$)] (**1a**) and H_2 after sitting at ambient temperature for 4 days in d_8-toluene (126 MHz, 176 K). * indicates peaks from **1a**, peaks labelled (a) are those from *transHGe*-[(dmpe)$_2$MnH(HGeHPh$_2$)] (***transHGe*-2a**), and peaks labelled (b) are from the low symmetry isomer(s) *central*-[(dmpe)$_2$Mn(H$_2$GeHPh$_2$)] (***central*-2a**) and/or *cis*-[(dmpe)$_2$Mn(GeHPh$_2$)(H$_2$)] (***cis*-2a**).

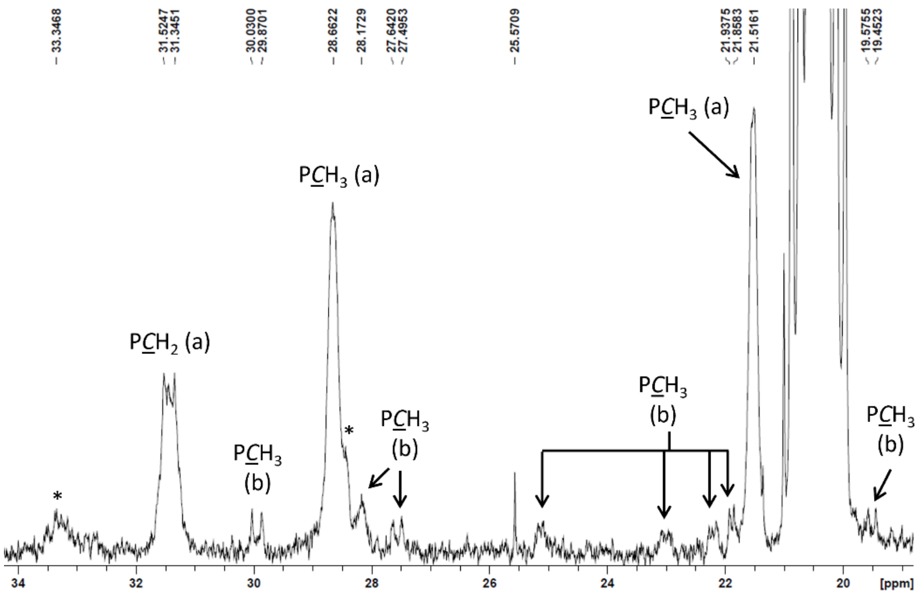

Figure S17. Expanded aliphatic region of the $^{13}C\{^{1}H\}$ NMR spectrum of a solution containing [(dmpe)$_2$MnH$_2$(GeHPh$_2$)] (**2a**) formed from the reaction of [(dmpe)$_2$MnH(=GePh$_2$)] (**1a**) and H$_2$ after sitting at ambient temperature for 4 days in *d*$_8$-toluene (126 MHz, 176 K). * indicates peaks from **1a**, peaks labelled (a) are those from *transHGe*-[(dmpe)$_2$MnH(HGeHPh$_2$)] (***transHGe*-2a**), and peaks labelled (b) are from the low symmetry isomer(s) *central*-[(dmpe)$_2$Mn(H$_2$GeHPh$_2$)] (***central*-2a**) and/or *cis*-[(dmpe)$_2$Mn(GeHPh$_2$)(H$_2$)] (***cis*-2a**).

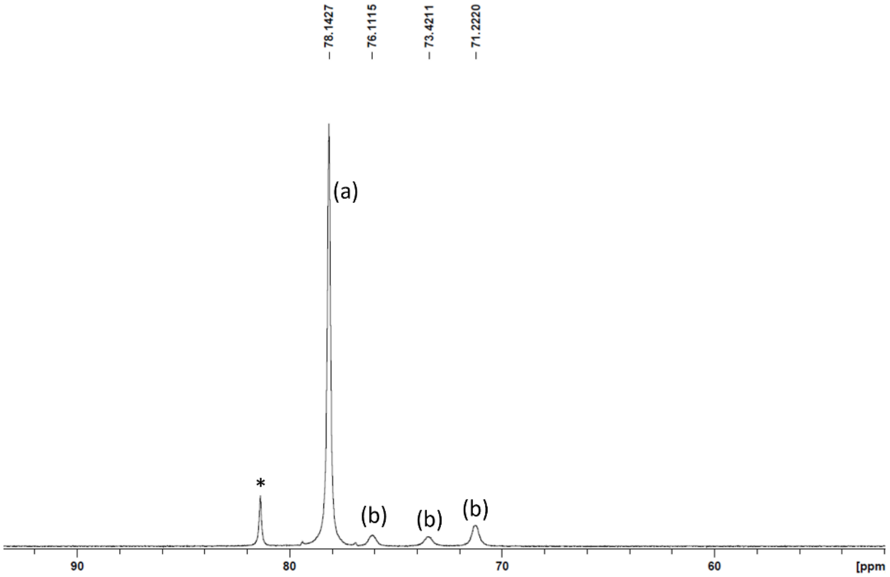

Figure S18. $^{31}P\{^{1}H\}$ NMR spectrum of a solution containing [(dmpe)$_2$MnH$_2$(GeHPh$_2$)] (**2a**) formed from the reaction of [(dmpe)$_2$MnH(=GePh$_2$)] (**1a**) and H$_2$ after sitting at ambient temperature for 4 days in *d*$_8$-toluene (202 MHz, 176 K). * indicates a peak from **1a**, the peak labelled (a) is from *transHGe*-[(dmpe)$_2$MnH(HGeHPh$_2$)] (***transHGe*-2a**), and peaks labelled (b) are from the low symmetry isomer(s) *central*-[(dmpe)$_2$Mn(H$_2$GeHPh$_2$)] (***central*-2a**) and/or *cis*-[(dmpe)$_2$Mn(GeHPh$_2$)(H$_2$)] (***cis*-2a**).

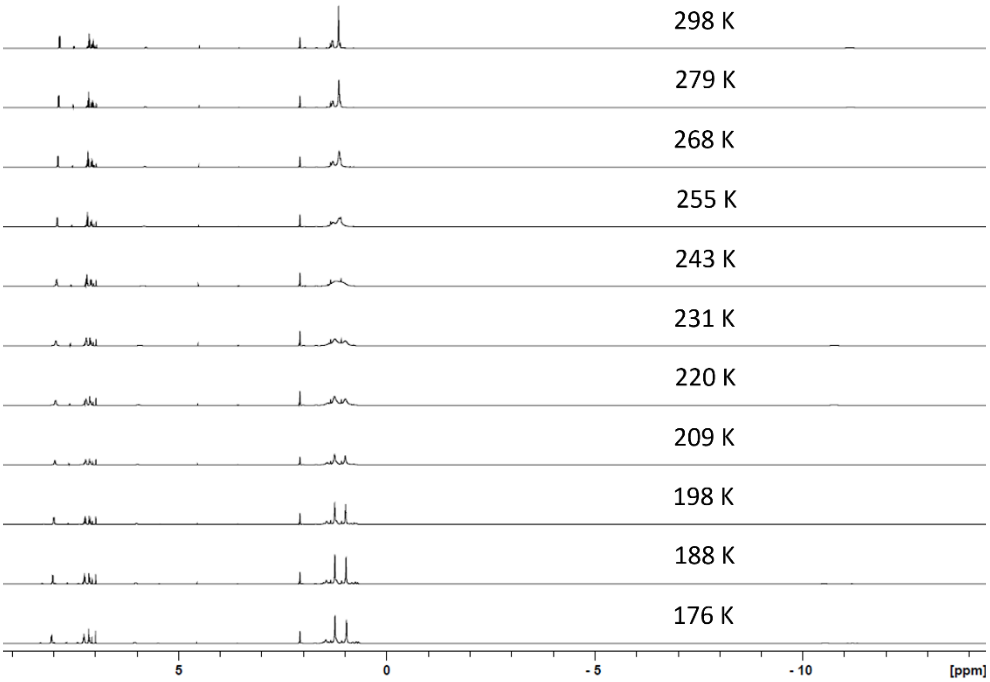

Figure S19. Variable temperature ^{1}H NMR spectra of a solution containing [(dmpe)$_2$MnH$_2$(GeHPh$_2$)] (**2a**) formed from the reaction of [(dmpe)$_2$MnH(=GePh$_2$)] (**1a**) and H_2 after sitting at ambient temperature for 4 days in d_8-toluene (500 MHz).

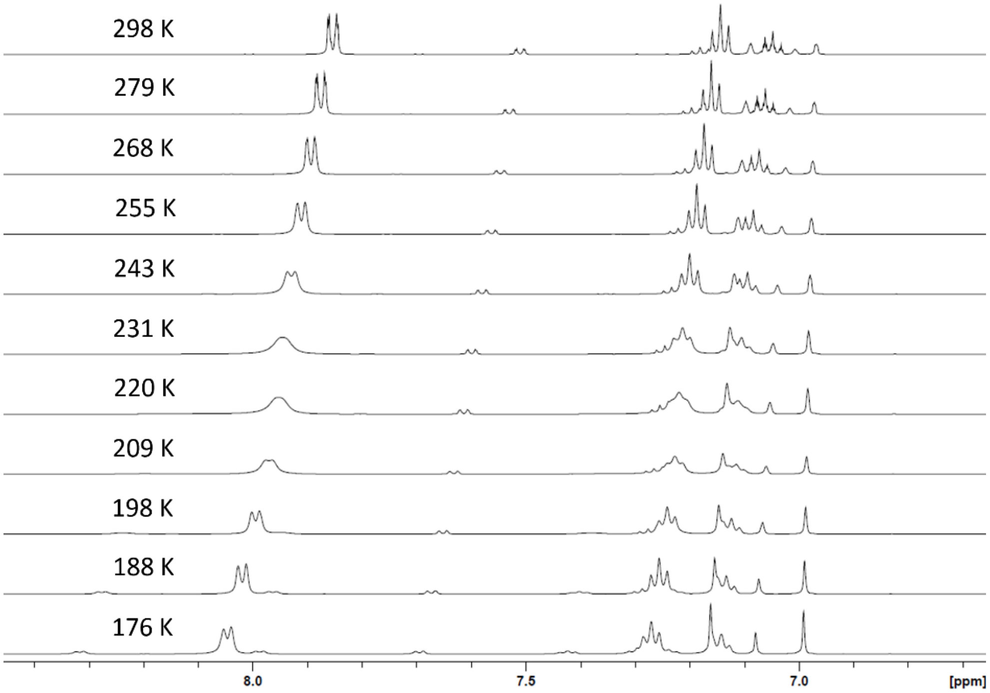

Figure S20. Expanded aromatic regions of variable temperature ^{1}H NMR spectra of a solution containing [(dmpe)$_2$MnH$_2$(GeHPh$_2$)] (**2a**) formed from the reaction of [(dmpe)$_2$MnH(=GePh$_2$)] (**1a**) and H_2 after sitting at ambient temperature for 4 days in d_8-toluene (500 MHz).

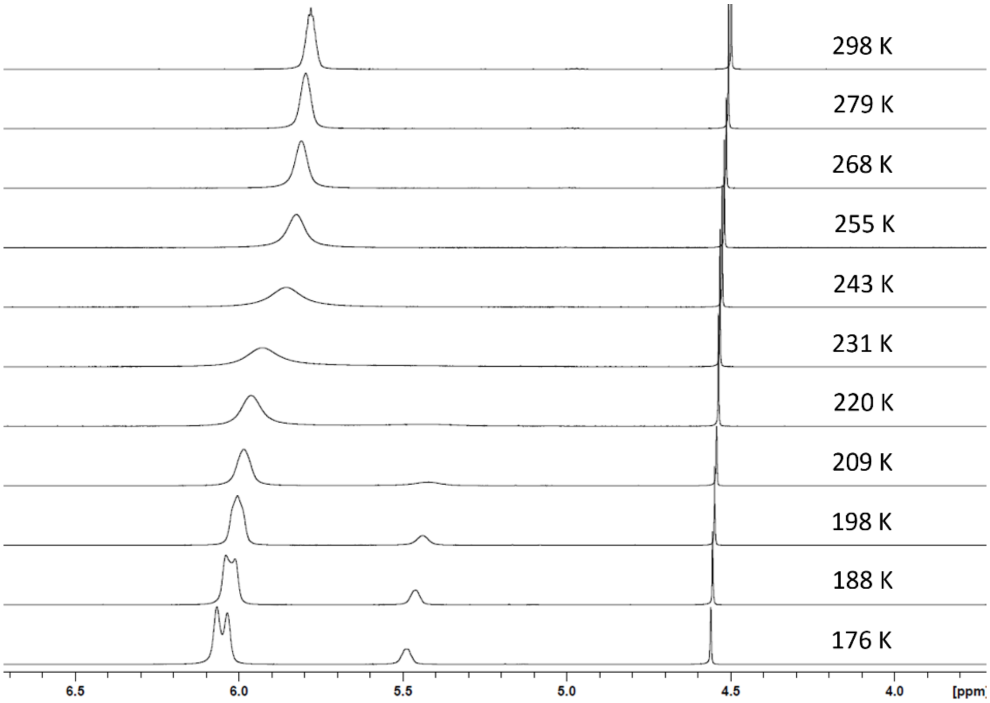

Figure S21. Expanded Ge*H* regions of variable temperature ^{1}H NMR spectra of a solution containing [(dmpe)$_2$MnH$_2$(GeHPh$_2$)] (**2a**) formed from the reaction of [(dmpe)$_2$MnH(=GePh$_2$)] (**1a**) and H$_2$ after sitting at ambient temperature for 4 days in d_8-toluene (500 MHz).

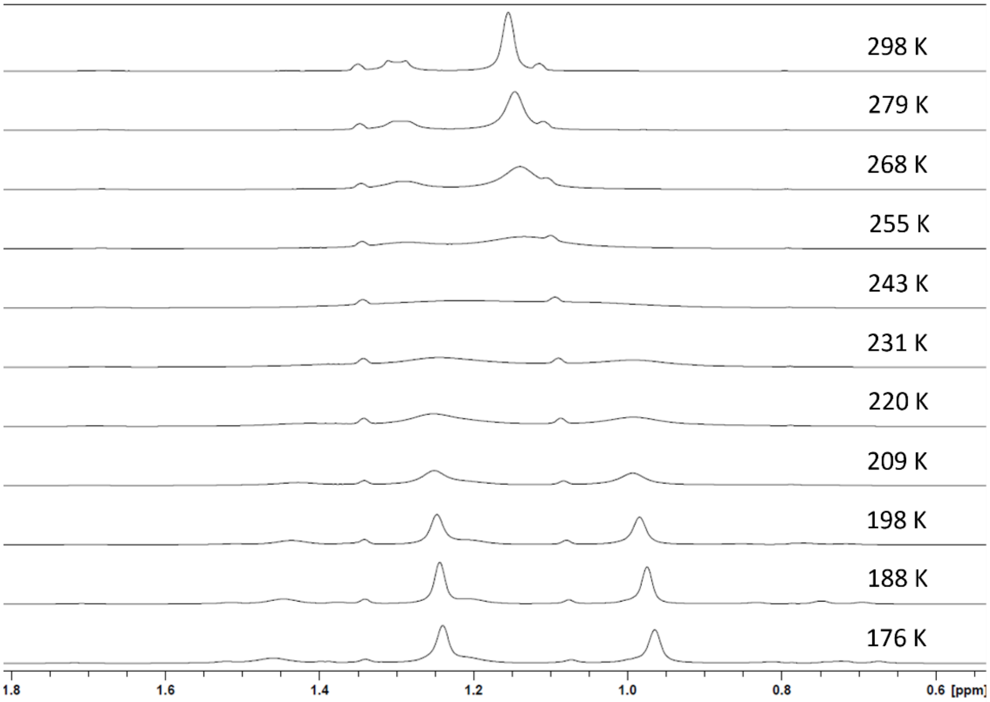

Figure S22. Expanded aliphatic regions of variable temperature ^{1}H NMR spectra of a solution containing [(dmpe)$_2$MnH$_2$(GeHPh$_2$)] (**2a**) formed from the reaction of [(dmpe)$_2$MnH(=GePh$_2$)] (**1a**) and H$_2$ after sitting at ambient temperature for 4 days in d_8-toluene (500 MHz).

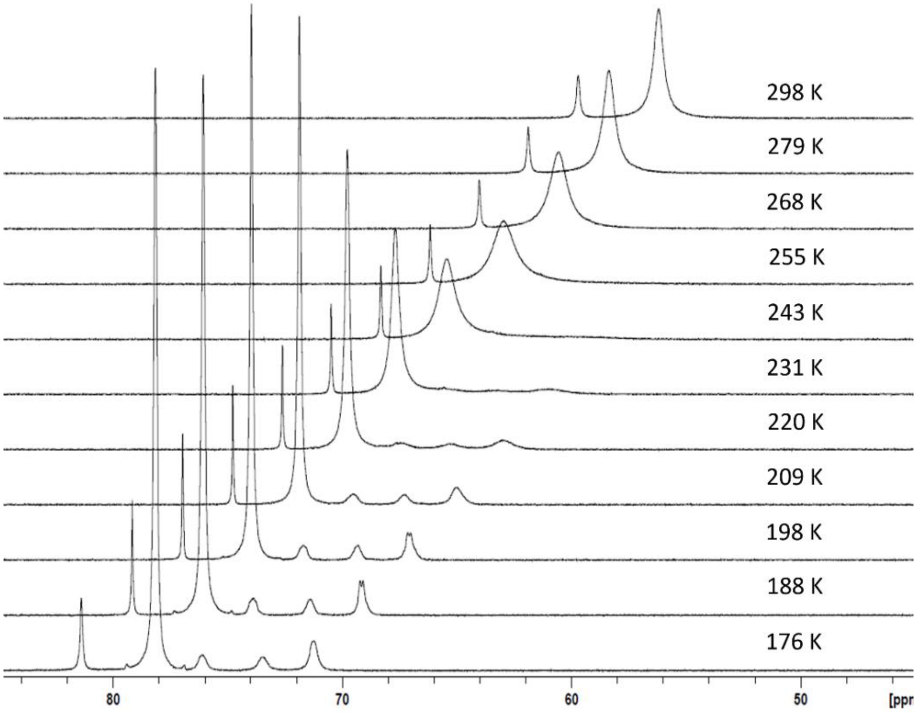

Figure S23. Variable temperature $^{31}P\{^{1}H\}$ NMR spectra of a solution containing [(dmpe)$_2$MnH$_2$(GeHPh$_2$)] (**2a**) formed from the reaction of [(dmpe)$_2$MnH(=GePh$_2$)] (**1a**) and H_2 after sitting at ambient temperature for 4 days in *d*$_8$-toluene (202 MHz). For clarity, each spectrum is shifted 2 ppm to lower frequency than the one below it, and the x-axis corresponds to the bottom spectrum.

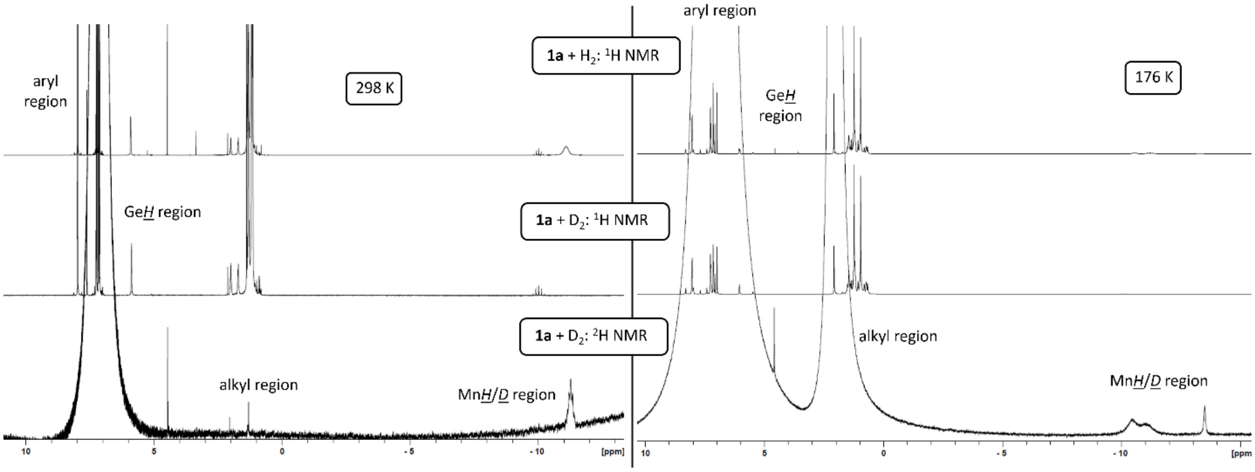

Figure S24. Top: ^{1}H NMR spectra of a solution containing [(dmpe)$_2$MnH$_2$(GeHPh$_2$)] (**2a**) formed from the reaction of [(dmpe)$_2$MnH(=GePh$_2$)] (**1a**) and H_2 after sitting at ambient temperature for 3 days in C_6D_6 (600 MHz, 298 K; left) or *d*$_8$-toluene (500 MHz, 176 K; right). Middle and bottom: ^{1}H NMR (middle; 500 MHz) and ^{2}H NMR (bottom; 77 MHz) spectra of a solution containing [(dmpe)$_2$MnD$_2$(GeHPh$_2$)] (***d*$_2$-2a**) formed from the reaction of [(dmpe)$_2$MnH(=GePh$_2$)] (**1a**) and D_2 after sitting at ambient temperature for 1 day in C_6D_6 (298 K; left) or 3 days in *d*$_8$-toluene (176 K; right).

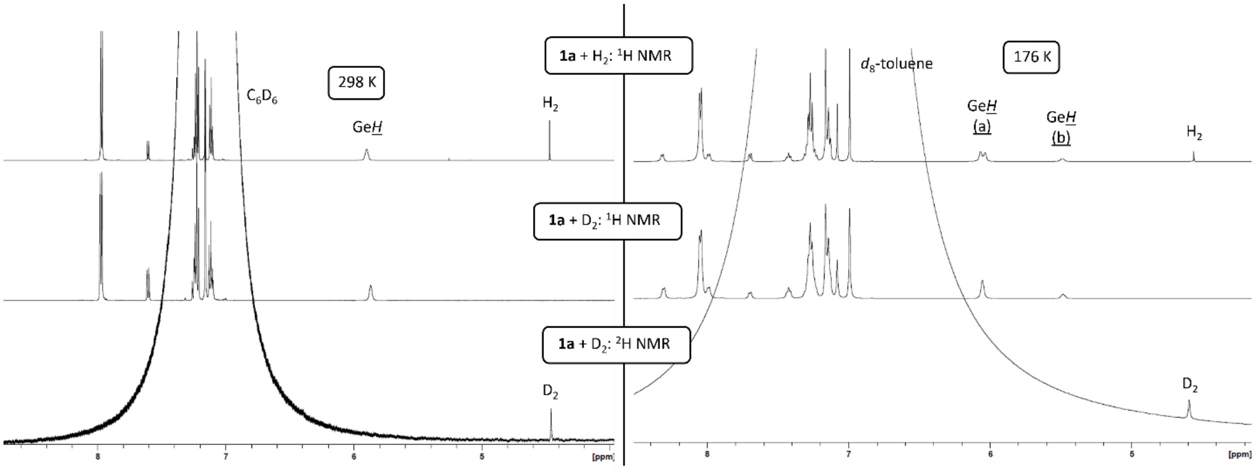

Figure S25. Top: Expanded aromatic and Ge*H* region of the ^{1}H NMR spectra of a solution containing [(dmpe)$_2$MnH$_2$(GeHPh$_2$)] (**2a**) formed from the reaction of [(dmpe)$_2$MnH(=GePh$_2$)] (**1a**) and H_2 after sitting at ambient temperature for 3 days in C_6D_6 (600 MHz, 298 K; left) or *d*$_8$-toluene (500 MHz, 176 K; right). The peaks labelled (a) are from the *transHGe* isomer of ***d*$_2$-2a**, and the peaks labelled (b) are from the *cis* and/or *central* isomer(s) of ***d*$_2$-2a**. Middle and bottom: Expanded aromatic and Ge*H* region of the ^{1}H NMR (middle; 500 MHz) and ^{2}H NMR (bottom; 77 MHz) spectra of a solution containing [(dmpe)$_2$MnD$_2$(GeHPh$_2$)] (***d*$_2$-2a**) formed from the reaction of [(dmpe)$_2$MnH(=GePh$_2$)] (**1a**) and D_2 after sitting at ambient temperature for 1 day in C_6D_6 (298 K; left) or 3 days in *d*$_8$-toluene (176 K; right).

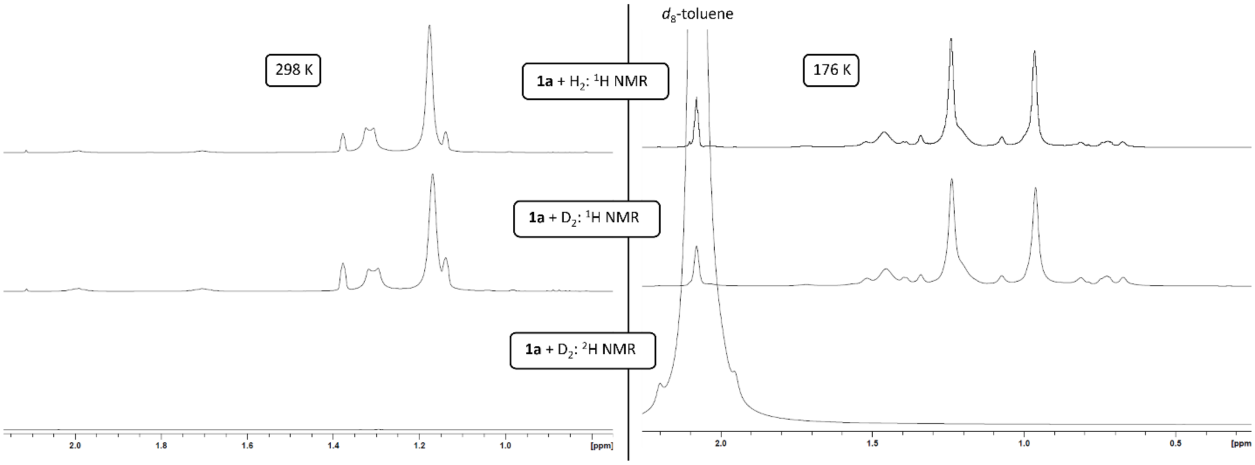

Figure S26. Top: Expanded aliphatic region of the ^{1}H NMR spectra of a solution containing [(dmpe)$_2$MnH$_2$(GeHPh$_2$)] (**2a**) formed from the reaction of [(dmpe)$_2$MnH(=GePh$_2$)] (**1a**) and H_2 after sitting at ambient temperature for 3 days in C_6D_6 (600 MHz, 298 K; left) or *d*$_8$-toluene (500 MHz, 176 K; right). Middle and bottom: Expanded aliphatic region of the ^{1}H NMR (middle; 500 MHz) and ^{2}H NMR (bottom; 77 MHz) spectra of a solution containing [(dmpe)$_2$MnD$_2$(GeHPh$_2$)] (***d*$_2$-2a**) formed from the reaction of [(dmpe)$_2$MnH(=GePh$_2$)] (**1a**) and D_2 after sitting at ambient temperature for 1 day in C_6D_6 (298 K; left) or 3 days in *d*$_8$-toluene (176 K; right).

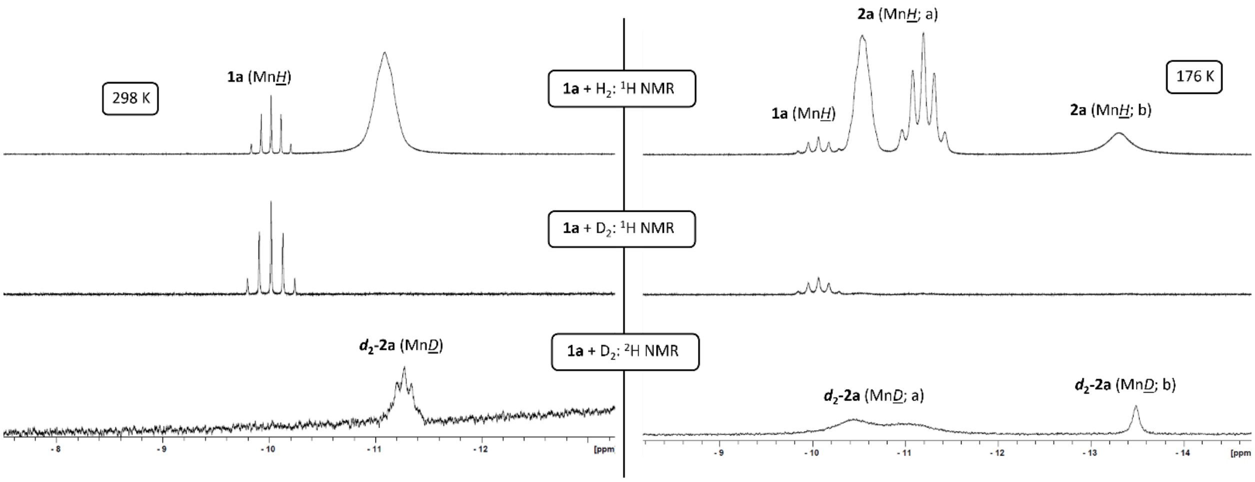

Figure S27. Top: Expanded metal hydride region of the ^{1}H NMR spectra of a solution containing [(dmpe)$_2$MnH$_2$(GeHPh$_2$)] (**2a**) formed from the reaction of [(dmpe)$_2$MnH(=GePh$_2$)] (**1a**) and H$_2$ after sitting at ambient temperature for 3 days in C$_6$D$_6$ (600 MHz, 298 K; left) or *d*$_8$-toluene (500 MHz, 176 K; right). The peaks labelled (a) are from the *transHGe* isomer of **2a** or ***d*$_2$-2a**, and the peaks labelled (b) are from the *cis* and/or *central* isomer(s) of **2a** or ***d*$_2$-2a**. Middle and bottom: Expanded metal hydride region of the ^{1}H NMR (middle; 500 MHz) and ^{2}H NMR (bottom; 77 MHz) spectra of a solution containing [(dmpe)$_2$MnD$_2$(GeHPh$_2$)] (***d*$_2$-2a**) formed from the reaction of [(dmpe)$_2$MnH(=GePh$_2$)] (**1a**) and D$_2$ after sitting at ambient temperature for 1 day in C$_6$D$_6$ (298 K; left) or 3 days in *d*$_8$-toluene (176 K; right).

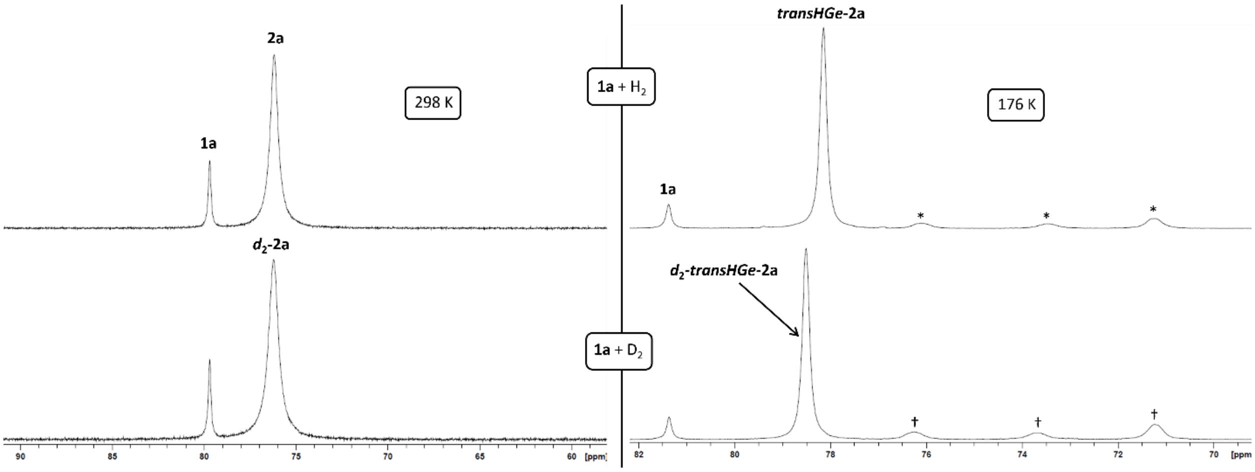

Figure S28. ^{31}P{^{1}H} NMR spectra (202 MHz) of a solution containing (top) [(dmpe)$_2$MnH$_2$(GeHPh$_2$)] (**2a**) formed from the reaction of [(dmpe)$_2$MnH(=GePh$_2$)] (**1a**) and H$_2$ after sitting at ambient temperature for 4 days in *d*$_8$-toluene (left; 298 K, right; 176 K) or (bottom) [(dmpe)$_2$MnD$_2$(GeHPh$_2$)] (***d*$_2$-2a**) formed from the reaction of [(dmpe)$_2$MnH(=GePh$_2$)] (**1a**) and D$_2$ after sitting at ambient temperature for 3 days in *d*$_8$-toluene (left; 298 K, right; 176 K). * indicates peaks from the *cis* and/or *central* isomer(s) of **2a**, and † indicates peaks from the *cis* and/or *central* isomer(s) of ***d*$_2$-2a**.

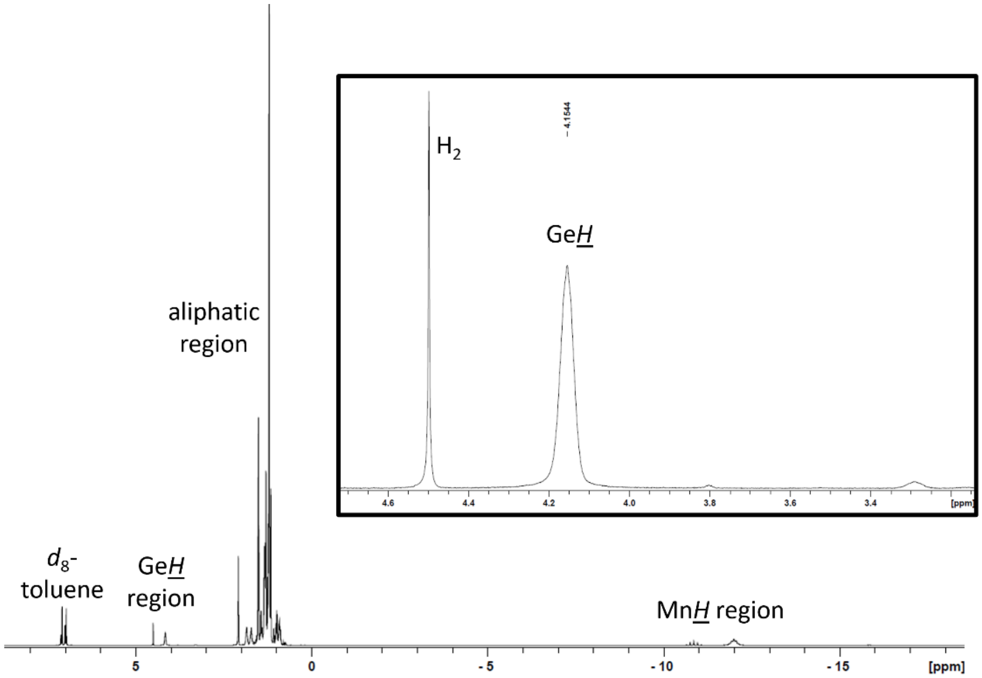

Figure S29. ^{1}H NMR spectrum of a solution containing [(dmpe)$_2$MnH$_2$(GeHEt$_2$)] (**2b**) formed from the reaction of [(dmpe)$_2$MnH(=GeEt$_2$)] (**1b**) and H$_2$ after sitting at ambient temperature for 3 days in d_8-toluene (500 MHz, 298 K). The inset shows the expanded Ge*H* region of this spectrum. The peak label is for a signal from **2b**.

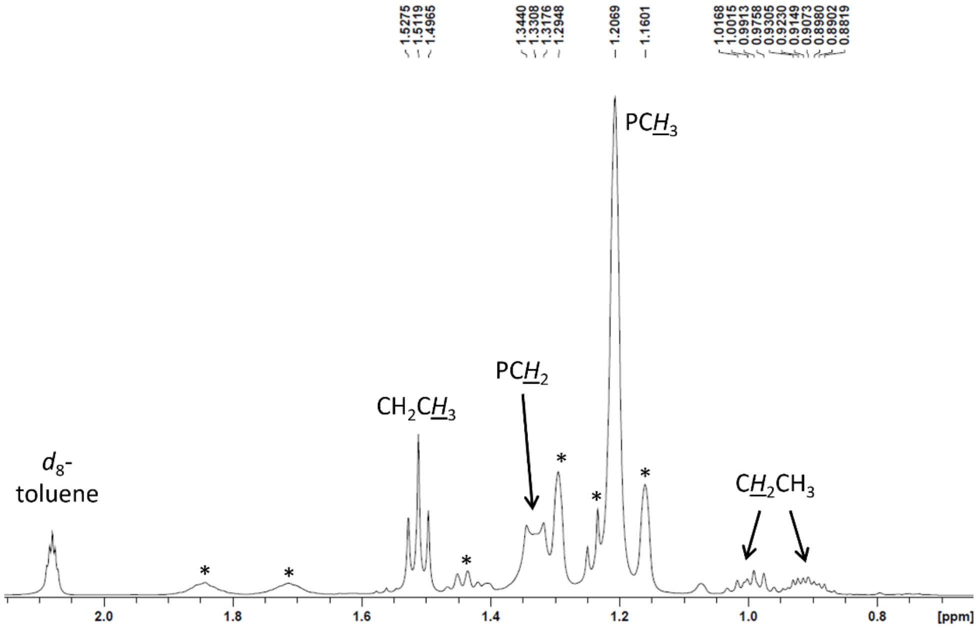

Figure S30. Expanded aliphatic region of the ^{1}H NMR spectrum of a solution containing [(dmpe)$_2$MnH$_2$(GeHEt$_2$)] (**2b**) formed from the reaction of [(dmpe)$_2$MnH(=GeEt$_2$)] (**1b**) and H$_2$ after sitting at ambient temperature for 3 days in d_8-toluene (500 MHz, 298 K). * indicates peaks from **1b**, and peak labels are for signals from **2b**.

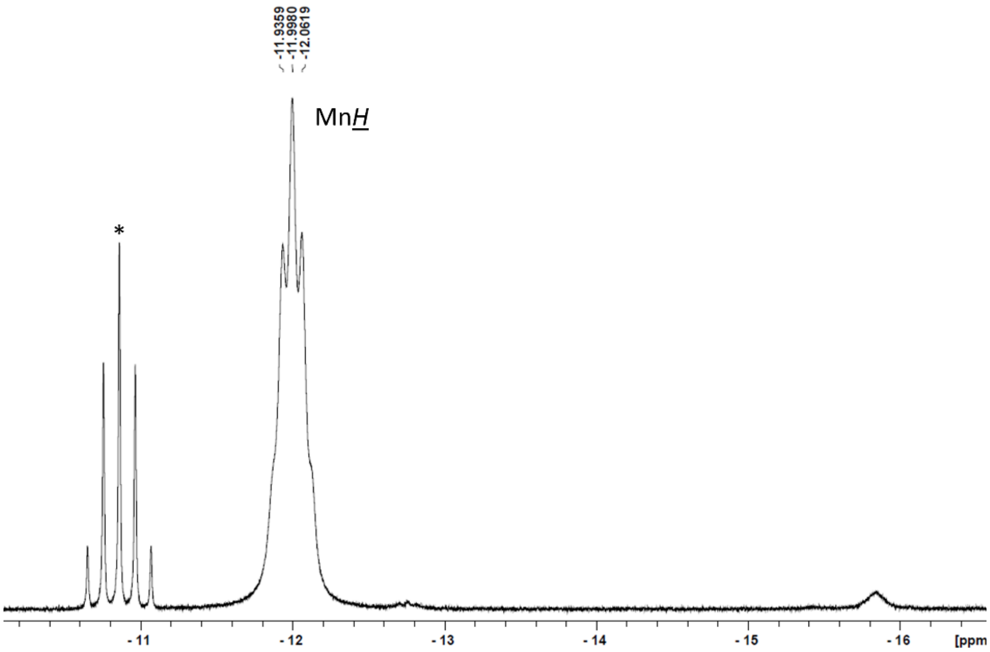

Figure S31. Expanded metal hydride region of the ^{1}H NMR spectrum of a solution containing [(dmpe)$_2$MnH$_2$(GeHEt$_2$)] (**2b**) formed from the reaction of [(dmpe)$_2$MnH(=GeEt$_2$)] (**1b**) and H_2 after sitting at ambient temperature for 3 days in *d*$_8$-toluene (500 MHz, 298 K). * indicates a peak from **1b**, and the peak label is for a signal from **2b**.

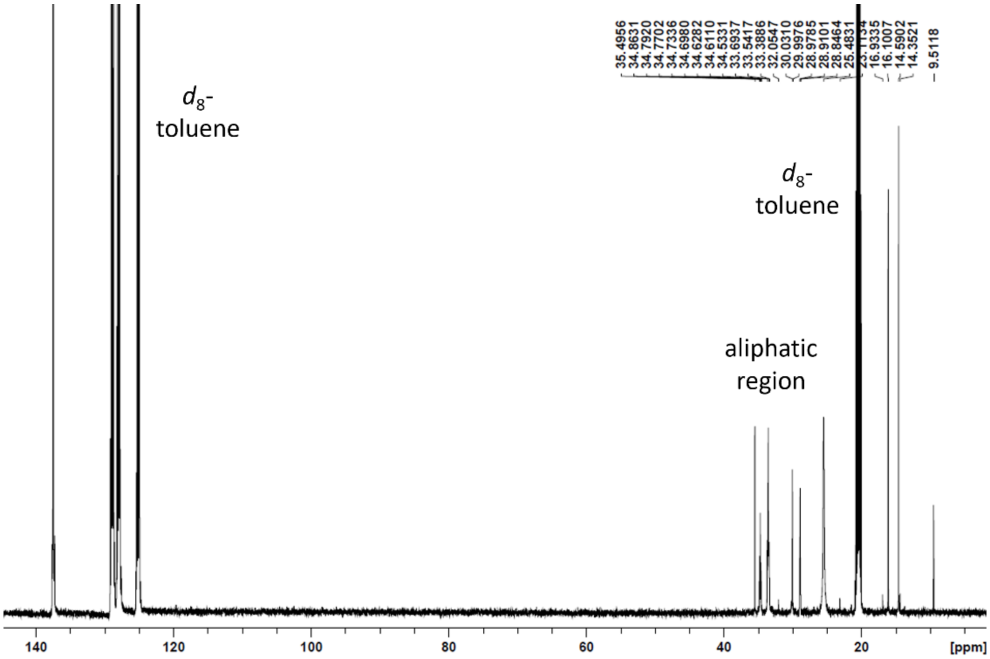

Figure S32. ^{13}C{^{1}H} NMR spectrum of a solution containing [(dmpe)$_2$MnH$_2$(GeHEt$_2$)] (**2b**) formed from the reaction of [(dmpe)$_2$MnH(=GeEt$_2$)] (**1b**) and H_2 after sitting at ambient temperature for 3 days in *d*$_8$-toluene (126 MHz, 298 K).

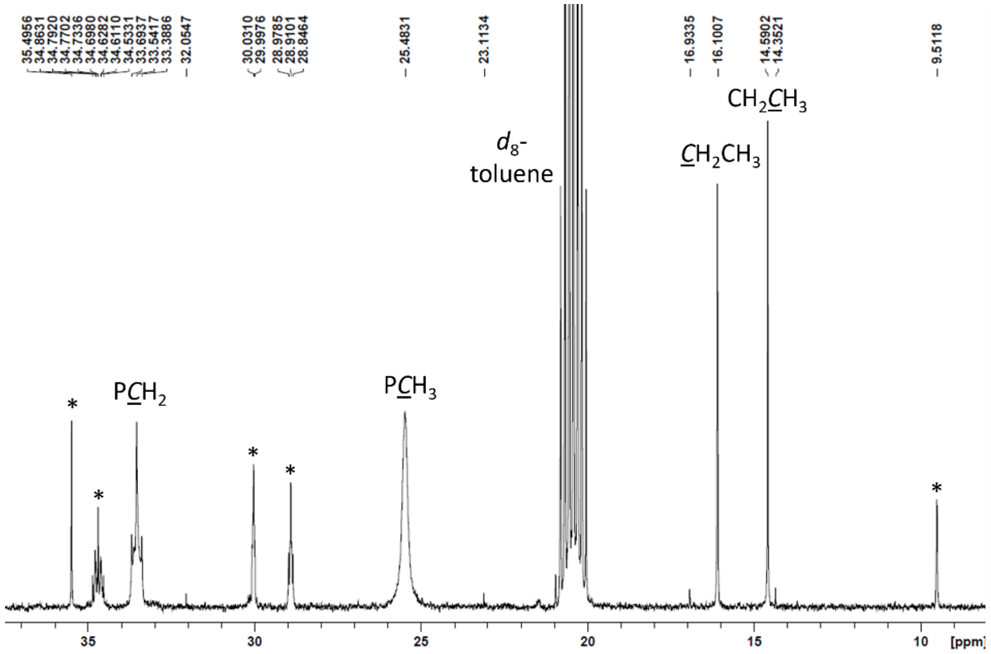

Figure S33. Expanded aliphatic region of the $^{13}C\{^1H\}$ NMR spectrum of a solution containing $[(dmpe)_2MnH_2(GeHEt_2)]$ (**2b**) formed from the reaction of $[(dmpe)_2MnH(=GeEt_2)]$ (**1b**) and H_2 after sitting at ambient temperature for 3 days in d_8-toluene (126 MHz, 298 K). * indicates peaks from **1b**, and peak labels are for signals from **2b**.

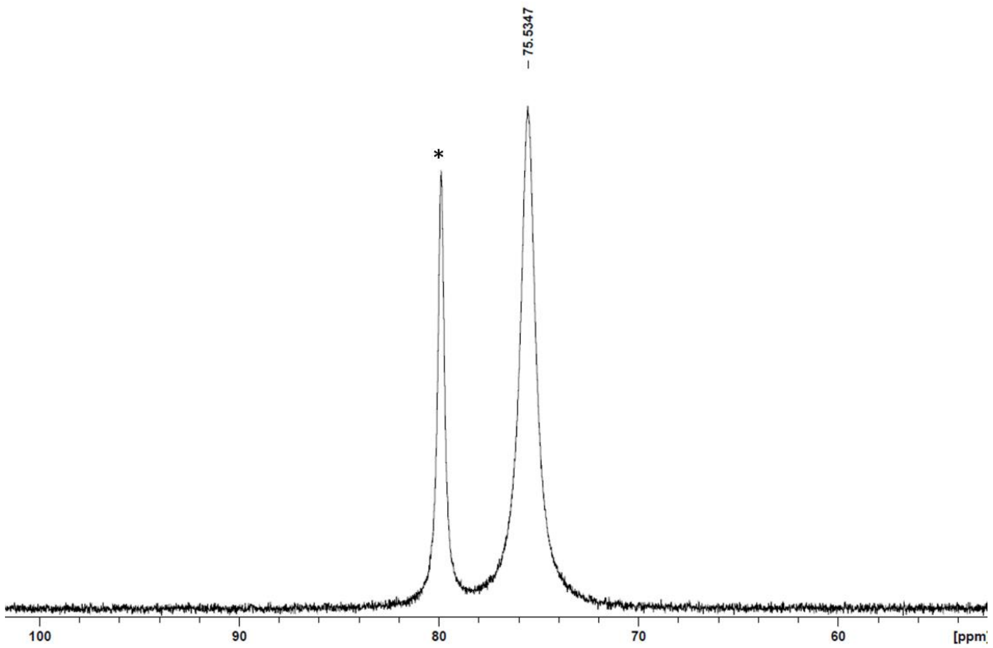

Figure S34. $^{31}P\{^1H\}$ NMR spectrum of a solution containing $[(dmpe)_2MnH_2(GeHEt_2)]$ (**2b**) formed from the reaction of $[(dmpe)_2MnH(=GeEt_2)]$ (**1b**) and H_2 after sitting at ambient temperature for 3 days in d_8-toluene (202 MHz, 298 K). * indicates a peak from **1b**, and the unlabelled peak is a signal from **2b**.

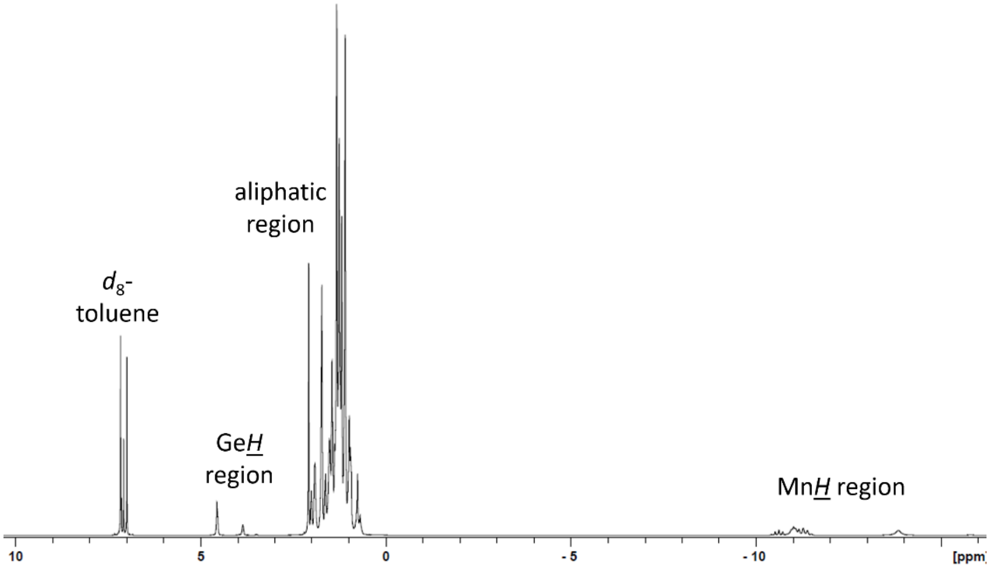

Figure S35. ^{1}H NMR spectrum of a solution containing [(dmpe)$_2$MnH$_2$(GeHEt$_2$)] (**2b**) formed from the reaction of [(dmpe)$_2$MnH(=GeEt$_2$)] (**1b**) and H_2 after sitting at ambient temperature for 3 days in d_8-toluene (500 MHz, 176 K).

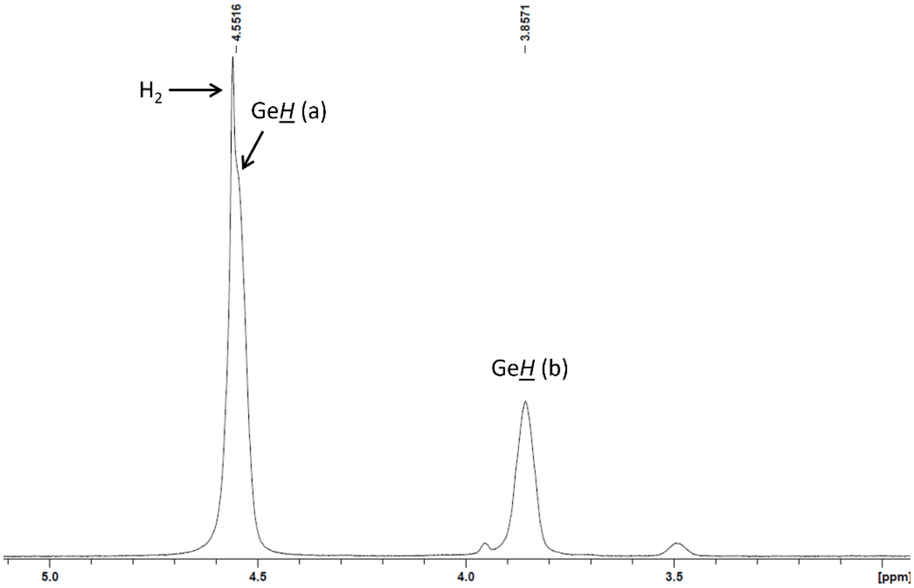

Figure S36. Expanded Ge*H* region of the ^{1}H NMR spectrum of a solution containing [(dmpe)$_2$MnH$_2$(GeHEt$_2$)] (**2b**) formed from the reaction of [(dmpe)$_2$MnH(=GeEt$_2$)] (**1b**) and H_2 after sitting at ambient temperature for 3 days in d_8-toluene (500 MHz, 176 K). The peaks labelled (a) is from *transHGe*-[(dmpe)$_2$MnH(HGeHEt$_2$)] (***transHGe*-2b**), and the peak labelled (b) is from the low symmetry isomer(s) *central*-[(dmpe)$_2$Mn(H$_2$GeHEt$_2$)] (***central*-2b**) and/or *cis*-[(dmpe)$_2$Mn(GeHEt$_2$)(H$_2$)] (***cis*-2b**).

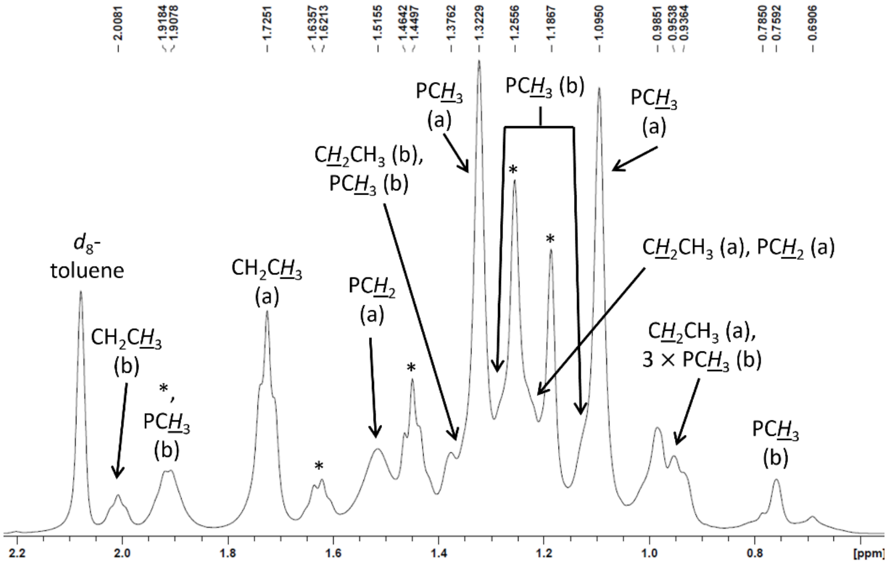

Figure S37. Expanded aliphatic region of the ^{1}H NMR spectrum of a solution containing [(dmpe)$_2$MnH$_2$(GeHEt$_2$)] (**2b**) formed from the reaction of [(dmpe)$_2$MnH(=GeEt$_2$)] (**1b**) and H$_2$ after sitting at ambient temperature for 3 days in d_8-toluene (500 MHz, 176 K). * indicates peaks from **1b**, peaks labelled (a) are those from *transHGe*-[(dmpe)$_2$MnH(HGeHEt$_2$)] (***transHGe*-2b**), and peaks labelled (b) are from the low symmetry isomer(s) *central*-[(dmpe)$_2$Mn(H$_2$GeHEt$_2$)] (***central*-2b**) and/or *cis*-[(dmpe)$_2$Mn(GeHEt$_2$)(H$_2$)] (***cis*-2b**).

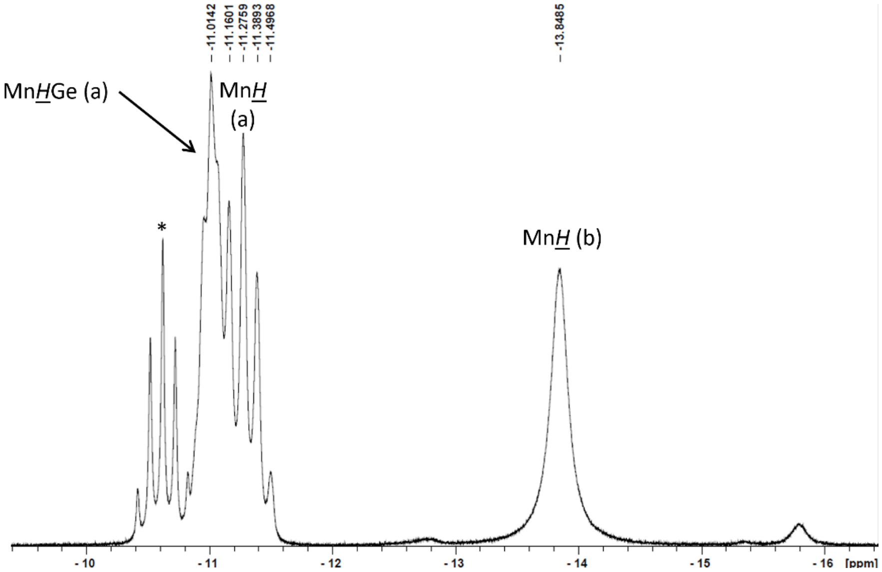

Figure S38. Expanded metal hydride region of the ^{1}H NMR spectrum of a solution containing [(dmpe)$_2$MnH$_2$(GeHEt$_2$)] (**2b**) formed from the reaction of [(dmpe)$_2$MnH(=GeEt$_2$)] (**1b**) and H$_2$ after sitting at ambient temperature for 3 days in d_8-toluene (500 MHz, 176 K). * indicates a peak from **1b**, peaks labelled (a) are those from *transHGe*-[(dmpe)$_2$MnH(HGeHEt$_2$)] (***transHGe*-2b**), and the peak labelled (b) is from the low symmetry isomer(s) *central*-[(dmpe)$_2$Mn(H$_2$GeHEt$_2$)] (***central*-2b**) and/or *cis*-[(dmpe)$_2$Mn(GeHEt$_2$)(H$_2$)] (***cis*-2b**).

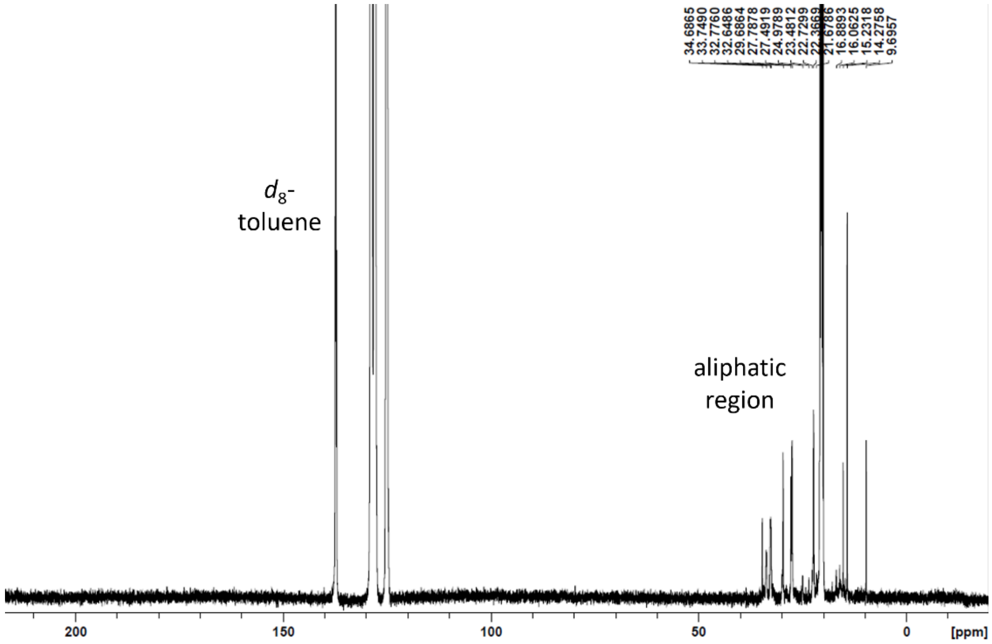

Figure S39. $^{13}C\{^1H\}$ NMR spectrum of a solution containing [(dmpe)$_2$MnH$_2$(GeHEt$_2$)] (**2b**) formed from the reaction of [(dmpe)$_2$MnH(=GeEt$_2$)] (**1b**) and H_2 after sitting at ambient temperature for 3 days in d_8-toluene (126 MHz, 176 K).

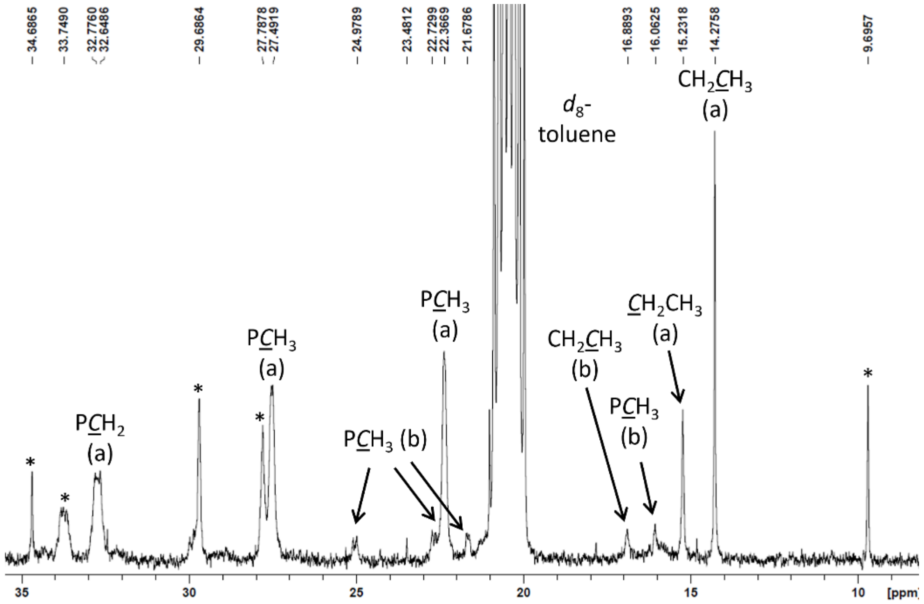

Figure S40. Expanded aliphatic region of the $^{13}C\{^1H\}$ NMR spectrum of a solution containing [(dmpe)$_2$MnH$_2$(GeHEt$_2$)] (**2b**) formed from the reaction of [(dmpe)$_2$MnH(=GeEt$_2$)] (**1b**) and H_2 after sitting at ambient temperature for 3 days in d_8-toluene (126 MHz, 176 K). * indicates peaks from **1b**, peaks labelled (a) are those from *transHGe*-[(dmpe)$_2$MnH(HGeHEt$_2$)] (***transHGe*-2b**), and peaks labelled (b) are from the low symmetry isomer(s) *central*-[(dmpe)$_2$Mn(H$_2$GeHEt$_2$)] (***central*-2b**) and/or *cis*-[(dmpe)$_2$Mn(GeHEt$_2$)(H$_2$)] (***cis*-2b**).

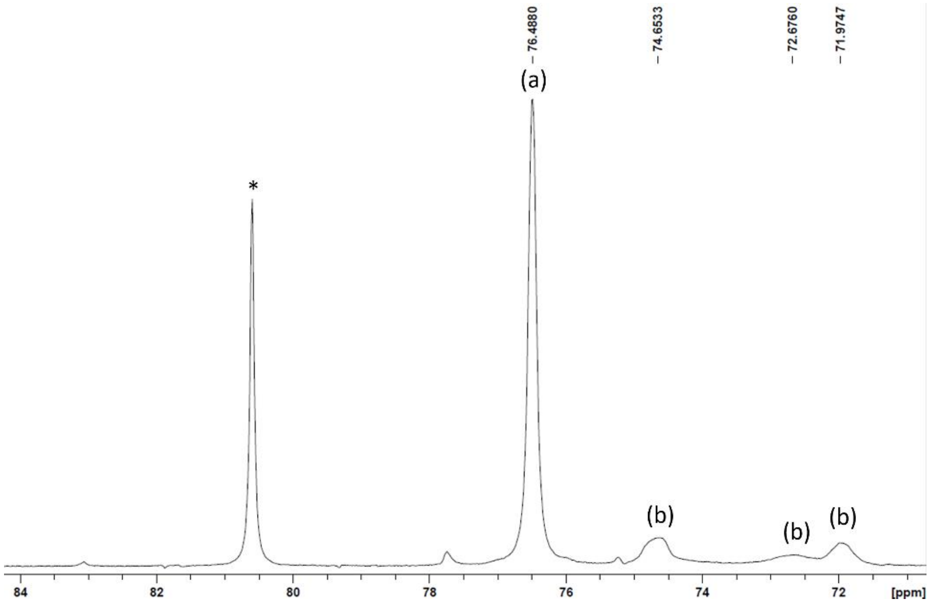

Figure S41. $^{31}P\{^1H\}$ NMR spectrum of a solution containing [(dmpe)$_2$MnH$_2$(GeHEt$_2$)] (**2b**) formed from the reaction of [(dmpe)$_2$MnH(=GeEt$_2$)] (**1b**) and H_2 after sitting at ambient temperature for 3 days in *d*$_8$-toluene (202 MHz, 176 K). * indicates a peak from **1b**, the peak labelled (a) is from *transHGe*-[(dmpe)$_2$MnH(HGeHEt$_2$)] (***transHGe*-2b**), and peaks labelled (b) are from the low symmetry isomer(s) *central*-[(dmpe)$_2$Mn(H$_2$GeHEt$_2$)] (***central*-2b**) and/or *cis*-[(dmpe)$_2$Mn(GeHEt$_2$)(H$_2$)] (***cis*-2b**).

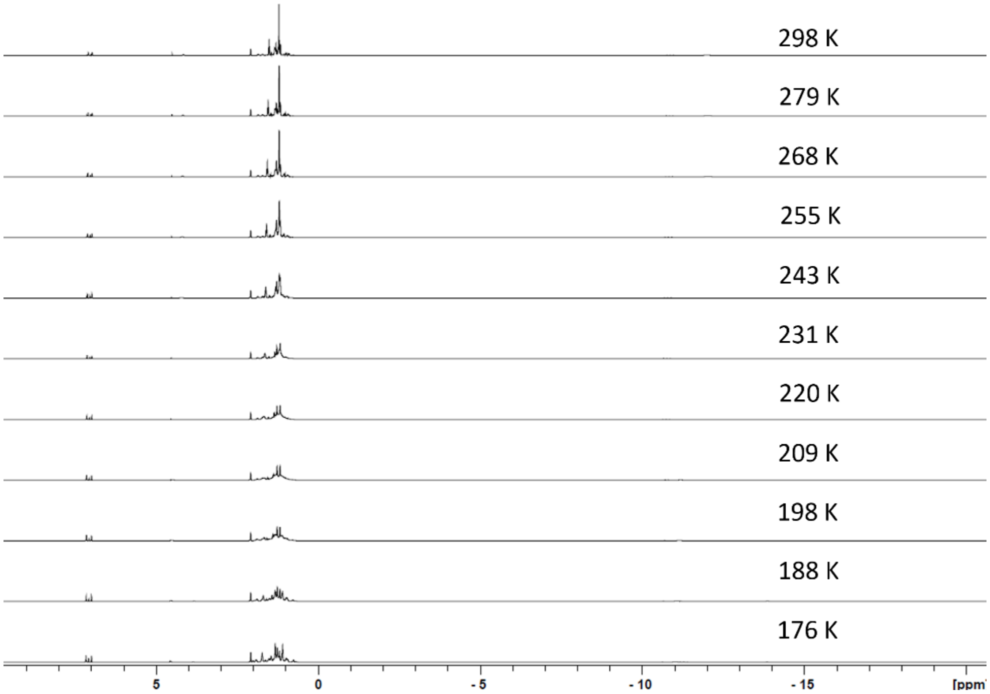

Figure S42. Variable temperature ^1H NMR spectra of a solution containing [(dmpe)$_2$MnH$_2$(GeHEt$_2$)] (**2b**) formed from the reaction of [(dmpe)$_2$MnH(=GeEt$_2$)] (**1b**) and H_2 after sitting at ambient temperature for 3 days in *d*$_8$-toluene (500 MHz).

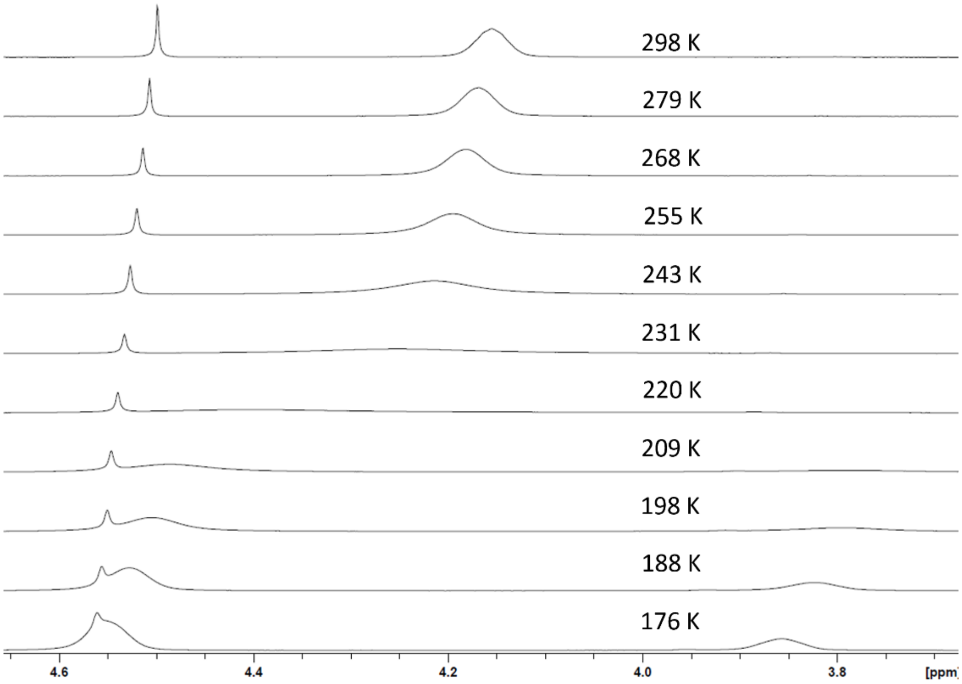

Figure S43. Expanded Ge*H* regions of the variable temperature ^{1}H NMR spectra of a solution containing [(dmpe)$_2$MnH$_2$(GeHEt$_2$)] (**2b**) formed from the reaction of [(dmpe)$_2$MnH(=GeEt$_2$)] (**1b**) and H$_2$ after sitting at ambient temperature for 3 days in *d*$_8$-toluene (500 MHz).

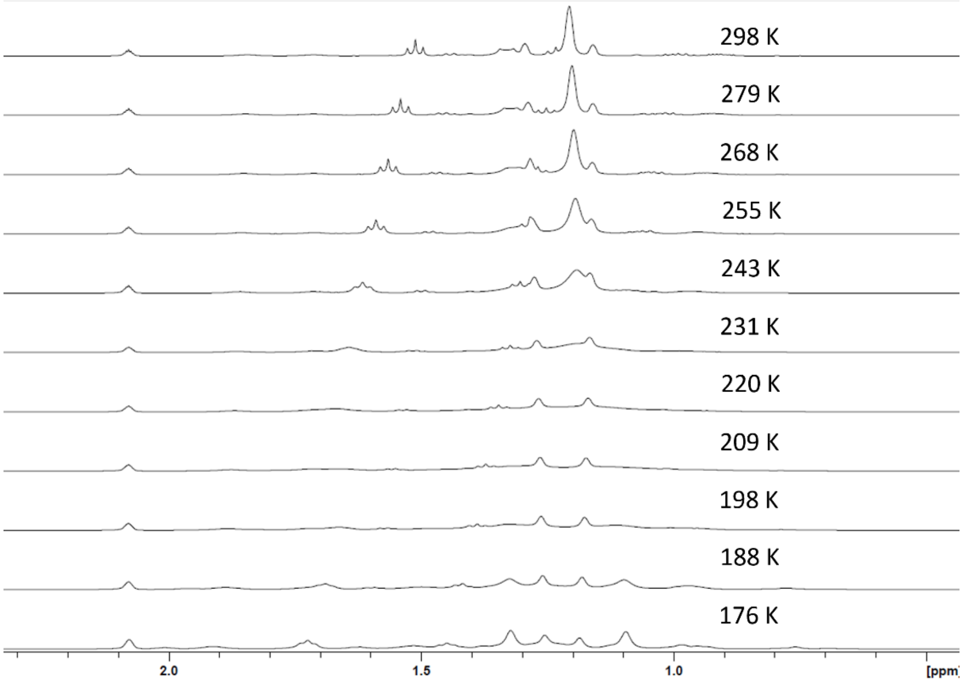

Figure S44. Expanded alkyl regions of the variable temperature ^{1}H NMR spectra of a solution containing [(dmpe)$_2$MnH$_2$(GeHEt$_2$)] (**2b**) formed from the reaction of [(dmpe)$_2$MnH(=GeEt$_2$)] (**1b**) and H$_2$ after sitting at ambient temperature for 3 days in *d*$_8$-toluene (500 MHz).

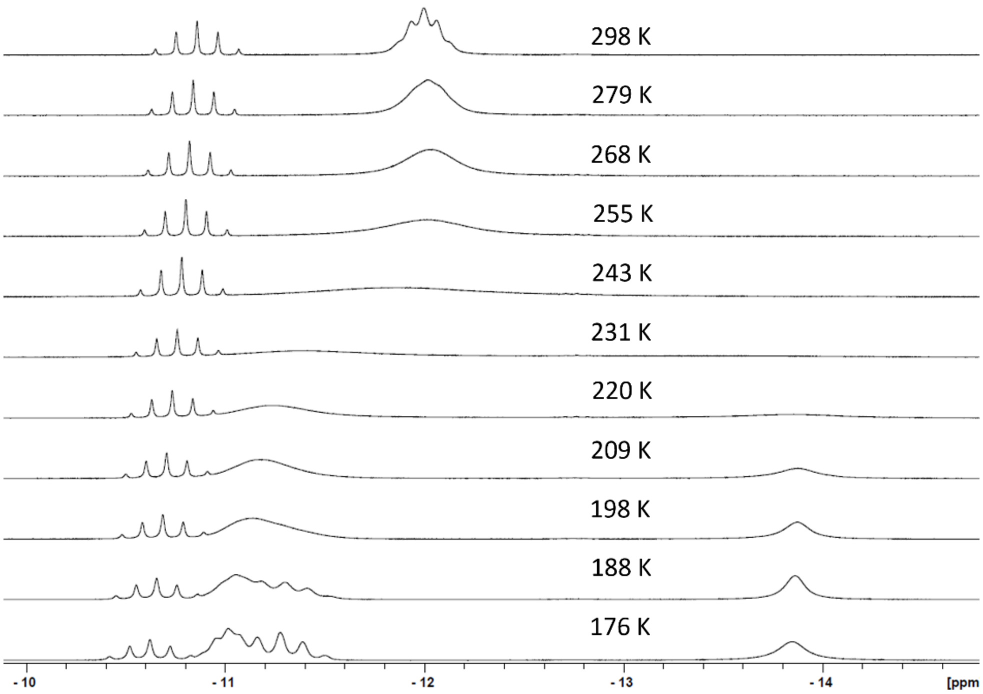

Figure S45. Expanded metal hydride regions of the variable temperature ^{1}H NMR spectra of a solution containing [(dmpe)$_2$MnH$_2$(GeHEt$_2$)] (**2b**) formed from the reaction of [(dmpe)$_2$MnH(=GeEt$_2$)] (**1b**) and H_2 after sitting at ambient temperature for 3 days in d_8-toluene (500 MHz).

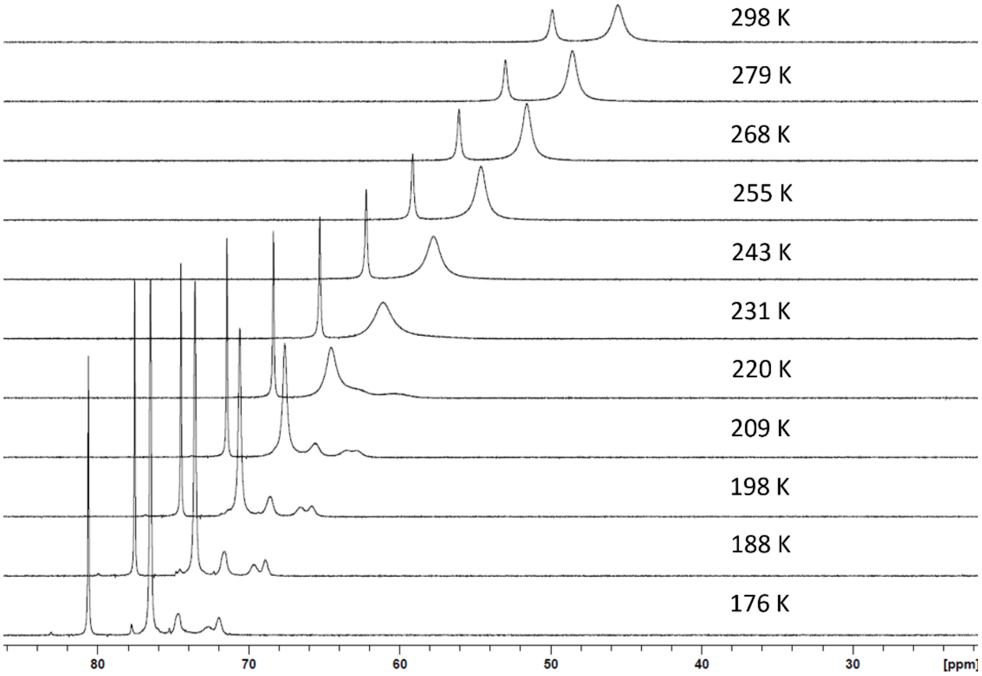

Figure S46. Variable temperature $^{31}P\{^{1}H\}$ NMR spectra of a solution containing [(dmpe)$_2$MnH$_2$(GeHEt$_2$)] (**2b**) formed from the reaction of [(dmpe)$_2$MnH(=GeEt$_2$)] (**1b**) and H_2 after sitting at ambient temperature for 3 days in d_8-toluene (202 MHz). For clarity, each spectrum is shifted 3 ppm to lower frequency than the one below it, and the x-axis corresponds to the bottom spectrum.

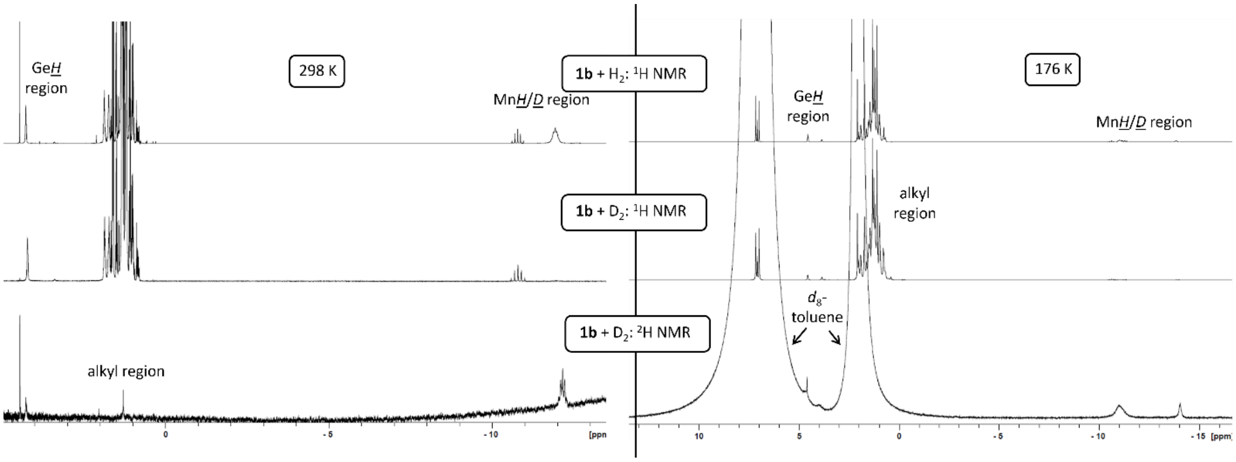

Figure S47. Top: ^{1}H NMR spectra of a solution containing [(dmpe)$_2$MnH$_2$(GeHEt$_2$)] (**2b**) formed from the reaction of [(dmpe)$_2$MnH(=GeEt$_2$)] (**1b**) and H$_2$ after sitting at ambient temperature for 4 days in C$_6$D$_6$ (600 MHz, 298 K; left) or d_8-toluene (500 MHz, 176 K; right). Middle and bottom: ^{1}H NMR (middle; 500 MHz) and ^{2}H NMR (bottom; 77 MHz) spectra of a solution containing [(dmpe)$_2$MnD$_2$(GeHEt$_2$)] and other isotopomers/isotopologues (***d*$_n$-2b**) formed from the reaction of [(dmpe)$_2$MnH(=GeEt$_2$)] (**1b**) and D$_2$ after sitting at ambient temperature for 1 day in C$_6$D$_6$ (298 K; left) or 4 days in d_8-toluene (176 K; right).

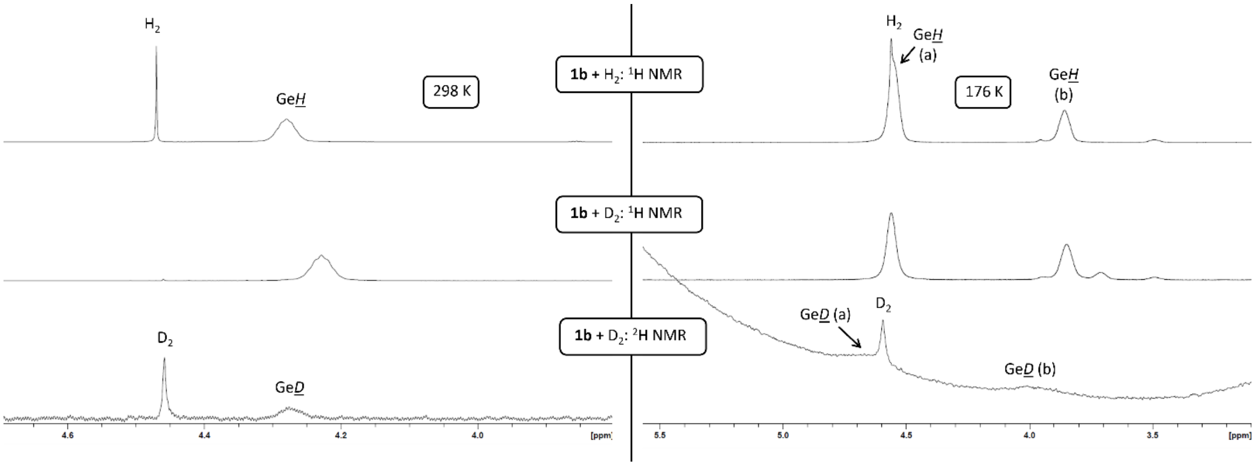

Figure S48. Top: Expanded Ge*H* region of ^{1}H NMR spectra of a solution containing [(dmpe)$_2$MnH$_2$(GeHEt$_2$)] (**2b**) formed from the reaction of [(dmpe)$_2$MnH(=GeEt$_2$)] (**1b**) and H$_2$ after sitting at ambient temperature for 4 days in C$_6$D$_6$ (600 MHz, 298 K; left) or d_8-toluene (500 MHz, 176 K; right). The peaks labelled (a) are from the *transHGe* isomer of **2b** or ***d*$_n$-2b**, and the peaks labelled (b) are from the *cis* and/or *central* isomer(s) of **2b** or ***d*$_n$-2b**. Middle and bottom: Expanded Ge*H* region of ^{1}H NMR (middle; 500 MHz) and ^{2}H NMR (bottom; 77 MHz) spectra of a solution containing [(dmpe)$_2$MnD$_2$(GeHEt$_2$)] and other isotopomers/isotopologues (***d*$_n$-2b**) formed from the reaction of [(dmpe)$_2$MnH(=GeEt$_2$)] (**1b**) and D$_2$ after sitting at ambient temperature for 1 day in C$_6$D$_6$ (298 K; left) or 4 days in d_8-toluene (176 K; right).

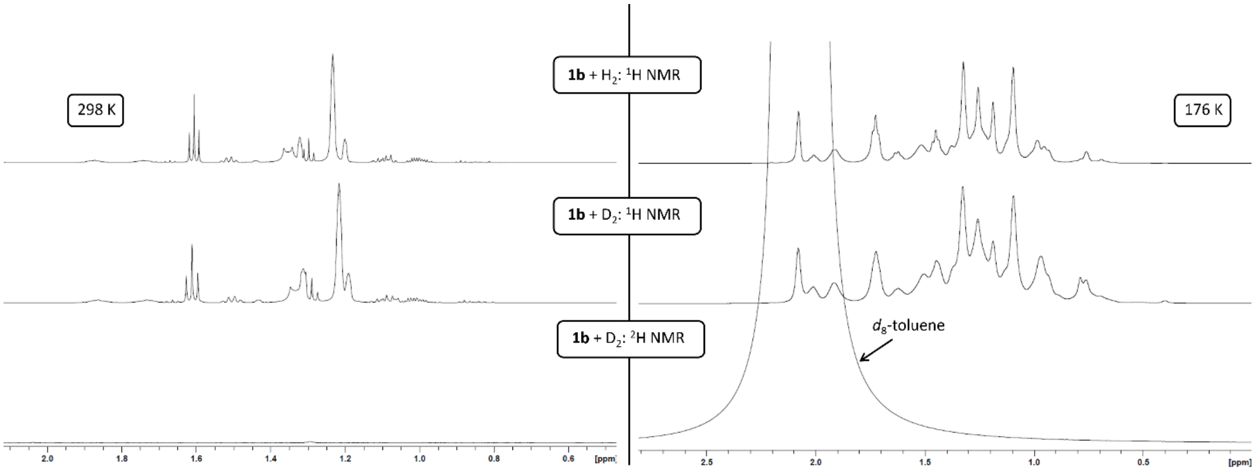

Figure S49. Top: Expanded aliphatic region of ^{1}H NMR spectra of a solution containing [(dmpe)$_2$MnH$_2$(GeHEt$_2$)] (**2b**) formed from the reaction of [(dmpe)$_2$MnH(=GeEt$_2$)] (**1b**) and H$_2$ after sitting at ambient temperature for 4 days in C$_6$D$_6$ (600 MHz, 298 K; left) or d_8-toluene (500 MHz, 176 K; right). Middle and bottom: Expanded aliphatic region of ^{1}H NMR (middle; 500 MHz) and ^{2}H NMR (bottom; 77 MHz) spectra of a solution containing [(dmpe)$_2$MnD$_2$(GeHEt$_2$)] and other isotopomers/isotopologues (***d*$_n$-2b**) formed from the reaction of [(dmpe)$_2$MnH(=GeEt$_2$)] (**1b**) and D$_2$ after sitting at ambient temperature for 1 day in C$_6$D$_6$ (298 K; left) or 4 days in d_8-toluene (176 K; right).

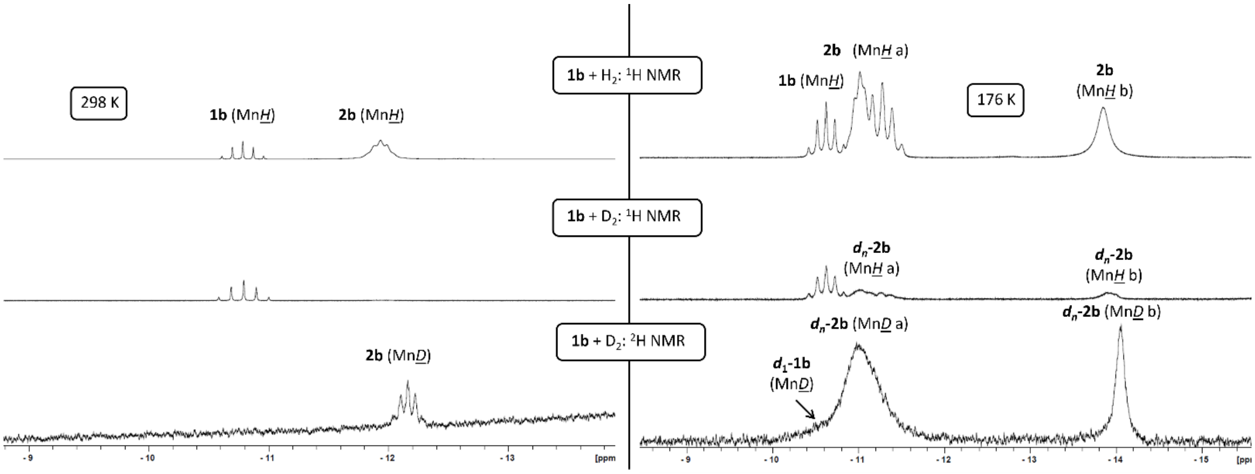

Figure S50. Top: Expanded metal hydride region of ^{1}H NMR spectra of a solution containing [(dmpe)$_2$MnH$_2$(GeHEt$_2$)] (**2b**) formed from the reaction of [(dmpe)$_2$MnH(=GeEt$_2$)] (**1b**) and H$_2$ after sitting at ambient temperature for 4 days in C$_6$D$_6$ (600 MHz, 298 K; left) or d_8-toluene (500 MHz, 176 K; right). The peaks labelled (a) are from the *transHGe* isomer of **2b** or ***d*$_n$-2b**, and the peaks labelled (b) are from the *cis* and/or *central* isomer(s) of **2b** or ***d*$_n$-2b**. Middle and bottom: Expanded metal hydride region of ^{1}H NMR (middle; 500 MHz) and ^{2}H NMR (bottom; 77 MHz) spectra of a solution containing [(dmpe)$_2$MnD$_2$(GeHEt$_2$)] and other isotopomers/isotopologues (***d*$_n$-2b**) formed from the reaction of [(dmpe)$_2$MnH(=GeEt$_2$)] (**1b**) and D$_2$ after sitting at ambient temperature for 1 day in C$_6$D$_6$ (298 K; left) or 4 days in d_8-toluene (176 K; right).

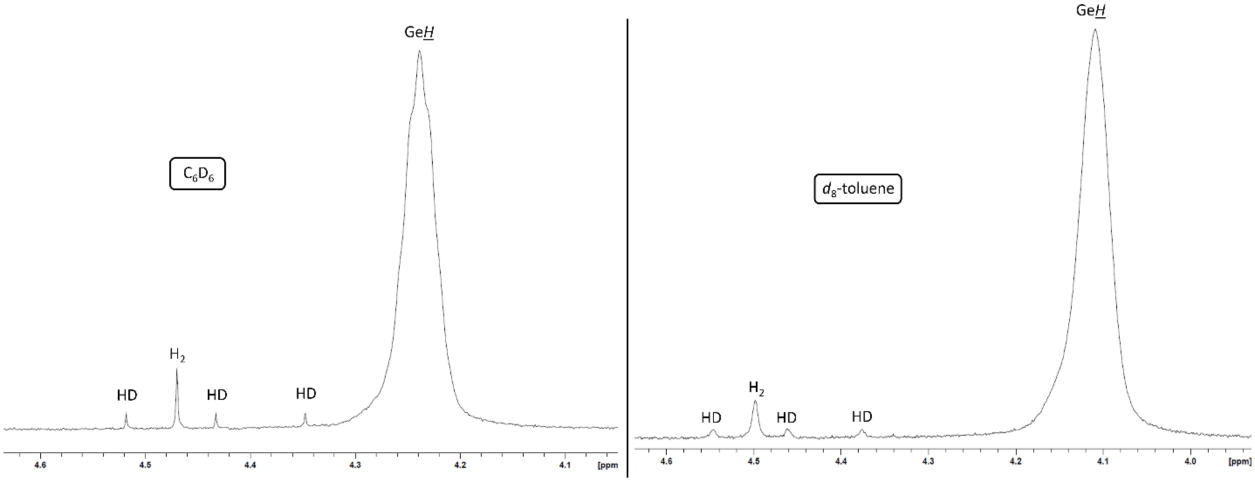

Figure S51. Expanded Ge*H* region of the ^{1}H NMR spectra of a solution containing [(dmpe)$_2$MnD$_2$(GeHEt$_2$)] and other isotopomers/isotopologues (***d*$_n$-2b**) formed from the reaction of [(dmpe)$_2$MnH(=GeEt$_2$)] (**1b**) and D$_2$ after sitting at ambient temperature for 3 days in C$_6$D$_6$ (500 MHz, 298 K; left) or 4 days in *d*$_8$-toluene (500 MHz, 298 K; right).

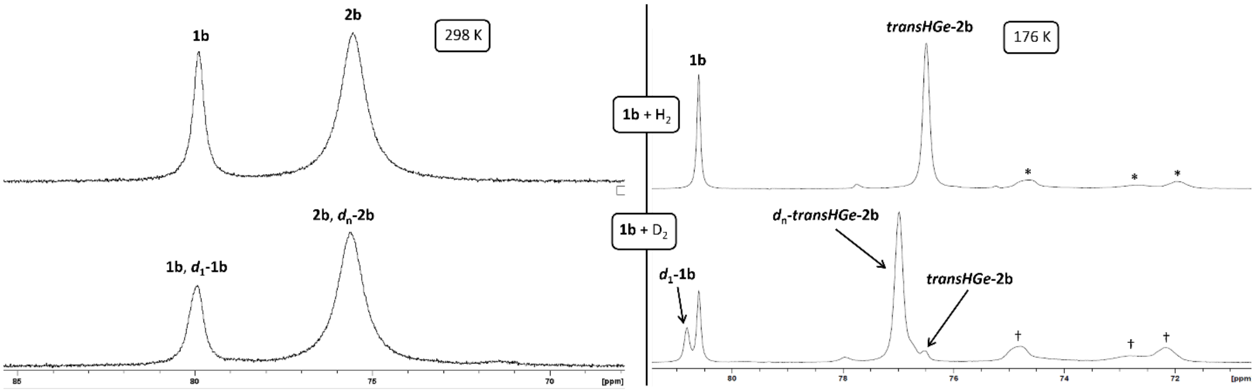

Figure S52. Top: ^{31}P{^{1}H} NMR spectra (202 MHz) of a solution containing [(dmpe)$_2$MnH$_2$(GeHEt$_2$)] (**2b**) formed from the reaction of [(dmpe)$_2$MnH(=GeEt$_2$)] (**1b**) and H$_2$ after sitting at ambient temperature for 3 days in *d*$_8$-toluene (left; 298 K, right; 176 K). Bottom: ^{31}P{^{1}H} NMR spectra (202 MHz) of a solution containing [(dmpe)$_2$MnD$_2$(GeHEt$_2$)] and other isotopomers/isotopologues (***d*$_n$-2b**) formed from the reaction of [(dmpe)$_2$MnH(=GeEt$_2$)] (**1b**) and D$_2$ after sitting at ambient temperature for four days in *d*$_8$-toluene (left; 298 K, right; 176 K). * indicates peaks from the *cis* and/or *central* isomer(s) of **2b**, and † indicates peaks from the *cis* and/or *central* isomer(s) of ***d*$_n$-2b**.

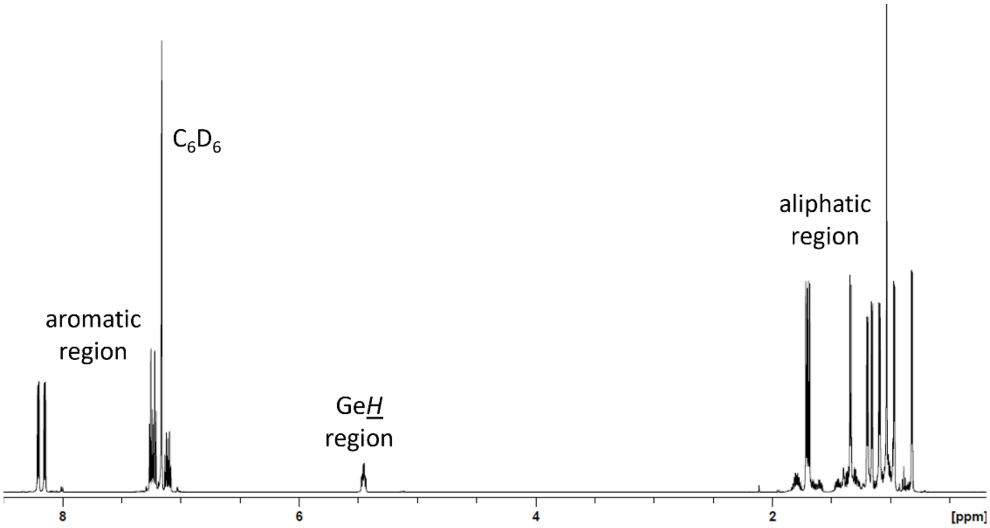

Figure S53. ^{1}H NMR spectrum of *cis*-[(dmpe)$_2$Mn(GeHPh$_2$)(CN^{t}Bu)] (***cis*-3a**) in C_6D_6 (600 MHz, 298 K).

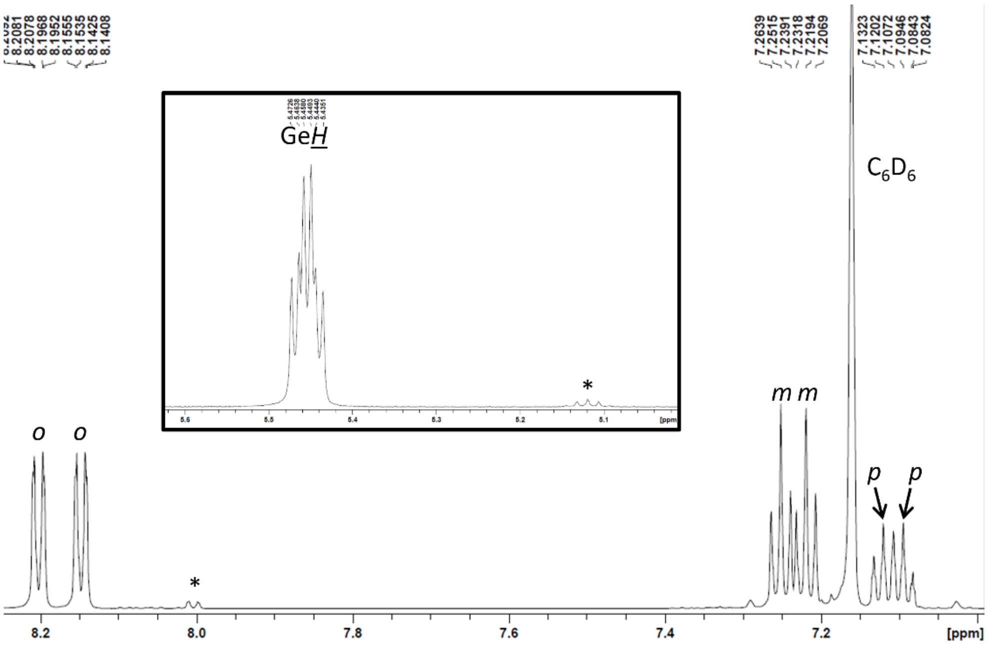

Figure S54. Expanded aromatic region of the ^{1}H NMR spectrum of *cis*-[(dmpe)$_2$Mn(GeHPh$_2$)(CN^{t}Bu)] (***cis*-3a**) in C_6D_6 (600 MHz, 298 K). The inset shows the expanded Ge*H* region of this spectrum. * indicates peaks from the *trans* isomer.

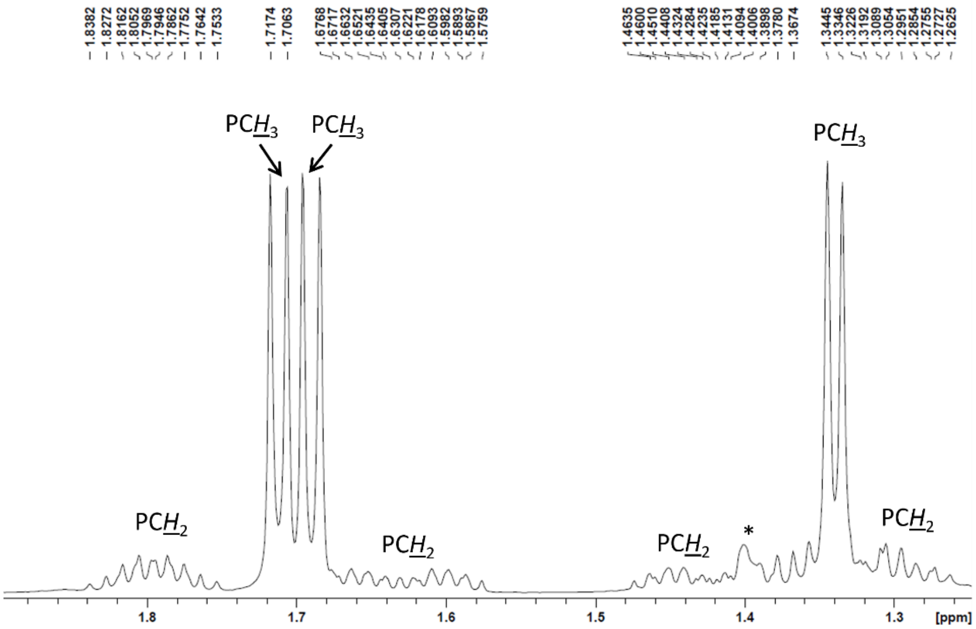

Figure S55. Expanded higher frequency aliphatic region of the ^{1}H NMR spectrum of *cis*-[(dmpe)$_2$Mn(GeHPh$_2$)(CN^{t}Bu)] (***cis*-3a**) in C_6D_6 (600 MHz, 298 K). * indicates a peak from the *trans* isomer.

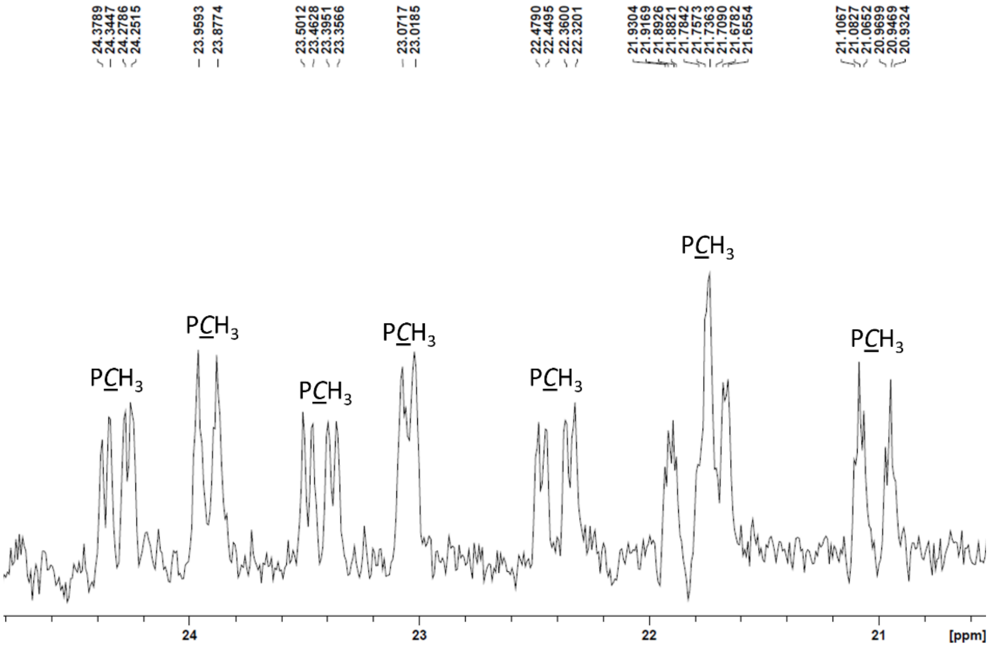

Figure S56. Expanded lower frequency aliphatic region of the ^{1}H NMR spectrum of *cis*-[(dmpe)$_2$Mn(GeHPh$_2$)(CN^{t}Bu)] (***cis*-3a**) in C_6D_6 (600 MHz, 298 K).

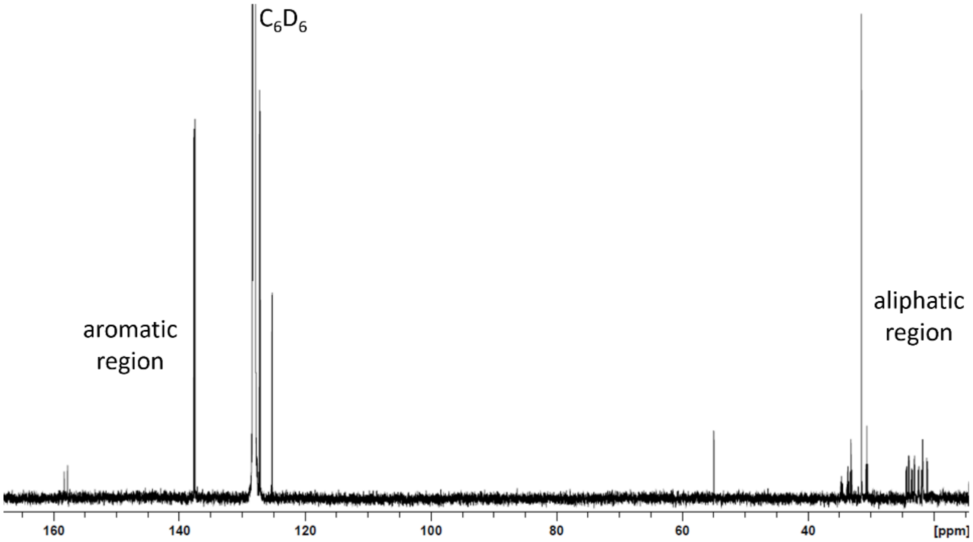

Figure S57. $^{13}C\{^1H\}$ NMR spectrum of *cis*-[(dmpe)$_2$Mn(GeHPh$_2$)(CN^{t}Bu)] (***cis*-3a**) in C_6D_6 (151 MHz, 298 K).

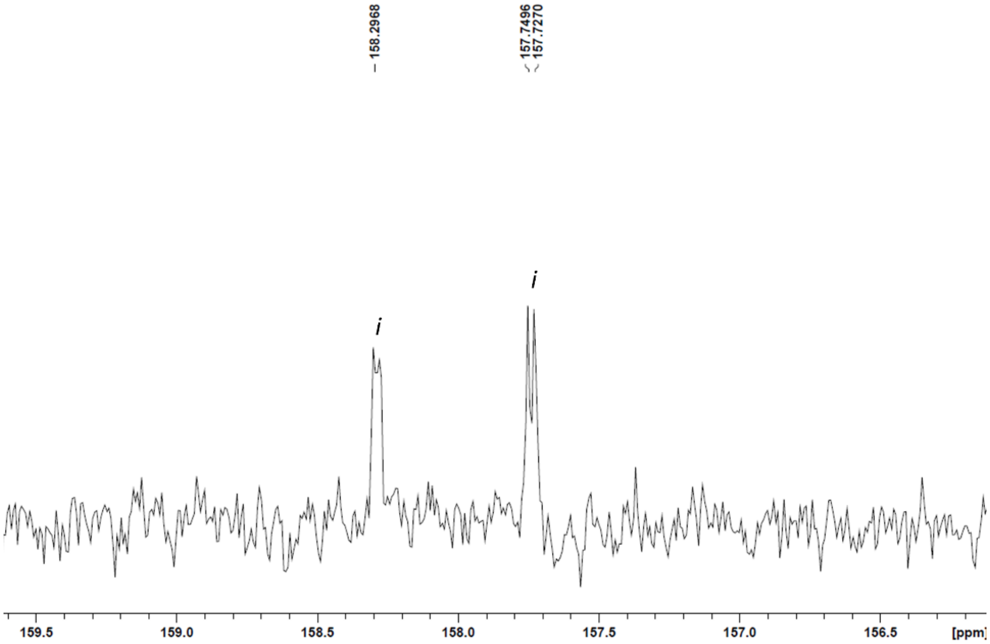

Figure S58. Expanded higher frequency aromatic region of the $^{13}C\{^1H\}$ NMR spectrum of *cis*-[(dmpe)$_2$Mn(GeHPh$_2$)(CN^{t}Bu)] (***cis*-3a**) in C_6D_6 (151 MHz, 298 K).

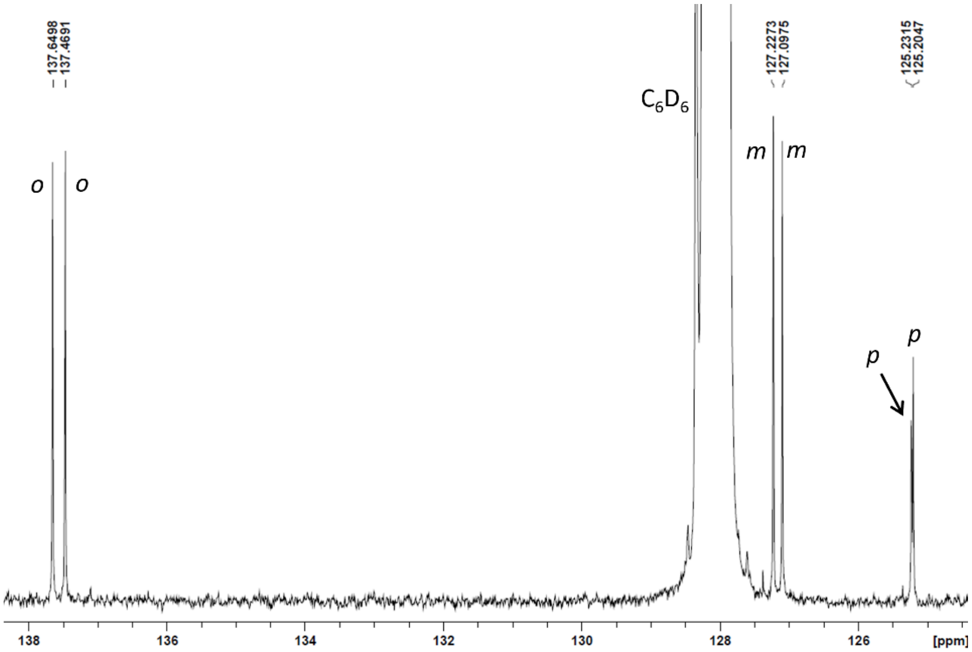

Figure S59. Expanded lower frequency aromatic region of the $^{13}C\{^1H\}$ NMR spectrum of *cis*-[(dmpe)$_2$Mn(GeHPh$_2$)(CN^{t}Bu)] (***cis*-3a**) in C_6D_6 (151 MHz, 298 K).

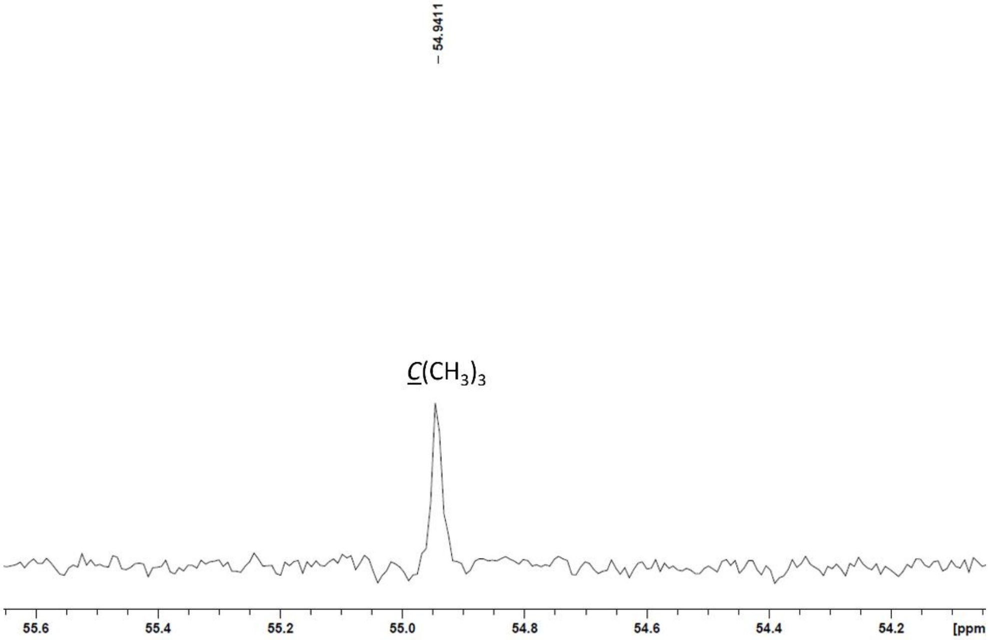

Figure S60. Expanded middle frequency region of the $^{13}C\{^1H\}$ NMR spectrum of *cis*-[(dmpe)$_2$Mn(GeHPh$_2$)(CN^{t}Bu)] (***cis*-3a**) in C_6D_6 (151 MHz, 298 K).

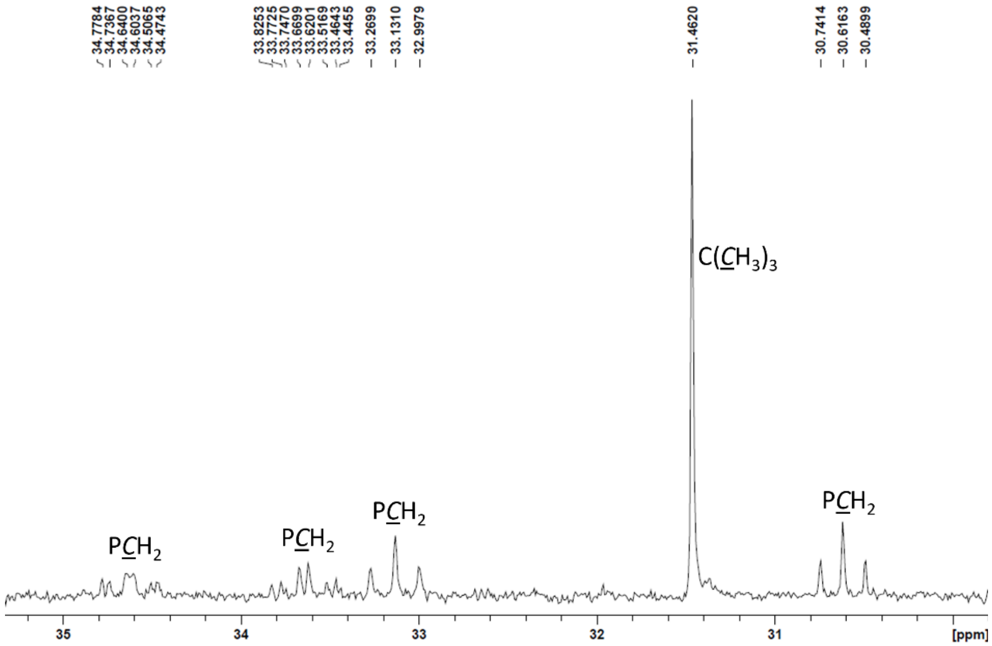

Figure S61. Expanded higher frequency aliphatic region of the $^{13}C\{^{1}H\}$ NMR spectrum of *cis*-[(dmpe)$_2$Mn(GeHPh$_2$)(CN^{t}Bu)] (***cis*-3a**) in C_6D_6 (151 MHz, 298 K).

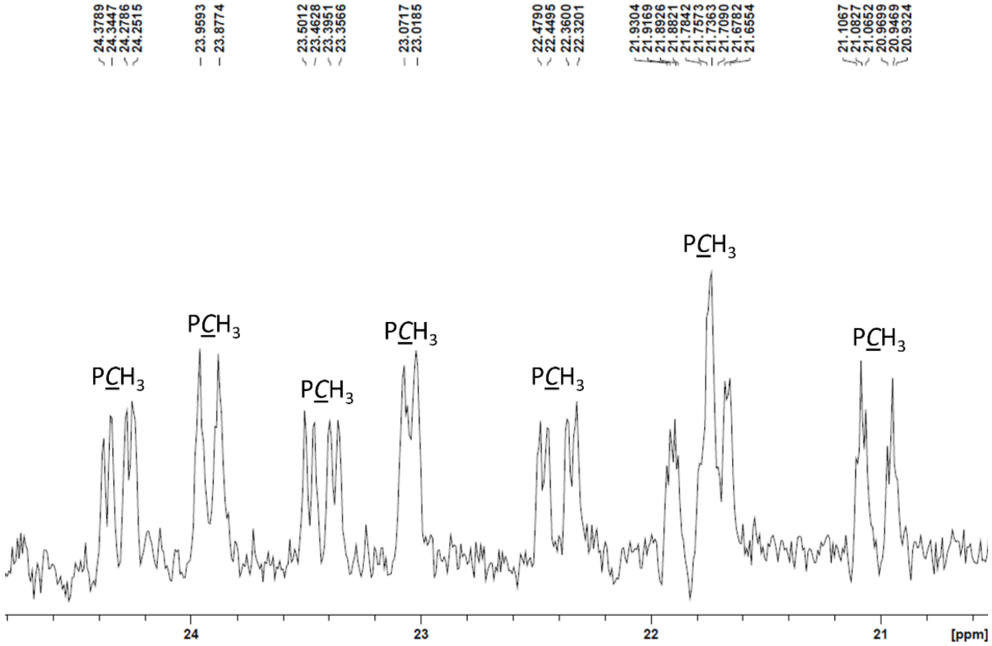

Figure S62. Expanded lower frequency aliphatic region of the $^{13}C\{^{1}H\}$ NMR spectrum of *cis*-[(dmpe)$_2$Mn(GeHPh$_2$)(CN^{t}Bu)] (***cis*-3a**) in C_6D_6 (151 MHz, 298 K).

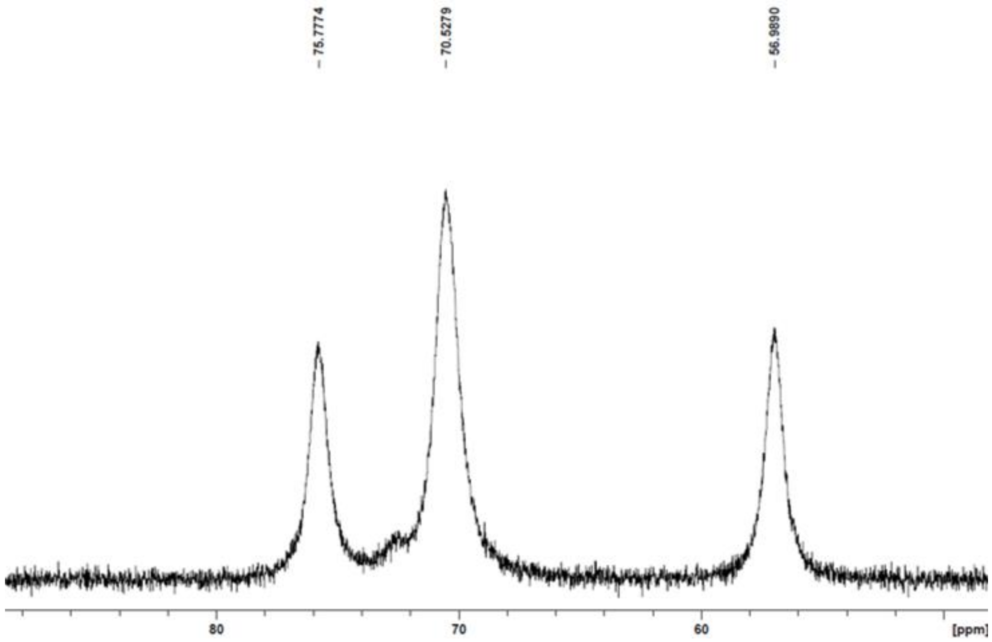

Figure S63. $^{31}P\{^{1}H\}$ NMR spectrum of *cis*-[(dmpe)$_2$Mn(GeHPh$_2$)(CN^{t}Bu)] (***cis*-3a**) in C_6D_6 (243 MHz, 298 K).

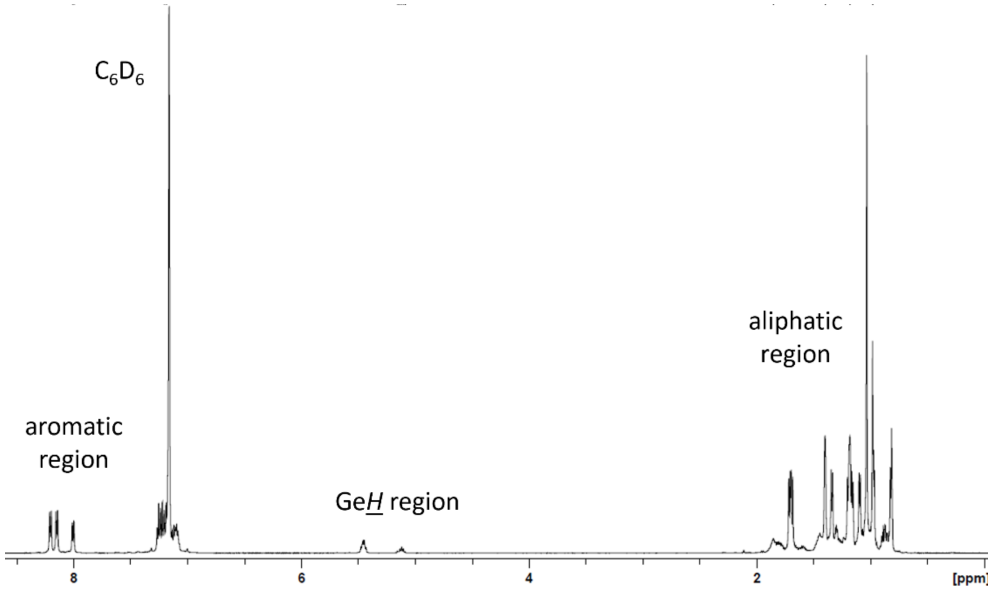

Figure S64. ^{1}H NMR spectrum of a mixture of *cis* and *trans* isomers of [(dmpe)$_2$Mn(GeHPh$_2$)(CN^{t}Bu)] (**3a**) in C_6D_6 (500 MHz, 298 K).

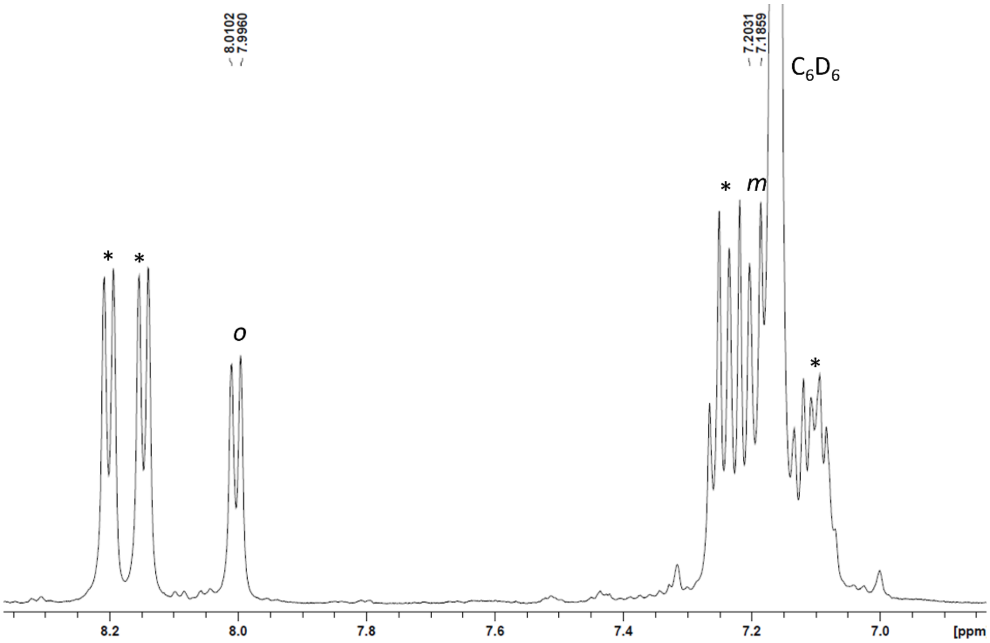

Figure S65. Expanded aromatic region of the ^{1}H NMR spectrum of a mixture of *cis* and *trans* isomers of [(dmpe)$_2$Mn(GeHPh$_2$)(CN^{t}Bu)] (**3a**) in C_6D_6 (500 MHz, 298 K). * indicates peaks arising from ***cis*-3a** and labelled peaks are from ***trans*-3a**.

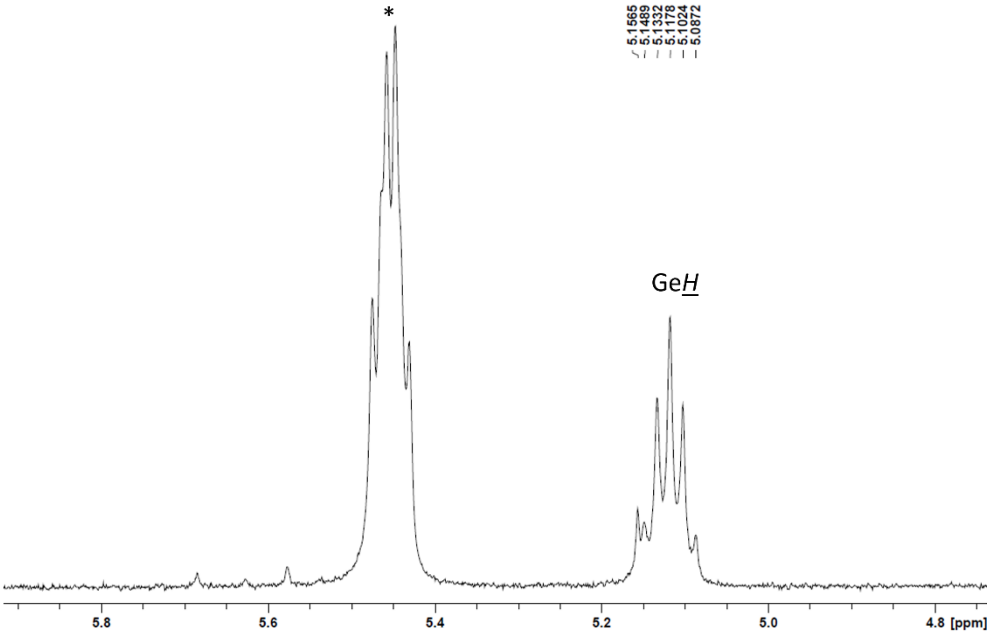

Figure S66. Expanded Ge*H* region of the ^{1}H NMR spectrum of a mixture of *cis* and *trans* isomers of [(dmpe)$_2$Mn(GeHPh$_2$)(CN^{t}Bu)] (**3a**) in C_6D_6 (500 MHz, 298 K). * indicates a peak arising from ***cis*-3a** and the labelled peak is from ***trans*-3a**.

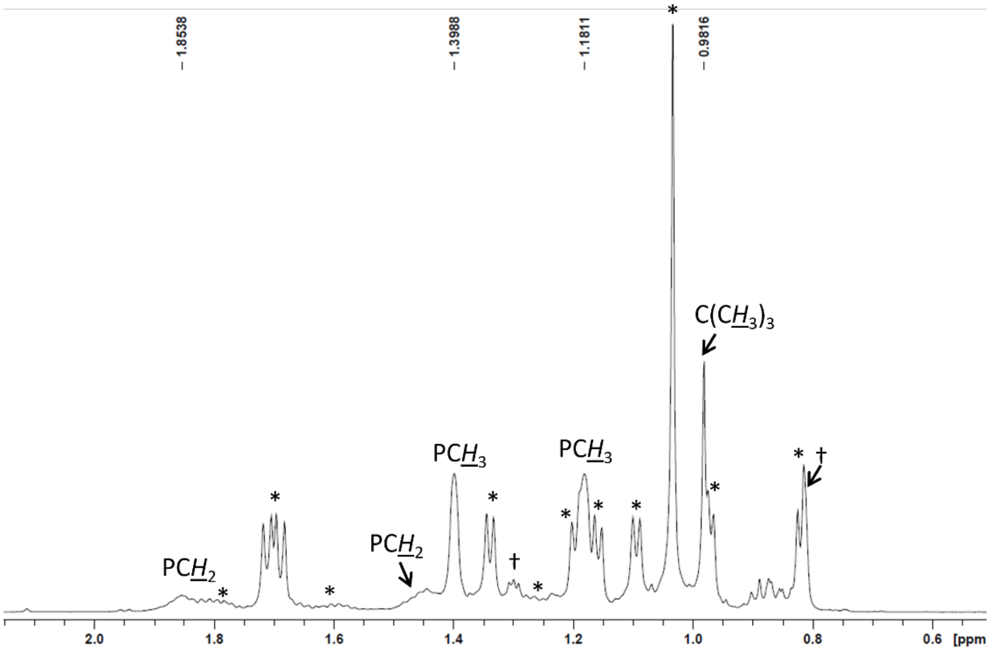

Figure S67. Expanded aliphatic region of the ^{1}H NMR spectrum of a mixture of *cis* and *trans* isomers of [(dmpe)$_2$Mn(GeHPh$_2$)(CN^{t}Bu)] (**3a**) in C_6D_6 (500 MHz, 298 K). * indicates peaks arising from ***cis*-3a** and labelled peaks are from ***trans*-3a**. † indicates signals from free dmpe.

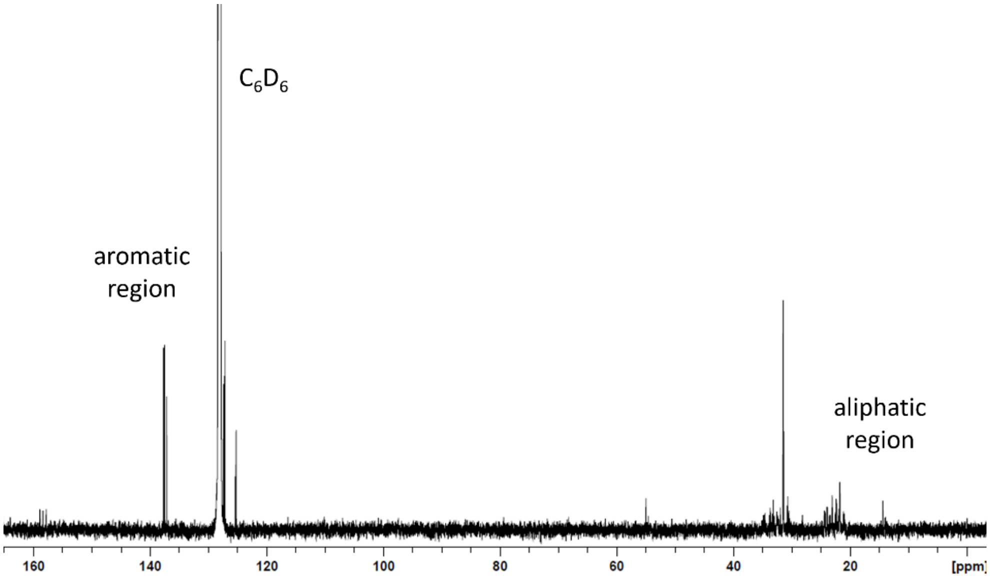

Figure S68. ^{13}C{^{1}H} NMR spectrum of a mixture of *cis* and *trans* isomers of [(dmpe)$_2$Mn(GeHPh$_2$)(CN^{t}Bu)] (**3a**) in C_6D_6 (126 MHz, 298 K).

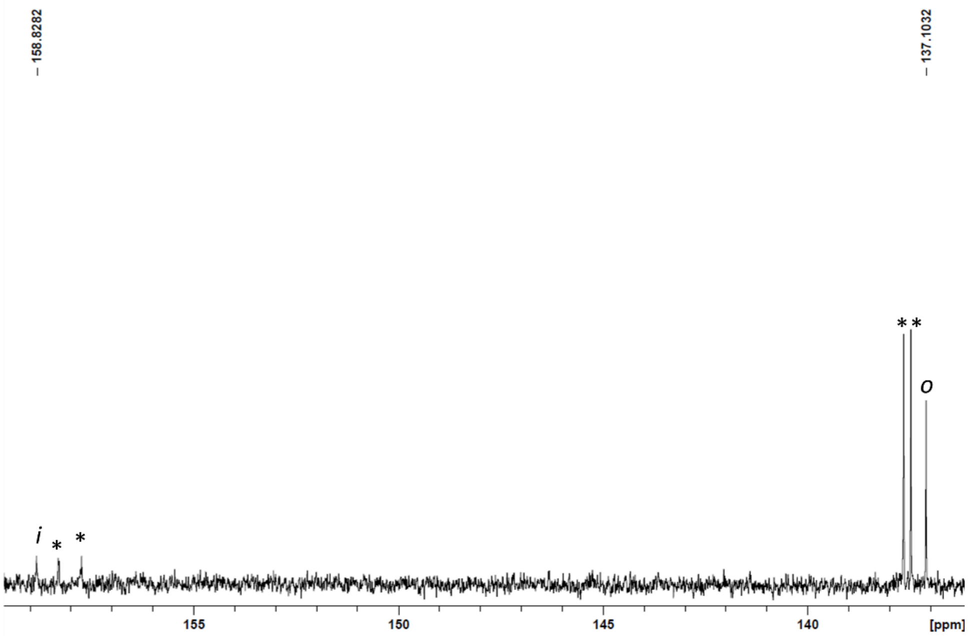

Figure S69. Expanded higher frequency aromatic region of the $^{13}C\{^1H\}$ NMR spectrum of a mixture of *cis* and *trans* isomers of [(dmpe)$_2$Mn(GeHPh$_2$)(CN^{t}Bu)] (**3a**) in C_6D_6 (126 MHz, 298 K). * indicates peaks arising from ***cis*-3a** and labelled peaks are from ***trans*-3a**.

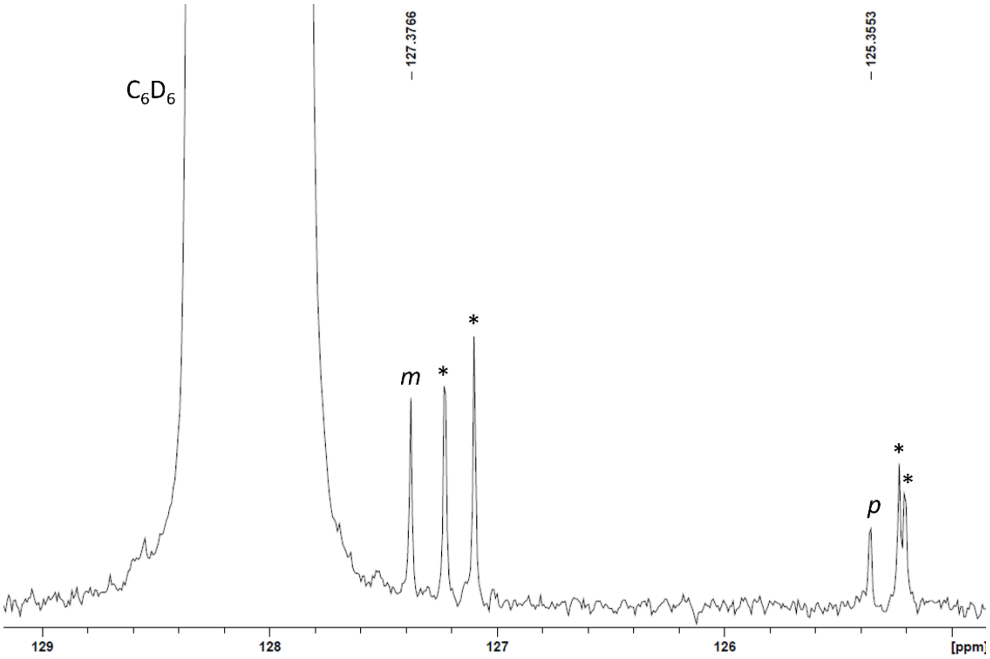

Figure S70. Expanded lower frequency aromatic region of the $^{13}C\{^1H\}$ NMR spectrum of a mixture of *cis* and *trans* isomers of (dmpe)$_2$Mn(GeHPh$_2$)(CN^{t}Bu)] (**3a**) in C_6D_6 (126 MHz, 298 K). * indicates peaks arising from ***cis*-3a** and labelled peaks are from ***trans*-3a**.

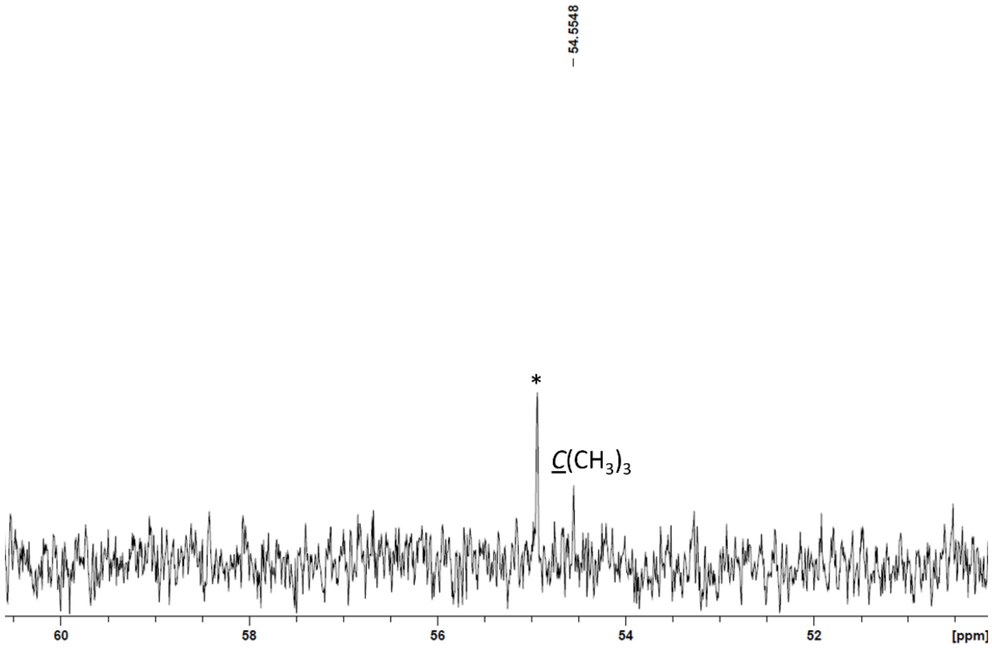

Figure S71. Expanded middle frequency region of the $^{13}C\{^1H\}$ NMR spectrum of a mixture of *cis* and *trans* isomers of (dmpe)$_2$Mn(GeHPh$_2$)(CN^{t}Bu)] (**3a**) in C_6D_6 (126 MHz, 298 K). * indicates a peak arising from ***cis*-3a** and the labelled peak is from ***trans*-3a**.

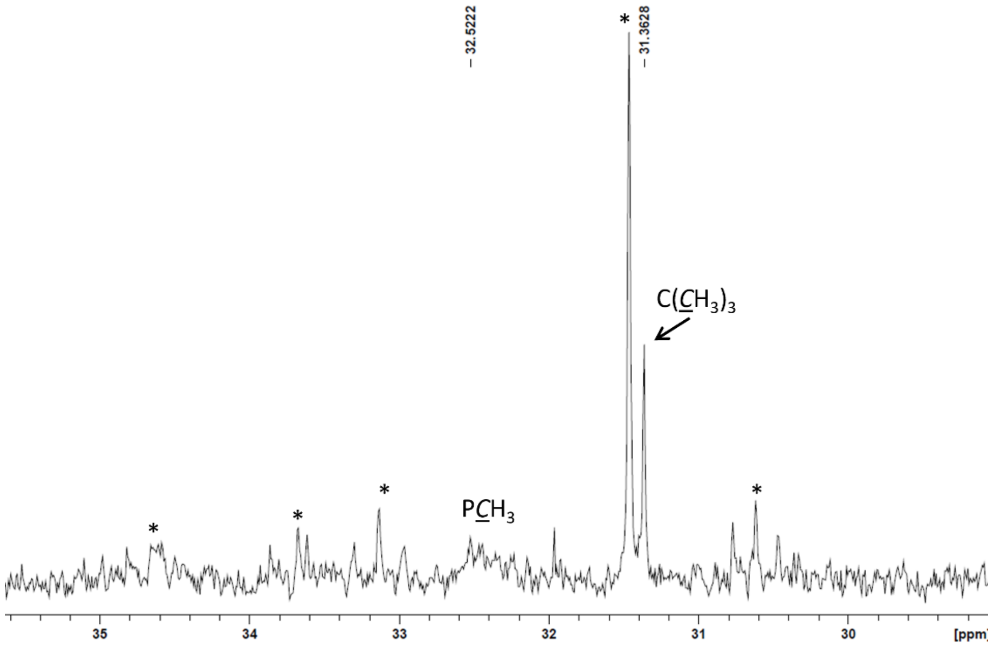

Figure S72. Expanded higher frequency aliphatic region of the $^{13}C\{^1H\}$ NMR spectrum of a mixture of *cis* and *trans* isomers of (dmpe)$_2$Mn(GeHPh$_2$)(CN^{t}Bu)] (**3a**) in C_6D_6 (126 MHz, 298 K). * indicates peaks arising from ***cis*-3a** and labelled peaks are from ***trans*-3a**.

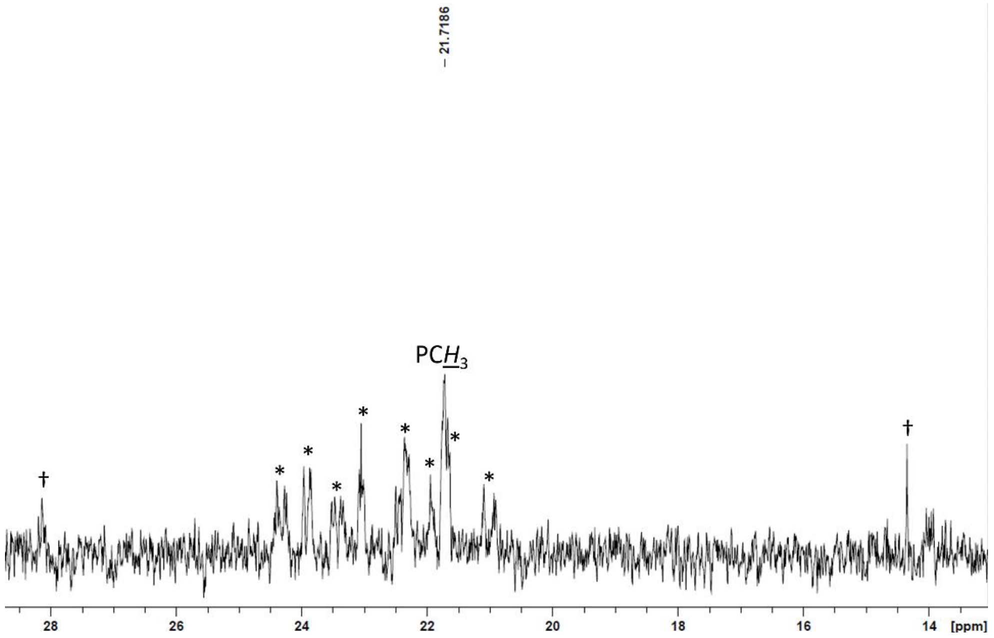

Figure S73. Expanded lower frequency aliphatic region of the $^{13}C\{^{1}H\}$ NMR spectrum of a mixture of *cis* and *trans* isomers of $(dmpe)_2Mn(GeHPh_2)(CN^tBu)]$ (**3a**) in C_6D_6 (126 MHz, 298 K). * indicates peaks arising from ***cis*-3a** and the labelled peak is from ***trans*-3a**. † indicates peaks from free dmpe.

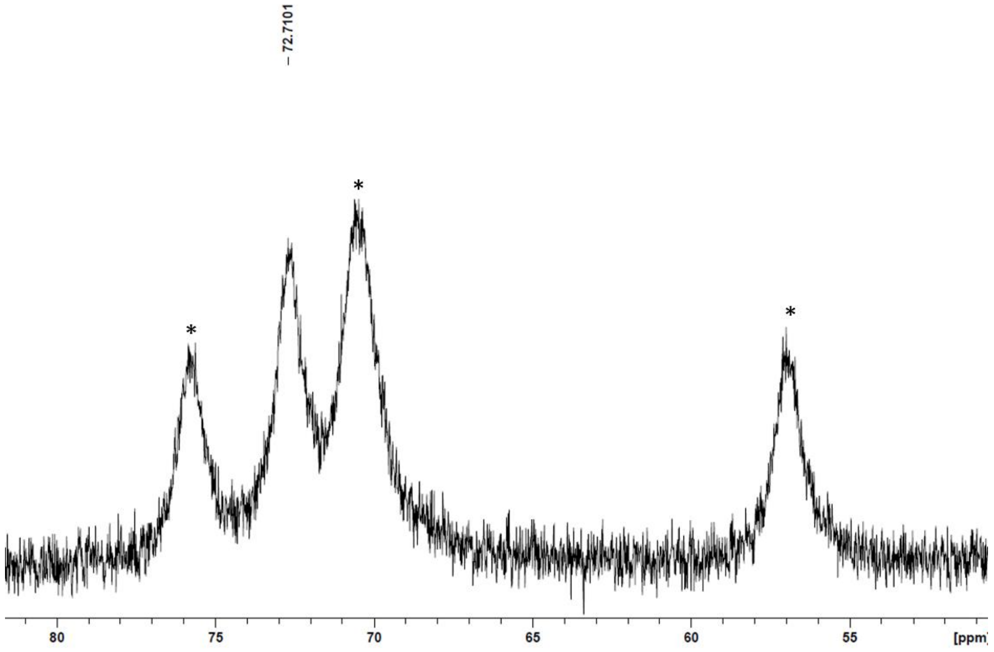

Figure S74. $^{31}P\{^{1}H\}$ NMR spectrum of a mixture of *cis* and *trans* isomers of $(dmpe)_2Mn(GeHPh_2)(CN^tBu)]$ (**3a**) in C_6D_6 (202 MHz, 298 K). * indicates peaks arising from ***cis*-3a** and the labelled peak is from ***trans*-3a**.

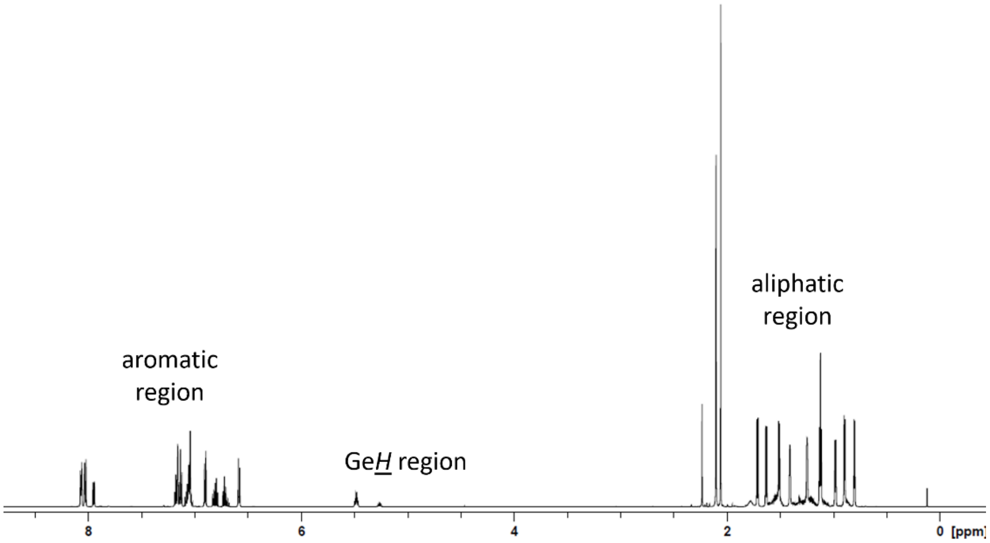

Figure S75. ^{1}H NMR spectrum of solution formed from the reaction of [(dmpe)$_2$MnH(=GePh$_2$)] (**1a**) and CNXyl containing a mixture of *cis* and *trans* isomers of [(dmpe)$_2$Mn(GeHPh$_2$)(CNXyl)] (**3b**) in C$_6$D$_6$ (600 MHz, 298 K). Xyl = *o*-xylyl.

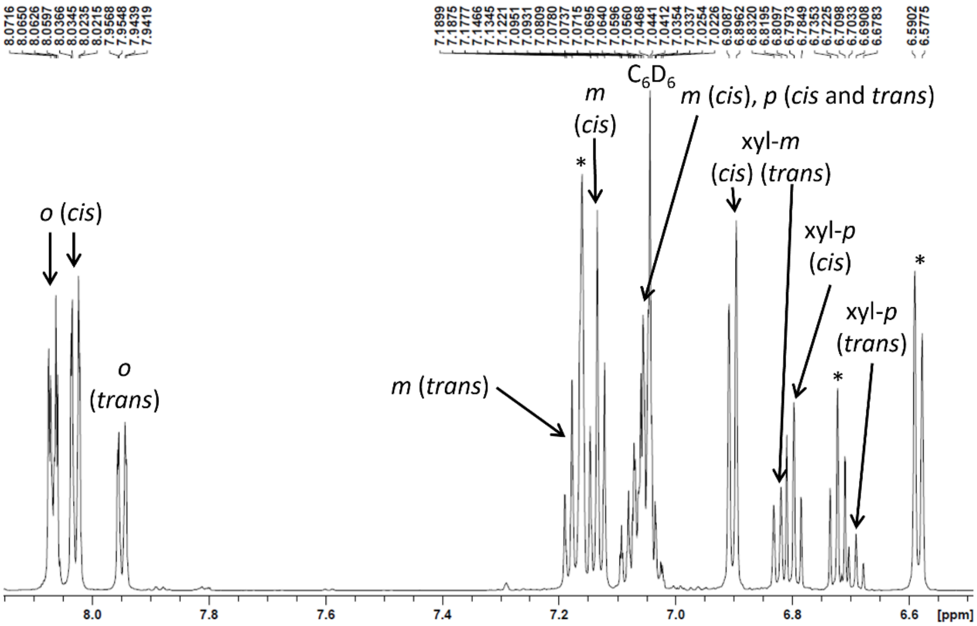

Figure S76. Expanded aromatic region of the ^{1}H NMR spectrum of solution formed from the reaction of [(dmpe)$_2$MnH(=GePh$_2$)] (**1a**) and CNXyl containing a mixture of *cis* and *trans* isomers of [(dmpe)$_2$Mn(GeHPh$_2$)(CNXyl)] (**3b**) in C$_6$D$_6$ (600 MHz, 298 K). Xyl = *o*-xylyl. * indicates peaks from CNXyl.

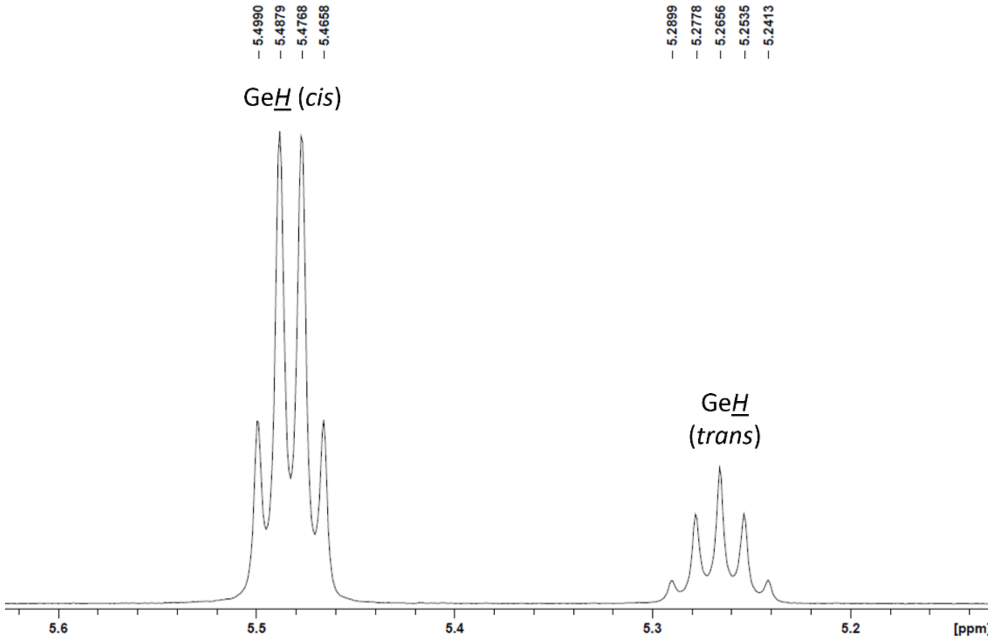

Figure S77. Expanded Ge*H* region of the ^{1}H NMR spectrum of solution formed from the reaction of [(dmpe)$_2$MnH(=GePh$_2$)] (**1a**) and CNXyl containing a mixture of *cis* and *trans* isomers of [(dmpe)$_2$Mn(GeHPh$_2$)(CNXyl)] (**3b**) in C$_6$D$_6$ (600 MHz, 298 K). Xyl = *o*-xylyl.

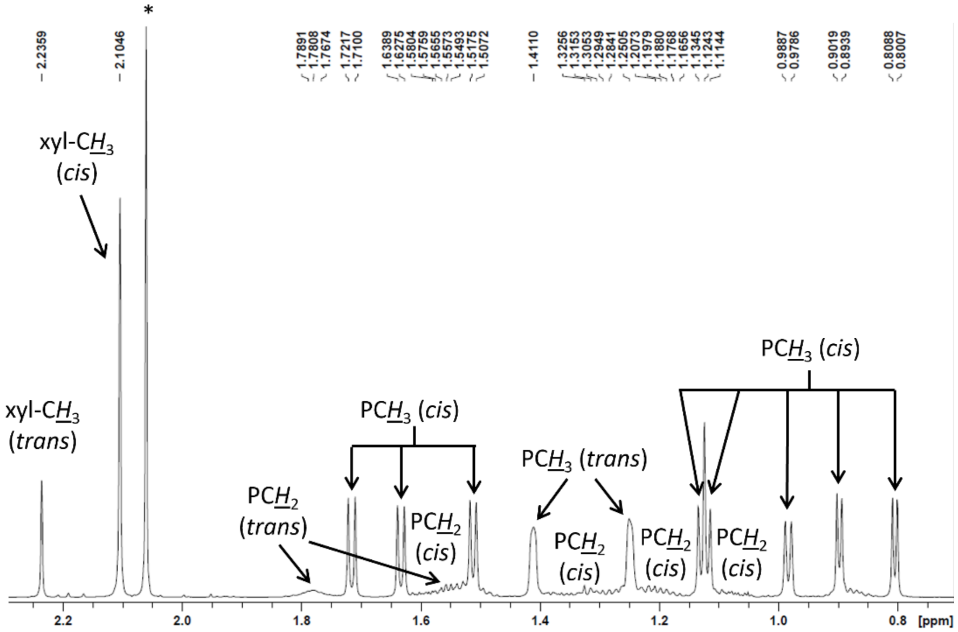

Figure S78. Expanded aliphatic region of the ^{1}H NMR spectrum of solution formed from the reaction of [(dmpe)$_2$MnH(=GePh$_2$)] (**1a**) and CNXyl containing a mixture of *cis* and *trans* isomers of [(dmpe)$_2$Mn(GeHPh$_2$)(CNXyl)] (**3b**) in C$_6$D$_6$ (600 MHz, 298 K). Xyl = *o*-xylyl. * indicates a peak from CNXyl.

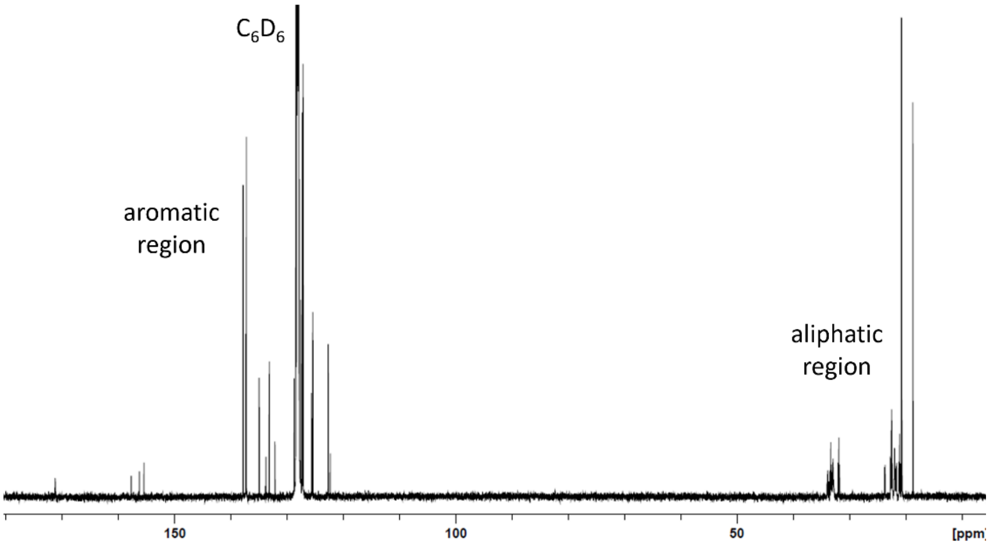

Figure S79. $^{13}C\{^1H\}$ NMR spectrum of solution formed from the reaction of [(dmpe)$_2$MnH(=GePh$_2$)] (**1a**) and CNXyl containing a mixture of *cis* and *trans* isomers of [(dmpe)$_2$Mn(GeHPh$_2$)(CNXyl)] (**3b**) in C_6D_6 (151 MHz, 298 K). Xyl = *o*-xylyl.

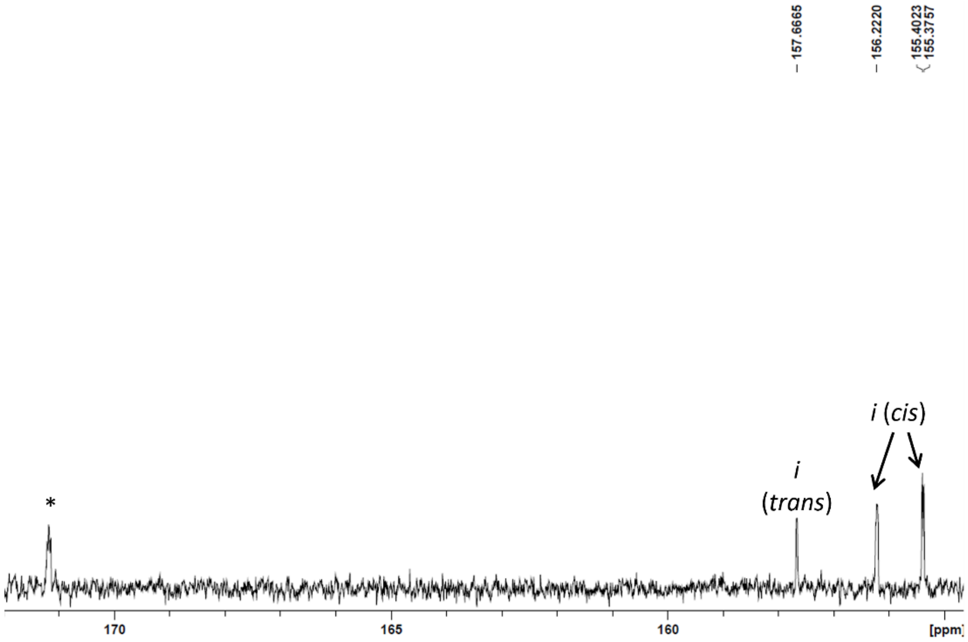

Figure S80. Expanded higher frequency aromatic region of the $^{13}C\{^1H\}$ NMR spectrum of solution formed from the reaction of [(dmpe)$_2$MnH(=GePh$_2$)] (**1a**) and CNXyl containing a mixture of *cis* and *trans* isomers of [(dmpe)$_2$Mn(GeHPh$_2$)(CNXyl)] (**3b**) in C_6D_6 (151 MHz, 298 K). Xyl = *o*-xylyl. * indicates a peak from CNXyl.

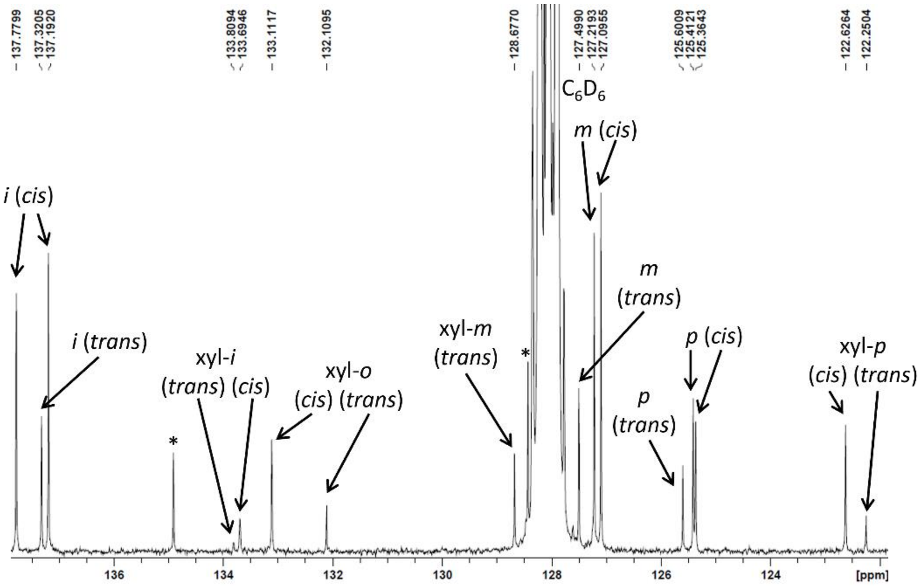

Figure S81. Expanded lower frequency aromatic region of the $^{13}C\{^1H\}$ NMR spectrum of solution formed from the reaction of [(dmpe)$_2$MnH(=GePh$_2$)] (**1a**) and CNXyl containing a mixture of *cis* and *trans* isomers of [(dmpe)$_2$Mn(GeHPh$_2$)(CNXyl)] (**3b**) in C_6D_6 (151 MHz, 298 K). Xyl = *o*-xylyl. * indicates peaks from CNXyl.

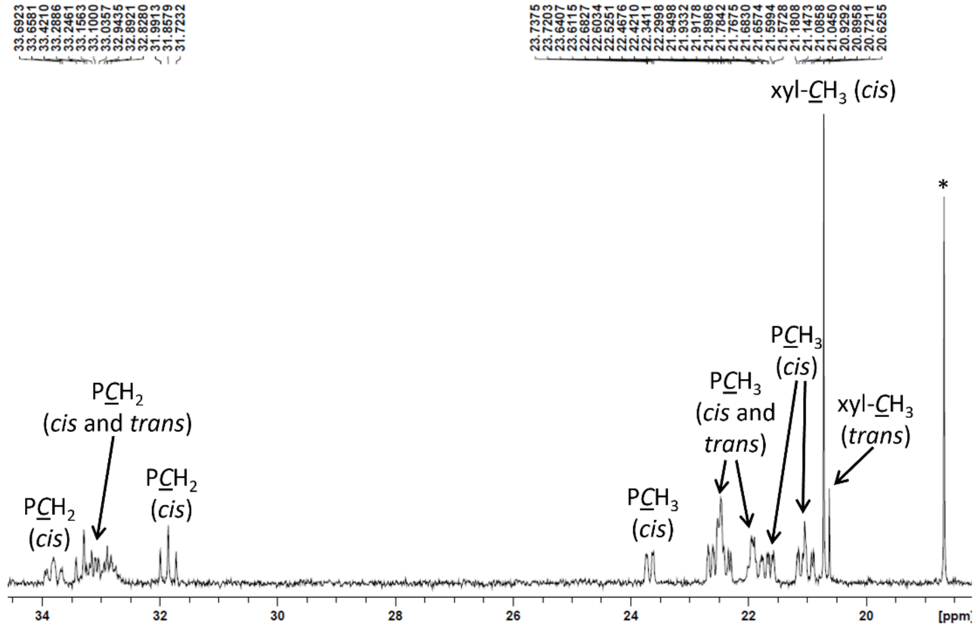

Figure S82. Expanded aliphatic region of the $^{13}C\{^1H\}$ NMR spectrum of solution formed from the reaction of [(dmpe)$_2$MnH(=GePh$_2$)] (**1a**) and CNXyl containing a mixture of *cis* and *trans* isomers of [(dmpe)$_2$Mn(GeHPh$_2$)(CNXyl)] (**3b**) in C_6D_6 (151 MHz, 298 K). Xyl = *o*-xylyl. * indicates a peak from CNXyl.

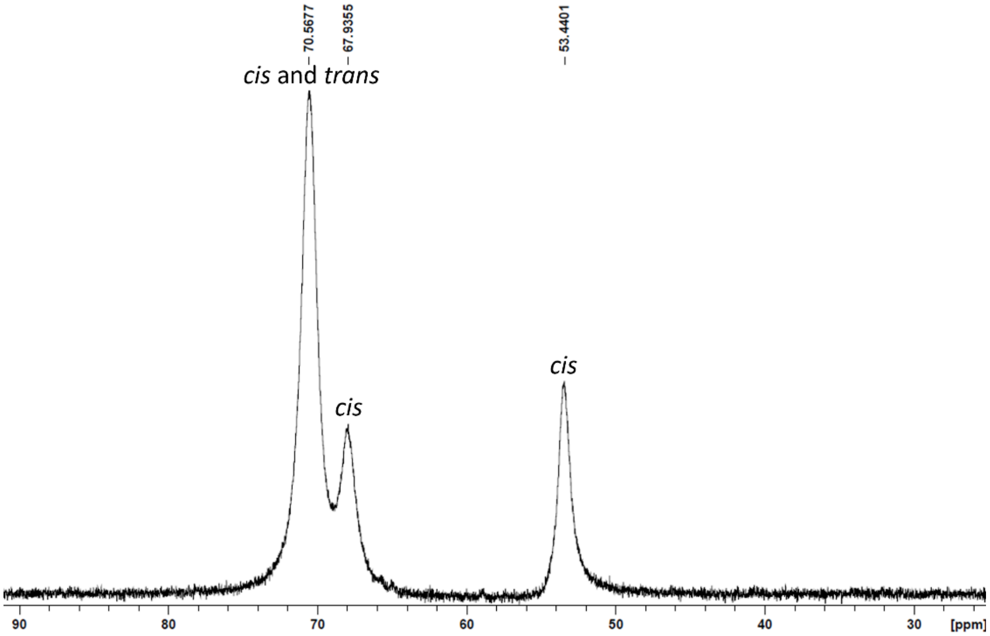

Figure S83. $^{31}P\{^{1}H\}$ NMR spectrum of solution formed from the reaction of [(dmpe)$_2$MnH(=GePh$_2$)] (**1a**) and CNXyl containing a mixture of *cis* and *trans* isomers of [(dmpe)$_2$Mn(GeHPh$_2$)(CNXyl)] (**3b**) in C_6D_6 (243 MHz, 298 K). Xyl = *o*-xylyl. * indicates a peak from CNXyl.

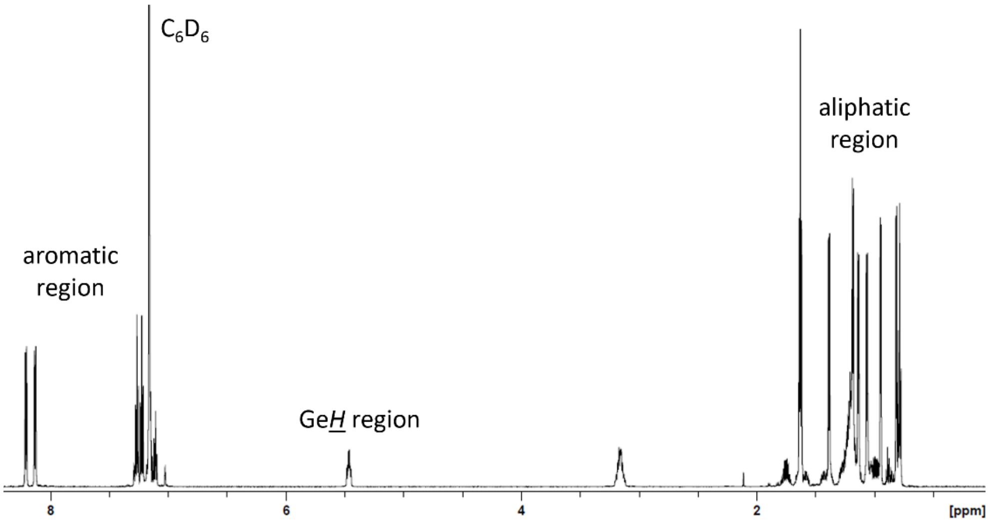

Figure S84. ^{1}H NMR spectrum of *cis*-[(dmpe)$_2$Mn(GeHPh$_2$)(CN^{n}Bu)] (***cis*-3c**) in C_6D_6 (600 MHz, 298 K).

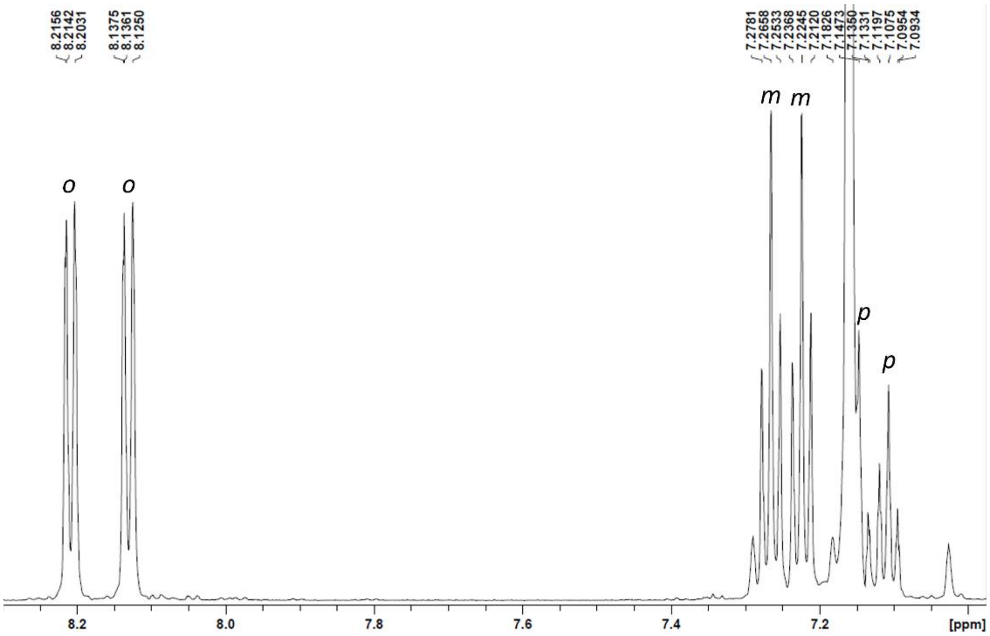

Figure S85. Expanded aromatic region of the ^{1}H NMR spectrum for *cis*-[(dmpe)$_2$Mn(GeHPh$_2$)(CN^{n}Bu)] (***cis*-3c**) in C_6D_6 (600 MHz, 298 K).

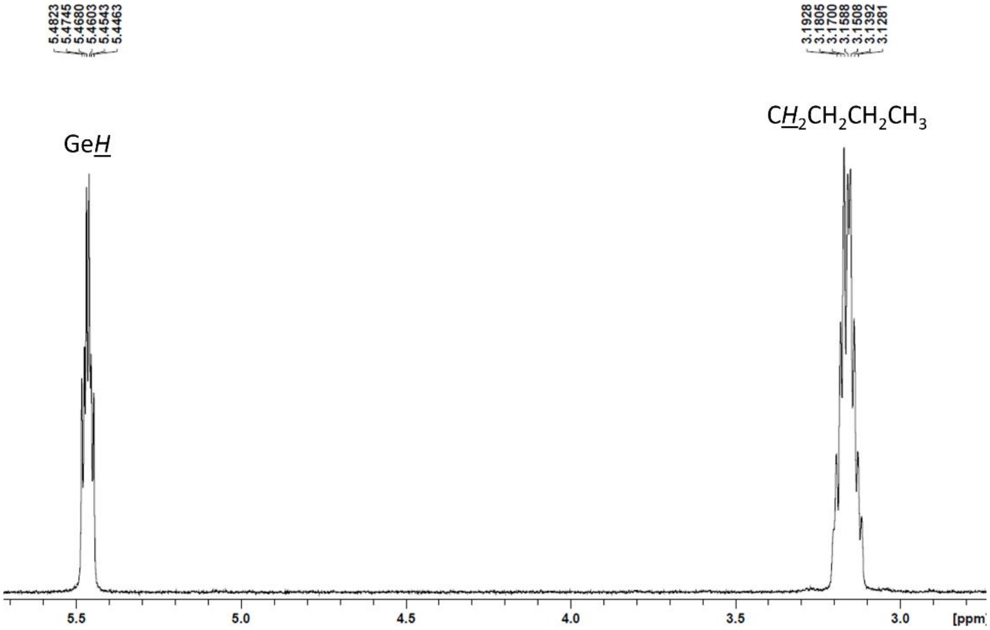

Figure S86. Expanded middle frequency region of the ^{1}H NMR spectrum for *cis*-[(dmpe)$_2$Mn(GeHPh$_2$)(CN^{n}Bu)] (***cis*-3c**) in C_6D_6 (600 MHz, 298 K).

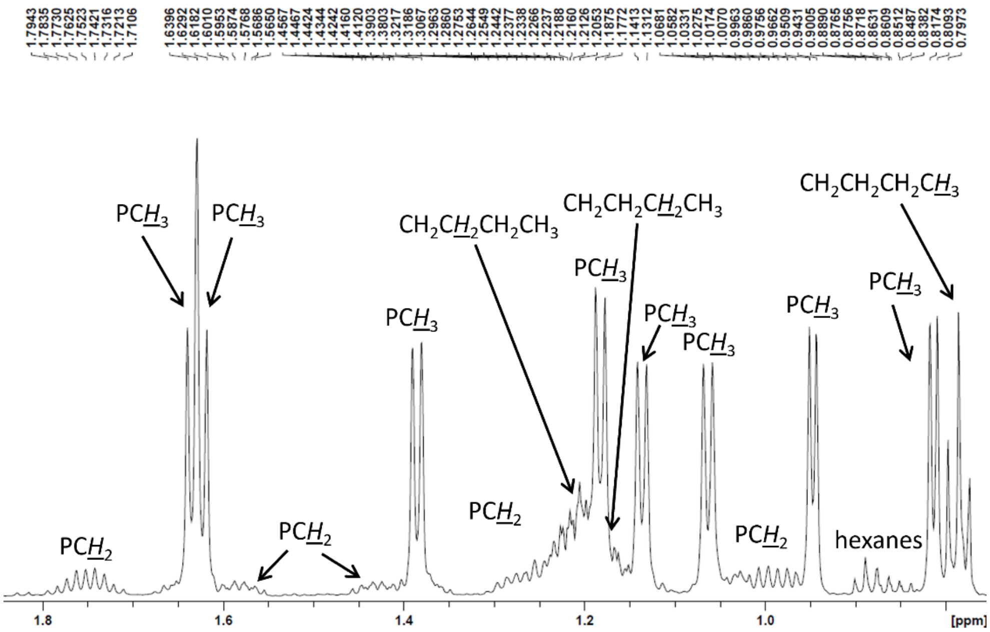

Figure S87. Expanded aliphatic region of the ^{1}H NMR spectrum for *cis*-[(dmpe)$_2$Mn(GeHPh$_2$)(CN^{n}Bu)] (***cis*-3c**) in C_6D_6 (600 MHz, 298 K).

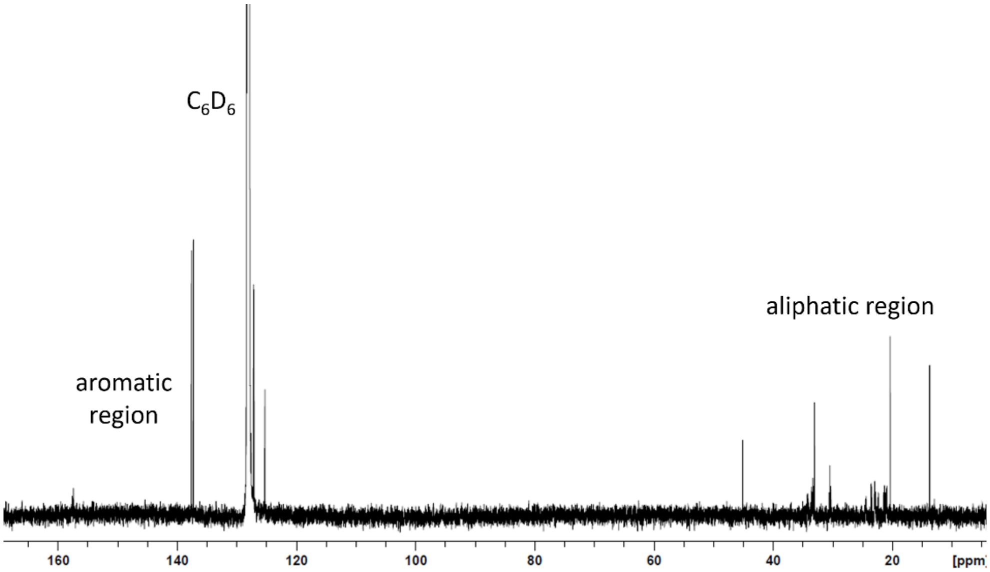

Figure S88. ^{13}C{^{1}H} NMR spectrum for *cis*-[(dmpe)$_2$Mn(GeHPh$_2$)(CN^{n}Bu)] (***cis*-3c**) in C_6D_6 (151 MHz, 298 K).

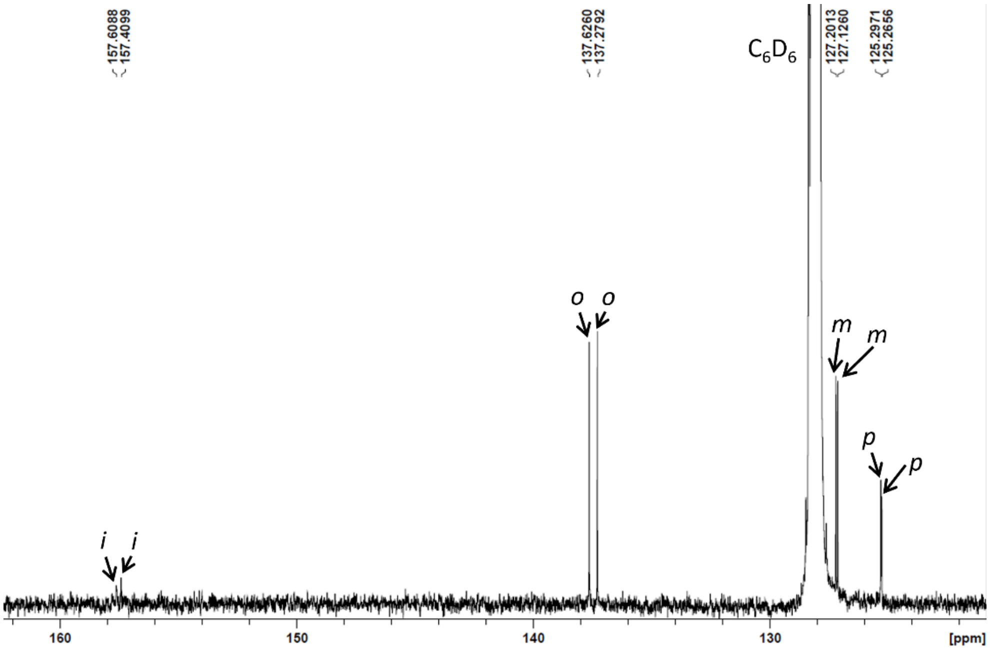

Figure S89. Expanded aromatic region of the $^{13}C\{^1H\}$ NMR spectrum for *cis*-[(dmpe)$_2$Mn(GeHPh$_2$)(CN^{n}Bu)] (***cis*-3c**) in C_6D_6 (151 MHz, 298 K).

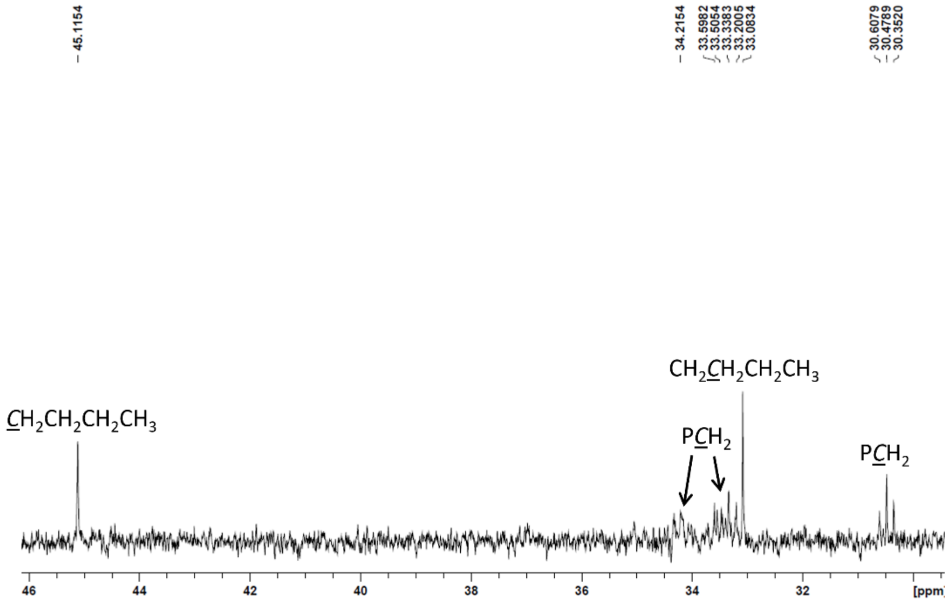

Figure S90. Expanded middle frequency region of the $^{13}C\{^1H\}$ NMR spectrum for *cis*-[(dmpe)$_2$Mn(GeHPh$_2$)(CN^{n}Bu)] (***cis*-3c**) in C_6D_6 (151 MHz, 298 K).

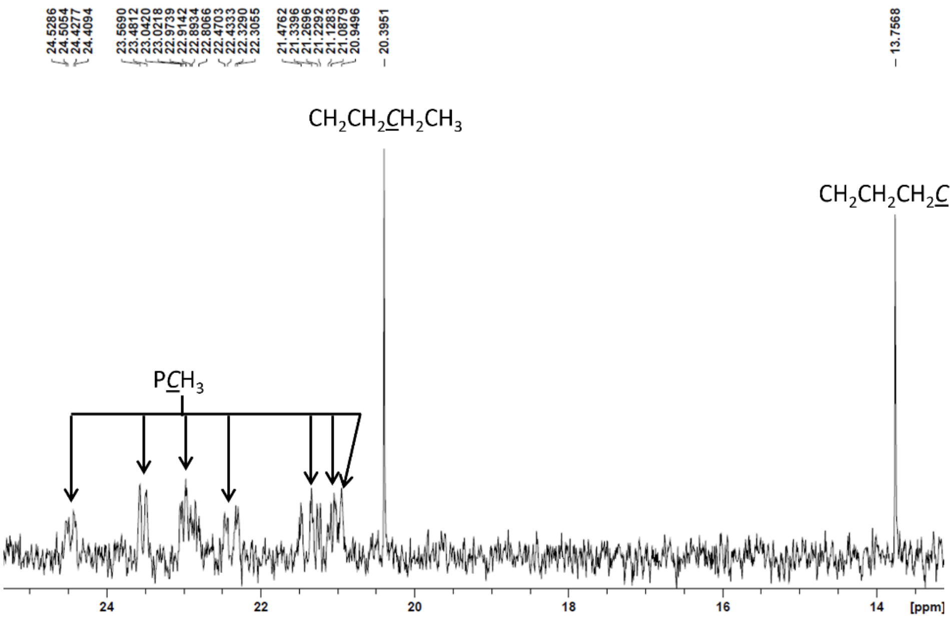

Figure S91. Expanded aliphatic region of the $^{13}C\{^{1}H\}$ NMR spectrum for *cis*-[(dmpe)$_2$Mn(GeHPh$_2$)(CN^{n}Bu)] (***cis*-3c**) in C_6D_6 (151 MHz, 298 K).

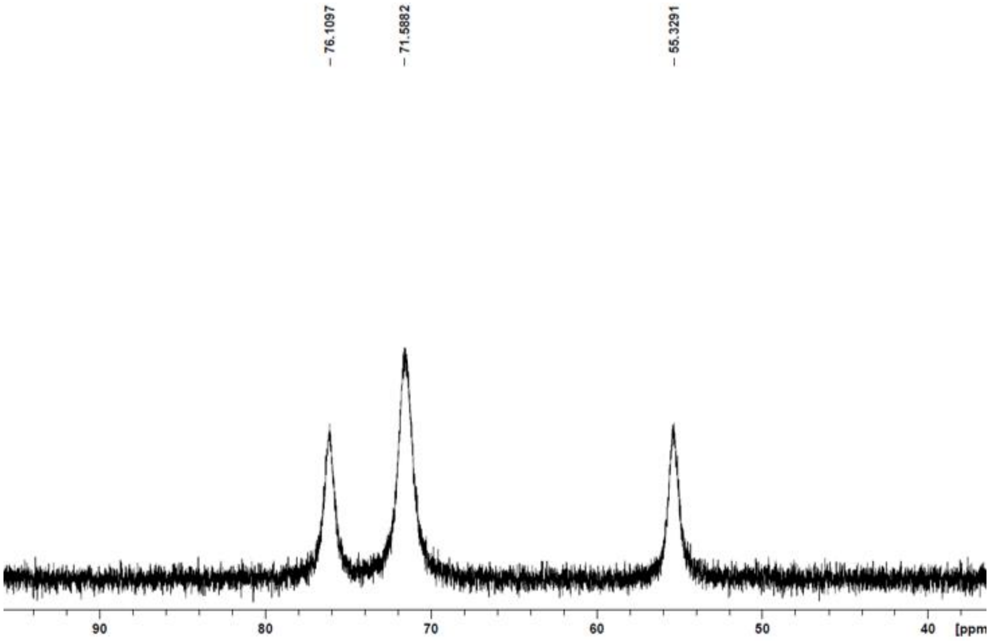

Figure S92. $^{31}P\{^{1}H\}$ NMR spectrum for *cis*-[(dmpe)$_2$Mn(GeHPh$_2$)(CN^{n}Bu)] (**3c**) in C_6D_6 (243 MHz, 298 K).

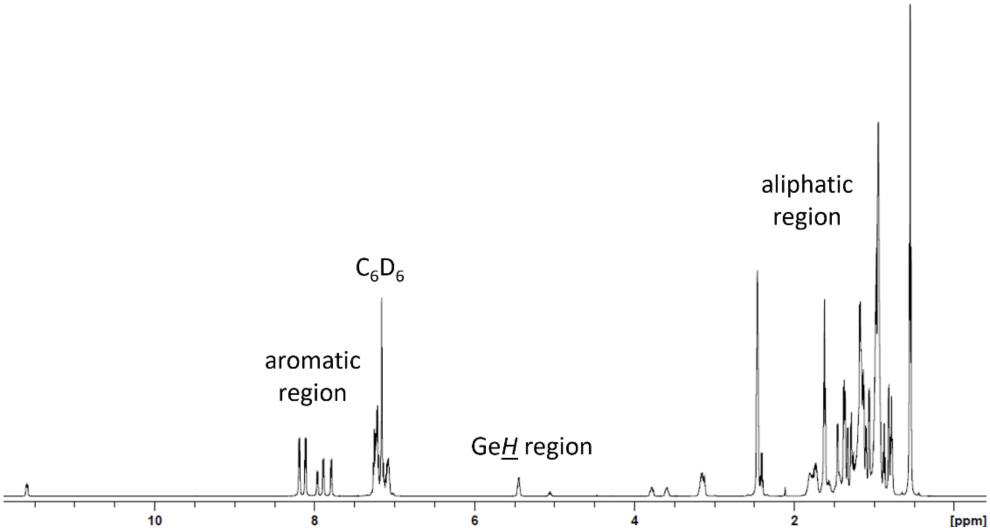

Figure S93. ^{1}H NMR spectrum of a solution containing *cis* and *trans* isomers of $[(dmpe)_2Mn(GeHPh_2)(CN^nBu)]$ (**3c**) formed from the reaction of $[(dmpe)_2MnH(=GePh_2)]$ (**1a**) and CN^nBu in C_6D_6 (600 MHz, 298 K).

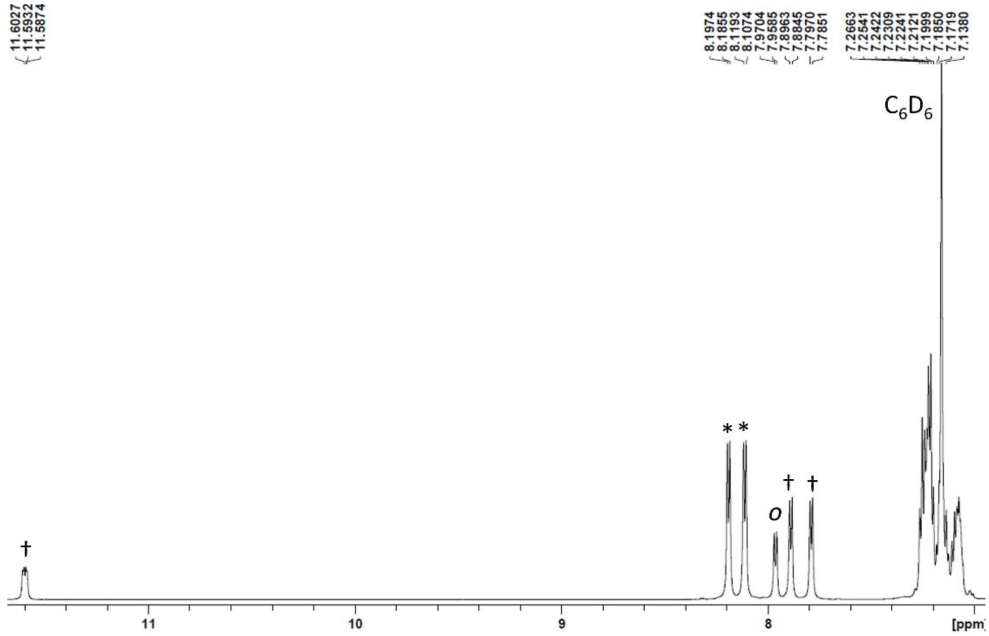

Figure S94. Expanded aromatic region of the ^{1}H NMR spectrum of a solution containing *cis* and *trans* isomers of $[(dmpe)_2Mn(GeHPh_2)(CN^nBu)]$ (**3c**) formed from the reaction of $[(dmpe)_2MnH(=GePh_2)]$ (**1a**) and CN^nBu in C_6D_6 (600 MHz, 298 K). * indicates peaks from ***cis*-3c**, † indicates peaks from an unidentified manganese-containing impurity, and labelled peaks are from ***trans*-3c**.

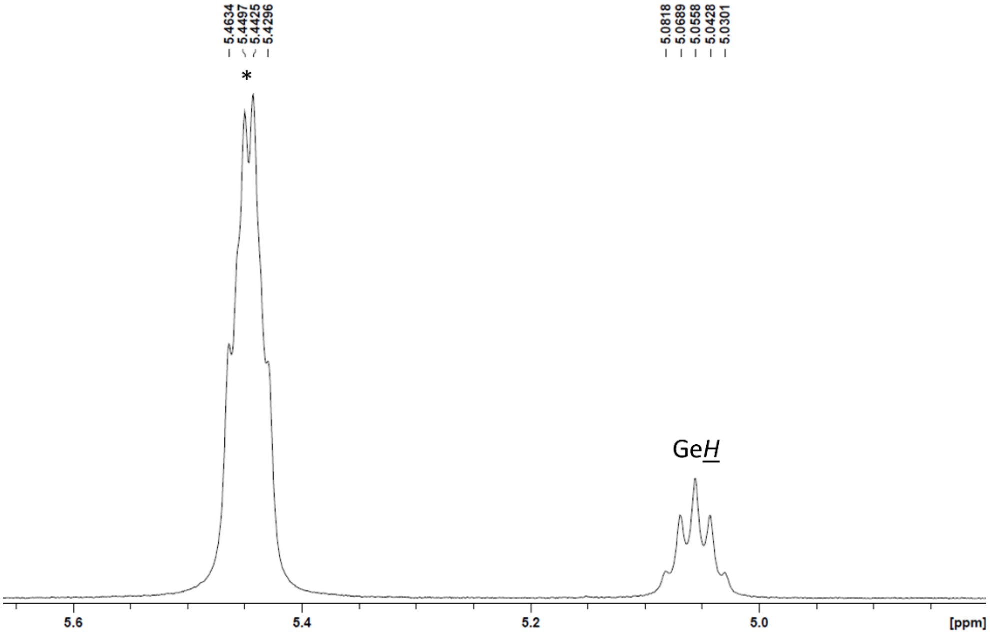

Figure S95. Expanded Ge*H* region of the ^{1}H NMR spectrum of a solution containing *cis* and *trans* isomers of [(dmpe)$_2$Mn(GeHPh$_2$)(CN^{n}Bu)] (**3c**) formed from the reaction of [(dmpe)$_2$MnH(=GePh$_2$)] (**1a**) and CN^{n}Bu in C_6D_6 (600 MHz, 298 K). * indicates a peak from ***cis*-3c** and the labelled peak is from ***trans*-3c**.

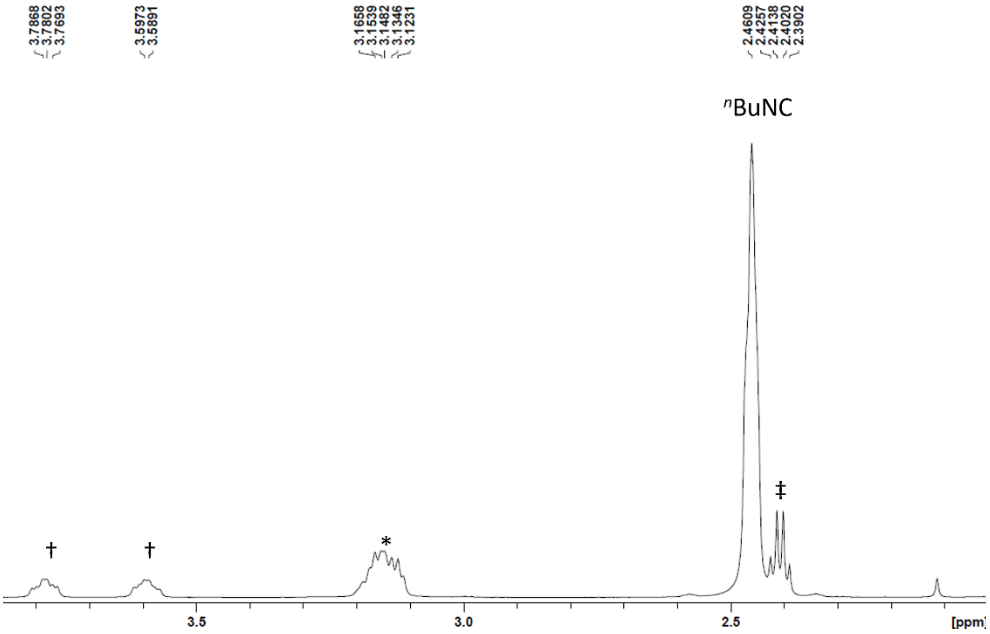

Figure S96. Expanded higher frequency aliphatic region of the ^{1}H NMR spectrum of a solution containing *cis* and *trans* isomers of [(dmpe)$_2$Mn(GeHPh$_2$)(CN^{n}Bu)] (**3c**) formed from the reaction of [(dmpe)$_2$MnH(=GePh$_2$)] (**1a**) and CN^{n}Bu in C_6D_6 (600 MHz, 298 K). * indicates a peak from ***cis*-3c**, † indicates peaks from an unidentified manganese-containing impurity, ‡ indicates an impurity present in the CN^{n}Bu used, and CN^{n}Bu indicates a peak from free CN^{n}Bu.

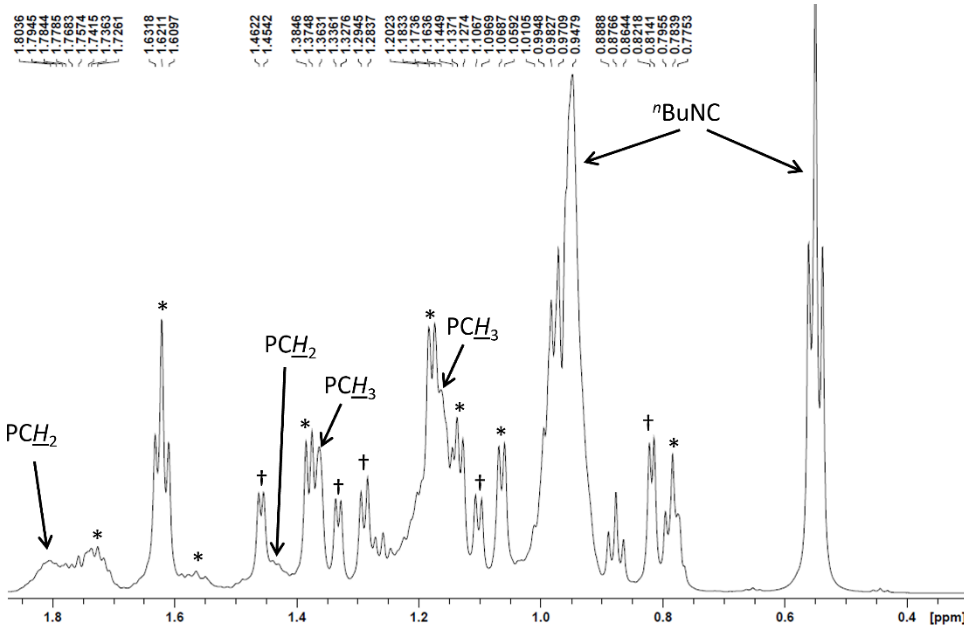

Figure S97. Expanded lower frequency aliphatic region of the ^{1}H NMR spectrum of a solution containing *cis* and *trans* isomers of [(dmpe)$_2$Mn(GeHPh$_2$)(CN^{n}Bu)] (**3c**) formed from the reaction of [(dmpe)$_2$MnH(=GePh$_2$)] (**1a**) and CN^{n}Bu in C$_6$D$_6$ (600 MHz, 298 K). * indicates peaks from ***cis*-3c**, † indicates peaks from an unidentified manganese-containing impurity, CN^{n}Bu indicates peaks from free CN^{n}Bu, and labelled peaks are from ***trans*-3c**.

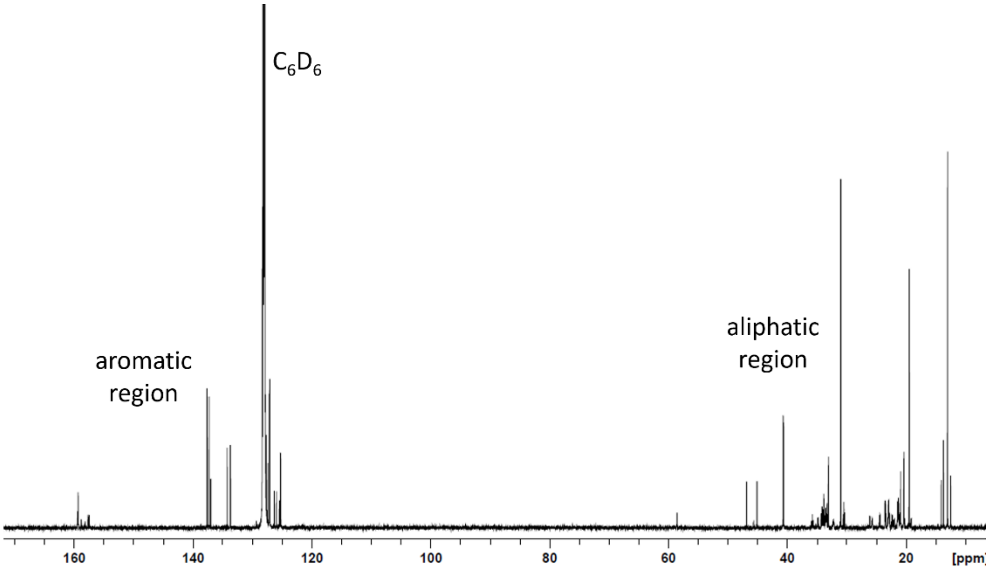

Figure S98. ^{13}C{^{1}H} NMR spectrum of a solution containing *cis* and *trans* isomers of [(dmpe)$_2$Mn(GeHPh$_2$)(CN^{n}Bu)] (**3c**) formed from the reaction of [(dmpe)$_2$MnH(=GePh$_2$)] (**1a**) and CN^{n}Bu in C$_6$D$_6$ (151 MHz, 298 K).

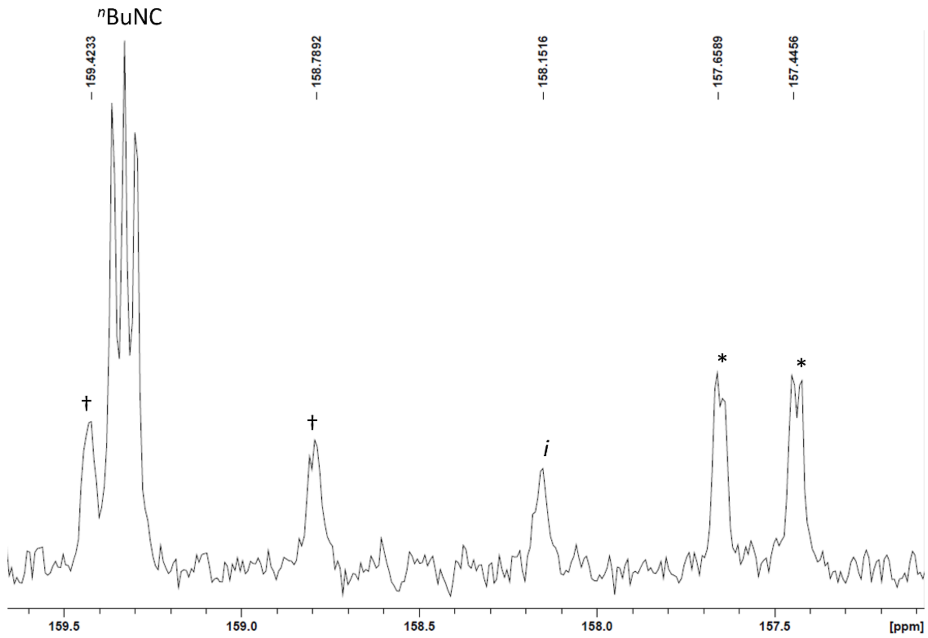

Figure S99. Expanded higher frequency aromatic region of the $^{13}C\{^{1}H\}$ NMR spectrum of a solution containing *cis* and *trans* isomers of [(dmpe)$_2$Mn(GeHPh$_2$)(CN^{n}Bu)] (**3c**) formed from the reaction of [(dmpe)$_2$MnH(=GePh$_2$)] (**1a**) and CN^{n}Bu in C_6D_6 (151 MHz, 298 K). * indicates peaks from ***cis*-3c**, † indicates peaks from an unidentified manganese-containing impurity, CN^{n}Bu indicates a peak from free CN^{n}Bu, and the labelled peak is from ***trans*-3c**.

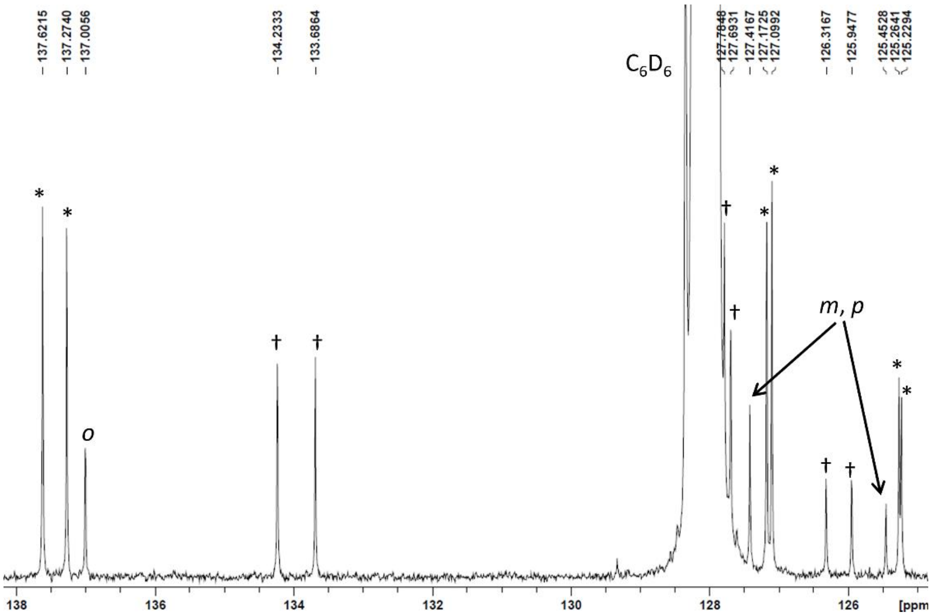

Figure S100. Expanded lower frequency aromatic region of the $^{13}C\{^{1}H\}$ NMR spectrum of a solution containing *cis* and *trans* isomers of [(dmpe)$_2$Mn(GeHPh$_2$)(CN^{n}Bu)] (**3c**) formed from the reaction of [(dmpe)$_2$MnH(=GePh$_2$)] (**1a**) and CN^{n}Bu in C_6D_6 (151 MHz, 298 K). * indicates peaks from ***cis*-3c** and † indicates peaks from an unidentified manganese-containing impurity.

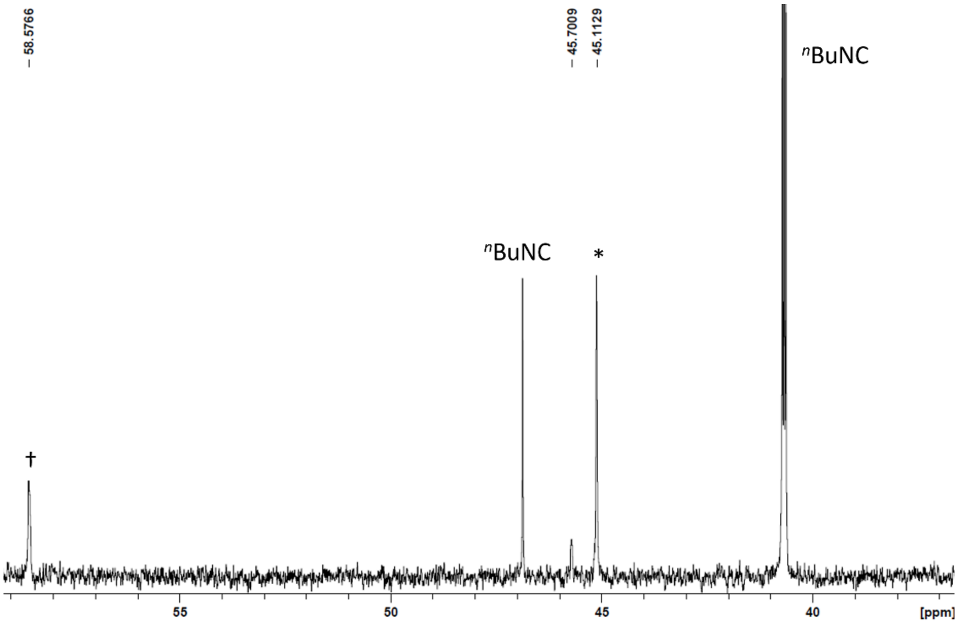

Figure S101. Expanded middle frequency region of the $^{13}C\{^1H\}$ NMR spectrum of a solution containing *cis* and *trans* isomers of $[(dmpe)_2Mn(GeHPh_2)(CN^nBu)]$ (**3c**) formed from the reaction of $[(dmpe)_2MnH(=GePh_2)]$ (**1a**) and CN^nBu in C_6D_6 (151 MHz, 298 K). * indicates a peak from ***cis*-3c**, † indicates a peak from an unidentified manganese-containing impurity, and CN^nBu indicates peaks from free CN^nBu.

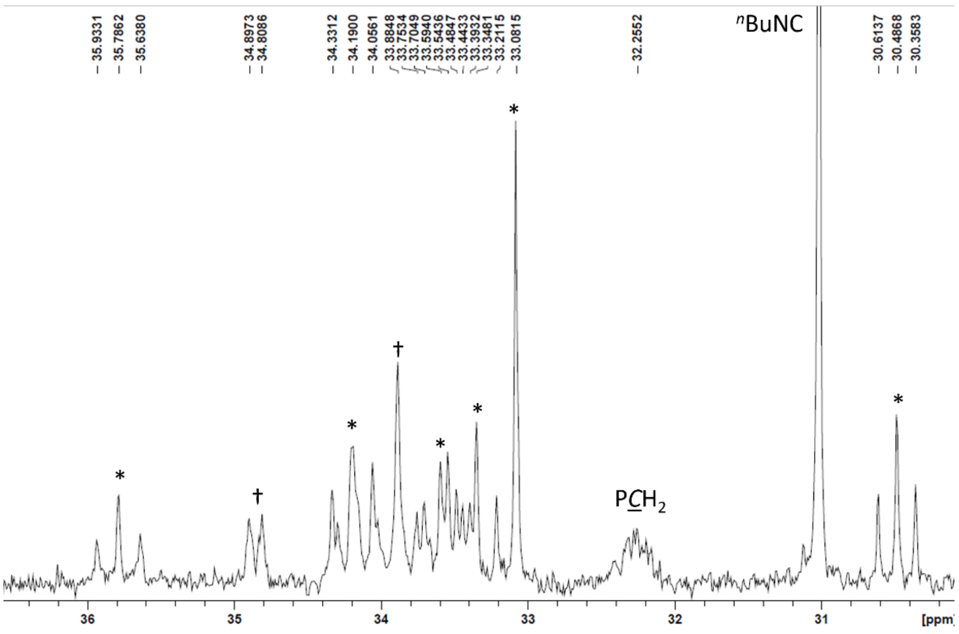

Figure S102. Expanded higher frequency aliphatic region of the $^{13}C\{^1H\}$ NMR spectrum of a solution containing *cis* and *trans* isomers of $[(dmpe)_2Mn(GeHPh_2)(CN^nBu)]$ (**3c**) formed from the reaction of $[(dmpe)_2MnH(=GePh_2)]$ (**1a**) and CN^nBu in C_6D_6 (151 MHz, 298 K). * indicates peaks from ***cis*-3c**, † indicates peaks from an unidentified manganese-containing impurity, CN^nBu indicates a peak from free CN^nBu, and the labelled peak is from ***trans*-3c**.

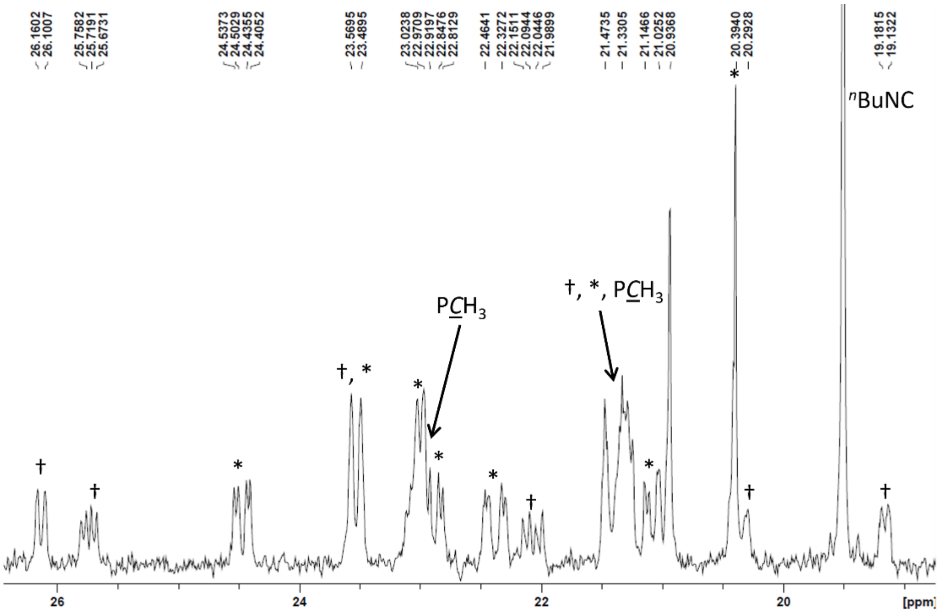

Figure S103. Expanded middle frequency aliphatic region of the $^{13}C\{^1H\}$ NMR spectrum of a solution containing *cis* and *trans* isomers of [(dmpe)$_2$Mn(GeHPh$_2$)(CN^{n}Bu)] (**3c**) formed from the reaction of [(dmpe)$_2$MnH(=GePh$_2$)] (**1a**) and CN^{n}Bu in C_6D_6 (151 MHz, 298 K). * indicates peaks from ***cis*-3c**, † indicates peaks from an unidentified manganese-containing impurity, CN^{n}Bu indicates a peak from free CN^{n}Bu, and labelled peaks are from ***trans*-3c**.

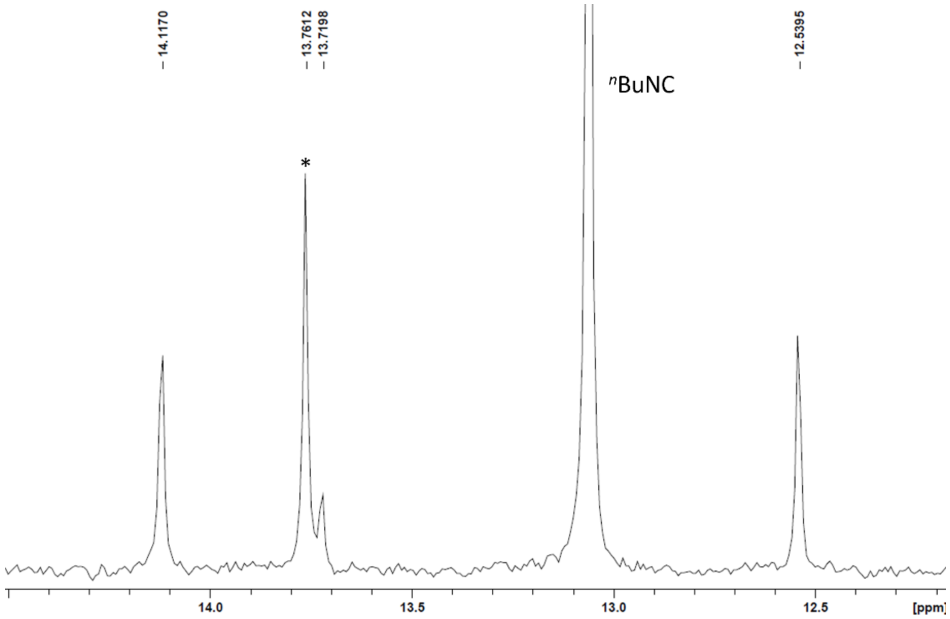

Figure S104. Expanded lower frequency aliphatic region of the $^{13}C\{^1H\}$ NMR spectrum of a solution containing *cis* and *trans* isomers of [(dmpe)$_2$Mn(GeHPh$_2$)(CN^{n}Bu)] (**3c**) formed from the reaction of [(dmpe)$_2$MnH(=GePh$_2$)] (**1a**) and CN^{n}Bu in C_6D_6 (151 MHz, 298 K). * indicates a peaks from ***cis*-3c** and CN^{n}Bu indicates a peak from free CN^{n}Bu.

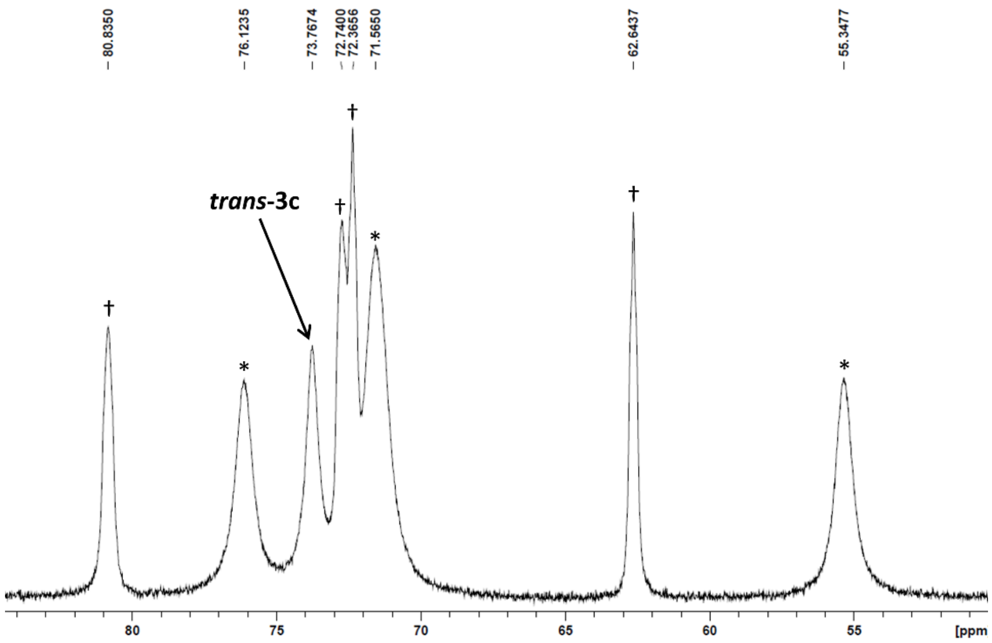

Figure S105. $^{31}P\{^{1}H\}$ NMR spectrum of a solution containing *cis* and *trans* isomers of $[(dmpe)_2Mn(GeHPh_2)(CN^{n}Bu)]$ (**3c**) formed from the reaction of $[(dmpe)_2MnH(=GePh_2)]$ (**1a**) and $CN^{n}Bu$ in C_6D_6 (243 MHz, 298 K). * indicates peaks from ***cis*-3c** and † indicates peaks from an unidentified manganese-containing impurity.

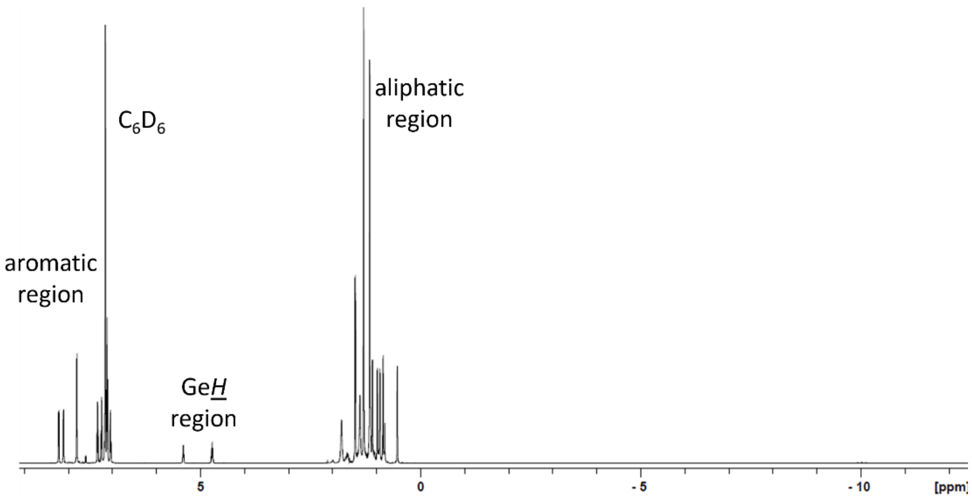

Figure S106. ^{1}H NMR spectrum of a solution containing *cis* and *trans* isomers of $[(dmpe)_2Mn(GeHPh_2)(N_2)]$ (**5a**) formed from the reaction of $[(dmpe)_2MnH(=GePh_2)]$ (**1a**) and N_2 after 7 days in C_6D_6 (600 MHz, 298 K).

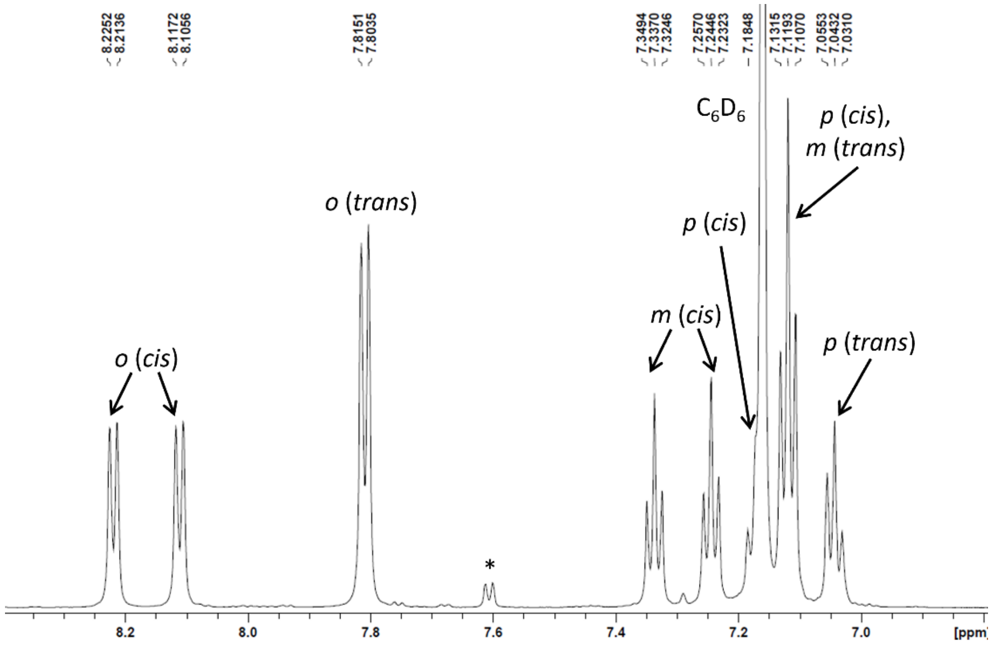

Figure S107. Expanded aromatic region of the ^{1}H NMR spectrum of a solution containing *cis* and *trans* isomers of [(dmpe)$_2$Mn(GeHPh$_2$)(N$_2$)] (**5a**) formed from the reaction of [(dmpe)$_2$MnH(=GePh$_2$)] (**1a**) and N$_2$ after 7 days in C$_6$D$_6$ (600 MHz, 298 K). * indicates a peak from **1a**.

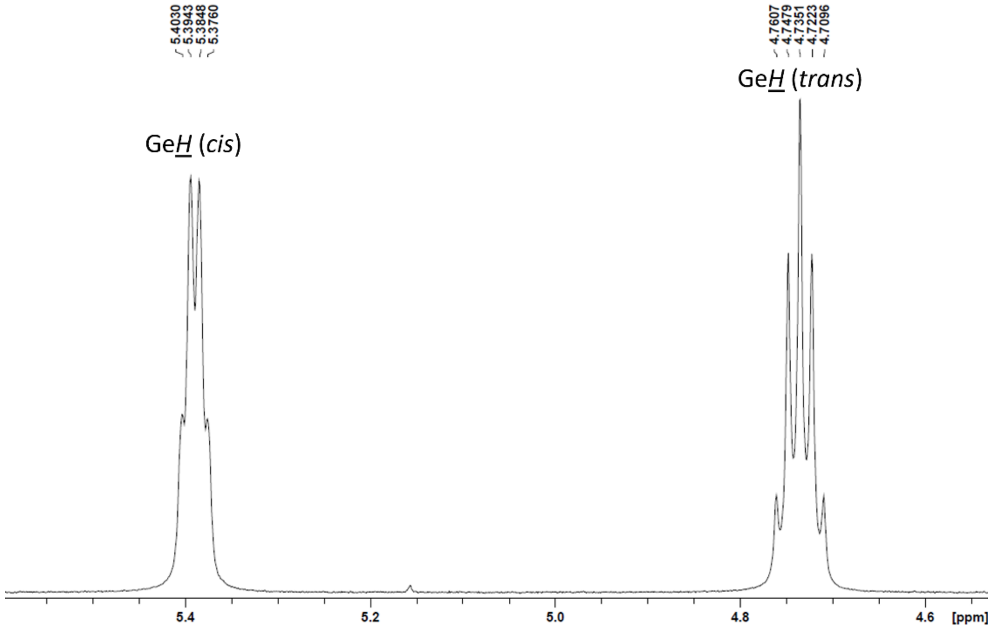

Figure S108. Expanded Ge*H* region of the ^{1}H NMR spectrum of a solution containing *cis* and *trans* isomers of [(dmpe)$_2$Mn(GeHPh$_2$)(N$_2$)] (**5a**) formed from the reaction of [(dmpe)$_2$MnH(=GePh$_2$)] (**1a**) and N$_2$ after 7 days in C$_6$D$_6$ (600 MHz, 298 K).

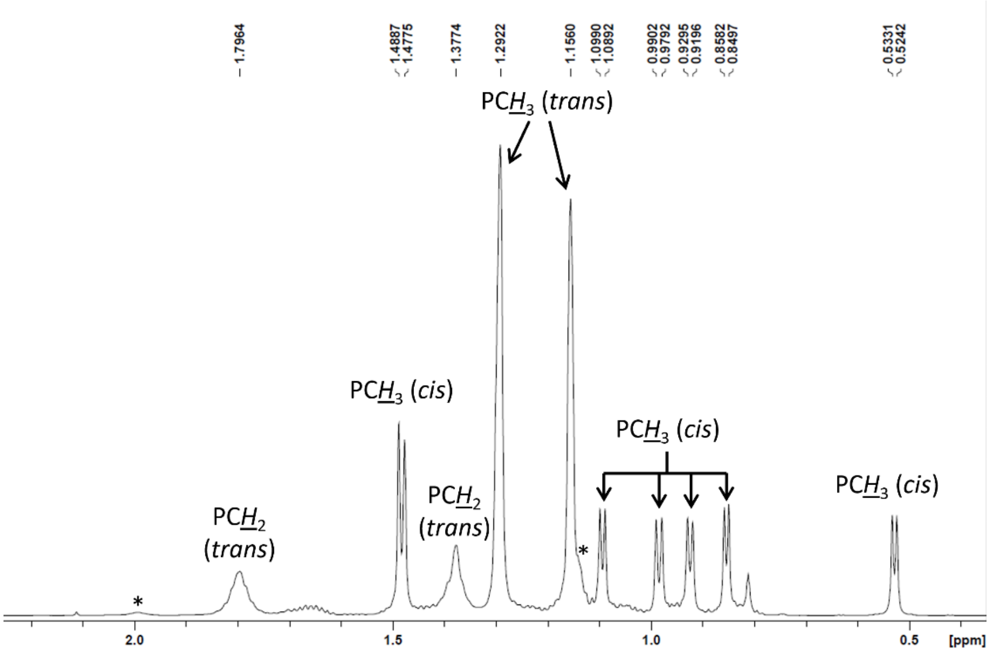

Figure S109. Expanded aliphatic region of the ^{1}H NMR spectrum of a solution containing *cis* and *trans* isomers of [(dmpe)$_2$Mn(GeHPh$_2$)(N$_2$)] (**5a**) formed from the reaction of [(dmpe)$_2$MnH(=GePh$_2$)] (**1a**) and N$_2$ after 7 days in C$_6$D$_6$ (600 MHz, 298 K). * indicates peaks from **1a**.

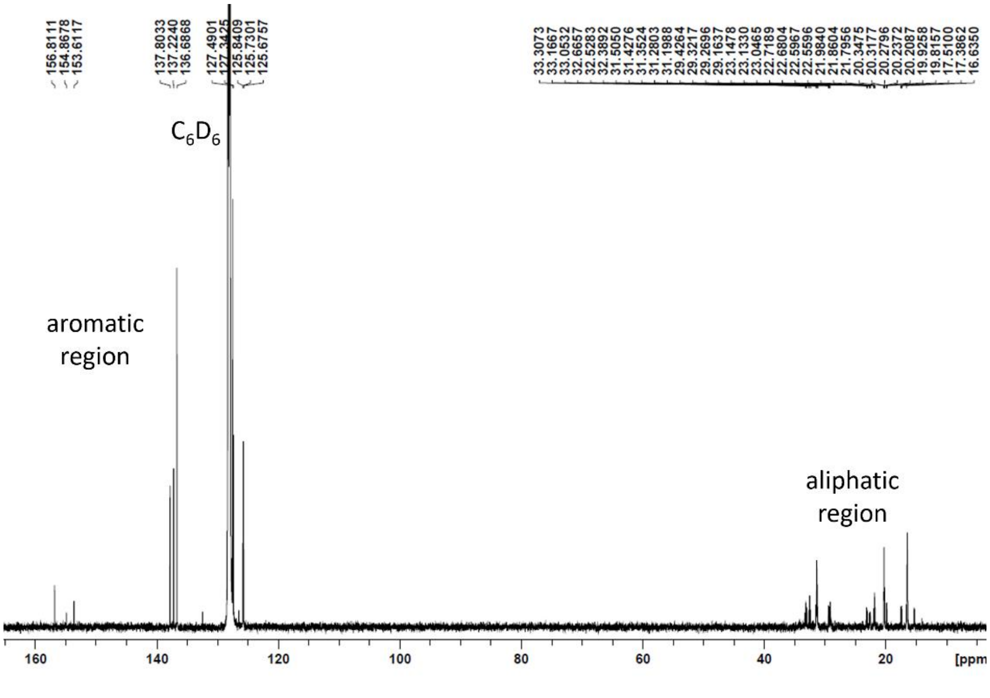

Figure S110. ^{13}C{^{1}H} NMR spectrum of a solution containing *cis* and *trans* isomers of [(dmpe)$_2$Mn(GeHPh$_2$)(N$_2$)] (**5a**) formed from the reaction of [(dmpe)$_2$MnH(=GePh$_2$)] (**1a**) and N$_2$ after 7 days in C$_6$D$_6$ (151 MHz, 298 K).

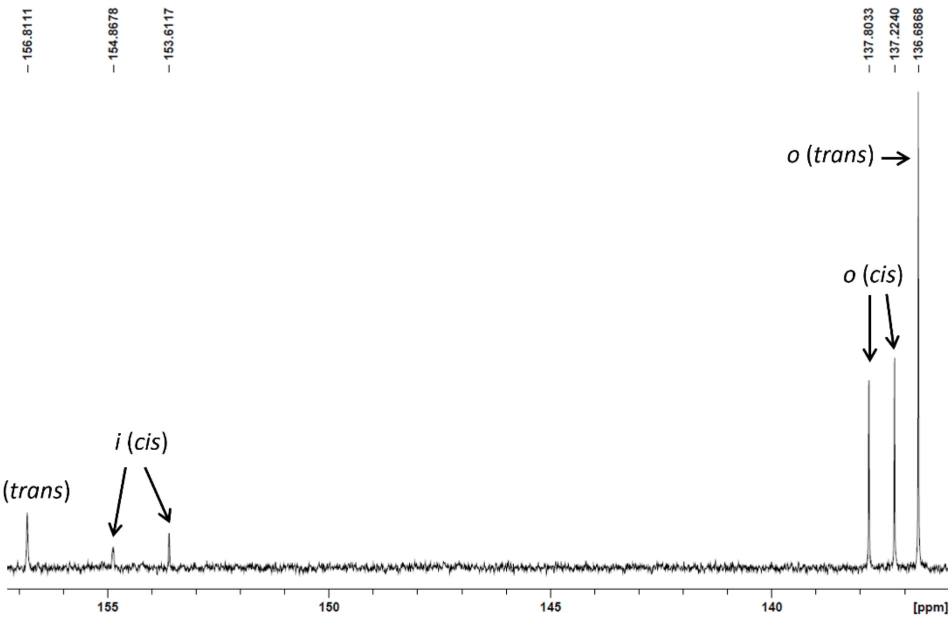

Figure S111. Expanded higher frequency aromatic region of the $^{13}C\{^1H\}$ NMR spectrum of a solution containing *cis* and *trans* isomers of [(dmpe)$_2$Mn(GeHPh$_2$)(N$_2$)] (**5a**) formed from the reaction of [(dmpe)$_2$MnH(=GePh$_2$)] (**1a**) and N_2 after 7 days in C_6D_6 (151 MHz, 298 K).

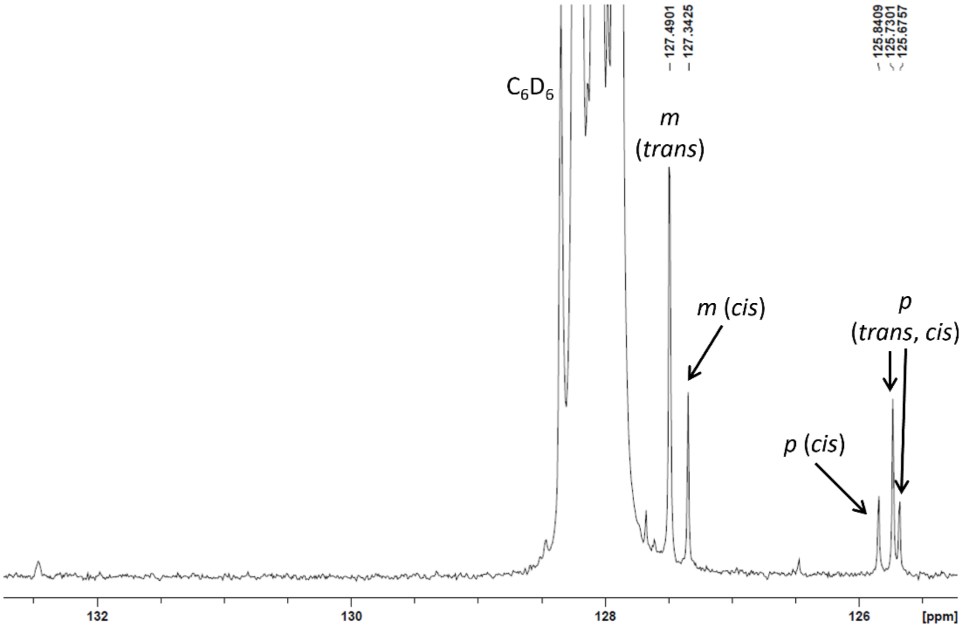

Figure S112. Expanded lower frequency aromatic region of the $^{13}C\{^1H\}$ NMR spectrum of a solution containing *cis* and *trans* isomers of [(dmpe)$_2$Mn(GeHPh$_2$)(N$_2$)] (**5a**) formed from the reaction of [(dmpe)$_2$MnH(=GePh$_2$)] (**1a**) and N_2 after 7 days in C_6D_6 (151 MHz, 298 K).

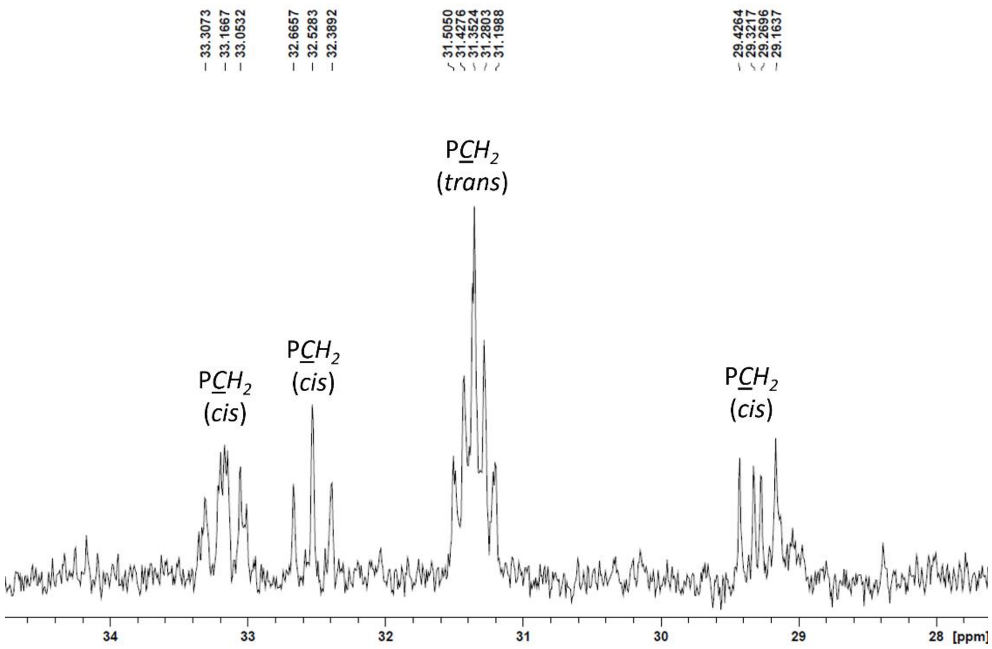

Figure S113. Expanded higher frequency aliphatic region of the $^{13}C\{^1H\}$ NMR spectrum of a solution containing *cis* and *trans* isomers of [(dmpe)$_2$Mn(GeHPh$_2$)(N$_2$)] (**5a**) formed from the reaction of [(dmpe)$_2$MnH(=GePh$_2$)] (**1a**) and N$_2$ after 7 days in C$_6$D$_6$ (151 MHz, 298 K).

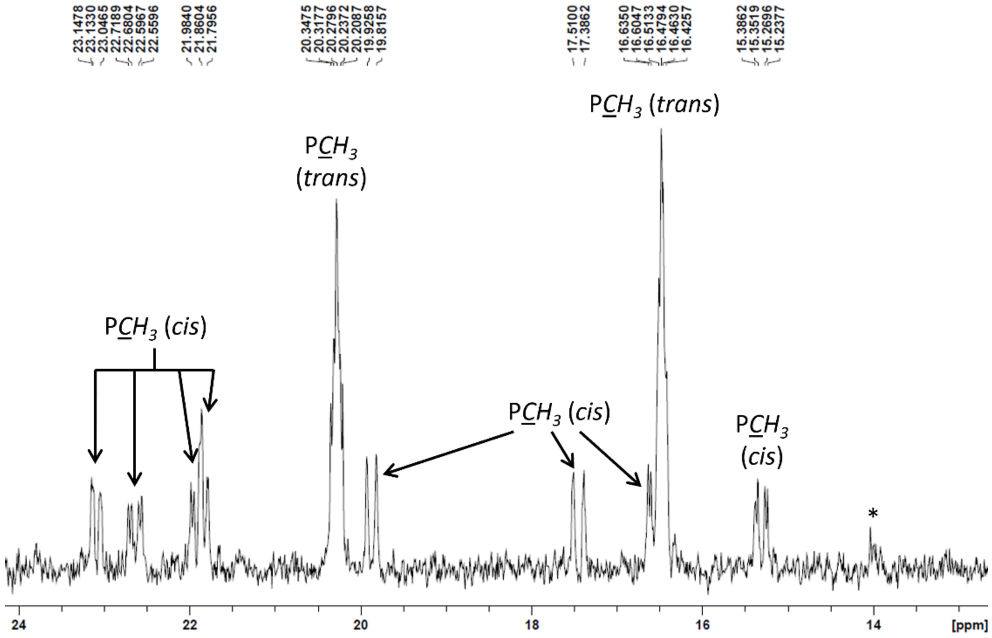

Figure S114. Expanded lower frequency aliphatic region of the $^{13}C\{^1H\}$ NMR spectrum of a solution containing *cis* and *trans* isomers of [(dmpe)$_2$Mn(GeHPh$_2$)(N$_2$)] (**5a**) formed from the reaction of [(dmpe)$_2$MnH(=GePh$_2$)] (**1a**) and N$_2$ after 7 days in C$_6$D$_6$ (151 MHz, 298 K). * is a peak from free dmpe.

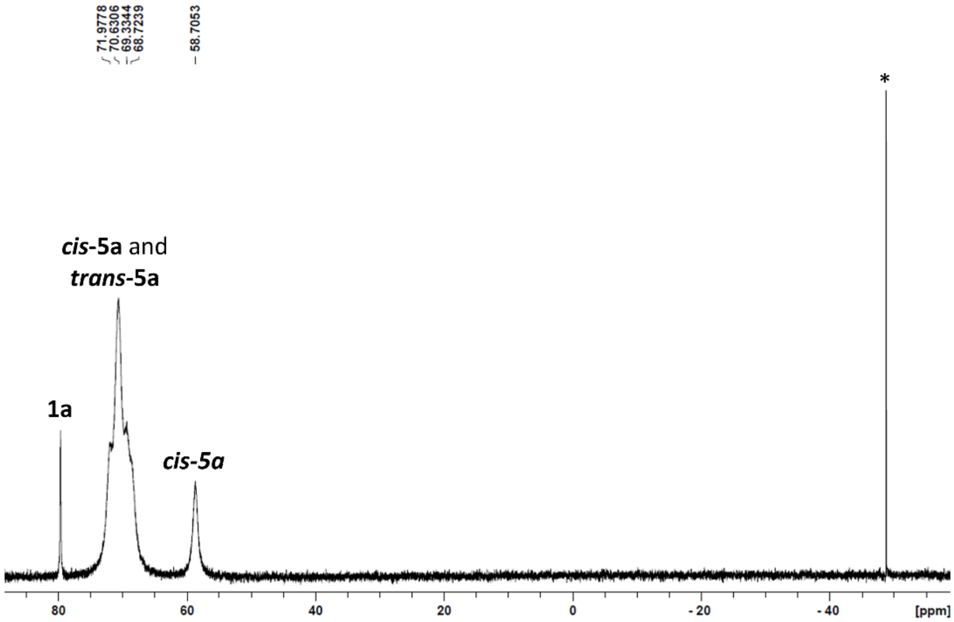

Figure S115. ^{31}P{^{1}H} NMR spectrum of a solution containing *cis* and *trans* isomers of [(dmpe)$_2$Mn(GeHPh$_2$)(N$_2$)] (**5a**) formed from the reaction of [(dmpe)$_2$MnH(=GePh$_2$)] (**1a**) and N$_2$ after 7 days in C$_6$D$_6$ (243 MHz, 298 K). * is a peak from free dmpe.

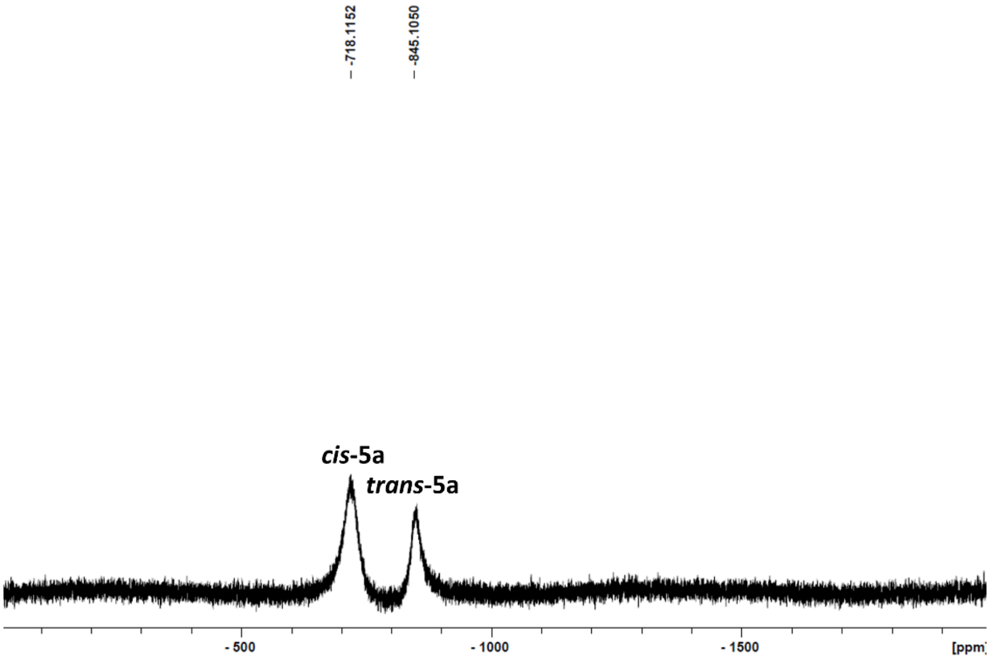

Figure S116. ^{55}Mn{^{1}H} NMR spectrum of a solution containing *cis* and *trans* isomers of [(dmpe)$_2$Mn(GeHPh$_2$)(N$_2$)] (**5a**) formed from the reaction of [(dmpe)$_2$MnH(=GePh$_2$)] (**1a**) and N$_2$ after 3 days in d_8-toluene (124 MHz, 298 K). [(dmpe)$_2$MnH(=GePh$_2$)] (**1a**) is present in solution, though at a concentration too dilute to be detected in this spectrum.

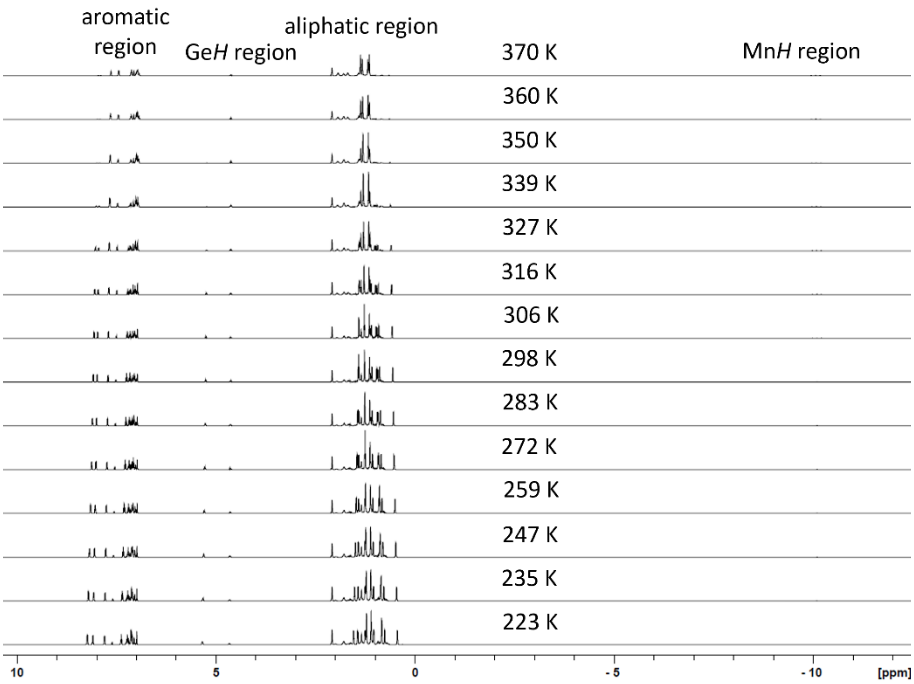

Figure S117. Variable temperature ^{1}H NMR spectra of a solution containing *cis* and *trans* isomers of [(dmpe)$_2$Mn(GeHPh$_2$)(N$_2$)] (**5a**) and *trans*-[(dmpe)$_2$MnH(=GePh$_2$)] (**1a**) formed from the reaction of **1a** and N$_2$ after 3 days in *d*$_8$-toluene (500 MHz, 298 K).

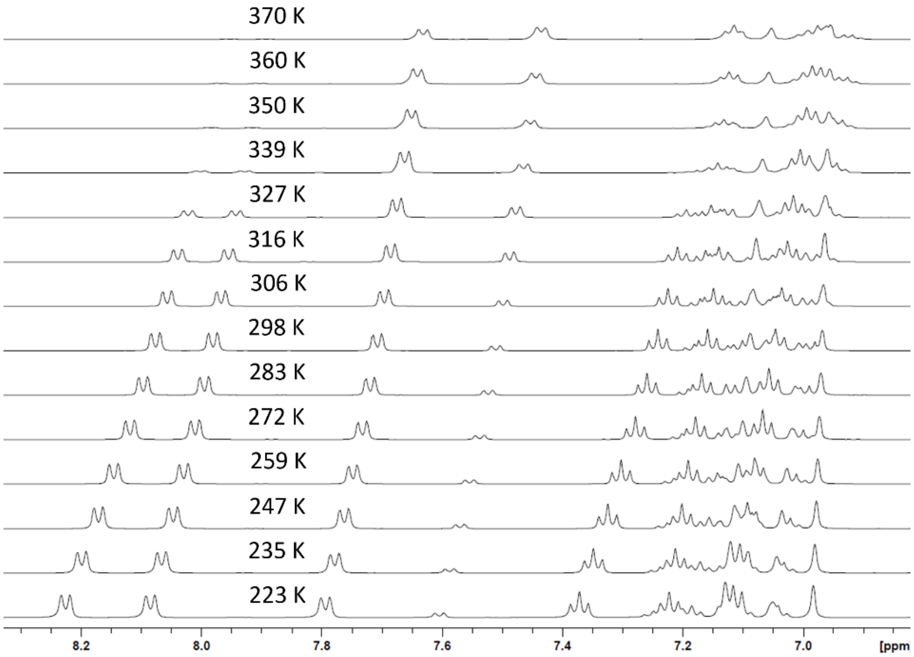

Figure S118. Expanded aromatic region of variable temperature ^{1}H NMR spectra of a solution containing *cis* and *trans* isomers of [(dmpe)$_2$Mn(GeHPh$_2$)(N$_2$)] (**5a**) and *trans*-[(dmpe)$_2$MnH(=GePh$_2$)] (**1a**) formed from the reaction of **1a** and N$_2$ after 3 days in *d*$_8$-toluene (500 MHz, 298 K).

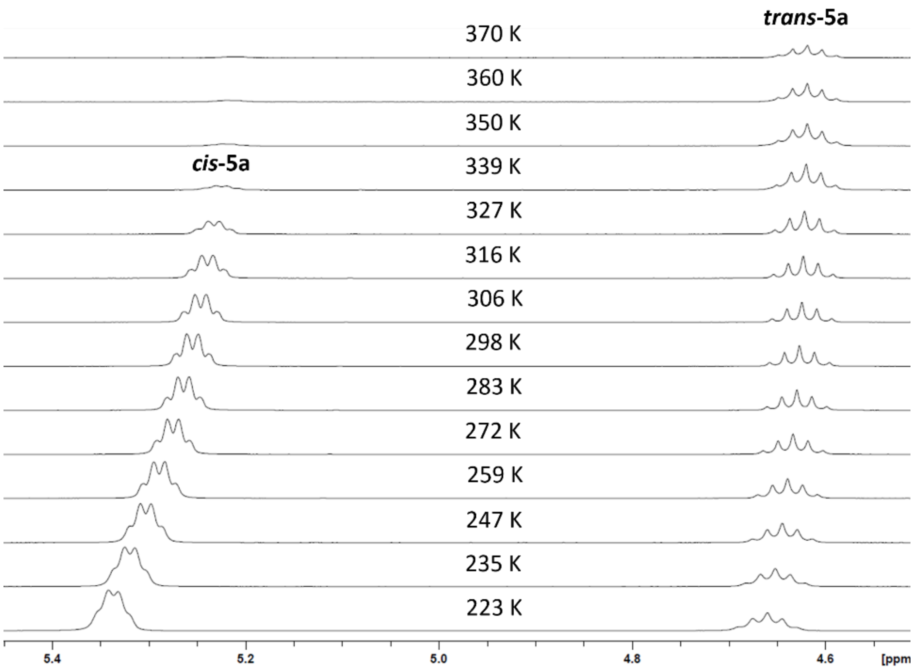

Figure S119. Expanded Ge*H* region of variable temperature ^{1}H NMR spectra of a solution containing *cis* and *trans* isomers of [(dmpe)$_2$Mn(GeHPh$_2$)(N$_2$)] (**5a**) and *trans*-[(dmpe)$_2$MnH(=GePh$_2$)] (**1a**) formed from the reaction of **1a** and N$_2$ after 3 days in *d*$_8$-toluene (500 MHz, 298 K).

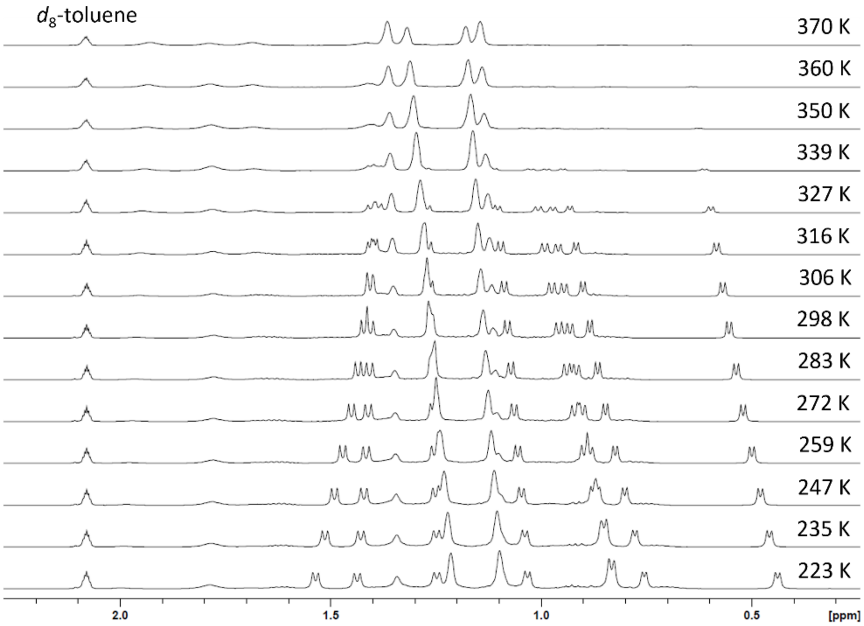

Figure S120. Expanded aliphatic region of variable temperature ^{1}H NMR spectra of a solution containing *cis* and *trans* isomers of [(dmpe)$_2$Mn(GeHPh$_2$)(N$_2$)] (**5a**) and *trans*-[(dmpe)$_2$MnH(=GePh$_2$)] (**1a**) formed from the reaction of **1a** and N$_2$ after 3 days in *d*$_8$-toluene (500 MHz, 298 K).

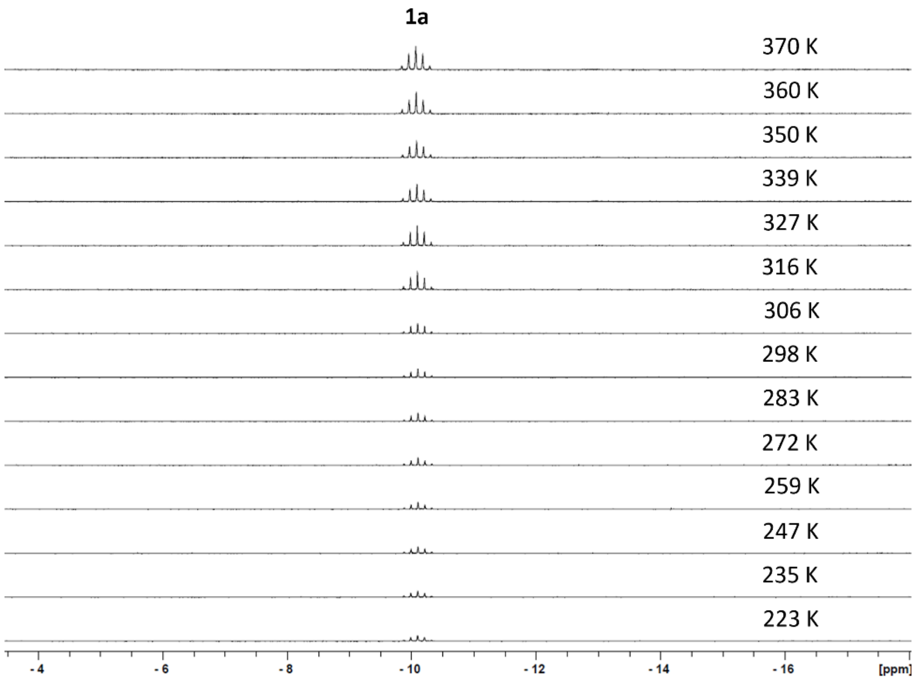

Figure S121. Expanded metal hydride region of variable temperature ^{1}H NMR spectra of a solution containing *cis* and *trans* isomers of [(dmpe)$_2$Mn(GeHPh$_2$)(N$_2$)] (**5a**) and *trans*-[(dmpe)$_2$MnH(=GePh$_2$)] (**1a**) formed from the reaction of **1a** and N$_2$ after 3 days in d_8-toluene (500 MHz, 298 K).

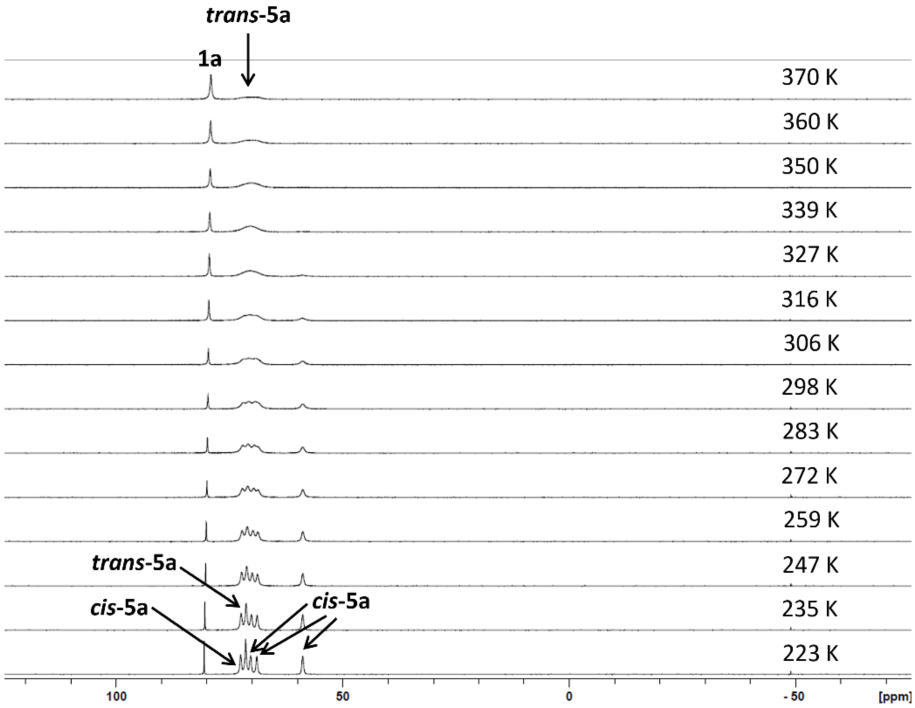

Figure S122. Variable temperature ^{31}P{^{1}H} NMR spectra of a solution containing *cis* and *trans* isomers of [(dmpe)$_2$Mn(GeHPh$_2$)(N$_2$)] (**5a**) and *trans*-[(dmpe)$_2$MnH(=GePh$_2$)] (**1a**) formed from the reaction of **1a** and N$_2$ after 3 days in d_8-toluene (202 MHz, 298 K).

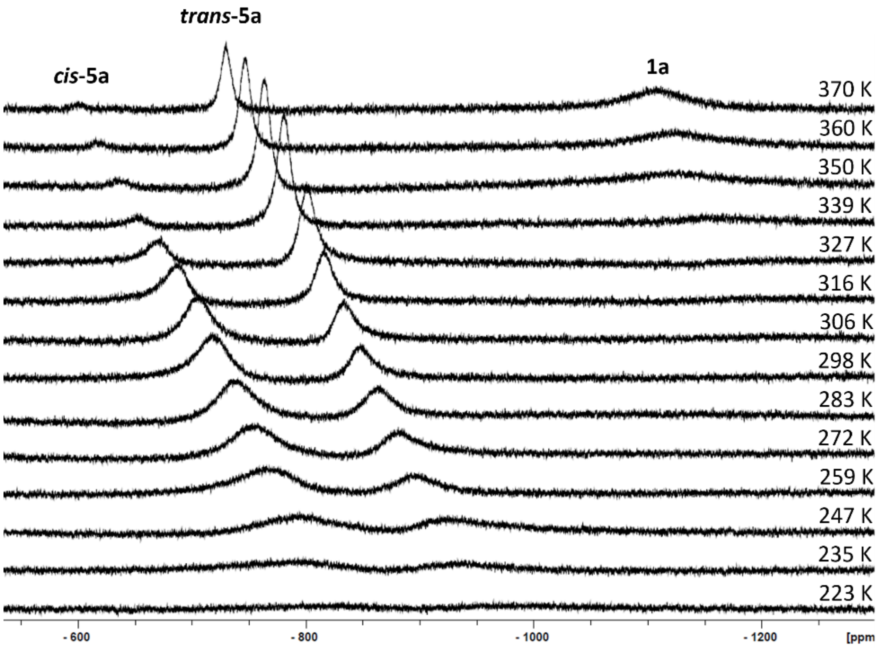

Figure S123. Variable temperature ^{55}Mn{^{1}H} NMR spectra of a solution containing *cis* and *trans* isomers of [(dmpe)$_2$Mn(GeHPh$_2$)(N$_2$)] (**5a**) and *trans*-[(dmpe)$_2$MnH(=GePh$_2$)] (**1a**) formed from the reaction of **1a** and N$_2$ after 3 days in d_8-toluene (124 MHz, 298 K).

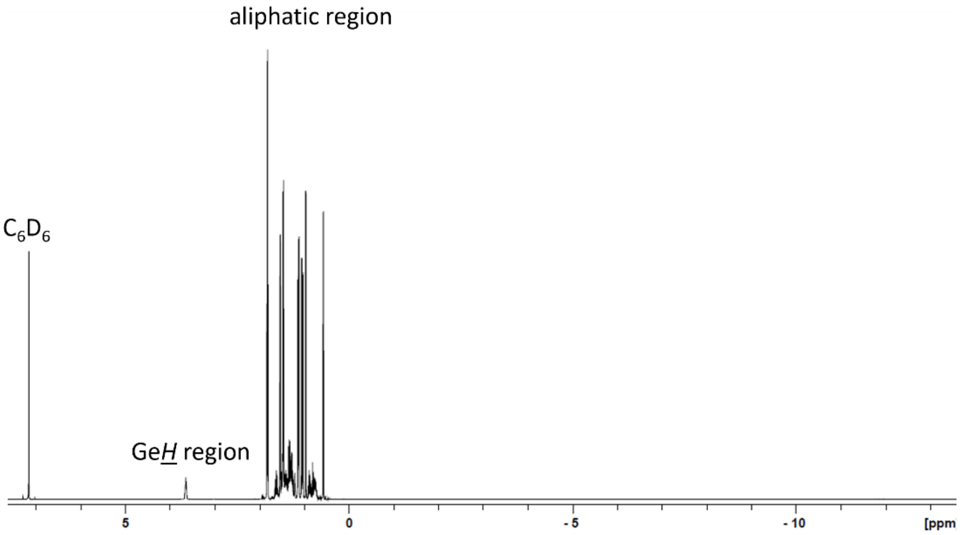

Figure S124. ^{1}H NMR spectrum of *cis*-[(dmpe)$_2$Mn(GeHEt$_2$)(N$_2$)] (***cis*-5b**) under an atmosphere of N$_2$ in C$_6$D$_6$ (600 MHz, 298 K).

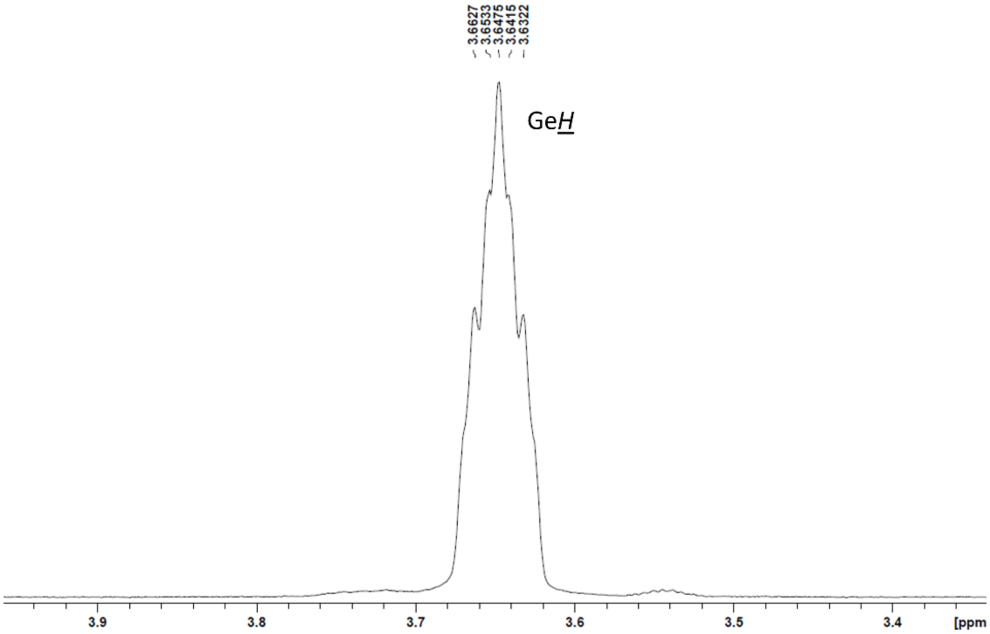

Figure S125. Expanded Ge*H* region of the ^{1}H NMR spectrum of *cis*-[(dmpe)$_2$Mn(GeHEt$_2$)(N$_2$)] (***cis*-5b**) under an atmosphere of N$_2$ in C$_6$D$_6$ (600 MHz, 298 K).

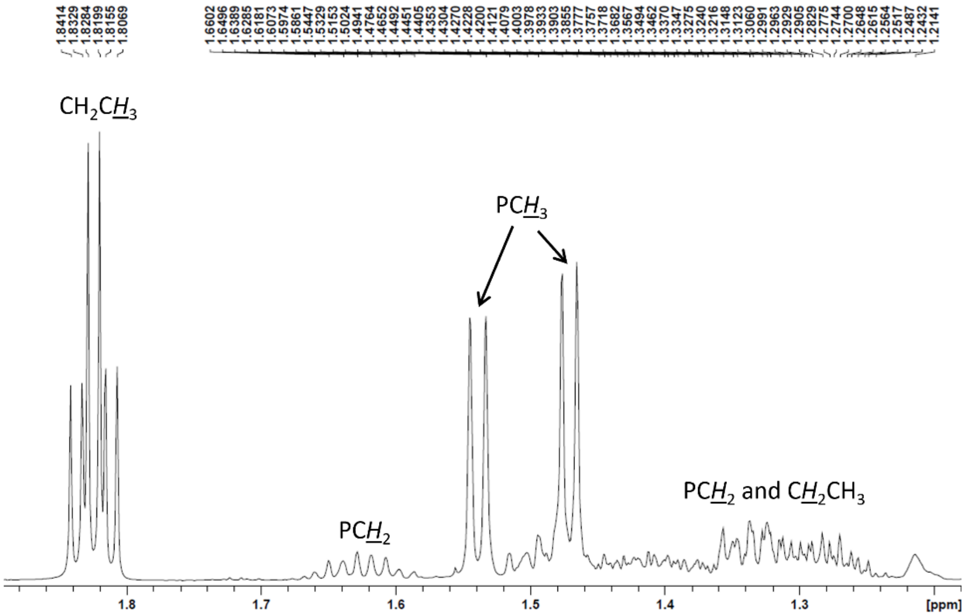

Figure S126. Expanded higher frequency aliphatic region of the ^{1}H NMR spectrum of *cis*-[(dmpe)$_2$Mn(GeHEt$_2$)(N$_2$)] (***cis*-5b**) under an atmosphere of N$_2$ in C$_6$D$_6$ (600 MHz, 298 K).

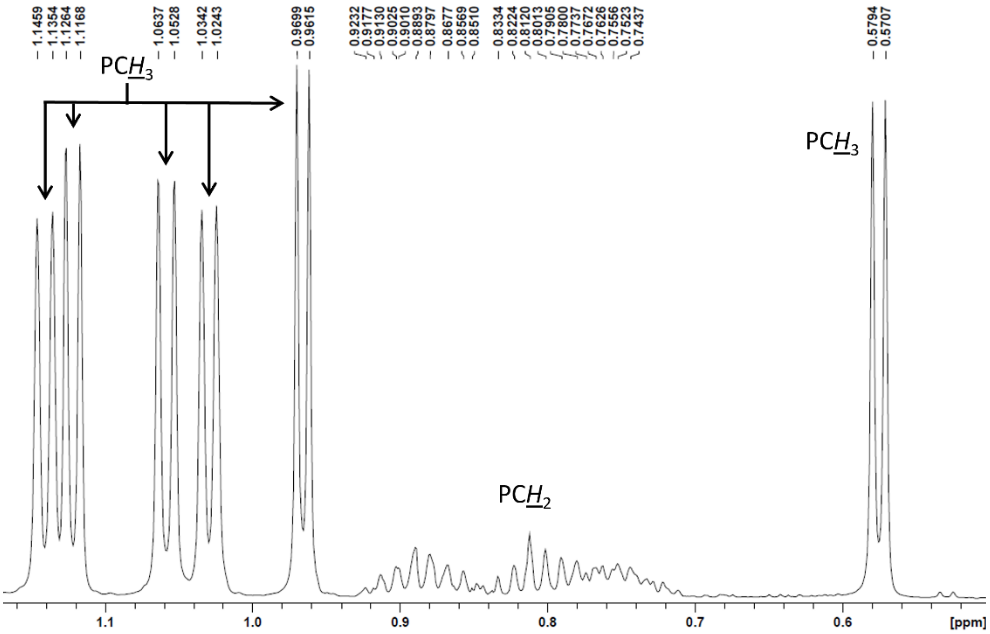

Figure S127. Expanded lower frequency aliphatic region of the ^{1}H NMR spectrum of *cis*-[(dmpe)$_2$Mn(GeHEt$_2$)(N$_2$)] (***cis*-5b**) under an atmosphere of N$_2$ in C$_6$D$_6$ (600 MHz, 298 K).

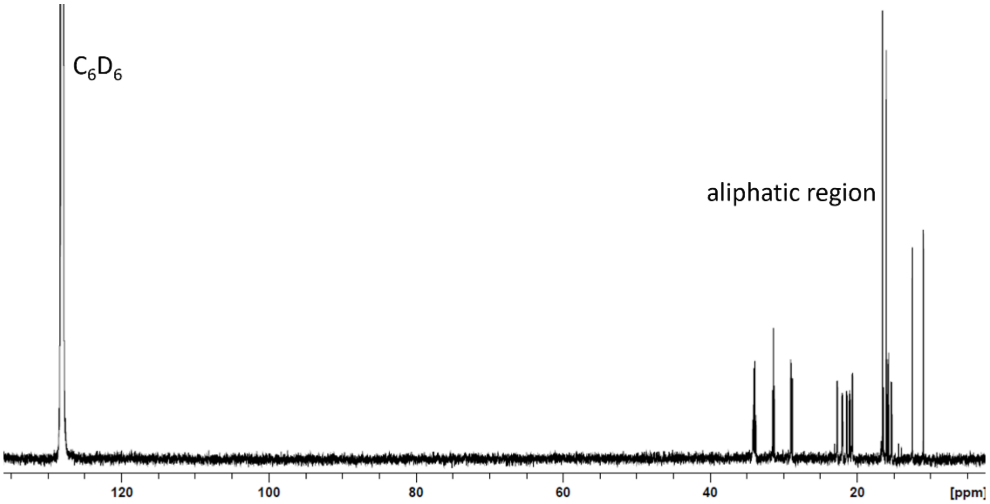

Figure S128. ^{13}C{^{1}H} NMR spectrum of *cis*-[(dmpe)$_2$Mn(GeHEt$_2$)(N$_2$)] (***cis*-5b**) under an atmosphere of N$_2$ in C$_6$D$_6$ (151 MHz, 298 K).

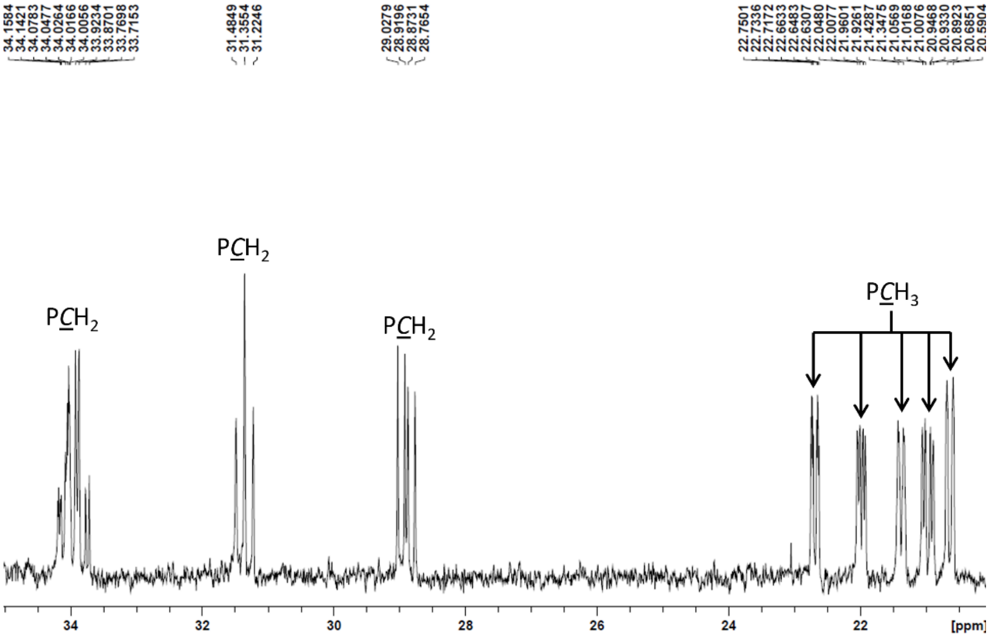

Figure S129. Expanded higher frequency aliphatic region of the $^{13}C\{^1H\}$ NMR spectrum of *cis*-[(dmpe)$_2$Mn(GeHEt$_2$)(N$_2$)] (***cis*-5b**) under an atmosphere of N_2 in C_6D_6 (151 MHz, 298 K).

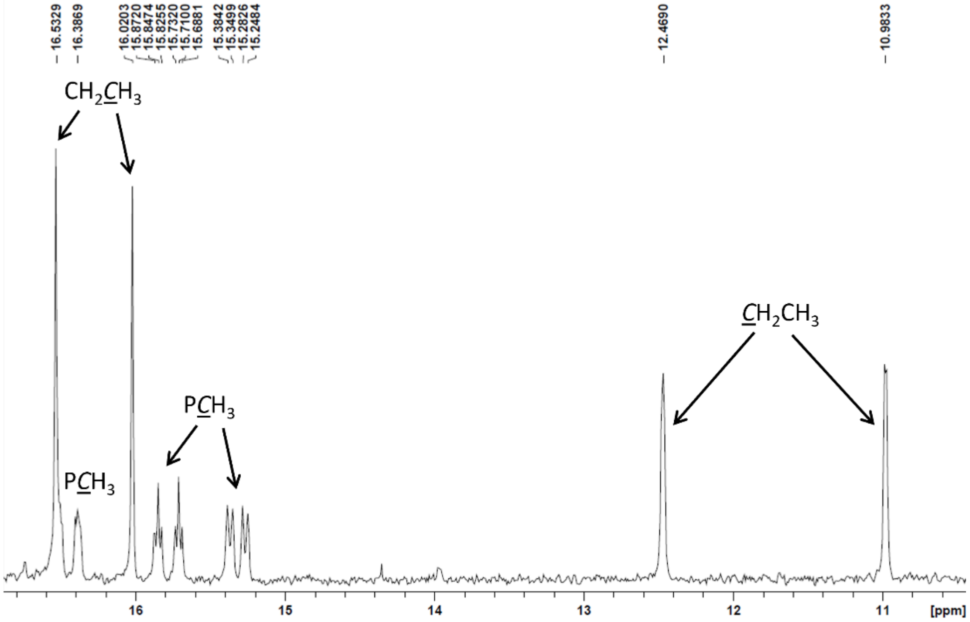

Figure S130. Expanded higher frequency aliphatic region of the $^{13}C\{^1H\}$ NMR spectrum of *cis*-[(dmpe)$_2$Mn(GeHEt$_2$)(N$_2$)] (***cis*-5b**) under an atmosphere of N_2 in C_6D_6 (151 MHz, 298 K).

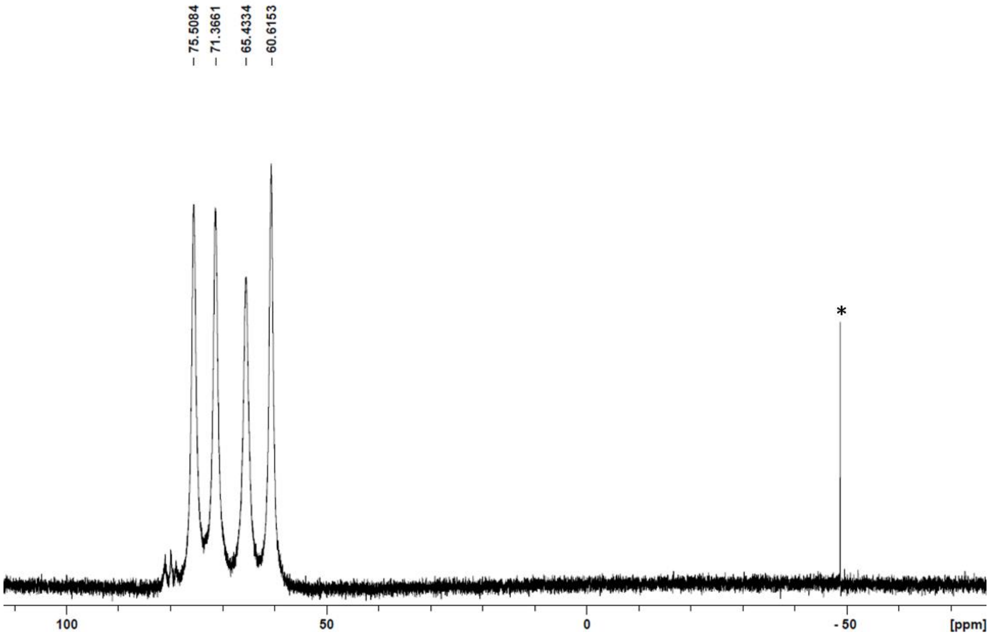

Figure S131. $^{31}P\{^1H\}$ NMR spectrum of *cis*-[(dmpe)$_2$Mn(GeHEt$_2$)(N$_2$)] (***cis*-5b**) under an atmosphere of N_2 in C_6D_6 (243 MHz, 298 K). * indicates a peak from free dmpe.

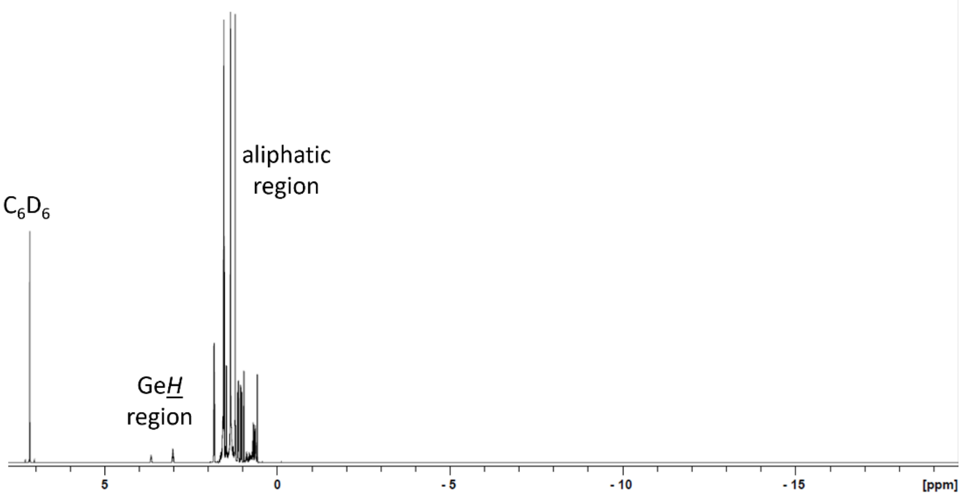

Figure S132. ^1H NMR spectrum of a solution containing *cis* and *trans* isomers of [(dmpe)$_2$Mn(GeHEt$_2$)(N$_2$)] (**5b**) formed from heating ***cis*-5b** under an atmosphere of N_2 for 1 day at 60 °C in C_6D_6 (600 MHz, 298 K).

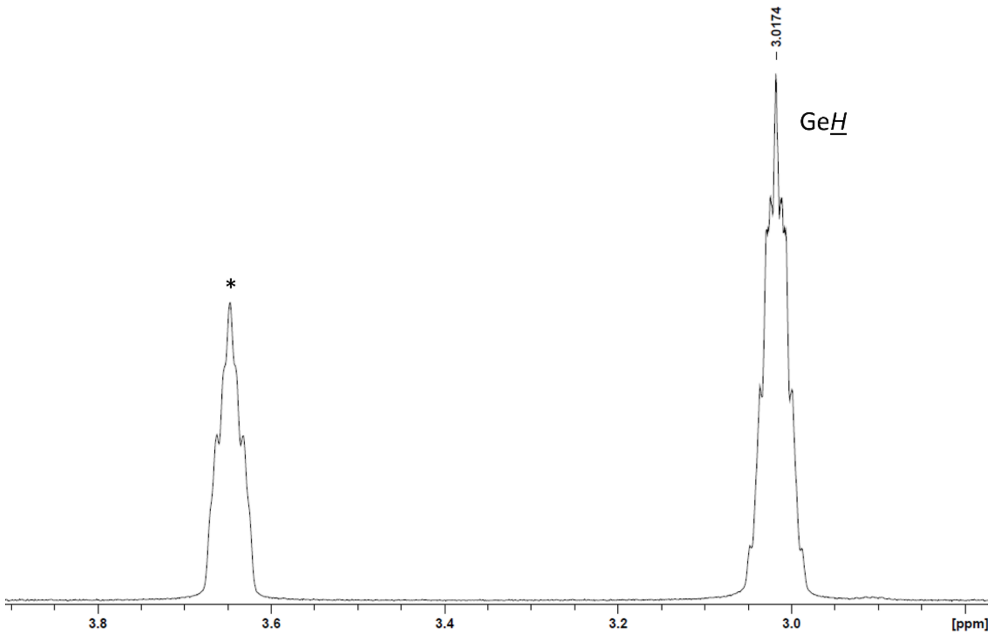

Figure S133. Expanded Ge*H* region of the ^{1}H NMR spectrum of a solution containing *cis* and *trans* isomers of [(dmpe)$_2$Mn(GeHEt$_2$)(N$_2$)] (**5b**) formed from heating ***cis*-5b** under an atmosphere of N$_2$ for 1 day at 60 °C in C$_6$D$_6$ (600 MHz, 298 K). * indicates a peak from ***cis*-5b** and the labelled peak is from ***trans*-5b**.

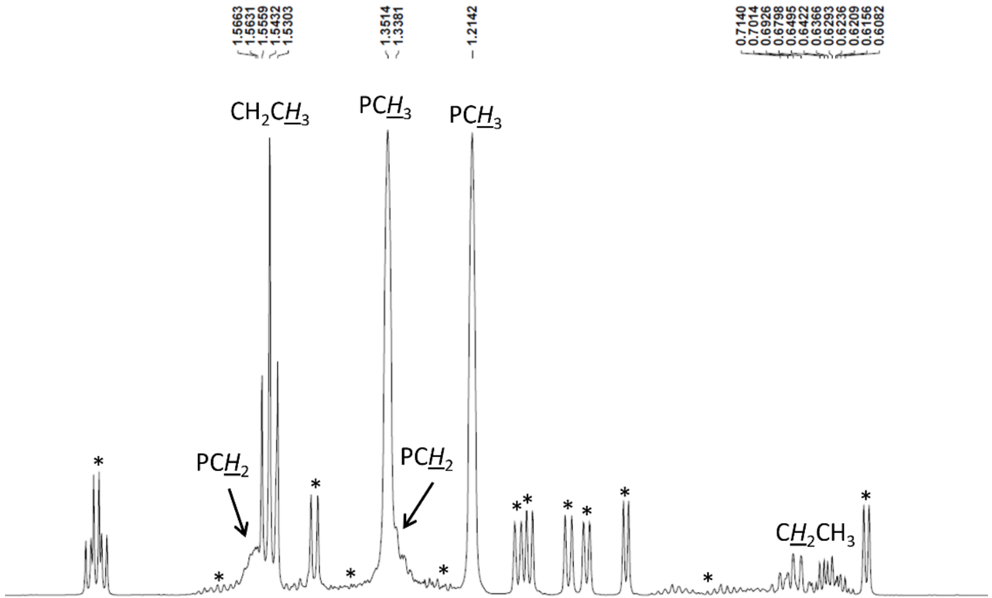

Figure S134. Expanded aliphatic region of the ^{1}H NMR spectrum of a solution containing *cis* and *trans* isomers of [(dmpe)$_2$Mn(GeHEt$_2$)(N$_2$)] (**5b**) formed from heating ***cis*-5b** under an atmosphere of N$_2$ for 1 day at 60 °C in C$_6$D$_6$ (600 MHz, 298 K). * indicates peaks from ***cis*-5b** and labelled peaks are from ***trans*-5b**.

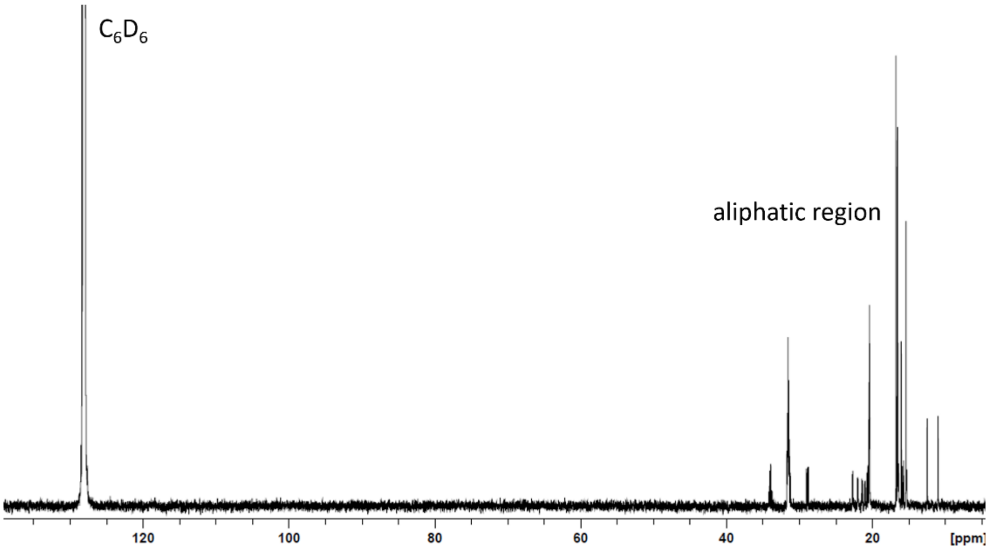

Figure S135. $^{13}C\{^1H\}$ NMR spectrum of a solution containing *cis* and *trans* isomers of $[(dmpe)_2Mn(GeHEt_2)(N_2)]$ (**5b**) formed from heating ***cis*-5b** under an atmosphere of N_2 for 1 day at 60 °C in C_6D_6 (151 MHz, 298 K).

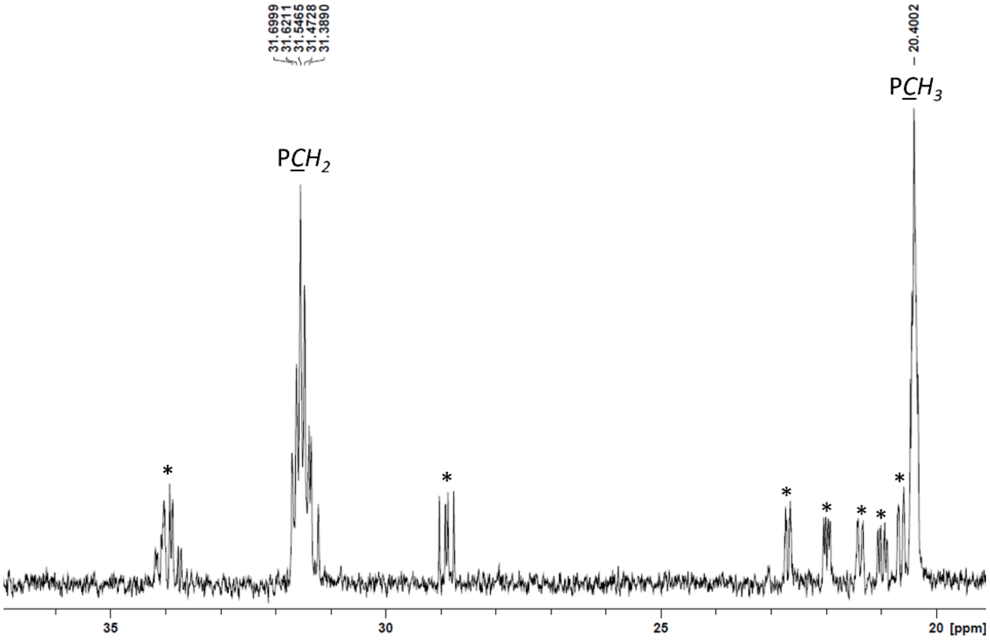

Figure S136. Expanded higher frequency aliphatic region of the $^{13}C\{^1H\}$ NMR spectrum of a solution containing *cis* and *trans* isomers of $[(dmpe)_2Mn(GeHEt_2)(N_2)]$ (**5b**) formed from heating ***cis*-5b** under an atmosphere of N_2 for 1 day at 60 °C in C_6D_6 (151 MHz, 298 K). * indicates peaks from ***cis*-5b** and labelled peaks are from ***trans*-5b**.

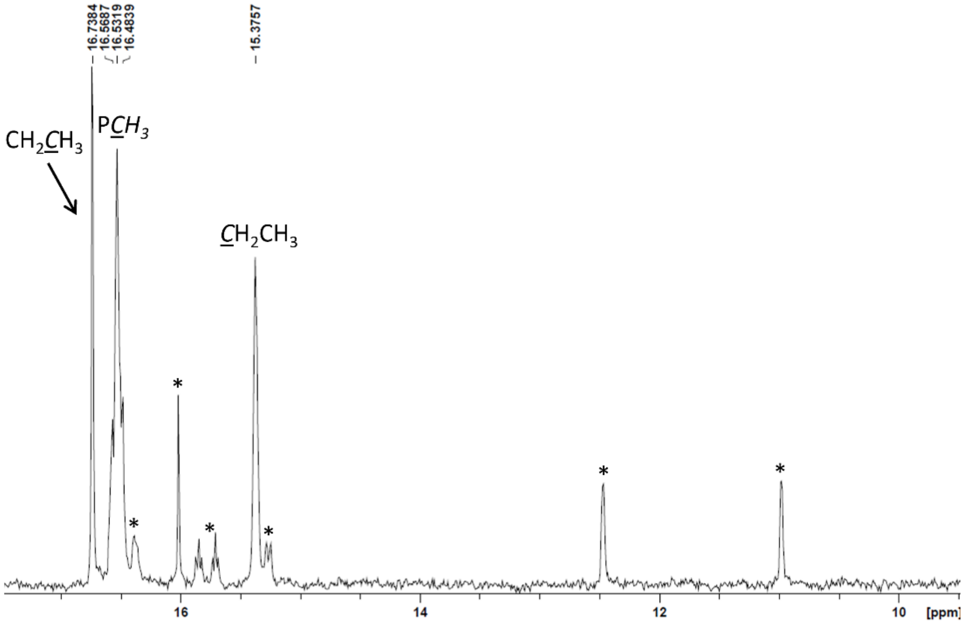

Figure S137. Expanded lower frequency aliphatic region of the $^{13}C\{^1H\}$ NMR spectrum of a solution containing *cis* and *trans* isomers of [(dmpe)$_2$Mn(GeHEt$_2$)(N$_2$)] (**5b**) formed from heating ***cis*-5b** under an atmosphere of N_2 for 1 day at 60 °C in C_6D_6 (151 MHz, 298 K). * indicates peaks from ***cis*-5b** and labelled peaks are from ***trans*-5b**.

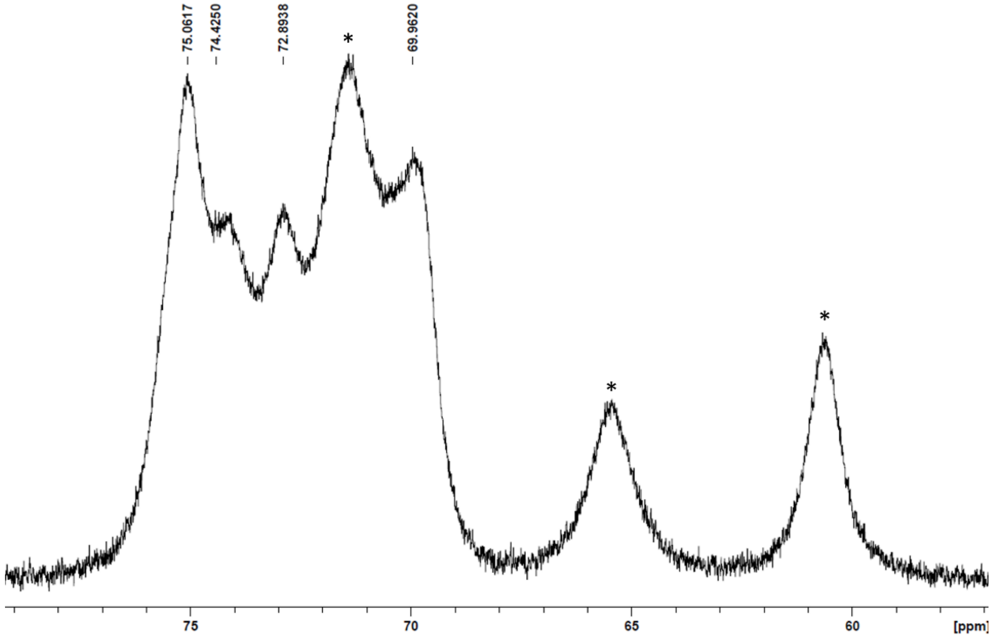

Figure S138. $^{31}P\{^1H\}$ NMR spectrum of a solution containing *cis* and *trans* isomers of [(dmpe)$_2$Mn(GeHEt$_2$)(N$_2$)] (**5b**) formed from heating ***cis*-5b** under an atmosphere of N_2 for 1 day at 60 °C in C_6D_6 (243 MHz, 298 K). * indicates peaks from ***cis*-5b**.

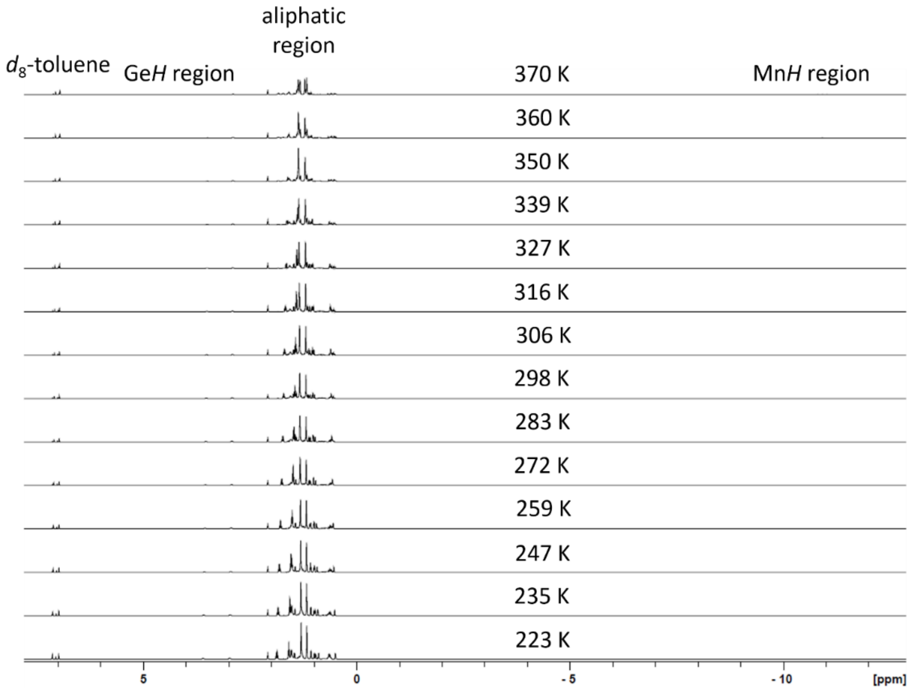

Figure S139. Variable temperature ^{1}H NMR spectra of a solution containing *cis* and *trans* isomers of $[(dmpe)_2Mn(GeHEt_2)(N_2)]$ (**5b**) and (at high temperatures only) *trans*-$[(dmpe)_2MnH(=GeEt_2)]$ (**1b**) formed from heating ***cis*-5b** under an atmosphere of N_2 for 1 day at 60 °C in d_8-toluene (500 MHz).

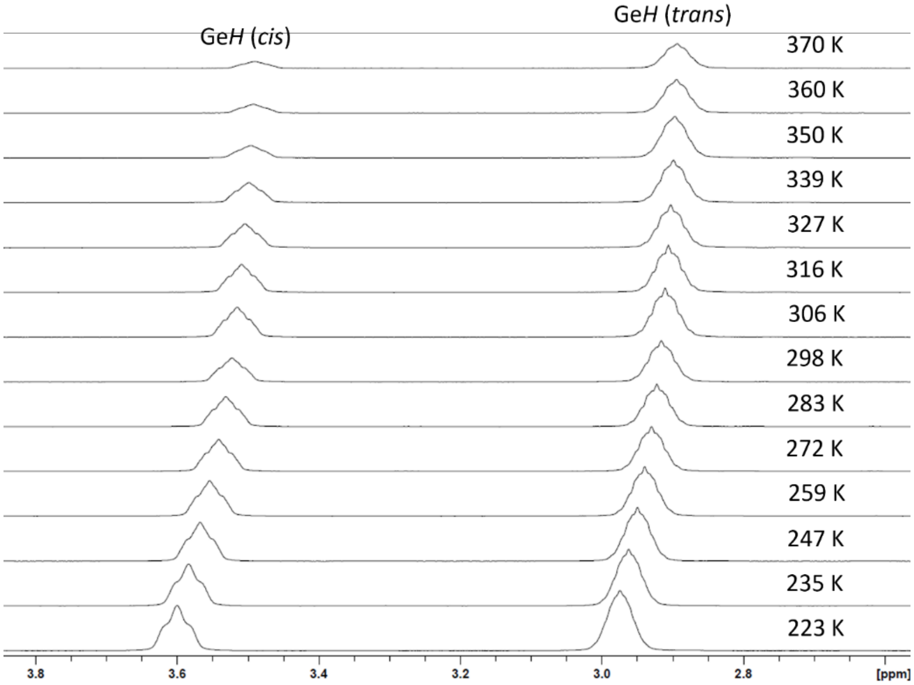

Figure S140. Expanded Ge*H* region of variable temperature ^{1}H NMR spectra of a solution containing *cis* and *trans* isomers of $[(dmpe)_2Mn(GeHEt_2)(N_2)]$ (**5b**) and (at high temperatures only) *trans*-$[(dmpe)_2MnH(=GeEt_2)]$ (**1b**) formed from heating ***cis*-5b** under an atmosphere of N_2 for 1 day at 60 °C in d_8-toluene (500 MHz).

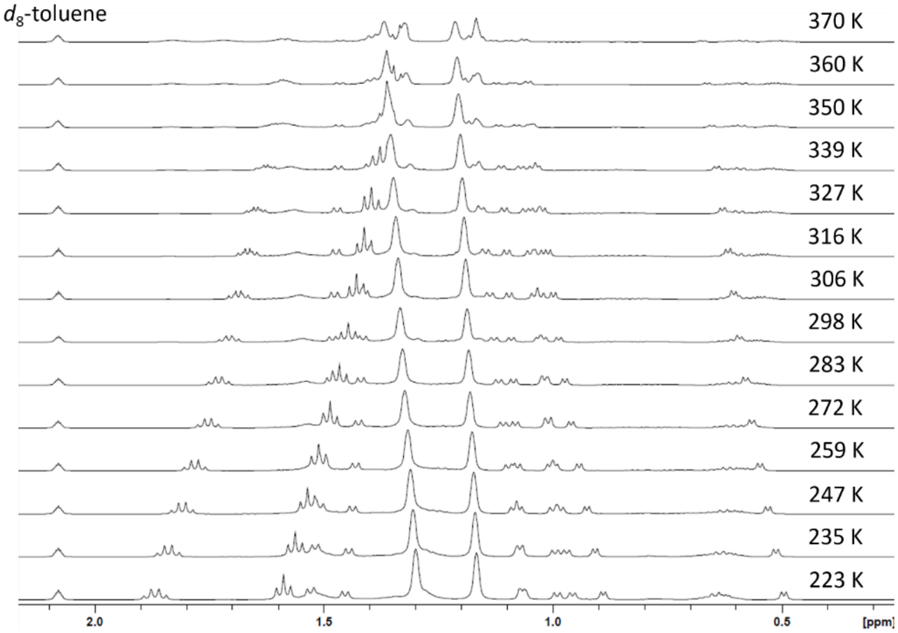

Figure S141. Expanded aliphatic region of variable temperature ^{1}H NMR spectra of a solution containing *cis* and *trans* isomers of [(dmpe)$_2$Mn(GeHEt$_2$)(N$_2$)] (**5b**) and (at high temperatures only) *trans*-[(dmpe)$_2$MnH(=GeEt$_2$)] (**1b**) formed from heating ***cis*-5b** under an atmosphere of N$_2$ for 1 day at 60 °C in d_8-toluene (500 MHz).

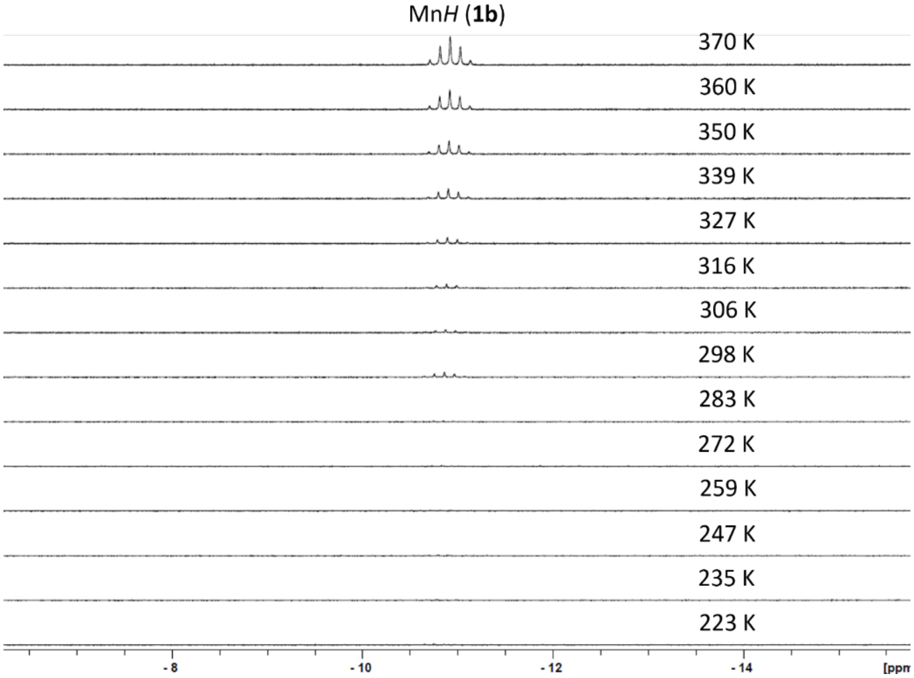

Figure S142. Expanded Mn*H* region of variable temperature ^{1}H NMR spectra of a solution containing *cis* and *trans* isomers of [(dmpe)$_2$Mn(GeHEt$_2$)(N$_2$)] (**5b**) and (at high temperatures only) *trans*-[(dmpe)$_2$MnH(=GeEt$_2$)] (**1b**) formed from heating ***cis*-5b** under an atmosphere of N$_2$ for 1 day at 60 °C in d_8-toluene (500 MHz).

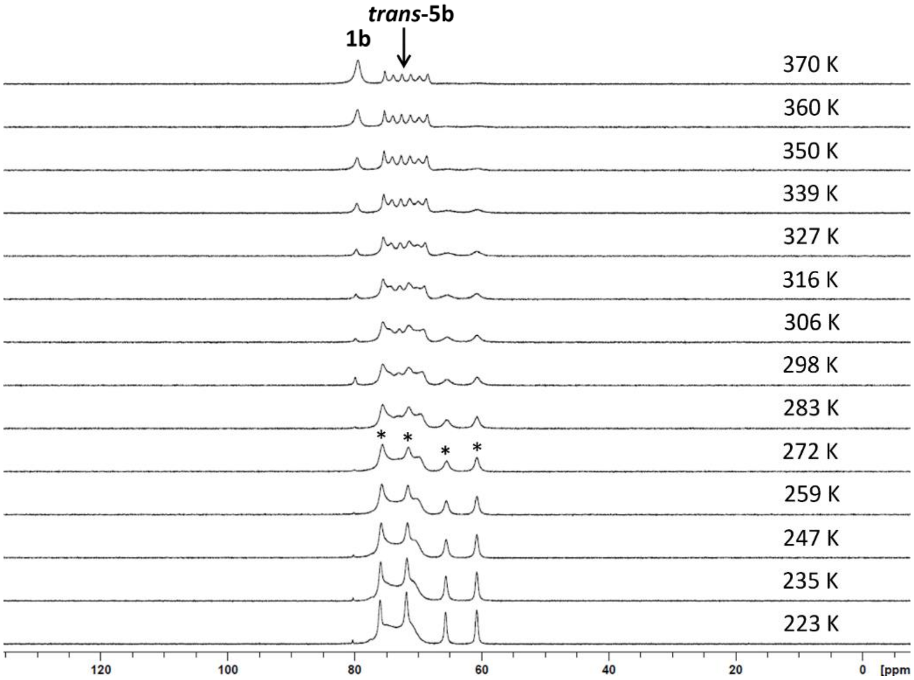

Figure S143. Variable temperature $^{31}P\{^1H\}$ NMR spectra of a solution containing *cis* and *trans* isomers of $[(dmpe)_2Mn(GeHEt_2)(N_2)]$ (**5b**) and (at high temperatures only) *trans*-$[(dmpe)_2MnH(=GeEt_2)]$ (**1b**) formed from heating ***cis*-5b** under an atmosphere of N_2 for 1 day at 60 °C in d_8-toluene (202 MHz). * indicates peaks from ***cis*-5b**.

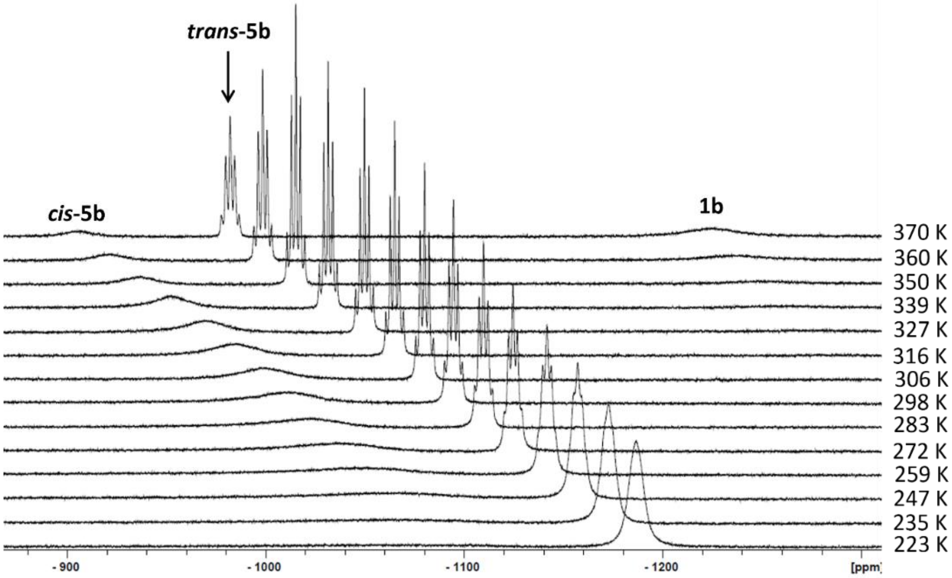

Figure S144. Variable temperature $^{55}Mn\{^1H\}$ NMR spectra of a solution containing *cis* and *trans* isomers of $[(dmpe)_2Mn(GeHEt_2)(N_2)]$ (**5b**) and (at high temperatures only) *trans*-$[(dmpe)_2MnH(=GeEt_2)]$ (**1b**) formed from heating ***cis*-5b** under an atmosphere of N_2 for 1 day at 60 °C in d_8-toluene (124 MHz).

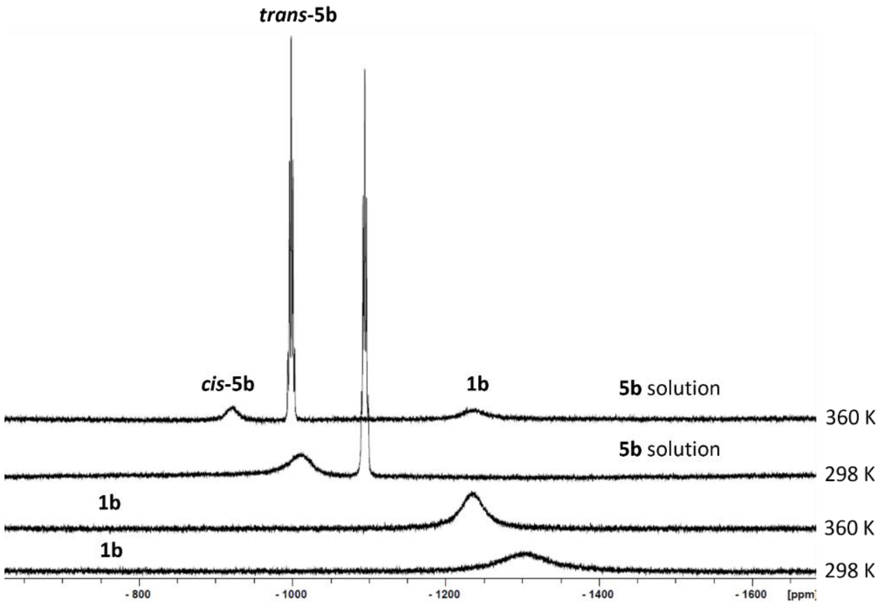

Figure S145. Top: $^{55}Mn\{^1H\}$ NMR spectra of a solution containing *cis* and *trans* isomers of [(dmpe)$_2$Mn(GeHEt$_2$)(N$_2$)] (**5b**) and (at 360 K only) *trans*-[(dmpe)$_2$MnH(=GeEt$_2$)] (**1b**) formed from heating ***cis*-5b** under an atmosphere of N$_2$ for 1 day at 60 °C in d_8-toluene (124 MHz; 298 and 360 K). Bottom: $^{55}Mn\{^1H\}$ NMR spectra of *trans*-[(dmpe)$_2$MnH(=GeEt$_2$)] (**1b**) in d_8-toluene (124 MHz; 298 and 360 K).

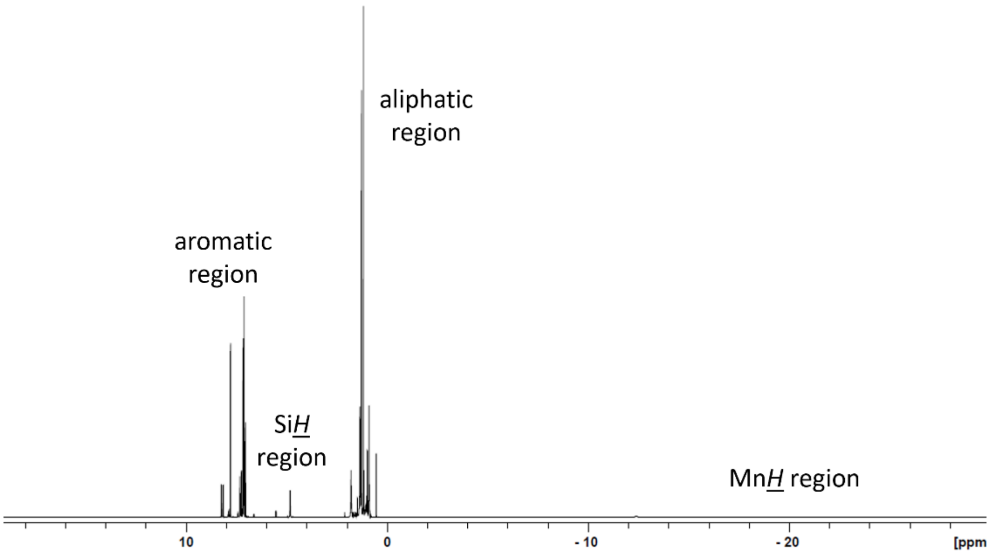

Figure S146. ^1H NMR spectrum of *cis* and *trans* isomers of [(dmpe)$_2$Mn(SiHPh$_2$)(N$_2$)] (**6**), along with [(dmpe)$_2$MnH$_2$(SiHPh$_2$)], under an atmosphere of N$_2$ in C_6D_6 (600 MHz, 298 K).

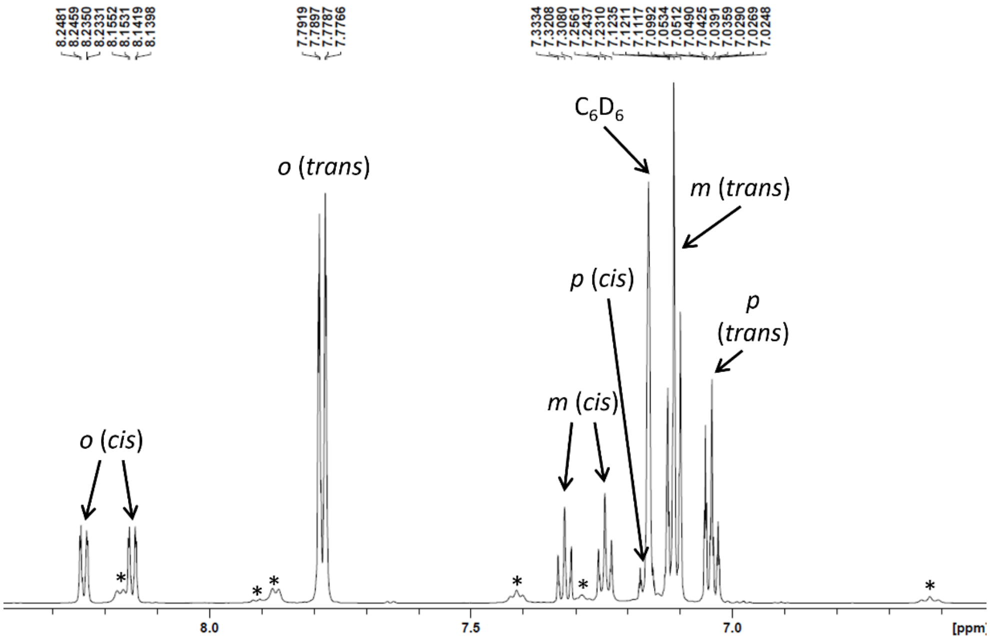

Figure S147. Expanded aromatic region of the ^{1}H NMR spectrum of *cis* and *trans* isomers of [(dmpe)$_2$Mn(SiHPh$_2$)(N$_2$)] (**6**), along with [(dmpe)$_2$MnH$_2$(SiHPh$_2$)], under an atmosphere of N_2 in C_6D_6 (600 MHz, 298 K). * indicates peaks from [(dmpe)$_2$MnH$_2$(SiHPh$_2$)] present in the starting material and labelled peaks are from **6**.

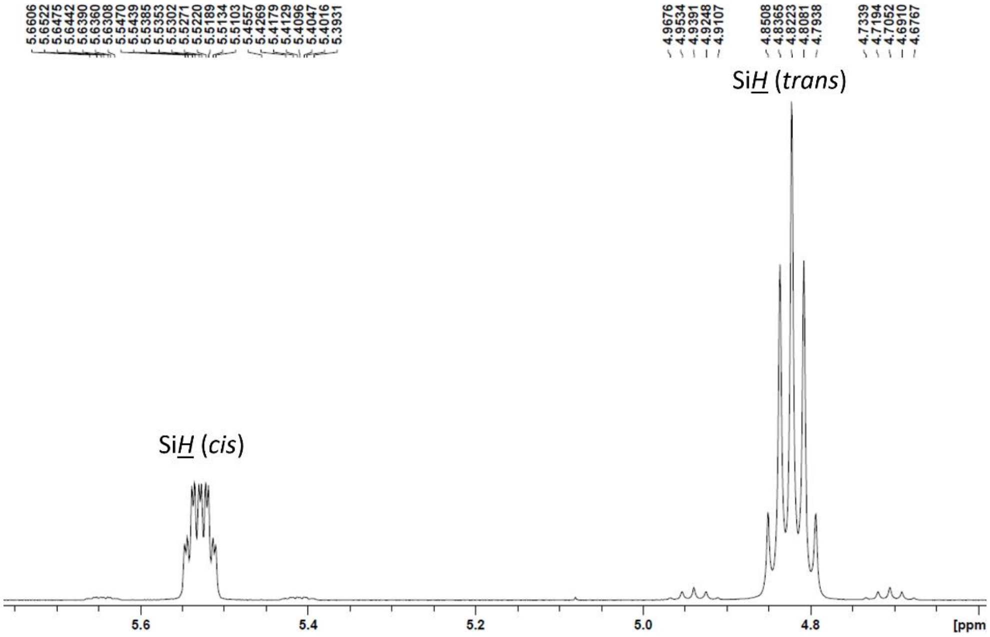

Figure S148. Expanded Si*H* region of the ^{1}H NMR spectrum of *cis* and *trans* isomers of [(dmpe)$_2$Mn(SiHPh$_2$)(N$_2$)] (**6**), along with [(dmpe)$_2$MnH$_2$(SiHPh$_2$)], under an atmosphere of N_2 in C_6D_6 (600 MHz, 298 K).

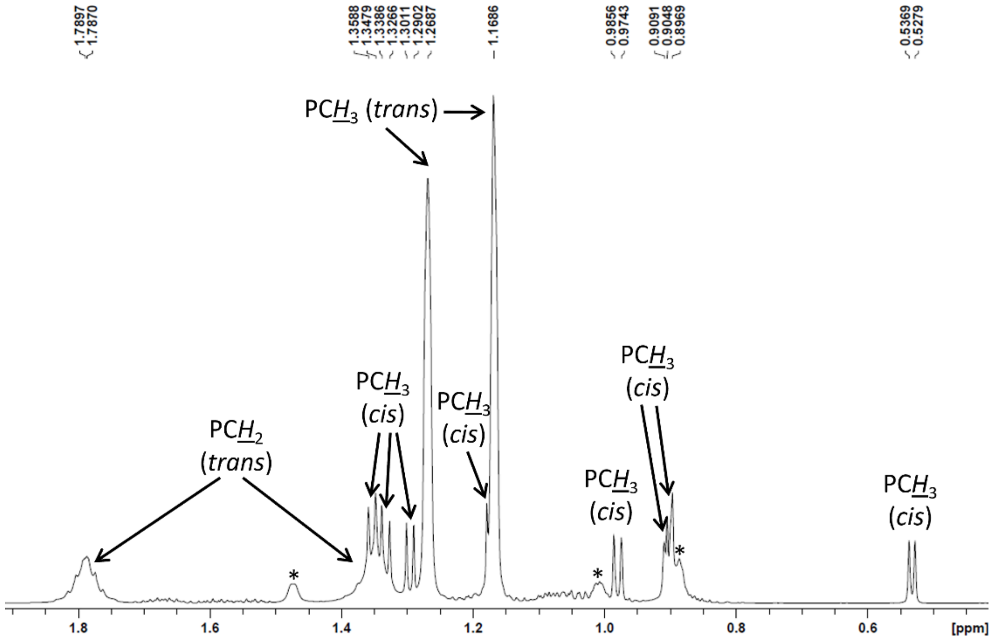

Figure S149. Expanded aliphatic region of the ^{1}H NMR spectrum of *cis* and *trans* isomers of [(dmpe)$_2$Mn(SiHPh$_2$)(N$_2$)] (**6**), along with [(dmpe)$_2$MnH$_2$(SiHPh$_2$)], under an atmosphere of N$_2$ in C$_6$D$_6$ (600 MHz, 298 K). * indicates peaks from [(dmpe)$_2$MnH$_2$(SiHPh$_2$)] present in the starting material and labelled peaks are from **6**.

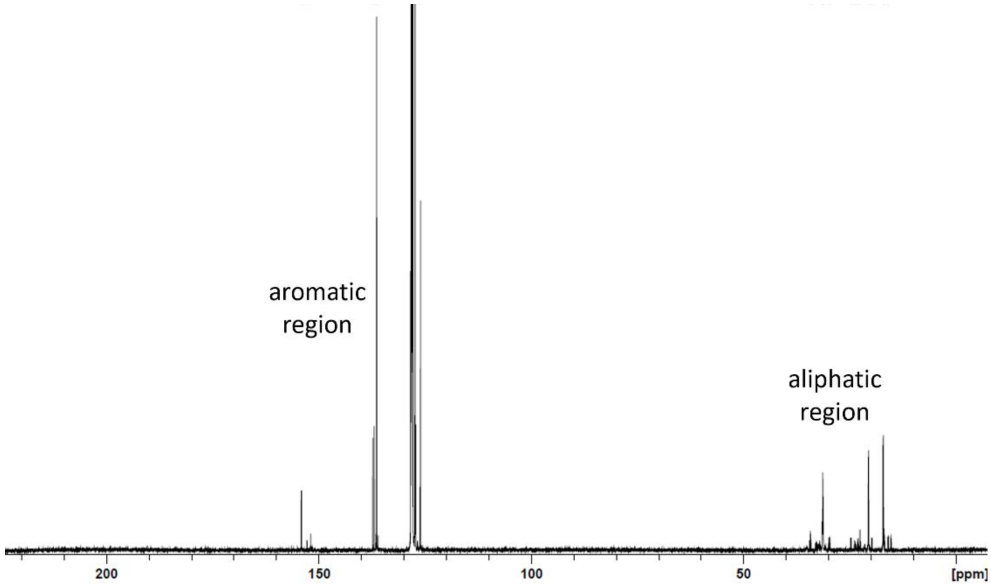

Figure S150. ^{13}C{^{1}H} NMR spectrum of *cis* and *trans* isomers of [(dmpe)$_2$Mn(SiHPh$_2$)(N$_2$)] (**6**), along with [(dmpe)$_2$MnH$_2$(SiHPh$_2$)], under an atmosphere of N$_2$ in C$_6$D$_6$ (151 MHz, 298 K).

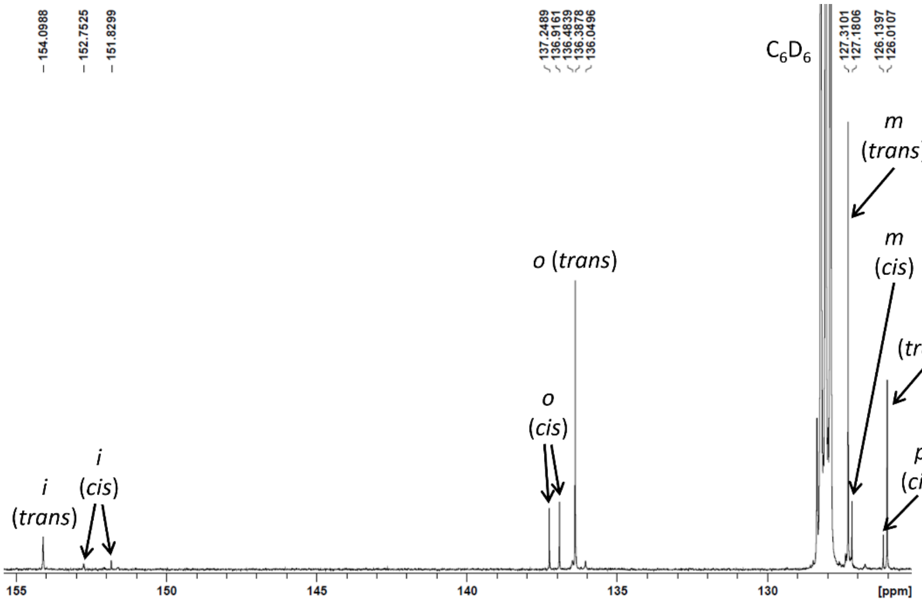

Figure S151. Expanded aliphatic region of the $^{13}C\{^1H\}$ NMR spectrum of *cis* and *trans* isomers of $[(dmpe)_2Mn(SiHPh_2)(N_2)]$ (**6**), along with $[(dmpe)_2MnH_2(SiHPh_2)]$, under an atmosphere of N_2 in C_6D_6 (151 MHz, 298 K).

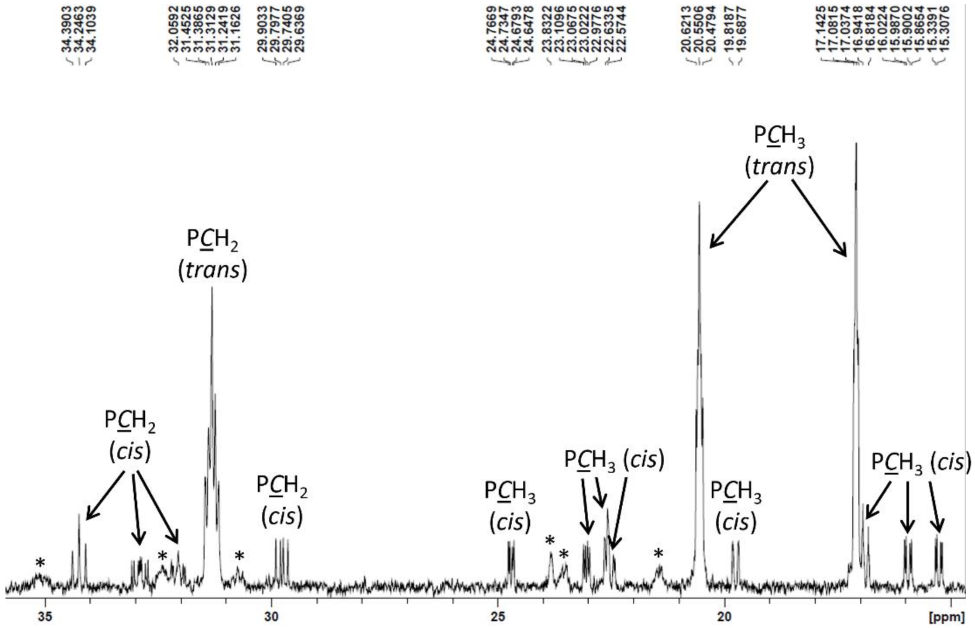

Figure S152. Expanded aliphatic region of the $^{13}C\{^1H\}$ NMR spectrum of *cis* and *trans* isomers of $[(dmpe)_2Mn(SiHPh_2)(N_2)]$ (**6**), along with $[(dmpe)_2MnH_2(SiHPh_2)]$, under an atmosphere of N_2 in C_6D_6 (151 MHz, 298 K). * indicates peaks from $[(dmpe)_2MnH_2(SiHPh_2)]$ present in the starting material and labelled peaks are from **6**.

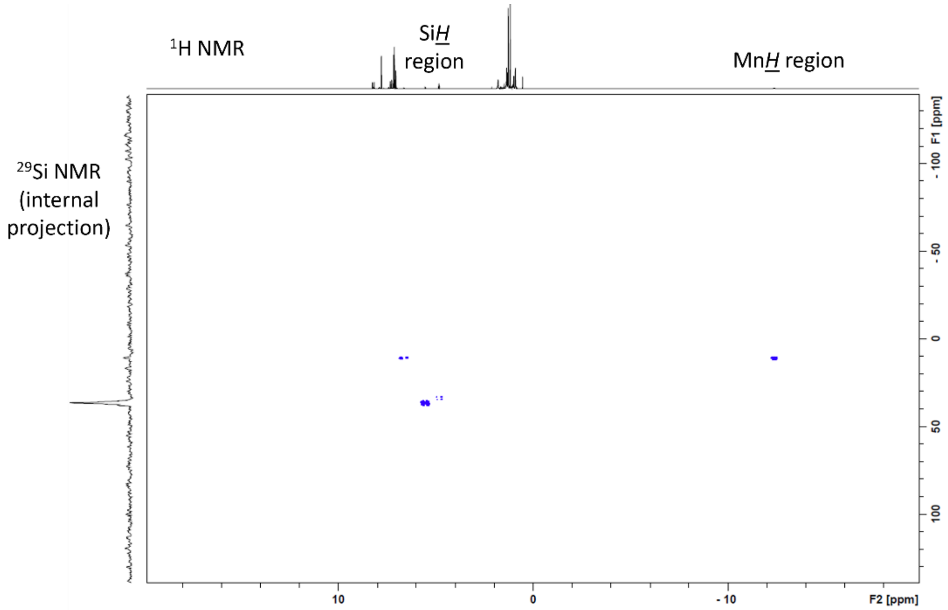

Figure S153. ^{1}H–^{29}Si HMBC NMR spectrum of *cis* and *trans* isomers of [(dmpe)$_2$Mn(SiHPh$_2$)(N$_2$)] (**6**), along with [(dmpe)$_2$MnH$_2$(SiHPh$_2$)], under an atmosphere of N$_2$ in C$_6$D$_6$ (119 MHz, 298 K).

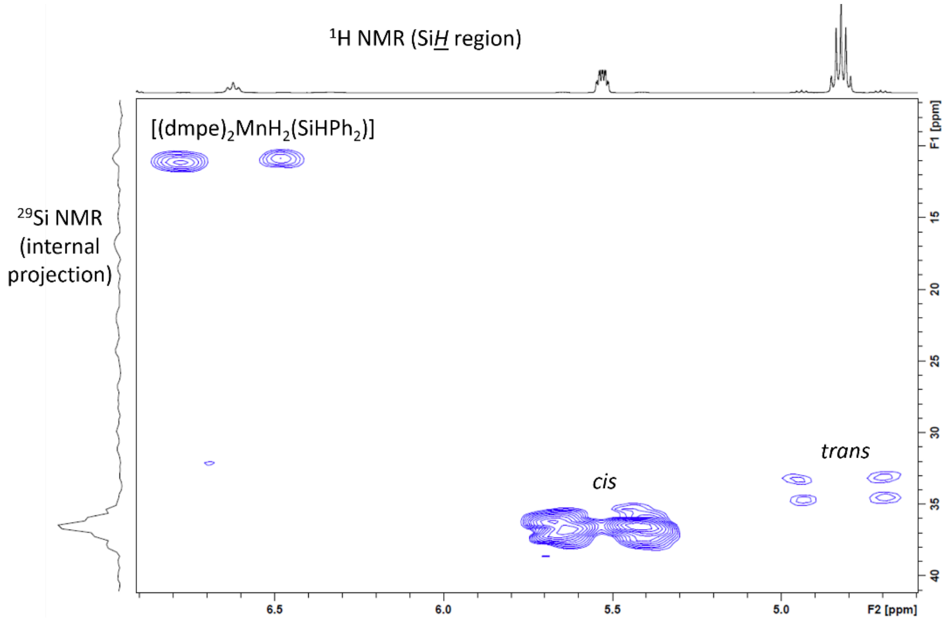

Figure S154. Expanded Si*H* region of the ^{1}H–^{29}Si HMBC NMR spectrum of *cis* and *trans* isomers of [(dmpe)$_2$Mn(SiHPh$_2$)(N$_2$)] (**6**), along with [(dmpe)$_2$MnH$_2$(SiHPh$_2$)], under an atmosphere of N$_2$ in C$_6$D$_6$ (119 MHz, 298 K).

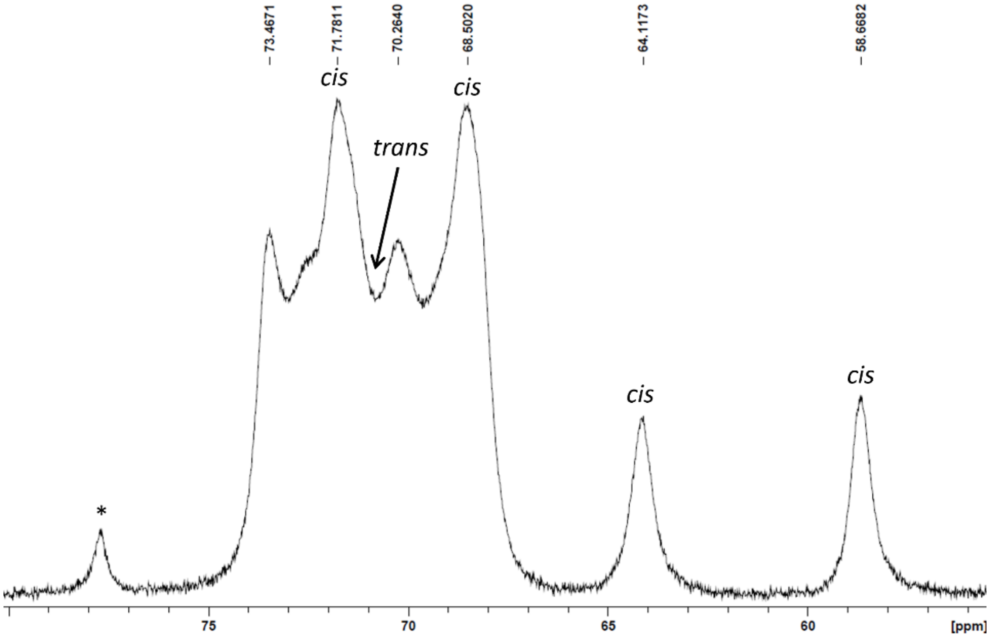

Figure S155. $^{31}P\{^{1}H\}$ NMR spectrum of *cis* and *trans* isomers of [(dmpe)$_2$Mn(SiHPh$_2$)(N$_2$)] (**6**), along with [(dmpe)$_2$MnH$_2$(SiHPh$_2$)], under an atmosphere of N$_2$ in C$_6$D$_6$ (243 MHz, 298 K). * indicates a peak from [(dmpe)$_2$MnH$_2$(SiHPh$_2$)] present in the starting material and labelled peaks are from **6**.

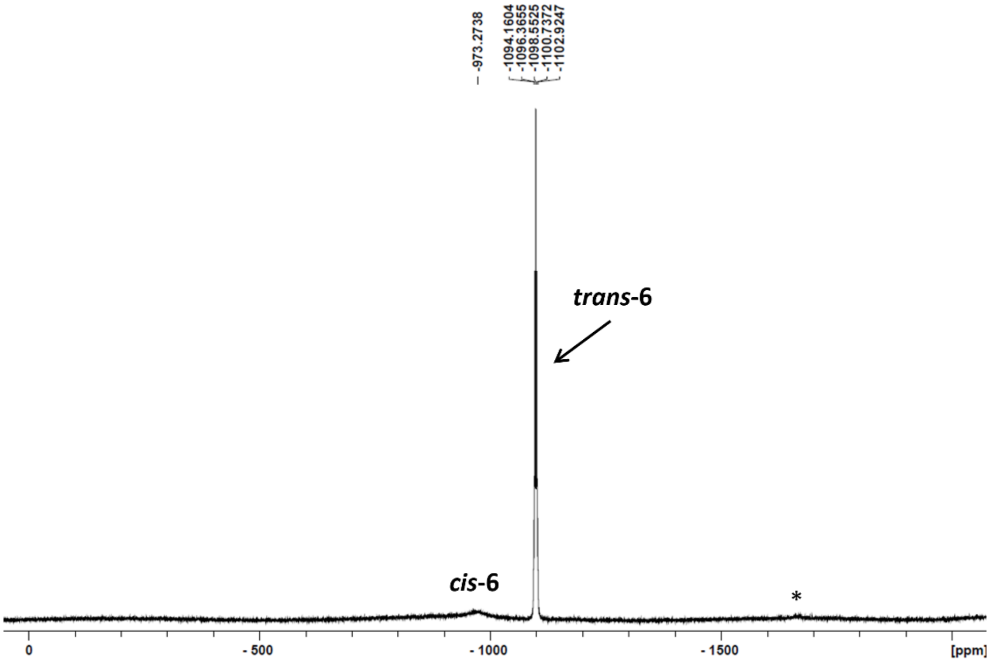

Figure S156. $^{55}Mn\{^{1}H\}$ NMR spectrum of *cis* and *trans* isomers of [(dmpe)$_2$Mn(SiHPh$_2$)(N$_2$)] (**6**), along with [(dmpe)$_2$MnH$_2$(SiHPh$_2$)], under an atmosphere of N$_2$ in C$_6$D$_6$ (124 MHz, 298 K). * indicates a peak from [(dmpe)$_2$MnH$_2$(SiHPh$_2$)] present in the starting material and labelled peaks are from **6**.

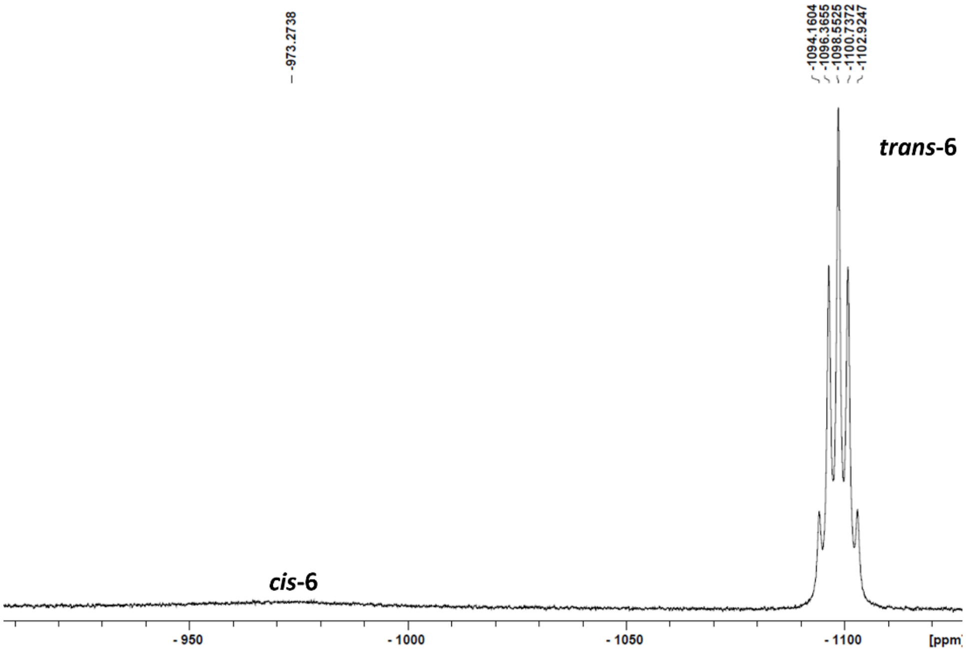

Figure S157. Expanded complex **6** region of the $^{55}Mn\{^1H\}$ NMR spectrum of *cis* and *trans* isomers of $[(dmpe)_2Mn(SiHPh_2)(N_2)]$ (**6**), along with $[(dmpe)_2MnH_2(SiHPh_2)]$, under an atmosphere of N_2 in C_6D_6 (124 MHz, 298 K).

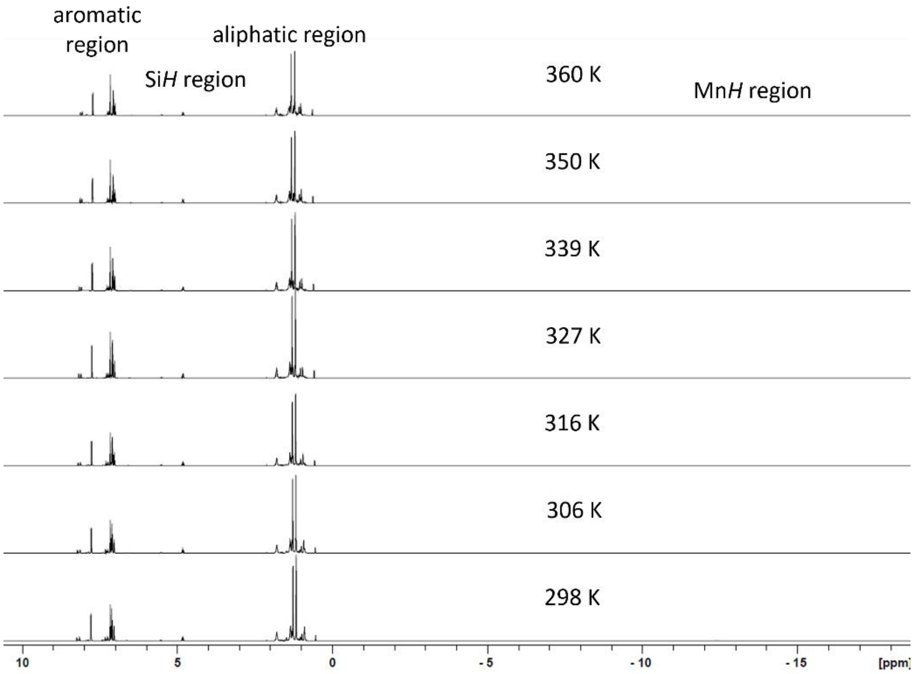

Figure S158. Variable temperature ^1H NMR spectra of a solution containing *cis* and *trans* isomers of $[(dmpe)_2Mn(SiHPh_2)(N_2)]$ (**6**), along with $[(dmpe)_2MnH_2(SiHPh_2)]$, under an atmosphere of N_2 in C_6D_6 (500 MHz).

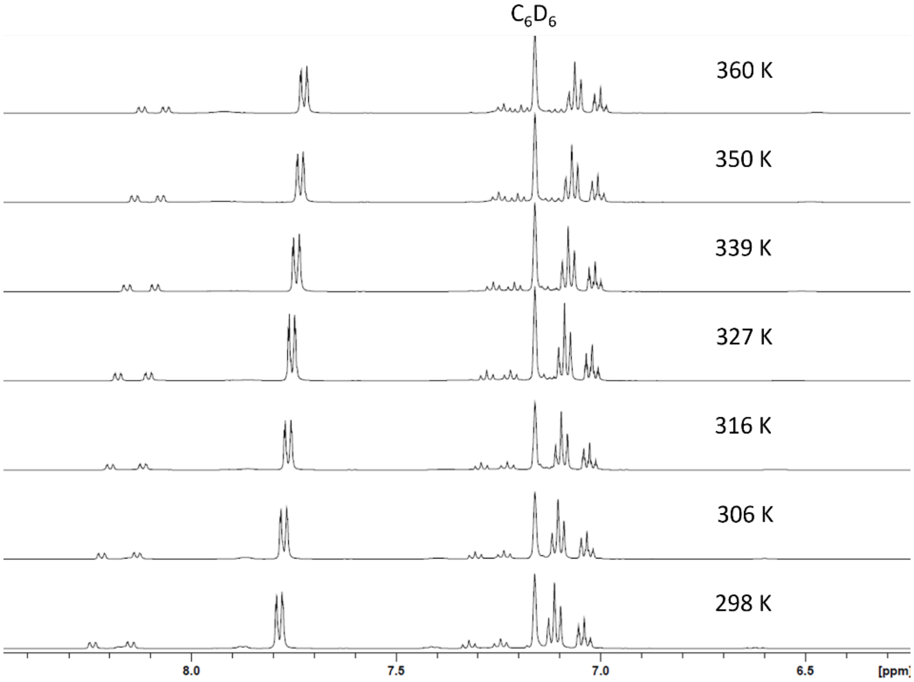

Figure S159. Expanded aromatic region of variable temperature ^1H NMR spectra of a solution containing *cis* and *trans* isomers of [(dmpe)$_2$Mn(SiHPh$_2$)(N$_2$)] (**6**), along with [(dmpe)$_2$MnH$_2$(SiHPh$_2$)], under an atmosphere of N_2 in C_6D_6 (500 MHz).

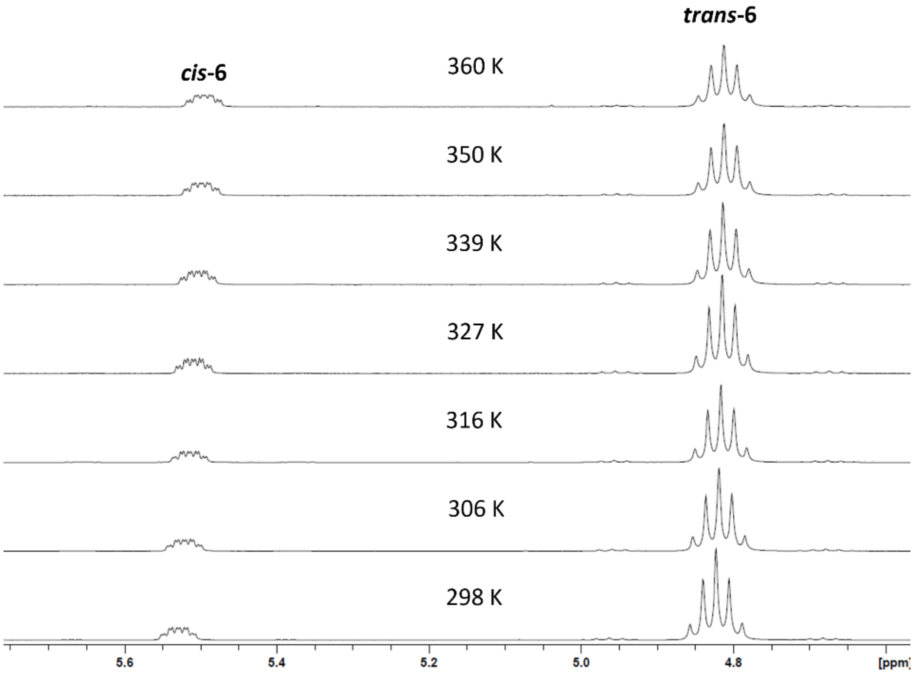

Figure S160. Expanded Si*H* region of variable temperature ^1H NMR spectra of a solution containing *cis* and *trans* isomers of [(dmpe)$_2$Mn(SiHPh$_2$)(N$_2$)] (**6**), along with [(dmpe)$_2$MnH$_2$(SiHPh$_2$)], under an atmosphere of N_2 in C_6D_6 (500 MHz).

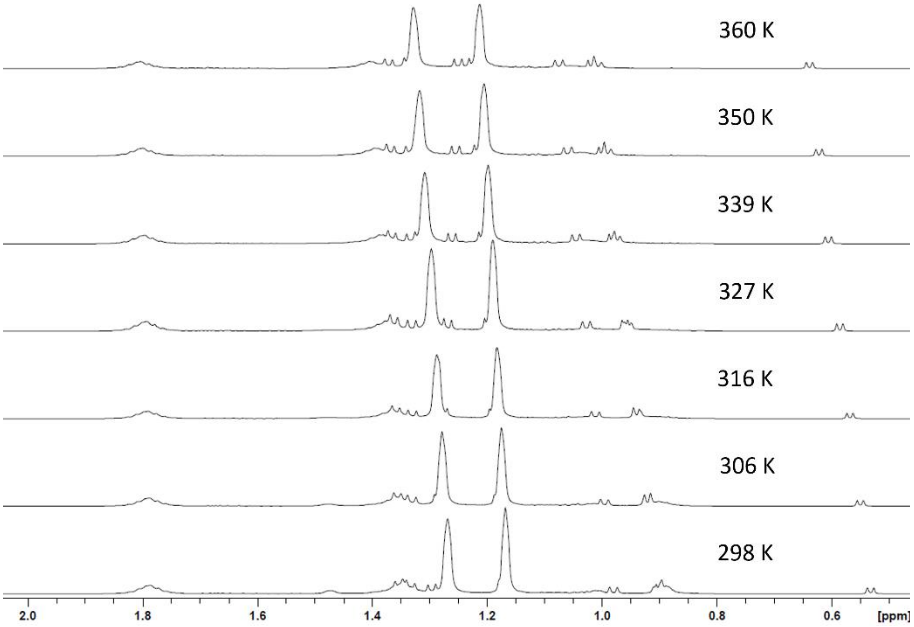

Figure S161. Expanded aliphatic region of variable temperature ^{1}H NMR spectra of a solution containing *cis* and *trans* isomers of [(dmpe)$_2$Mn(SiHPh$_2$)(N$_2$)] (**6**), along with [(dmpe)$_2$MnH$_2$(SiHPh$_2$)], under an atmosphere of N$_2$ in C$_6$D$_6$ (500 MHz).

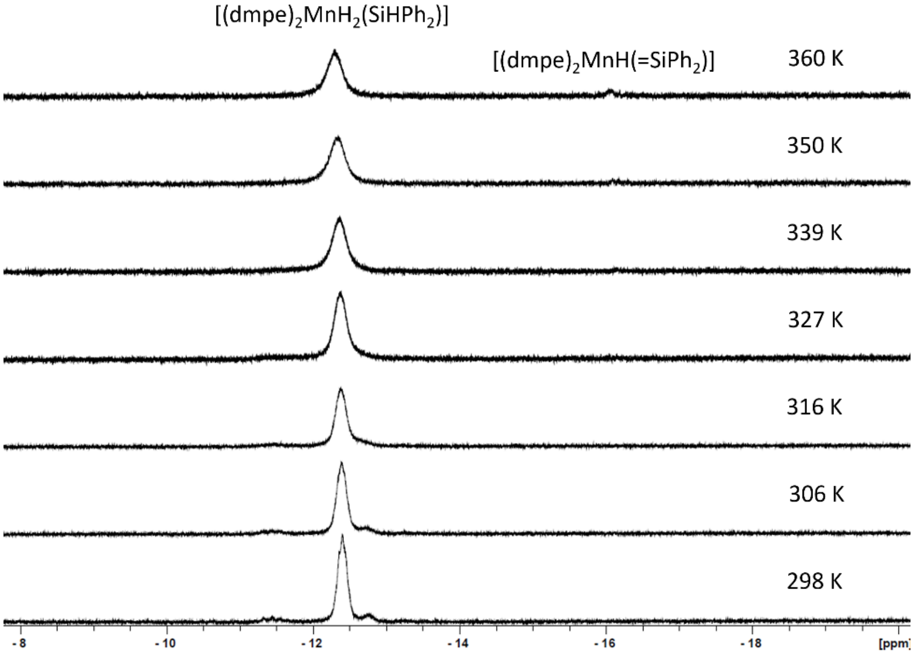

Figure S162. Expanded metal hydride region of variable temperature ^{1}H NMR spectra of a solution containing *cis* and *trans* isomers of [(dmpe)$_2$Mn(SiHPh$_2$)(N$_2$)] (**6**), along with [(dmpe)$_2$MnH$_2$(SiHPh$_2$)], under an atmosphere of N$_2$ in C$_6$D$_6$ (500 MHz).

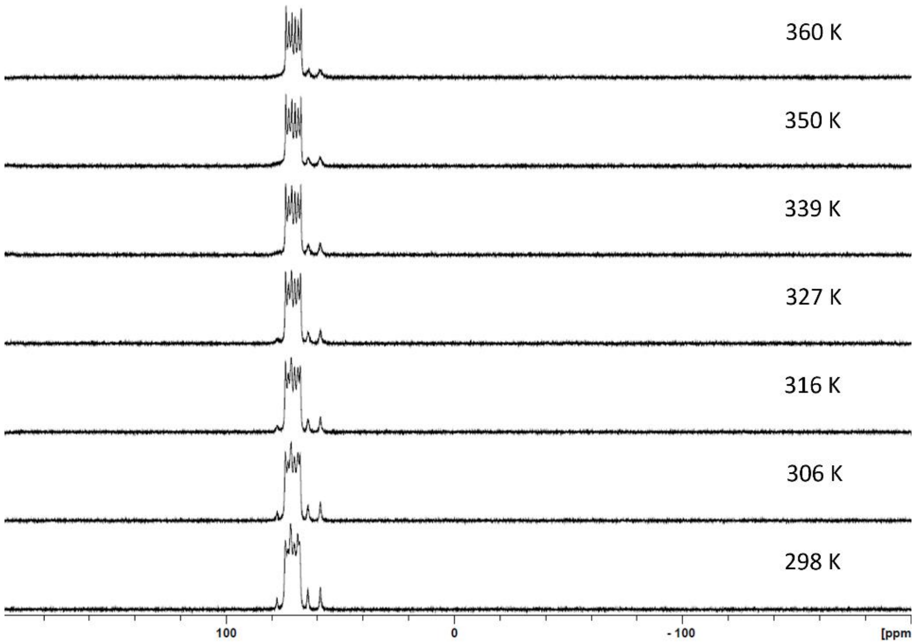

Figure S163. Variable temperature $^{31}P\{^1H\}$ NMR spectra of a solution containing *cis* and *trans* isomers of $[(dmpe)_2Mn(SiHPh_2)(N_2)]$ (**6**), along with $[(dmpe)_2MnH_2(SiHPh_2)]$, under an atmosphere of N_2 in C_6D_6 (202 MHz).

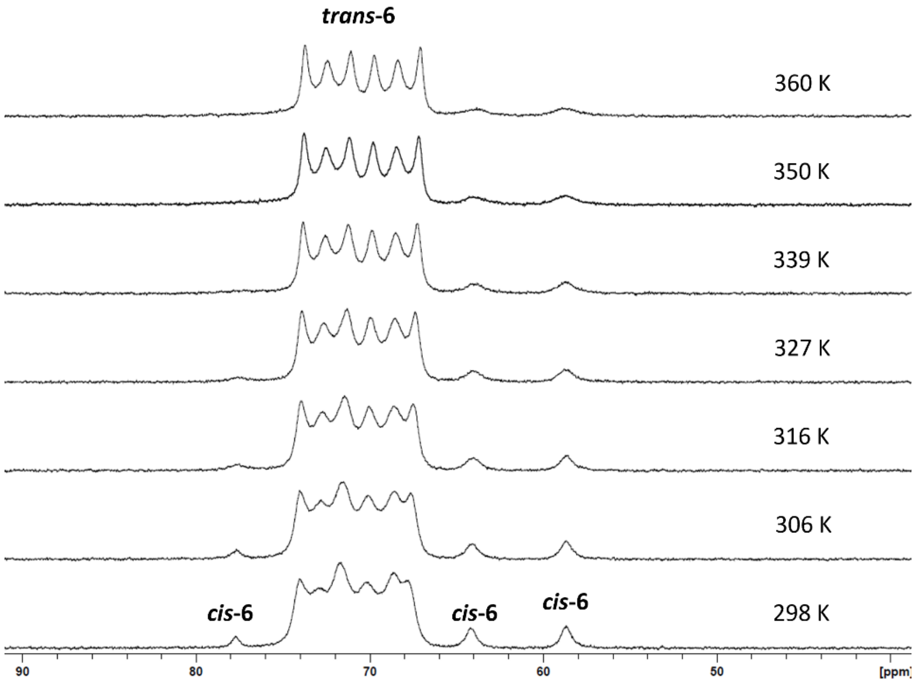

Figure S164. Expanded complex **6** region of variable temperature $^{31}P\{^1H\}$ NMR spectra of a solution containing *cis* and *trans* isomers of $[(dmpe)_2Mn(SiHPh_2)(N_2)]$ (**6**), along with $[(dmpe)_2MnH_2(SiHPh_2)]$, under an atmosphere of N_2 in C_6D_6 (202 MHz).

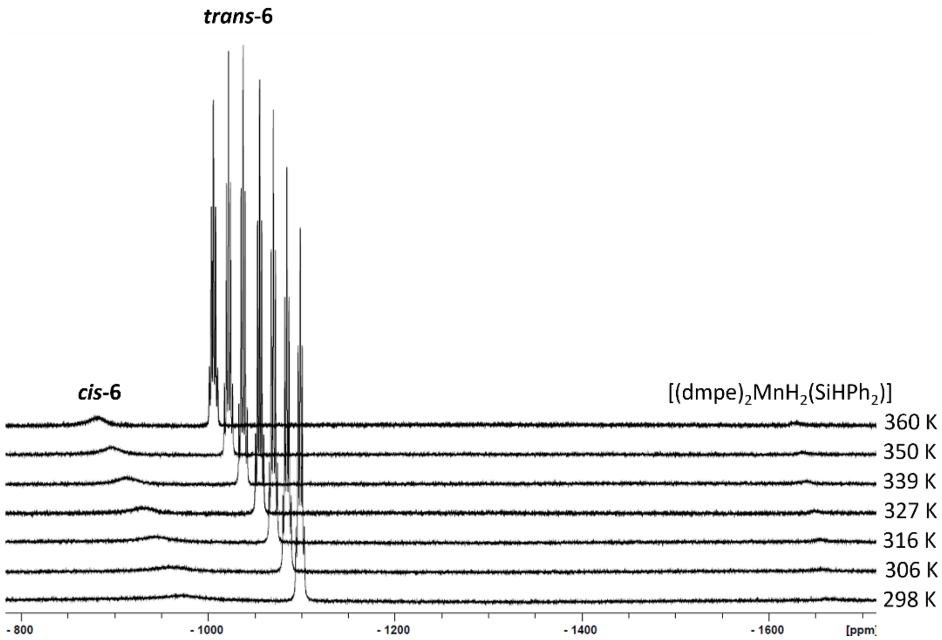

Figure S165. Variable temperature ^{55}Mn{^{1}H} NMR spectra of a solution containing *cis* and *trans* isomers of [(dmpe)$_2$Mn(SiHPh$_2$)(N$_2$)] (**6**), along with [(dmpe)$_2$MnH$_2$(SiHPh$_2$)], under an atmosphere of N$_2$ in C$_6$D$_6$ (124 MHz).

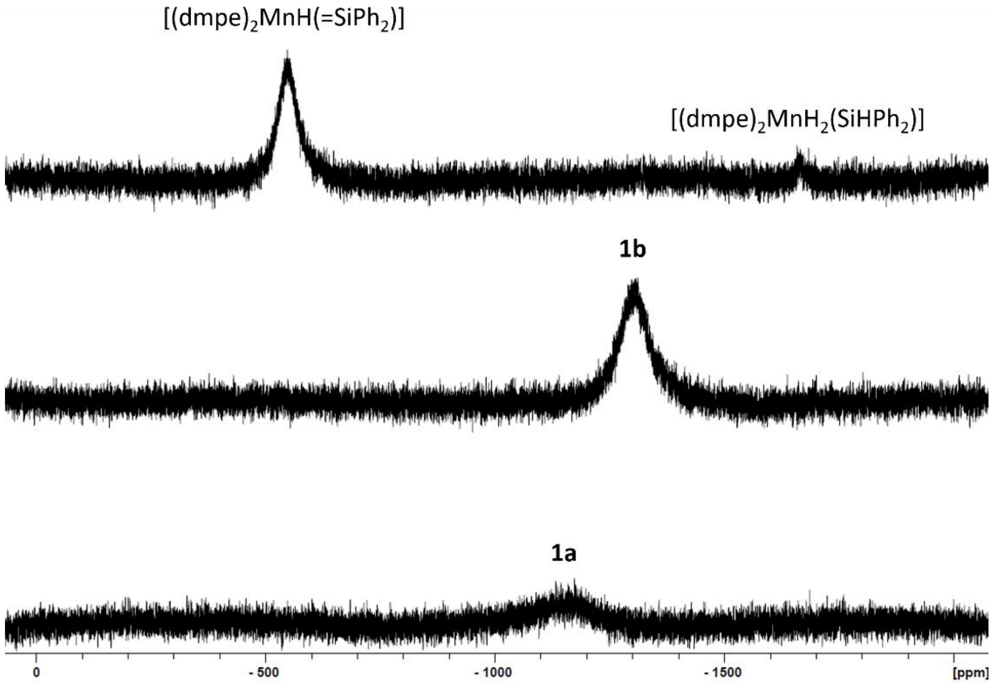

Figure S166. ^{55}Mn{^{1}H} NMR spectra of (bottom, in d_8-toluene) [(dmpe)$_2$MnH(=GePh$_2$)] (**1a**), (middle, in d_8-toluene) [(dmpe)$_2$MnH(=GeEt$_2$)] (**1b**), and (top, in C$_6$D$_6$) an 8 : 1 mixture of [(dmpe)$_2$MnH(=SiPh$_2$)] : [(dmpe)$_2$MnH$_2$(SiHPh$_2$)] (124 MHz, 298 K).

Figures of X-ray Crystal Structures of Complexes *cis*-3b, 4, *cis*-5a, and *trans*-5a

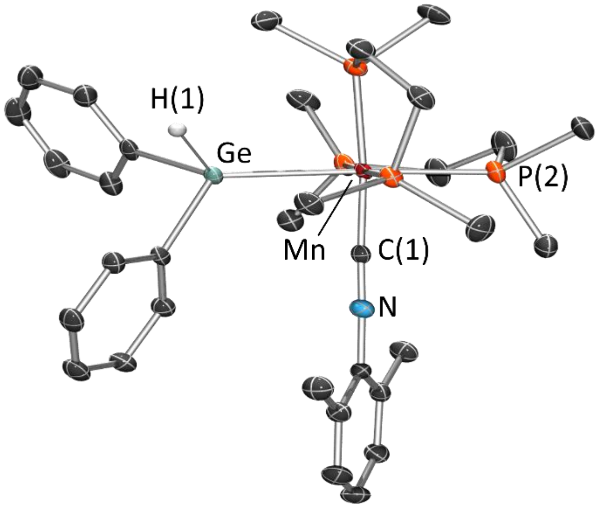

Figure S167. X-ray crystal structure of [(dmpe)$_2$Mn(GeHPh$_2$)(CNXyl)]·0.5(toluene) (***cis*-3b**) with ellipsoids shown at 50 % probability. A second essentially isostructural ***cis*-3b** molecule, a toluene molecule, and most hydrogen atoms (with the exception of the hydrogen on Ge, which was located from the difference map and refined isotropically) are omitted for clarity. Xyl = *o*-xylyl.

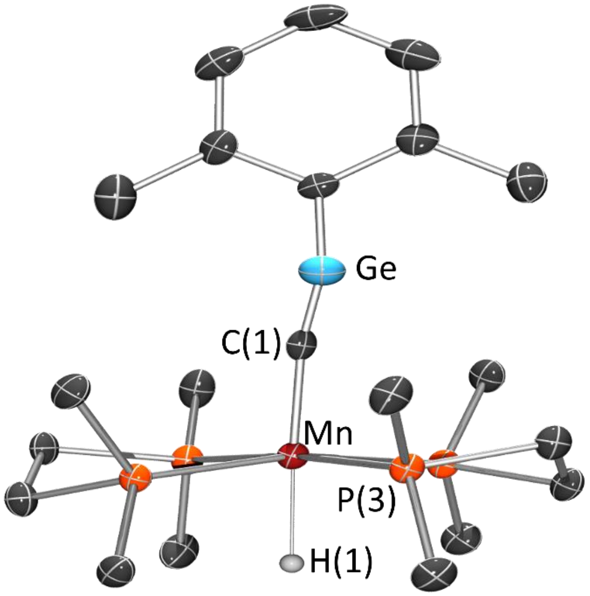

Figure S168. X-ray crystal structure of [(dmpe)$_2$MnH(CNXyl)] (**4**) with ellipsoids shown at 50 % probability. Most hydrogen atoms (with the exception of the hydrogen on Mn, which was located from the difference map and refined isotropically) were omitted for clarity. Xyl = *o*-xylyl.

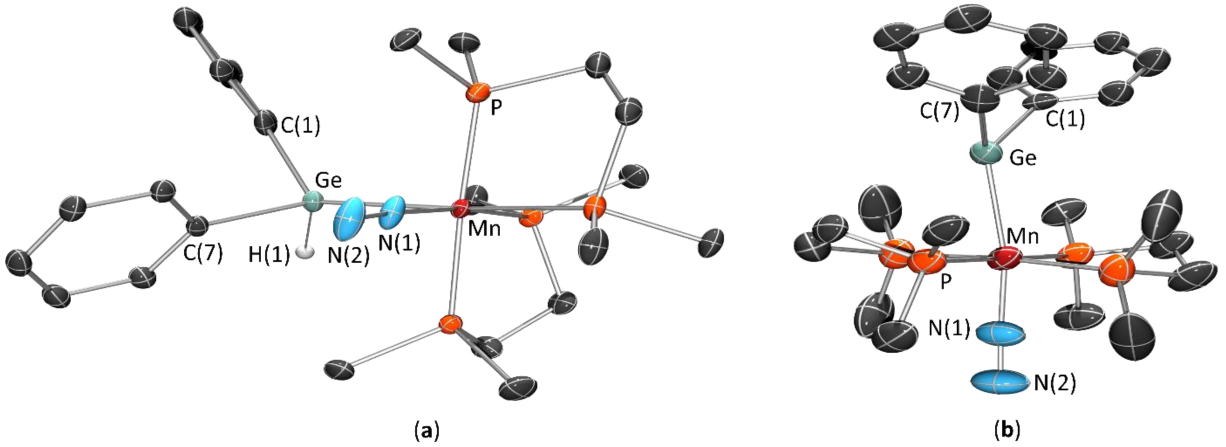

Figure S169. X-ray crystal structure of (a) *cis*-[(dmpe)$_2$Mn(GeHPh$_2$)(N$_2$)] (***cis*-5a**) and (b) *trans*-[(dmpe)$_2$Mn(GeHPh$_2$)(N$_2$)] (***trans*-5a**) with ellipsoids shown at 50 % probability. Most hydrogen atoms (with the exception of the hydrogen on Ge for ***cis*-5a**, which was located from the difference map and refined isotropically) were omitted for clarity. The germyl ligand in ***trans*-5a** was disordered over two positions and only the major component (67.9(4) %) is shown, and no hydrogen atom was located on the Ge atom from the difference map due to a combination of germyl ligand disorder and poor crystal quality.

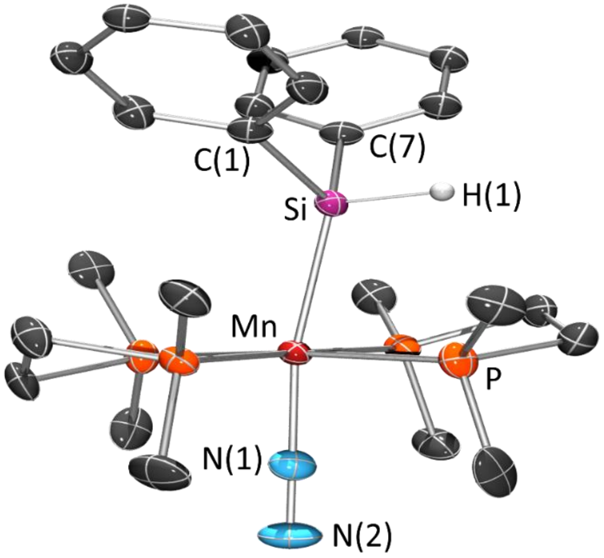

Figure S170. X-ray crystal structure of *trans*-[(dmpe)$_2$Mn(SiHPh$_2$)(N$_2$)] (***trans*-6**) with ellipsoids shown at 50 % probability. Most hydrogen atoms (with the exception of the hydrogen on Si, which was located from the difference map and refined isotropically) were omitted for clarity. The silyl ligand and part of both dmpe ligands were disordered over two positions and only the major component (69.8(3) %) is shown. No hydrogen atom was located on the Si atom from the difference map in the minor disorder component.

Tables of X-ray Crystal Data and Crystal Structure Refinement

Table S1. Crystal and structure refinement data for *trans*-[(dmpe)$_2$MnH(HGeHEt$_2$)] (***trans*-2b**) co-crystalized with *trans*-[(dmpe)$_2$MnH(=GeEt$_2$)] (**1b**).

Identification code	MnGeHEt2_H2_trans
Empirical formula	$C_{16}H_{43.92}GeMnP_4$
Formula weight	487.84
Temperature/K	100.00
Crystal system	triclinic
Space group	P-1
a/Å	9.159(3)
b/Å	9.8098(18)
c/Å	14.115(3)
α/°	88.987(10)
β/°	75.985(19)
γ/°	75.957(14)
Volume/Å^3	1192.6(5)
Z	2
ρ_{calc}g/cm^3	1.359
μ/mm^{-1}	2.055
F(000)	514.0
Crystal size/mm^3	0.6 × 0.5 × 0.45
Radiation	MoKα (λ = 0.71073)
2Θ range for data collection/°	4.284 to 59.32
Index ranges	$-12 \le h \le 12$, $-13 \le k \le 13$, $-19 \le l \le 19$
Reflections collected	20812
Independent reflections	20812 [R_{int} = ?, R_{sigma} = 0.0755]
Data/restraints/parameters	20812/24/264
Goodness-of-fit on F^2	1.150
Final R indexes [I>=2σ (I)]	R_1 = 0.0424, wR_2 = 0.1254
Final R indexes [all data]	R_1 = 0.0667, wR_2 = 0.1322
Largest diff. peak/hole / e Å^{-3}	2.87/-1.16

Table S2. Crystal and structure refinement data for *cis*-[(dmpe)$_2$Mn(GeHPh$_2$)(CN^{t}Bu)] (***cis*-3a**).

Identification code	MnGeHPh2_CNtBu_cis
Empirical formula	$C_{29}H_{52}GeMnNP_4$
Formula weight	666.12
Temperature/K	100
Crystal system	triclinic
Space group	P-1
a/Å	9.255(3)
b/Å	9.797(4)
c/Å	19.964(5)
α/°	76.88(2)
β/°	87.088(11)
γ/°	68.91(3)
Volume/Å^3	1643.8(9)
Z	2
ρ_{calc}g/cm^3	1.346
μ/mm^{-1}	1.512
F(000)	700.0
Crystal size/mm^3	0.45 × 0.25 × 0.15
Radiation	MoKα (λ = 0.71073)
2Θ range for data collection/°	4.192 to 59.26
Index ranges	$-11 \leq h \leq 12$, $-13 \leq k \leq 13$, $-27 \leq l \leq 27$
Reflections collected	19363
Independent reflections	9183 [R_{int} = 0.0305, R_{sigma} = 0.0651]
Data/restraints/parameters	9183/0/340
Goodness-of-fit on F^2	1.028
Final R indexes [I>=2σ (I)]	R_1 = 0.0483, wR_2 = 0.1134
Final R indexes [all data]	R_1 = 0.0601, wR_2 = 0.1181
Largest diff. peak/hole / e Å^{-3}	2.56/-1.26

Table S3. Crystal and structure refinement data for *cis*-[(dmpe)$_2$Mn(GeHPh$_2$)(CNXyl)]·0.5(toluene) (***cis*-3b**).

Identification code	MnGeHPh2_CNXyl_cis
Empirical formula	$C_{36.5}H_{56}GeMnNP_4$
Formula weight	760.23
Temperature/K	100.00
Crystal system	triclinic
Space group	P-1
a/Å	10.896(4)
b/Å	15.146(4)
c/Å	23.533(7)
α/°	93.122(18)
β/°	98.196(19)
γ/°	101.38(3)
Volume/Å^3	3755(2)
Z	4
ρ_{calc}g/cm^3	1.345
μ/mm^{-1}	1.333
F(000)	1596.0
Crystal size/mm^3	0.5 × 0.3 × 0.1
Radiation	MoKα (λ = 0.71073)
2Θ range for data collection/°	3.388 to 59.244
Index ranges	$-15 \le h \le 14$, $-21 \le k \le 18$, $-32 \le l \le 32$
Reflections collected	44723
Independent reflections	20889 [R_{int} = 0.0474, R_{sigma} = 0.0978]
Data/restraints/parameters	20889/7/804
Goodness-of-fit on F^2	1.059
Final R indexes [I>=2σ (I)]	R_1 = 0.0541, wR_2 = 0.1359
Final R indexes [all data]	R_1 = 0.0825, wR_2 = 0.1493
Largest diff. peak/hole / e Å^{-3}	1.41/-1.02

Table S4. Crystal and structure refinement data for *trans*-[(dmpe)$_2$Mn(GeHPh$_2$)(CN^{n}Bu)] (***trans*-3c**).

Identification code	MnGeHPh2_CNnBu_trans
Empirical formula	$C_{29}H_{52}GeMnNP_4$
Formula weight	666.12
Temperature/K	100.00
Crystal system	monoclinic
Space group	$P2_1/n$
a/Å	9.459(4)
b/Å	20.844(10)
c/Å	16.251(10)
α/°	90
β/°	90.97(3)
γ/°	90
Volume/Å^3	3204(3)
Z	4
ρ_{calc}g/cm^3	1.381
μ/mm^{-1}	1.551
F(000)	1400.0
Crystal size/mm^3	0.3 × 0.15 × 0.15
Radiation	MoKα (λ = 0.71073)
2Θ range for data collection/°	3.178 to 52.85
Index ranges	$-10 \le h \le 11$, $-26 \le k \le 26$, $-20 \le l \le 20$
Reflections collected	26664
Independent reflections	6577 [R_{int} = 0.0841, R_{sigma} = 0.0811]
Data/restraints/parameters	6577/0/338
Goodness-of-fit on F^2	1.022
Final R indexes [I>=2σ (I)]	R_1 = 0.0521, wR_2 = 0.1211
Final R indexes [all data]	R_1 = 0.0813, wR_2 = 0.1336
Largest diff. peak/hole / e Å^{-3}	2.79/-0.52

Table S5. Crystal and structure refinement data for *trans*-[(dmpe)$_2$MnH(CNXyl] (**4**).

Identification code	MnHXyl
Empirical formula	$C_{21}H_{42}MnNP_4$
Formula weight	487.37
Temperature/K	100.00
Crystal system	monoclinic
Space group	$P2_1/n$
a/Å	11.946(9)
b/Å	12.950(8)
c/Å	17.304(13)
α/°	90
β/°	108.69(3)
γ/°	90
Volume/Å^3	2536(3)
Z	4
ρ_{calc}g/cm^3	1.277
μ/mm^{-1}	0.780
F(000)	1040.0
Crystal size/mm^3	0.35 × 0.1 × 0.02
Radiation	MoKα (λ = 0.71073)
2Θ range for data collection/°	4.008 to 52.798
Index ranges	$-14 \le h \le 14$, $-16 \le k \le 15$, $-21 \le l \le 21$
Reflections collected	20450
Independent reflections	5171 [R_{int} = 0.1230, R_{sigma} = 0.1114]
Data/restraints/parameters	5171/0/258
Goodness-of-fit on F^2	0.993
Final R indexes [I>=2σ (I)]	R_1 = 0.0610, wR_2 = 0.1366
Final R indexes [all data]	R_1 = 0.1217, wR_2 = 0.1615
Largest diff. peak/hole / e Å^{-3}	0.81/-0.61

Table S6. Crystal and structure refinement data for *cis*-[(dmpe)$_2$Mn(GeHPh$_2$)(N$_2$)] (***cis*-5a**).

Identification code	MnGeHPh2_N2_cis
Empirical formula	$C_{24}H_{43}GeMnN_2P_4$
Formula weight	611.01
Temperature/K	100
Crystal system	triclinic
Space group	P-1
a/Å	9.636(2)
b/Å	10.981(3)
c/Å	14.658(3)
α/°	71.401(12)
β/°	83.524(16)
γ/°	77.39(2)
Volume/Å^3	1433.0(6)
Z	2
ρ_{calc}g/cm^3	1.416
μ/mm^{-1}	1.728
F(000)	636.0
Crystal size/mm^3	0.4 × 0.3 × 0.2
Radiation	MoKα (λ = 0.71073)
2Θ range for data collection/°	3.99 to 59.236
Index ranges	$-13 \le h \le 13$, $-15 \le k \le 15$, $-16 \le l \le 20$
Reflections collected	16604
Independent reflections	7994 [R_{int} = 0.0219, R_{sigma} = 0.0575]
Data/restraints/parameters	7994/311/357
Goodness-of-fit on F^2	1.041
Final R indexes [I>=2σ (I)]	R_1 = 0.0376, wR_2 = 0.0912
Final R indexes [all data]	R_1 = 0.0458, wR_2 = 0.0945
Largest diff. peak/hole / e Å^{-3}	0.99/-0.80

Table S7. Crystal and structure refinement data for *trans*-[$(dmpe)_2Mn(GeHPh_2)(N_2)$] (***trans*-5a**).

Identification code	MnGeHPh2_N2_trans
Empirical formula	$C_{24}H_{43}GeMnN_2P_4$
Formula weight	611.01
Temperature/K	100
Crystal system	monoclinic
Space group	Cc
a/Å	10.333(2)
b/Å	16.308(3)
c/Å	17.760(4)
α/°	90
β/°	105.80(3)
γ/°	90
Volume/Å^3	2879.9(11)
Z	4
ρ_{calc}g/cm^3	1.409
μ/mm^{-1}	1.720
F(000)	1272.0
Crystal size/mm^3	0.5 × 0.33 × 0.2
Radiation	Mo Kα (λ = 0.71073)
2Θ range for data collection/°	4.798 to 52.744
Index ranges	$-11 \leq h \leq 12$, $-20 \leq k \leq 20$, $-22 \leq l \leq 21$
Reflections collected	9837
Independent reflections	5401 [R_{int} = 0.1929, R_{sigma} = 0.2176]
Data/restraints/parameters	5401/710/337
Goodness-of-fit on F^2	0.872
Final R indexes [I>=2σ (I)]	R_1 = 0.0852, wR_2 = 0.1881
Final R indexes [all data]	R_1 = 0.1865, wR_2 = 0.2392
Largest diff. peak/hole / e Å^{-3}	0.84/-0.77
Flack parameter	-0.08(5)

Table S8. Crystal and structure refinement data for *cis*-[(dmpe)$_2$Mn(GeHEt$_2$)(N$_2$)] (***cis*-5b**).

Identification code	MnGeHEt2_N2_cis
Empirical formula	$C_{16}H_{43}GeMnN_2P_4$
Formula weight	514.93
Temperature/K	100
Crystal system	monoclinic
Space group	$P2_1/n$
a/Å	9.295(3)
b/Å	16.194(4)
c/Å	16.278(4)
α/°	90
β/°	90.674(14)
γ/°	90
Volume/Å^3	2450.1(11)
Z	4
ρ_{calc}g/cm^3	1.396
μ/mm^{-1}	2.006
F(000)	1080.0
Crystal size/mm^3	0.4 × 0.35 × 0.25
Radiation	MoKα (λ = 0.71073)
2Θ range for data collection/°	5.006 to 61.236
Index ranges	$-10 \leq h \leq 13$, $-23 \leq k \leq 22$, $-23 \leq l \leq 23$
Reflections collected	30837
Independent reflections	7531 [R_{int} = 0.0232, R_{sigma} = 0.0391]
Data/restraints/parameters	7531/409/306
Goodness-of-fit on F^2	1.201
Final R indexes [I>=2σ (I)]	R_1 = 0.0337, wR_2 = 0.0864
Final R indexes [all data]	R_1 = 0.0381, wR_2 = 0.0878
Largest diff. peak/hole / e Å^{-3}	0.67/-0.72

Table S9. Crystal and structure refinement data for *trans*-[(dmpe)$_2$Mn(GeHEt$_2$)(N$_2$)] (***trans*-5b**).

Identification code	MnGeHEt2_N2_trans
Empirical formula	$C_{16}H_{43}GeMnN_2P_4$
Formula weight	514.93
Temperature/K	100.00
Crystal system	monoclinic
Space group	$P2_1/n$
a/Å	8.921(4)
b/Å	30.056(8)
c/Å	9.232(3)
α/°	90
β/°	96.37(3)
γ/°	90
Volume/Å^3	2460.2(15)
Z	4
ρ_{calc}g/cm^3	1.390
μ/mm^{-1}	1.998
F(000)	1080.0
Crystal size/mm^3	0.2 × 0.15 × 0.05
Radiation	MoKα (λ = 0.71073)
2Θ range for data collection/°	4.642 to 56.848
Index ranges	$-11 \le h \le 11$, $-40 \le k \le 40$, $-12 \le l \le 12$
Reflections collected	27879
Independent reflections	6158 [R_{int} = 0.0799, R_{sigma} = 0.0757]
Data/restraints/parameters	6158/0/231
Goodness-of-fit on F^2	0.977
Final R indexes [I>=2σ (I)]	R_1 = 0.0344, wR_2 = 0.0693
Final R indexes [all data]	R_1 = 0.0601, wR_2 = 0.0757
Largest diff. peak/hole / e Å^{-3}	0.39/-0.50

Table S10. Crystal and structure refinement data for *trans*-[(dmpe)$_2$Mn(SiHPh$_2$)(N$_2$)] (***trans*-6**).

Identification code	MnHSiPh2_N2_trans
Empirical formula	$C_{24}H_{42.7}MnN_2P_4Si$
Formula weight	566.21
Temperature/K	100.00
Crystal system	monoclinic
Space group	Cc
a/Å	10.300(6)
b/Å	16.285(9)
c/Å	17.635(12)
α/°	90
β/°	105.91(2)
γ/°	90
Volume/Å^3	2845(3)
Z	4
ρ_{calc}g/cm^3	1.322
μ/mm^{-1}	0.747
F(000)	1199.0
Crystal size/mm^3	0.15 × 0.15 × 0.1
Radiation	MoKα (λ = 0.71073)
2Θ range for data collection/°	4.85 to 59.478
Index ranges	-14 ≤ h ≤ 14, -22 ≤ k ≤ 22, -24 ≤ l ≤ 24
Reflections collected	31909
Independent reflections	7794 [R_{int} = 0.0770, R_{sigma} = 0.0937]
Data/restraints/parameters	7794/194/362
Goodness-of-fit on F^2	1.019
Final R indexes [I>=2σ (I)]	R_1 = 0.0585, wR_2 = 0.1246
Final R indexes [all data]	R_1 = 0.1018, wR_2 = 0.1464
Largest diff. peak/hole / e Å^{-3}	1.01/-0.52
Flack parameter	0.046(14)

Tables of Selected Crystallographic Metrics for Complexes 3a-c and 4

Table S11. Selected X-ray crystallography bond metrics (Å or °) for isonitrile germyl complexes [(dmpe)$_2$Mn(GeHPh$_2$)(CNR)] (**3a-c**) and isonitrile hydride complex [(dmpe)$_2$MnH(CNXyl)] (**4**). Xyl represents *o*-xylyl.

	GeHPh$_2$ or H	CNR	Mn–Ge or Mn–H	Mn–C	C≡N	Ge–Mn–C or H–Mn–C	C–N–C
***cis*-3a**	GeHPh$_2$	CN^{t}Bu	2.475(1)	1.837(3)	1.184(5)	88.28(9)	168.1(3)
***cis*-3b**[a]	GeHPh$_2$	CNXyl	2.481(1)	1.821(3)	1.192(4)	86.84(8)	172.6(3)
***trans*-3c**	GeHPh$_2$	CN^{n}Bu	2.528(1)	1.804(4)	1.190(6)	177.1(1)	144.9(4)
4	H	CNXyl	1.75(7)	1.789(6)	1.221(8)	177(2)	160.4(5)
4 (lit.)[12]	H	CNXyl	1.84	1.935(6)	1.303(8)	180.00	180.00

a. The unit cell in ***cis*-3b** contains two independent but isostructural complexes (in addition to a co-crystallized toluene molecule). In one of these structures, there is evidence for significant disorder of the dmpe ligands which could not be properly modelled, so metrics in this table are only from the other structure.

Tables of Selected NMR Spectroscopic Data for Complexes 3a-c

Table S12. Selected NMR spectroscopy information for germyl isonitrile complexes [(dmpe)$_2$Mn(GeHPh$_2$)(CNR)] (**3a-c**). Xyl represents *o*-xylyl. C$_6$D$_6$, 500 or 600 MHz, 298 K.

		^{1}H NMR GeH	^{31}P NMR	^{1}H NMR GeH	^{31}P NMR	*cis* : *trans* after complete conversion
	R	*cis*		*trans*		
3a	Ph	5.45	75.8, 70.5 (2P), 57.0	5.12	72.7	77 : 23
3b	Xyl	5.48	70.6 (2P), 67.9, 53.4	5.27	70.6	78 : 22
3c	^{n}Bu	5.45	76.1, 71.6 (2P), 55.4	5.06	73.8	83 : 17

2D Powder X-ray Diffractograms for Complexes 5a-b

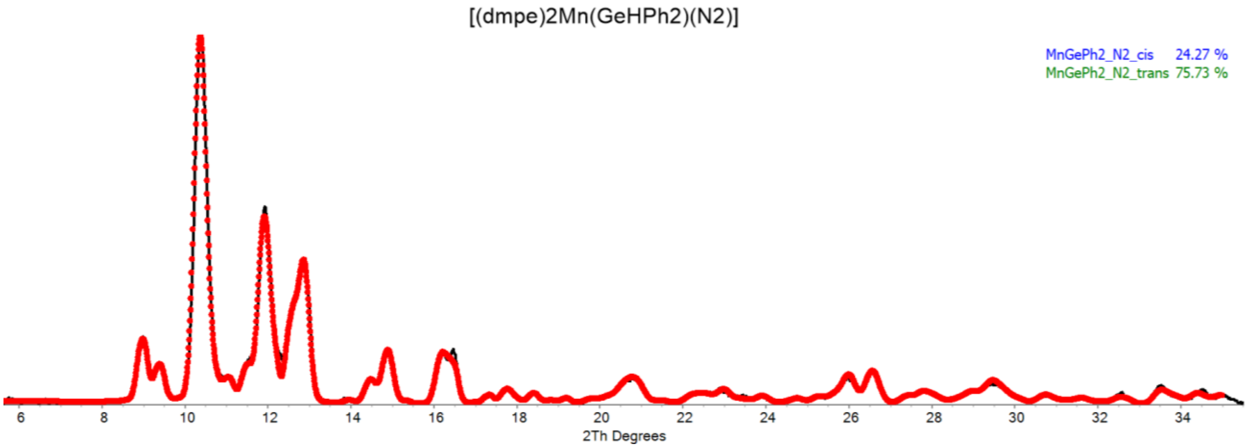

Figure S171. Overlay of (black) the 2D power X-ray diffractogram of the isolated bulk solid of [(dmpe)$_2$Mn(GeHPh$_2$)(N$_2$)] (**5a**) and (red) the theoretical diffractogram calculated from a combination of the single crystal X-ray structures of ***cis*-5a** and ***trans*-5a** after conducting Rietveld refinement, indicating that the bulk sample exists as a mixture of the two isomers (24.27 : 75.73 ratio). λ = 1.54056 Å, T = 298 K.

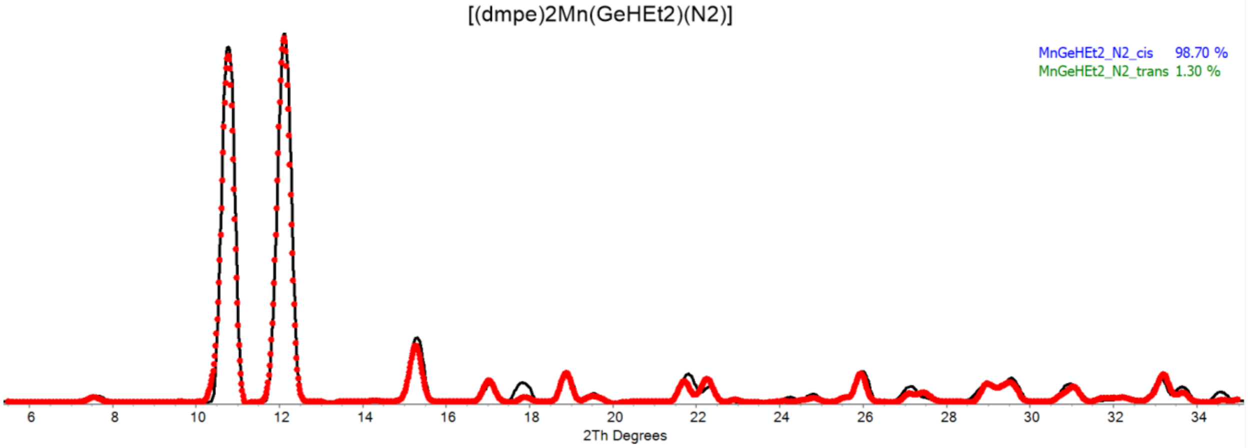

Figure S172. Overlay of (black) the 2D power X-ray diffractogram of the isolated bulk solid of [(dmpe)$_2$Mn(GeHEt$_2$)(N$_2$)] (**5b**) and (red) the theoretical diffractogram calculated from a combination of the single crystal X-ray structures of ***cis*-5b** and ***trans*-5b** after conducting Rietveld refinement, indicating that the bulk sample exists as almost exclusively (~99 %) as the *cis* isomer. λ = 1.54056 Å, T = 298 K.

IR Spectra for Complexes 5a-b

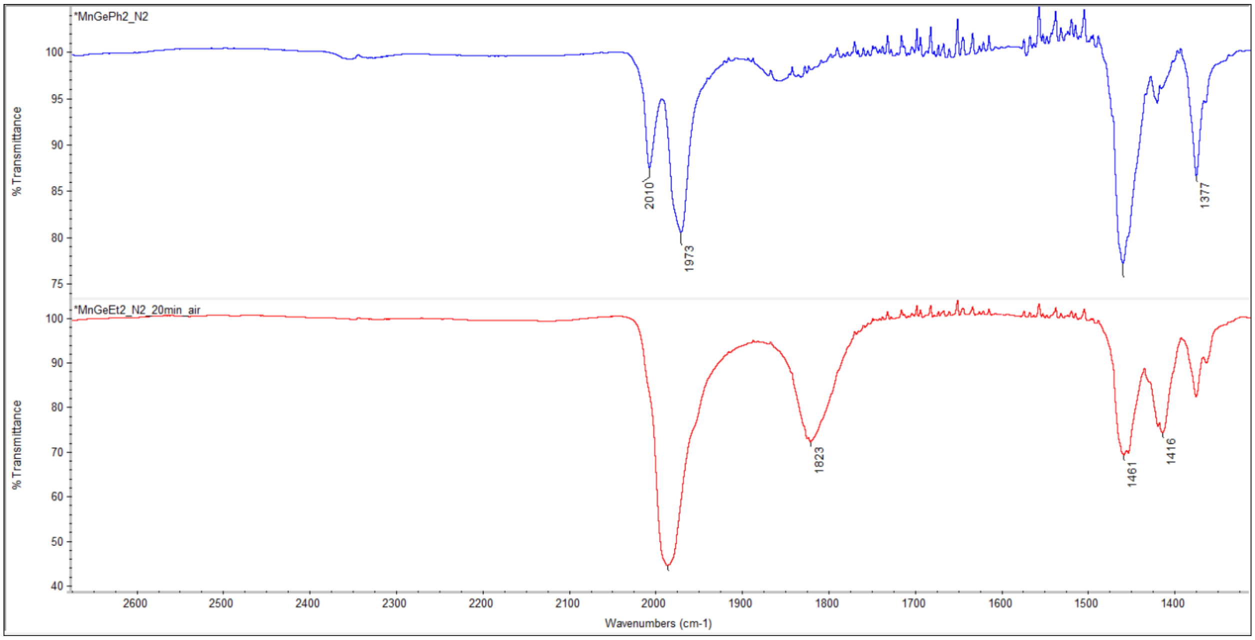

Figure S173. IR spectra for (top) [(dmpe)$_2$Mn(GeHPh$_2$)(N$_2$)] (**5a**) and (bottom) [(dmpe)$_2$Mn(GeHEt$_2$)(N$_2$)] (**5b**) in a Nujol mull.

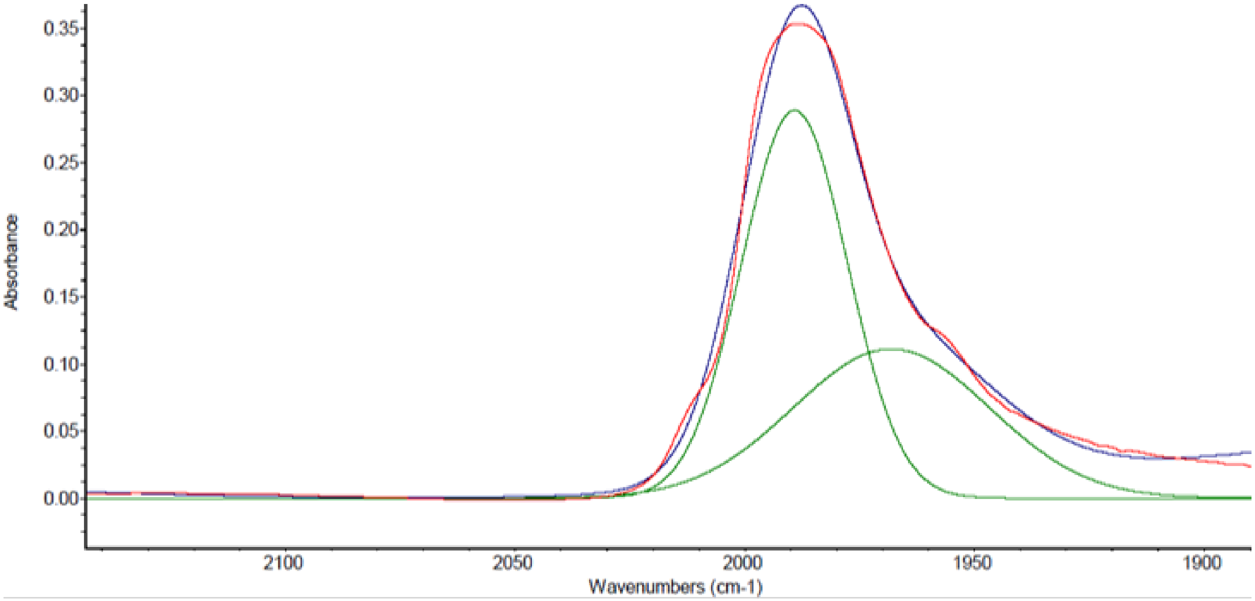

Figure S174. Expanded $\nu_{N\equiv N}$ region of the IR spectrum of [(dmpe)$_2$Mn(GeHEt$_2$)(N$_2$)] (**5b**; red) showing the peaks resolved for the *cis* (green; left) and *trans* (green; right) isomers, and the resulting predicted spectrum (purple). Gaussian lineshapes and a quadradic baseline correction were employed within the 1887-2144 cm^{-1} region, resulting in a standard error of 5.81 and an F statistic of 0.34.

DFT Calculated Structures for Complex 2a and the Geometry Optimized Fragment of [(dmpe)$_2$Mn(GeHPh$_2$)]

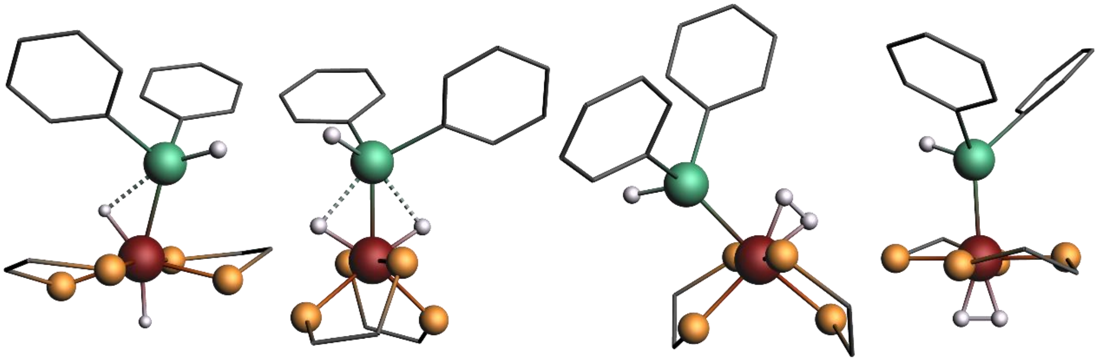

transHGe-2a ***central-2a*** ***cis-2a*** ***transH$_2$-2a***

Figure S175. Geometry optimized DFT calculated structures for the (left to right) *transHGe*, *central*, *cis*, and *transH$_2$* isomers of [(dmpe)$_2$MnH(=GePh$_2$)] (**2a**). Spheres represent Mn (red), Ge (green), P (orange), and H (white), whereas carbon atoms are represented by grey vertices. *P*-methyl groups and most H atoms have been omitted for clarity. Solid bonds are those with Mayer bond orders >0.40, while dashed bonds are those with Mayer bond orders between 0.20 and 0.24.

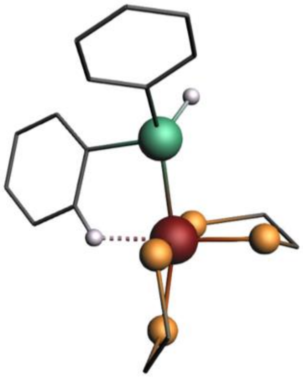

Figure S176. Geometry optimized DFT calculated structure of [(dmpe)$_2$Mn(GeHPh$_2$)] (**A**), the fragment of *cis*-[(dmpe)$_2$Mn(GeHPh$_2$)(N$_2$)] (***cis*-5b**) used in the fragment interaction calculation. Spheres represent Mn (red), Ge (green), P (orange), C (grey), and H (white). Most H atoms (with the exceptions of the one on Ge and the one involved in the agostic interaction) have been omitted for clarity, as have *P*-methyl groups. The dotted line represents the agostic interaction.

Figures Showing Superimposed Calculated and X-ray Structures of 5a-b

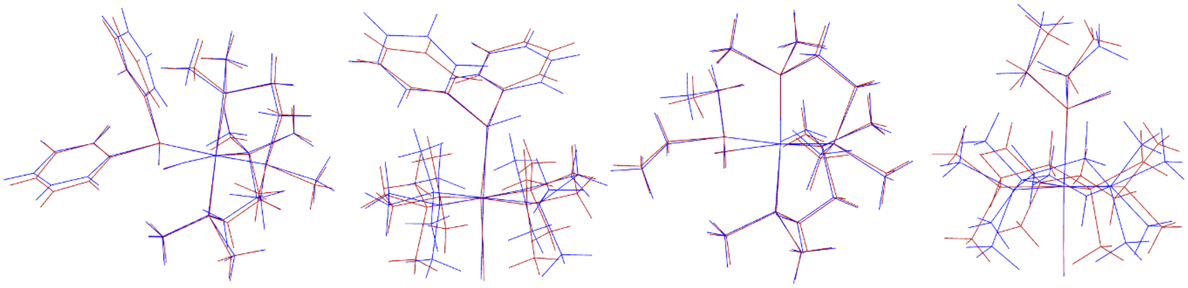

Figure S177. Superimposed DFT-calculated (blue) and X-ray (red) structures of, from left to right, *cis*-[(dmpe)$_2$Mn(GeHPh$_2$)(N$_2$)] (***cis*-5a**), *trans*-[(dmpe)$_2$Mn(GeHPh$_2$)(N$_2$)] (***trans*-5a**), *cis*-[(dmpe)$_2$Mn(GeHEt$_2$)(N$_2$)] (***cis*-5b**), and *trans*-[(dmpe)$_2$Mn(GeHEt$_2$)(N$_2$)] (***trans*-5b**).

Overall Deformation Densities of *cis* and *trans* 5a,b

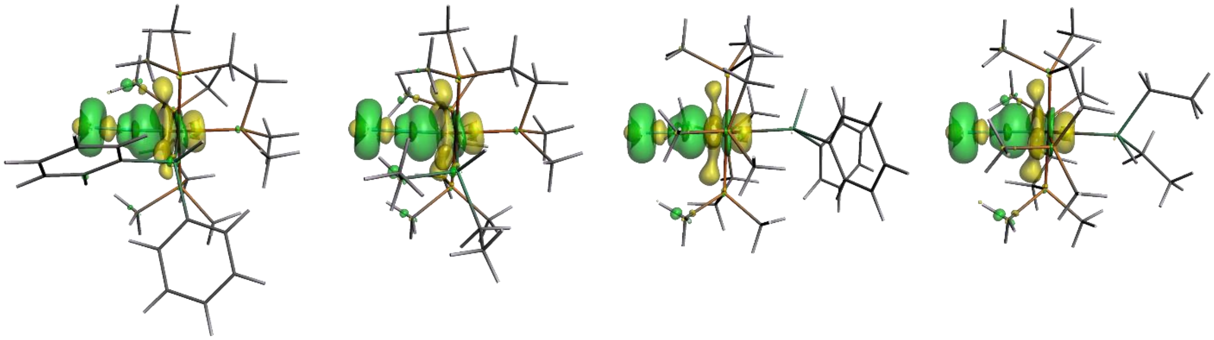

Figure S178. Overall deformation densities of (left to right) *cis*-[(dmpe)$_2$Mn(GeHPh$_2$)(N$_2$)] (***cis*-5a**), *cis*-[(dmpe)$_2$Mn(GeHEt$_2$)(N$_2$)] (***cis*-5b**), *trans*-[(dmpe)$_2$Mn(GeHPh$_2$)(N$_2$)] (***trans*-5a**), and trans-[(dmpe)$_2$Mn(GeHEt$_2$)(N$_2$)] (***trans*-5b**). Deformation density isosurfaces (set to 0.003) correspond to increased (green) and decreased (yellow) electron density relative to the non-interacting fragments.

Selected ETS-NOCV Deformation Densities, NOCV Orbitals, and Fragment Orbital Contributors for *cis* and *trans*-5

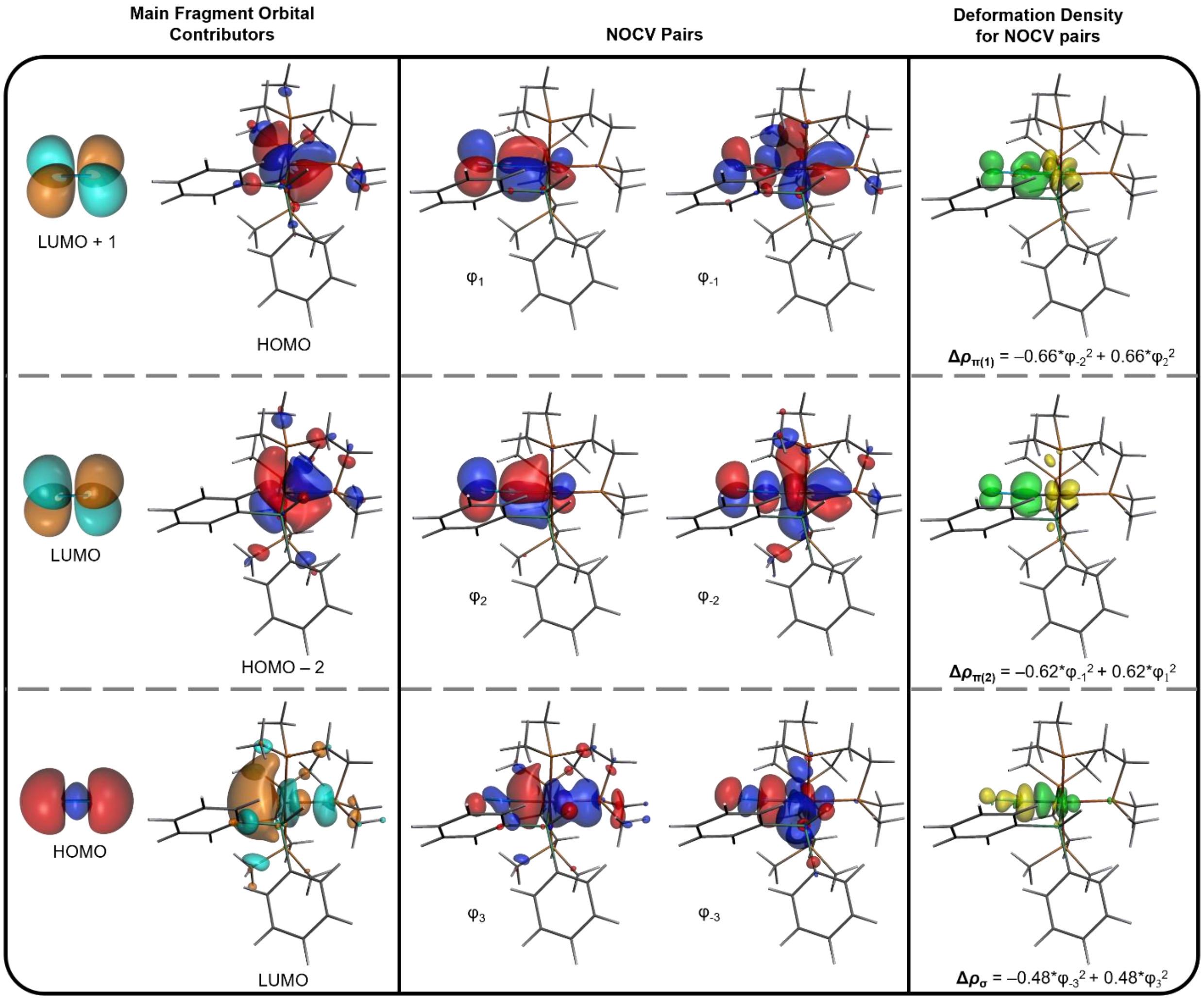

Figure S179. ETS-NOCV main fragment orbital contributors (left), NOCV orbitals (middle), and deformation densities (right) from interaction calculation using neutral [(dmpe)$_2$Mn(GeHPh$_2$)] and N$_2$ fragments for *cis*-[(dmpe)$_2$Mn(GeHPh$_2$)(N$_2$)] (***cis*-5a**). Deformation density isosurfaces (set to 0.003) correspond to increased (green) and decreased (yellow) electron density relative to the non-interacting fragments. Orbital isosurfaces are set to 0.03.

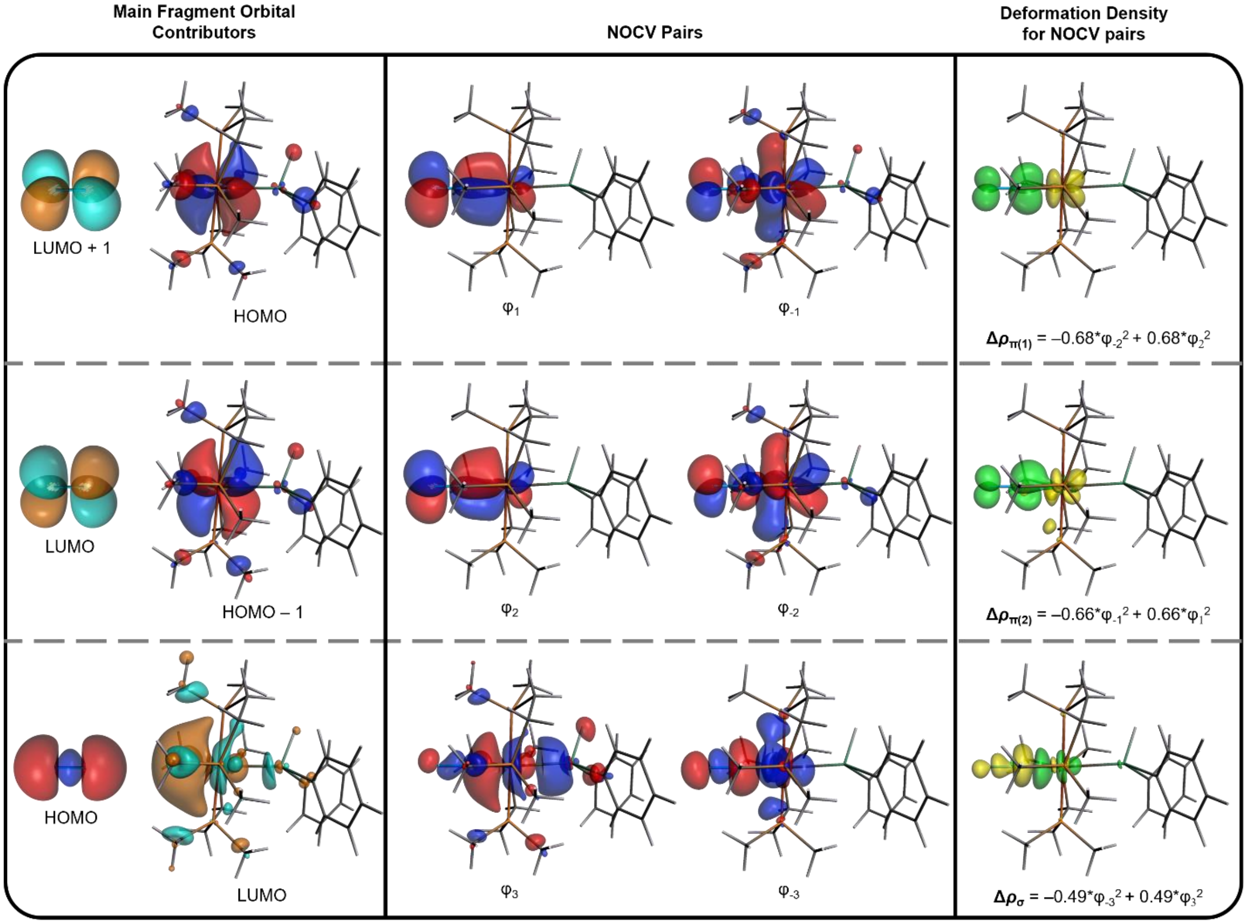

Figure S180. ETS-NOCV main fragment orbital contributors (left), NOCV orbitals (middle), and deformation densities (right) from interaction calculation using neutral [(dmpe)$_2$Mn(GeHPh$_2$)] and N$_2$ fragments for *trans*-[(dmpe)$_2$Mn(GeHPh$_2$)(N$_2$)] (***trans*-5a**). Deformation density isosurfaces (set to 0.003) correspond to increased (green) and decreased (yellow) electron density relative to the non-interacting fragments. Orbital isosurfaces are set to 0.03.

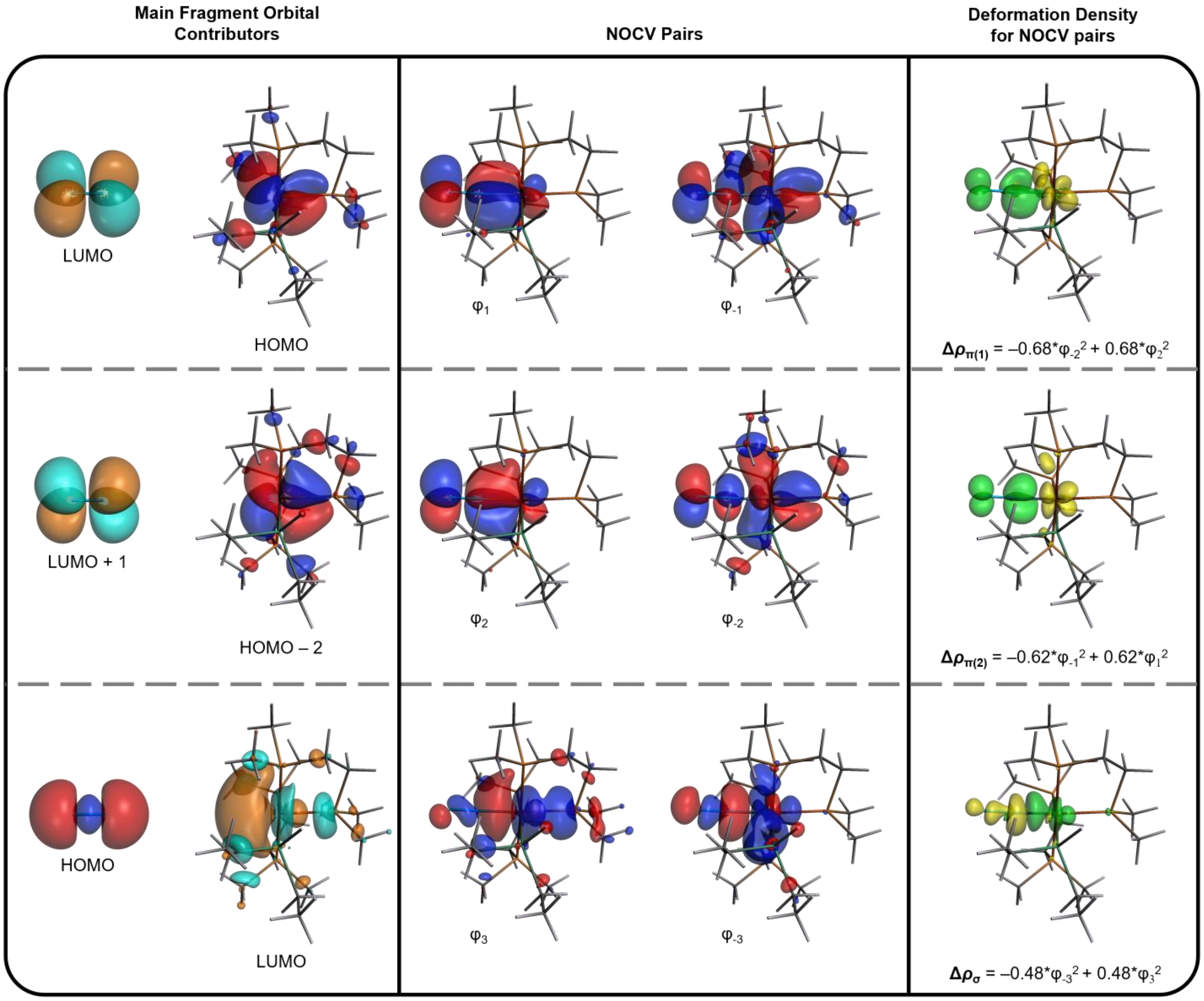

Figure S181. ETS-NOCV main fragment orbital contributors (left), NOCV orbitals (middle), and deformation densities (right) from interaction calculation using neutral [(dmpe)$_2$Mn(GeHEt$_2$)] and N$_2$ fragments for *cis*-[(dmpe)$_2$Mn(GeHEt$_2$)(N$_2$)] (***cis*-5b**). Deformation density isosurfaces (set to 0.003) correspond to increased (green) and decreased (yellow) electron density relative to the non-interacting fragments. Orbital isosurfaces are set to 0.03.

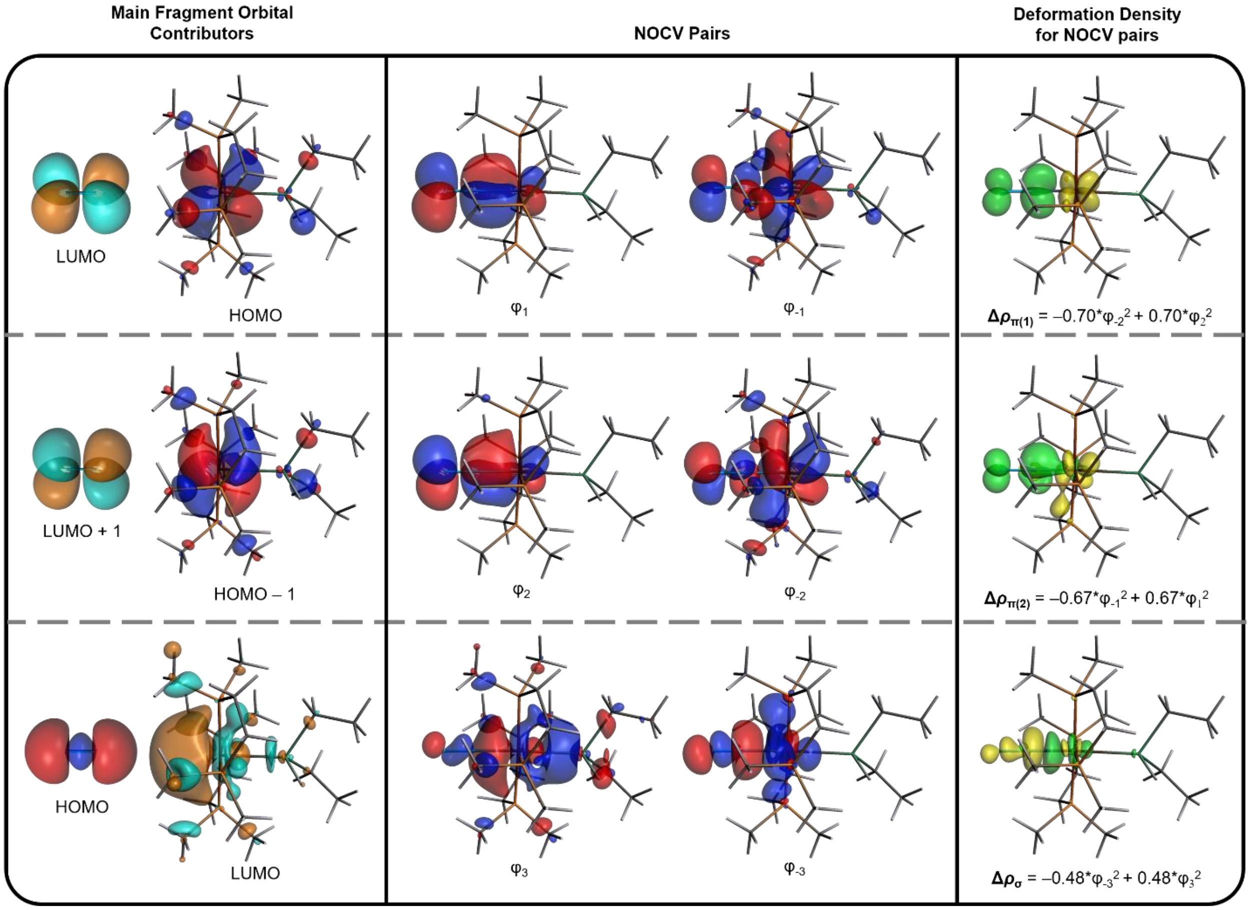

Figure S182. ETS-NOCV main fragment orbital contributors (left), NOCV orbitals (middle), and deformation densities (right) from interaction calculation using neutral [(dmpe)$_2$Mn(GeHEt$_2$)] and N$_2$ fragments for *trans*-[(dmpe)$_2$Mn(GeHEt$_2$)(N$_2$)] (***trans*-5b**). Deformation density isosurfaces (set to 0.003) correspond to increased (green) and decreased (yellow) electron density relative to the non-interacting fragments. Orbital isosurfaces are set to 0.03.

Tables of Calculated Bond Metrics, Mayer Bond Orders, and Hirshfeld Charges for 2a-b, 5a-b, and the geometry optimized [(dmpe)$_2$Mn(GeHPh$_2$)] fragment from the fragment interaction calculation for *cis*-5a

Table S13. Selected DFT calculated {and X-ray crystal structure} bond distances in Å, angles in °, (and Mayer bond orders) for the four isomers of the germyl dihydride complexes [(dmpe)$_2$MnH$_2$(GeHR$_2$)] (**2a**: R = Ph, **2b**: R = Et). Gibbs free energies of formation (Gibbs) are included in kJ mol^{-1} at 176 K, and are relative to the isomer with the lowest Gibbs free energy of formation at 176 K. H$_t$ indicates a terminal hydrogen, and H$_{br}$ indicates a hydrogen atom bridging between Mn and Ge. H$_1$ and H$_2$ represent H atoms in a dihydrogen ligand (for the *cis* isomer, they indicate the one closest and furthest, respectively, to Ge).

	GeHR$_2$	GeHPh$_2$ (**2a**)	GeHEt$_2$ (**2b**)
transHGe	Gibbs (176 K)	0	0
	Ge–H$_t$	1.58 (0.84)	1.58 {1.42(8)} (0.84)
	Ge–H$_{br}$	2.08 (0.22)	2.00 {1.77(7)} (0.23)
	Mn–H$_t$	1.54 (0.83)	1.55 {1.55(4)} (0.82)
	Mn–H$_{br}$	1.57 (0.65)	1.56 {1.50(8)} (0.65)
	Mn–Ge	2.43 (0.78)	2.46 {2.530(2), 2.530(4)} (0.74)
	Mn–Ge–H$_t$	116.3	114.9
	H$_t$–Mn–Ge	160.9	162.3
	H$_t$–Mn–GeH$_{br}$(centroid)	179.0	177.1
	Mn–Ge–C	118.6, 119.1	115.1, 121.1
	Ge–Mn–H$_{br}$	50.8	54.3
central	Gibbs (176 K)	11.1	9.9
	Ge–H$_t$	1.57 (0.88)	1.58 (0.84)
	Ge–H$_{br}$	2.03, 2.13 (0.24, 0.20)	2.11, 2.20 (0.17, 0.13)
	Mn–H$_{br}$	1.56, 1.57 (0.69, 0.70)	1.55, 1.56 (0.77, 0.70)
	Mn–Ge	2.39 (0.69)	2.43 (0.79)
	H$_{Br}$–Mn–Ge	57.0, 61.0	59.4, 62.7
	H$_{Br}$–Mn–H$_{Br}$	114.3	121.9
	Mn–Ge–C	117.0, 118.3	116.4, 121.7
	Mn–Ge–H$_t$	115.8	111.7
	H$_{Br}$–Mn–H$_{Br}$ plane to H$_{Br}$–Ge–H$_{Br}$ plane	27.7	6.0
cis	Gibbs (176 K)	8.9	10.2
	Ge–H$_t$	1.58 (0.86)	1.59 (0.86)
	Ge–H$_1$	2.34 (0.08)	2.28 (0.11)
	Mn–H$_1$	1.59 (0.46)	1.59 (0.48)
	Mn–H$_2$	1.60 (0.58)	1.60 (0.58)
	Mn–Ge	2.47 (0.83)	2.48 (0.85)
	H$_1$–H$_2$	0.95 (0.44)	0.95 (0.45)
	H$_1$–Mn–Ge	66.3	63.7
	H$_1$–Mn–H$_2$	34.6	34.7
	H$_2$(centroid)–Mn–Ge	82.2	80.6
	Mn–Ge–C	116.1, 126.3	116.7, 123.9
	Mn–Ge–H$_t$	115.1	113.0
transH$_2$	Gibbs (176 K)	16.3	14.1
	Ge–H$_t$	1.58 (0.85)	1.59 (0.88)
	Mn–H$_1$	1.57, 1.58 (0.59)	1.58 (0.62, 0.63)
	Mn–Ge	2.49 (0.82)	2.48 (0.79)
	H$_1$–H$_1$	0.98 (0.41)	0.97 (0.42)
	H$_1$–Mn–H$_1$	36.2	36.0
	H$_2$(centroid)–Mn–Ge	175.5	175.2
	Mn–Ge–C	119.6, 128.1	123.2, 124.3
	Mn–Ge–H$_t$	112.1	110.3

Table S14. Selected DFT calculated bond distances, angles, and Mayer bond orders for the geometry optimized fragment [(dmpe)$_2$Mn(GeHPh$_2$)] (**A**; Figure S176) used in the fragment interaction calculation for *cis*-[(dmpe)$_2$Mn(GeHPh$_2$)(N$_2$)] (***cis*-5a**). H$_a$ is the hydrogen involved in the γ-agostic interaction, C$_{i(1)}$ and C$_{i(2)}$ are the *ispo* carbon atoms on the phenyl ring involved in the γ-agostic interaction and the phenyl ring not involved in the γ-agostic interaction, respectively. C$_{o(1)}$ is the *ortho* carbon bonded to H$_a$ and C$_{o(2)}$ are the other three *ortho* carbon atoms.

	Bond distance (Å) or angle (°)	Mayer bond order
Mn–H$_a$	1.91	0.24
Mn–Ge	2.44	0.88
Ge–C$_{i(1)}$	1.99	0.89
Ge–C$_{i(2)}$	1.99	0.91
C$_{o(1)}$–H$_a$	1.13	0.81
C$_{o(2)}$–H	1.09	1.03, 1.05
Ge–H	1.58	0.87
Mn–Ge–C$_{i(1)}$	87.8	N/A
Mn–Ge–C$_{i(2)}$	130.4	N/A
Mn–Ge–H$_{Ge}$	123.2	N/A
Mn–H$_a$–C$_{o(1)}$	118.6	N/A

Table S15. Selected Hirshfeld charges for the four isomers of the germyl dihydride complexes [(dmpe)$_2$MnH$_2$(GeHR$_2$)] (**2a**: R = Ph, **2b**: R = Et), the two isomers of germyl dinitrogen complexes [(dmpe)$_2$Mn(GeHR$_2$)(N$_2$)] (**5a**: R = Ph, **5b**: R = Et), and the geometry optimized fragment [(dmpe)$_2$Mn(GeHPh$_2$)] (**A**) used in the fragment interaction calculation for *cis*-[(dmpe)$_2$Mn(GeHPh$_2$)(N$_2$)] (***cis*-5a**). For ***cis*-2a,b**, dihydrogen atoms are listed with the one closer to Ge first.

	Mn	Ge	H$_t$ (Ge)	H$_t$ (Mn)	H$_{br}$ or H$_2$	Nα	Nβ
***transHGe*-2a**	–0.23	0.21	–0.09	–0.08	–0.07	–	–
***central*-2a**	–0.24	0.24	–0.09	–	–0.07, –0.08	–	–
***cis*-2a**	–0.23	0.19	–0.10	–	–0.02, –0.02	–	–
***transH$_2$*-2a**	–0.23	0.17	–0.09	–	–0.03, –0.03	–	–
***transHGe*-2b**	–0.23	0.22	–0.10	–0.09	–0.07	–	–
***central*-2b**	–0.24	0.24	–0.10	–	–0.07, –0.08	–	–
***cis*-2b**	–0.23	0.20	–0.10	–	–0.02, –0.02	–	–
***transH$_2$*-2b**	–0.23	0.18	–0.11	–	–0.03, –0.03	–	–
***trans*-5a**	–0.20	0.17	–0.09	–	–	–0.02	–0.13
***cis*-5a**	–0.21	0.18	–0.10	–	–	–0.01	–0.10
***trans*-5b**	–0.21	0.18	–0.10	–	–	–0.02	–0.14
***cis*-5b**	–0.21	0.19	–0.10	–	–	–0.01	–0.11
	Mn	Ge	H$_t$ (Ge)	H$_{agostic}$	H$_{o\text{-Ph(not agostic)}}$		
A	–0.21	0.17	–0.10	0.01	0.04, 0.04, 0.05		

References

1. D. Sellmann, *Angew Chem Int Ed Engl*, 1972, **11**, 534-534.
2. S. M. Howdle and M. Poliakoff, *J. Chem. Soc., Chem. Commun.*, 1989, 1099-1101.
3. J. A. Banister, P. D. Lee and M. Poliakoff, *Organometallics*, 1995, **14**, 3876-3885.
4. P. D. Lee, J. L. King, S. Seebald and M. Poliakoff, *Organometallics*, 1998, **17**, 524-533.
5. R. K. Merwin, A. C. Ontko, J. F. Houlis and D. M. Roddick, *Polyhedron*, 2004, **23**, 2873-2878.
6. J. A. Banister, M. W. George, S. Grubert, S. M. Howdle, M. Jobling, F. P. A. Johnson, S. L. Morrison, M. Poliakoff, U. Schubert and J. R. Westwell, *J. Organomet. Chem.*, 1994, **484**, 129-135.
7. S. M. Howdle, M. A. Healy and M. Poliakoff, *J. Am. Chem. Soc.*, 1990, **112**, 4804-4813.
8. Y. Zheng, W. Wang, J. Lin, Y. She and K. Fu, *J. Phys. Chem.*, 1992, **96**, 9821-9827.
9. W. T. Boese and P. C. Ford, *Organometallics*, 1994, **13**, 3525-3531.
10. J. B. Eastwood, L. A. Hammarback, M. T. McRobie, I. P. Clark, M. Towrie, I. J. S. Fairlamb and J. M. Lynam, *Dalton Trans.*, 2020, **49**, 5463-5470.
11. B. H. G. Swennenhuis, R. Poland, N. J. DeYonker, C. E. Webster, D. J. Darensbourg and A. A. Bengali, *Organometallics*, 2011, **30**, 3054-3063.
12. C. Perthuisot, M. Fan and W. D. Jones, *Organometallics*, 1992, **11**, 3622-3629.
13. Y.-Q. Zou, S. Chakraborty, A. Nerush, D. Oren, Y. Diskin-Posner, Y. Ben-David and D. Milstein, *ACS Catal.*, 2018, **8**, 8014-8019.
14. W. A. King, X.-L. Luo, B. L. Scott, G. J. Kubas and K. W. Zilm, *J. Am. Chem. Soc.*, 1996, **118**, 6782-6783.
15. W. A. King, B. L. Scott, J. Eckert and G. J. Kubas, *Inorg. Chem.*, 1999, **38**, 1069-1084.
16. K. D. Welch, W. G. Dougherty, W. S. Kassel, D. L. DuBois and R. M. Bullock, *Organometallics*, 2010, **29**, 4532-4540.